

Carbon against PFAS

Adsorption at low concentrations

Marko Pranić

Propositions

1. The design of adsorbents for PFAS removal requires improving adsorption kinetics over increasing adsorption capacity
   (This Thesis)
2. No PFAS treatment is effective without prior removal of natural organic matter.
   (This Thesis)
3. Experimental designs that minimize reliance on statistics result in more reliable data and conclusions.
4. Creative ideas to scientific problems emerge when the mind is relaxed.
5. Scientific papers are well written when Master-level students understand them
6. Reliance on artificial intelligence contributes to a decline in human intelligence.
7. The adoption of English as a single working language benefits the European Union economy and welfare of its citizens.
8. Societies that value altruism over individual interests are less polarized and therefore more stable.

Propositions belonging to the thesis, entitled
Carbon against PFAS. Adsorption at Low Concentration,

Marko Pranić
Wageningen, 01.07.2026

CARBON AGAINST PFAS

Adsorption at Low Concentration

Marko Pranić

Thesis Committee

Promotors
Prof. Dr ir. A. van der Wal
Special Professor, Environmental Technology
Wageningen University and Research

Dr ir. J.E. Dykstra
Associate Professor, Environmental Technology
Wageningen University and Research

Other members:
Prof. Dr A.A. Koelmans, Wageningen University and Research
Prof. Dr E.R. Cornelissen, Ghent University, Belgium
Dr A. Georgi, Helmholtz Centre for Environmental Research, Leipzig, Germany
Dr C.H.M. Hofman-Caris, KWR Water Research Institute, Nieuwegein

This research was conducted under the auspices of the Graduate School for Socio-Economic and Natural Sciences of the Environment (SENSE).

Carbon against PFAS

Adsorption at Low Concentration

Marko Pranić

Thesis

submitted in fulfilment of the requirements for the degree of doctor
at Wageningen University
by the authority of the Rector Magnificus,
Prof. Dr C. Kroeze,
in the presence of the
Thesis Committee appointed by the Academic Board
to be defended in public
on Wednesday 1 July 2026
at 10:30 a.m. in the Omnia Auditorium.

Marko Pranić
Carbon against PFAS. Adsorption at Low Concentration,
284 pages.

PhD thesis, Wageningen University, Wageningen, the Netherlands (2026)
With references, with summary in English

ISBN: 978-94-6534-458-4
DOI: 10.18174/681560

To all students

Table of Contents:

Chapter 1	General Introduction	9
Chapter 2	Kinetic and Isotherm Study for the Adsorption of Per- and Polyfluoroalkyl substances (PFAS) on Activated Carbon in the Low ng/L Range	35
Chapter 3	Total PFAS Isotherms as a Framework to Select Adsorbents for PFAS Removal	85
Chapter 4	Temperature impacts PFAS adsorption on Activated Carbon	109
Chapter 5	Which Natural Organic Matter Components Limit PFAS Removal by Activated Carbon	137
Chapter 6	Electroregeneration of Activated Carbon Filters: Concentrating Short-Chain PFAS	171
Chapter 7	General Discussion	197
References		239
Summary		259
Acknowledgments		263

CHAPTER 1

General Introduction



1.1. General background

Clean drinking water is a limited and increasingly stressed resource, yet it is essential for public health, economic activity, and societal stability. At the same time, modern societies rely on thousands of synthetic chemicals that enable advanced technologies and everyday products, but may unintentionally contaminate water resources. Among these, per- and polyfluoroalkyl substances (PFAS) have become a particular concern: PFAS are widely used, extremely persistent, and detected in water at concentrations that can pose potential risks to human health and environment.[1]

This Thesis addresses the challenge of removing PFAS from drinking water using adsorption by granular activated carbon (GAC) under environmentally relevant conditions. It focuses on identifying the mechanisms that limit PFAS adsorption, particularly for short-chain PFAS and in the presence of natural organic matter, and on evaluating strategies to improve treatment performance and regeneration efficiency to meet increasingly stringent regulatory requirements.

The History of Teflon

In 1938, DuPont chemist R. J. Plunkett and his assistant J. Rebok were working on synthesizing a new non-flammable refrigerator coolant, tetrafluoroethylene (C_2F_4). During one experiment, C_2F_4 gas did not come out from a pressurized cylinder, and upon cutting cylinder open, they found a white powder coating the interior. They had unintentionally created a new polymer inside the cylinder. A spontaneous polymerization of C_2F_4 had occurred, producing polytetrafluoroethylene (PTFE), a material that later became globally known as Teflon.[2]

Plunkett soon realized that Teflon was indestructible. It did not dissolve in water, it did not melt in the strongest acids or bases, and it would not burn. Fortunately for DuPont, this discovery came during the Second World War, a time when indestructible materials were in great demand. One of the first applications of Teflon was to coat pipes and reactors used to produce uranium hexafluoride, an extremely corrosive chemical required for the Manhattan Project. The U.S. military soon adopted Teflon, using it to coat aircraft fuel tanks and engine components to prevent corrosion. Teflon also enabled the safe handling of concentrated nitric acid in explosive manufacturing processes.[3]

The remarkable durability of Teflon comes from the carbon–fluorine (C–F) bond. Fluorine is the most electronegative element, meaning it strongly attracts shared electrons, and the C–F bond is the strongest single bonds carbon can form. As a result, high temperatures of around 800 °C are required to break these bonds and thermally

decompose Teflon.[4] After the war, DuPont began exploring civilian applications for this nearly indestructible material. From the post-war period onward, Teflon has found widespread use across numerous industries. It is used as insulation for electrical cables exposed to extreme temperatures; as a dry lubricant; and as a coat for pipes requiring exceptional chemical resistance. Teflon also entered everyday life through non-stick coatings on cookware and waterproof layers in outdoor clothing.[5]

Teflon was also adopted in medical applications, a development on which Plunkett reflected nearly 50 years after its discovery:[2]

"It has been exciting to see something I worked on become of such great benefit to mankind in general as well as to real people I know. Some years ago, at a social affair, I was introduced by a doctor friend to a man who had been suffering from a serious heart defect. 'See that fellow dancing over there,' asked my friend, 'he's alive today because he is wearing a Teflon aorta which I installed.' … I believe I've been more than just helpful; I've made a real contribution."

So how are PFAS related to Teflon? One of the most efficient ways to produce Teflon is in aqueous phase, with PFAS as a surfactant that stabilizes the growing polymer particles in water. Because commercial Teflon products typically require very high purity (~99.99%), the raw polymer must be thoroughly washed after production.[5] The resulting wastewater contains large amounts of PFAS. In the second half of the 20th century, these toxic wastewaters were released into the environment with little or no treatment, leading to severe local contamination, multiple environmental incidents, high-profile lawsuits and substantial financial settlements.[6]

1.2. What are PFAS?

1.2.1. Definition and classification

PFAS stands for per- and polyfluoroalkyl substances, where the prefix per- (Latin: completely) denotes fully fluorinated carbon chains in which all hydrogen atoms are replaced by fluorine, while the prefix poly- (Greek: many) denotes partially fluorinated chains that retain at least one carbon–hydrogen bond. In older literature, particularly before 2011, the term PFC (perfluorinated compounds) was often used, but this created confusion, as "PFC" was also used to describe perfluorocarbons, a completely different class of chemicals. To address this issue, Buck et al. (2011) recommended the scientific community to adopt the term PFAS and avoid using PFC. This terminology was widely accepted, and Buck et al. (2011) also further defined PFAS as follows:[7]

„PFASs are aliphatic substances containing one or more C atoms on which all the H substituents present in the nonfluorinated analogues from which they are notionally derived have been replaced by F atoms, in such a manner that PFASs contain the perfluoroalkyl moiety C_nF_{2n+1}*-"*

This definition encompasses the well-studied PFAS, including long-chain compounds such as PFOA and PFOS, as well as their shorter-chain and branched replacements, such as PFPeA and GenX.

About a decade later, the Organisation for Economic Co-operation and Development (OECD) proposed a broader definition:[8]

„…with a few noted exceptions, any chemical with at least a perfluorinated methyl group (–CF3) or a perfluorinated methylene group (–CF2–) is a PFAS."

Compared with the Buck et al. (2011) definition, the OECD framework is much more expansive. It includes fluorinated gases, fluoropolymers such as Teflon, and low-molecular-weight compounds like trifluoroacetic acid (TFA). Figure 1.1 illustrates examples of chemicals classified as PFAS under each definition.

The definition of PFAS remains an active topic of debate.[9,10] Scientists, industry, and regulatory agencies all recognize that the definition chosen has direct consequences for environmental monitoring, regulatory limits, and treatment requirements.[4] In drinking water regulation how "PFAS" is defined determines which compounds are subject to regulatory limits. Under current EU rules, the total allowable concentration of all PFAS (PFAS Total) in drinking water is 500 ng/L.[11] Achieving this limit would become significantly more challenging if the broader OECD definition, rather than the narrower Buck et al. (2011), were applied. The International Union of Pure and Applied Chemistry (IUPAC) is currently developing a unified definition, which is expected to strongly influence future legislation and scientific practice.[5]

The research for this PhD Thesis was conducted between 2021 and 2025. During this period, the definition proposed by Buck et al. (2011) remained the most widely used in the scientific community, and this definition is applied throughout this Thesis. For the purpose of this Thesis, two additional PFAS classifications are particularly important. First, PFAS can be grouped according to their functional headgroup into per- and polyfluorocarboxylic acids (PFCAs), which contain a terminal carboxylic acid group, and per- and polyfluorosulfonic acids (PFSAs), which contain a terminal sulfonic acid group. Second, PFAS are commonly classified by carbon-chain length. Under the Buck et al. (2011) framework, short-chain PFAS are defined as PFCAs with six or fewer perfluorinated carbons and PFSAs with five or fewer perfluorinated carbons. These classification conventions are used throughout this Thesis and are consistent with much of the literature cited herein.

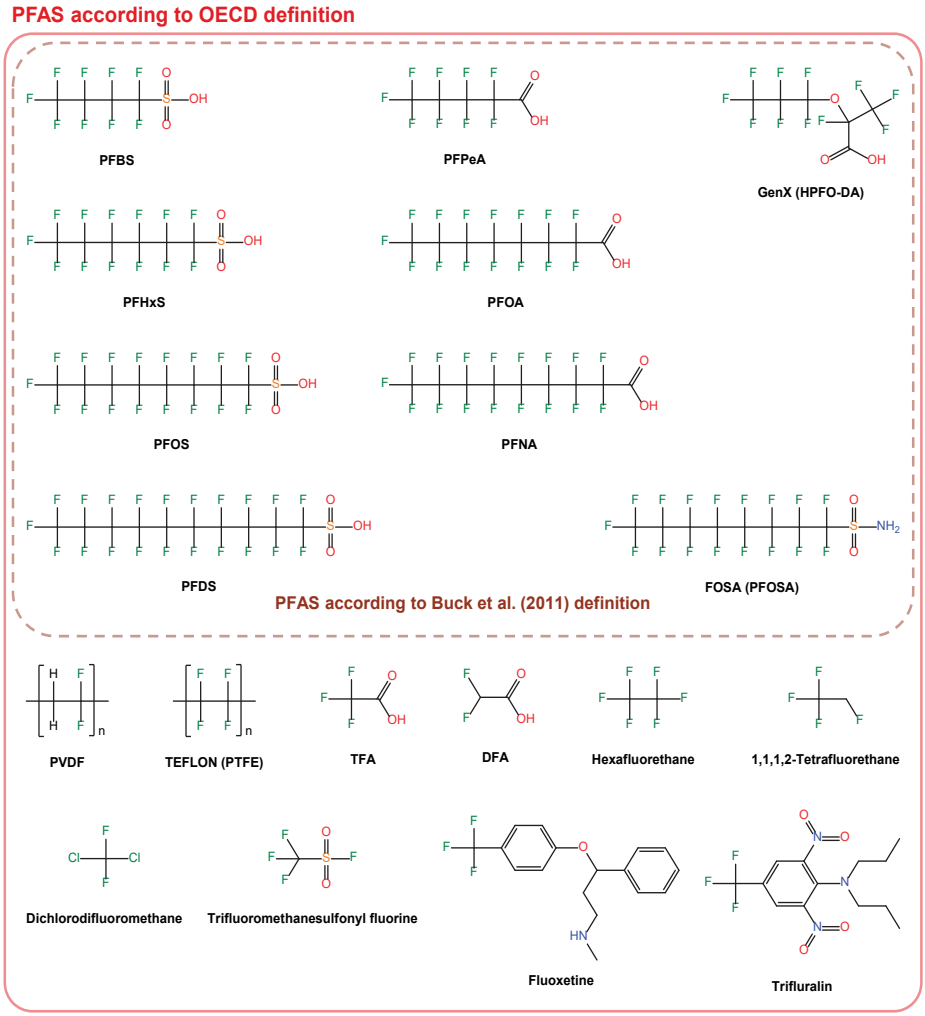


Figure 1.1. Examples of substances classified as PFAS under the definition proposed by Buck et al. (2011)[7] and under the broader OECD definition.[8] The Buck et al. (2011) framework is restricted to aliphatic substances containing a perfluoroalkyl moiety (C_nF_{2n+1}–), whereas the OECD definition additionally includes substances containing at least one perfluorinated methyl (–CF_3) or methylene (–CF_2–) group.

1.2.2. Properties and uses

The properties of PFASs arise directly from their chemical structure (Figure 1.2A). The fluorinated carbon backbone provides hydrophobicity, thermal stability, and chemical resistance, while the polar headgroup adds hydrophilicity and polarity.[12,13] This amphiphilic nature makes many PFAS effective surfactants capable of forming micelles in water (Figure 1.2B), and makes them mobile in the environment. Recent studies, however, suggest that some

PFAS may self-associate in aqueous solution as large, concentration-dependent aggregates rather than forming classical, size-limited micelles (Figure 1.2C).[14]

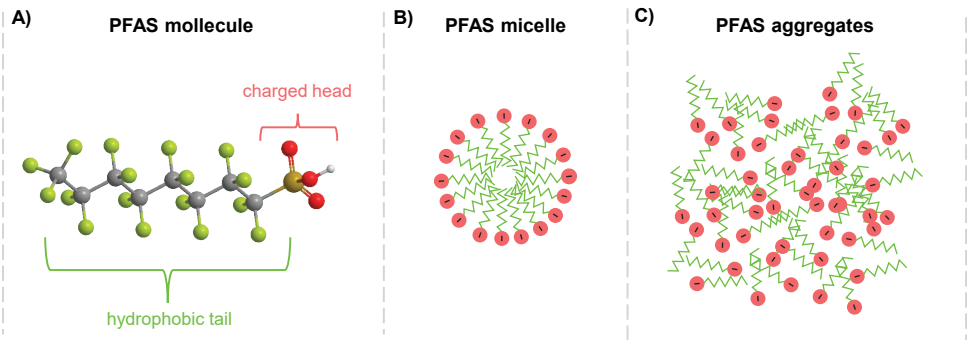


Figure 1.2. PFAS structure and self-association in water. (A) Three-dimensional representation of long-chain PFOS, with atoms shown as carbon (grey), fluorine (green), oxygen (red), and sulfur (yellow). (B) Classical micelle formation by PFAS surfactants. (C) Alternative non-micellar aggregation behaviour reported for some PFAS, forming larger aggregates rather than size-limited micelles. In all panels, the hydrophobic perfluorinated tail is shown in green and the charged headgroup in red.[14]

The strength of the carbon–fluorine bond, combined with the low surface energy of the fluorinated chain, gives PFAS their characteristic performance properties: the ability to lower surface tension, resistance to acids and oxidants, non-flammability, high gas solubility, low dielectric constant, and stability across wide temperature ranges. In addition, PFAS exhibit extremely low reactivity, high dielectric breakdown strength, good heat conductivity, low refractive index, low volatility under vacuum, the ability to generate strong acids, and even partial impenetrability to radiation.[15] Together, these properties explain their widespread use in industrial processes and consumer products.

An overview of industrial PFAS uses was provided in a study by Glüge et al. (2020), which compiled non-confidential volume data reported under the U.S. Toxic Substances Control Act Chemical Data Reporting system. Although this Act requires companies to report chemical use volumes, more than 80% of entries are classified as confidential business information, meaning the completeness and reliability of available data is low. Nevertheless, using the non-confidential data reported for Denmark, Norway, Sweden, and Finland in 2016, general trends of industrial PFAS uses can still be identified. PFAS use is dominated by the electrical equipment and machinery manufacturing sectors, where PFAS serve primarily as functional fluids, with each sector using more than 2000 tonnes of PFAS per year. Uses in the 100–500 tonnes include basic inorganic chemical manufacturing, where PFAS are applied as refrigerants and heat-transfer fluids, as well as the production of fire-fighting foam agents. Uses around 1-2 tonnes include computer and electronic product manufacturing and

miscellaneous manufacturing, where PFAS are reported as solvents for cleaning, degreasing, or surface treatment.. All remaining sectors, such as paints and coatings, textiles, oil and gas operations, printing inks, rubber processing, and cleaning products, report volumes below 1 ton in the non-confidential data.

Because their use is so widespread, PFAS are inevitably released into the environment, either directly during product use or indirectly through industrial effluents, municipal wastewater treatment plants, landfills, recycling and incineration, or atmospheric deposition. With advances in analytical methods capable of detecting PFAS at ng/L levels, they have now been found globally in water, soil, biota, and human serum. Although the chronic effects of long-term exposure to low concentrations are not fully understood, their persistence and potential for bioaccumulation have prompted strict regulations for allowable concentrations in drinking water and food.

In response to these concerns, long-chain PFAS have gradually been replaced by short-chain alternatives, such as replacing PFOA with GenX.[16] However, short-chain PFAS remain highly mobile, environmentally persistent, and difficult to remove from water. Consequently, regulatory and scientific efforts are now increasingly directed at promoting completely non-fluorinated alternatives, as part of a broader push in the EU to restrict PFAS uses to those considered essential.

For a substance to serve as a PFAS alternative, it must satisfy three criteria: it must be non-hazardous, provide comparable technical performance, and be commercially available. A recent study by Figueroa et al. (2025) evaluated PFAS use across 325 identified applications and found that potential alternatives exist for only 40 of them. Viable substitutes were identified mainly for applications such as firefighting foams, paper and packaging, and certain textile treatments. Crucially, the study found no suitable alternatives for many industrial uses, particularly those requiring extreme thermal stability, chemical resistance, or durability. These industrial sectors are also among the largest users of PFAS. This highlights that, although reducing PFAS production is essential, a full phase-out is currently not technically feasible without further innovation.

Therefore, while long-term mitigation requires reducing PFAS use and developing reliable alternatives, PFAS will continue to enter the environment for the foreseeable future. As a result, effective treatment technologies must be applied to reduce PFAS levels in the environment.

The following Section 1.3 discusses current PFAS concentrations in drinking water sources and the regulatory thresholds that utilities must meet, providing the context for the use of advanced removal processes, such as adsorption onto activated carbon.

1.3. PFAS in drinking water

1.3.1. Regulations of PFAS concentrations

The current EU Drinking Water Directive (2020) sets a maximum concentration of 100 ng/L for the sum of 20 regulated PFAS, along with a broader PFAS Total limit (all compounds considered PFAS) of 500 ng/L.[11] In contrast, the United States has recently adopted stricter national standards: the U.S. EPA now enforces 4 – 10 ng/L for concentration of five PFAS of concern in drinking water[17]

In Europe, PFAS regulation is increasingly guided by health-based exposure limits. The European Food Safety Authority (EFSA) defined a tolerable weekly intake (TWI) of 4.4 ng /kg of body weight per week for the combined exposure to four PFAS (PFOA, PFOS, PFNA, and PFHxS), based on observed immunotoxic effects.[1] To translate this TWI into drinking water guidance, the Dutch National Institute for Public Health and the Environment (RIVM) applied a Relative Potency Factor (RPF) approach. In this framework the toxicity of individual PFAS is expressed relative to PFOA as the reference compound; longer-chain PFAS such as PFOS receive higher RPF values due to greater suspected toxicity, whereas shorter-chain PFAS receive lower values (Table 1.1).[18] Using this framework, RIVM derived an advised maximum concentration of 4.4 ng PFOA-equivalents per liter (4.4 ng PEQ/L) for the sum of 23 PFAS in drinking water, although this value is not incorporated in law. At the European level, the same PEQ-based threshold has been incorporated into a recent proposal for the revision of the Environmental Quality Standards Directive, where it is applied to the protection of surface waters from 25 PFAS, indicating a broader regulatory shift toward potency-weighted PFAS limits.[19]

1.3.2. Detected levels of PFAS in raw and produced drinking water in Europe and The Netherlands

In drinking water sources, the combined concentration of PFAS typically ranges from below 1 ng/L to approximately 1 µg/L. These levels are referred to in this Thesis as environmentally relevant concentrations. The Netherlands provides an especially informative case for examining PFAS occurrence and treatment challenges: the country has extensive and systematic monitoring programs, relies heavily on surface water for drinking water production that can have high PFAS concentrations, and follows some of the strictest PFAS guidelines in Europe. As a result, many high-quality datasets are available.

A study by Zafeiraki et al. (2015) analysed tap water samples from The Netherlands and Greece.[20] In The Netherlands, PFAS concentrations in drinking water were generally higher: 11 of 37 samples exceeded 15 ng/L, and the maximum measured value reached 54 ng/L. For comparison, in Greece only 5 of 43 samples contained PFAS above 2 ng/L, with a highest reported total PFAS concentration of 5.9 ng/L. Zafeiraki et al. (2015) also summarized PFAS monitoring studies conducted across Europe between 2007 and 2012. In most countries, total PFAS levels in tap water ranged from below 10 ng/L up to roughly 40 ng/L. An exception was

reported by Skutlarek et al. (2006), who measured PFAS concentrations of approximately 200 ng/L in groundwater in Germany, attributed to the application of PFAS-contaminated soil improvers on agricultural land.[21]

More severe contamination in The Netherlands has been observed near industrial point sources. Gebbink et al. (2017) reported elevated GenX concentrations downstream of a Dutch fluorochemical plant, ranging from 1.7 to 812 ng/L, while other PFAS summed to 36–65 ng/L depending on the location. Importantly, drinking water in nearby cities showed much lower levels, with total PFAS ranging from 0.56 to 58 ng/L (with GenX included), demonstrating either significant removal through treatment or accumulation of GenX somewhere in the environment.[16]

Two more recent studies evaluated PFAS concentrations using the EFSA RPF approach. The first, by Sadia et al. (2023), measured 56 PFAS in raw and treated water from 18 Dutch drinking water facilities employing a wide range of treatment processes.[22] In raw water, total PFAS concentrations ranged from 50 to 1150 ng/L for surface waters and from 90 to 530 ng/L for groundwater. All facilities succeeded in meeting the current EU requirement of <100 ng/L for the sum of 20 PFAS. However, many surface-water facilities did not meet the much stricter national guideline of 4.4 ng PEQ/L proposed by EFSA with 9 out of 11 produced drinking waters exceeding this threshold. The primary reason was the presence of the ultrashort-chain PFAS trifluoroacetic acid (TFA), which contributed to 49–99% of the total PEQ. TFA concentrations ranged from 30 to 1100 ng/L, and similarly elevated levels have been reported in German drinking water.[22]

The second study, conducted by Grung et al. (2024), examined PFAS levels in 17 source waters and corresponding treated waters across Norway.[23] In source waters, the sum of measured PFAS ranged from 0.5 to 15 ng/L, while concentrations expressed as PEQ ranged from 0.7 to 19 ng PEQ/L. In treated water, none of the samples exceeded the current EU limit of 100 ng/L for the sum of 20 PFAS, and only 1 out of 142 drinking water samples exceeded the EFSA-proposed limit of 4.4 ng PEQ/L. It is important to highlight, however, that this study did not include TFA in its measurements.

These studies show that current drinking water in The Netherlands generally complies with the existing EU standard of 100 ng/L but does not meet the much stricter national guideline of 4.4 ng PEQ/L. As a result, considerable effort in recent years has focused on understanding PFAS removal mechanisms and improving treatment strategies.

1.3.3. Removal of PFAS from drinking water

A range of technologies is available for PFAS removal from drinking water, differing in maturity, effectiveness, and applicability at full scale. The most established and widely implemented approaches are separation-based technologies. In practice, PFAS removal in drinking

water treatment is achieved predominantly through adsorption onto granular or powdered activated carbon, and in some cases through ion-exchange resins.[24–27] Membrane processes such as nanofiltration and reverse osmosis are also highly effective and can achieve very low effluent concentrations; however, their application is typically limited to specific contexts due to high energy demand and the need to manage concentrated reject streams.[25,28]

Beyond these established options, increasing research attention is directed towards alternative and emerging technologies that aim to destroy PFAS rather than separate them. These include electrochemical treatment, advanced oxidation and reduction processes, plasma-based methods, and sonochemical approaches.[25,29] Although many of these techniques demonstrate promising removal or degradation efficiencies at laboratory or pilot scale, their broader implementation is currently constrained by high energy requirements, operational complexity, and cost. Consequently, adsorption-based technologies remain the backbone of PFAS removal in drinking water treatment, while destructive technologies are primarily considered complementary or prospective future solutions.

1.4. Removal of PFAS with adsorption by activated carbon

1.4.1. What is adsorption?

Adsorption is a phase-transfer process in which chemical species from gas or liquid accumulate at the surface of a solid or liquid phase.[30–32] In the context of PFAS removal, adsorption typically involves a porous solid material on which PFAS molecules can adsorb. Adsorption technology is widely applied in drinking water production as well as in the treatment of industrial and municipal wastewater streams containing PFAS. The basic terminology used in adsorption is illustrated in Figure 1.3. The solid material providing surface sites for adsorption is referred to as the adsorbent, while the species removed from solution are termed the adsorbate. The reverse process, in which adsorbed molecules detach from the surface and return to the fluid phase, is known as desorption. Adsorption and desorption are governed by thermodynamic principles: physical adsorption is typically exothermic and associated with change in entropy, favouring lower temperatures, whereas desorption becomes increasingly favourable at elevated temperatures.[32]

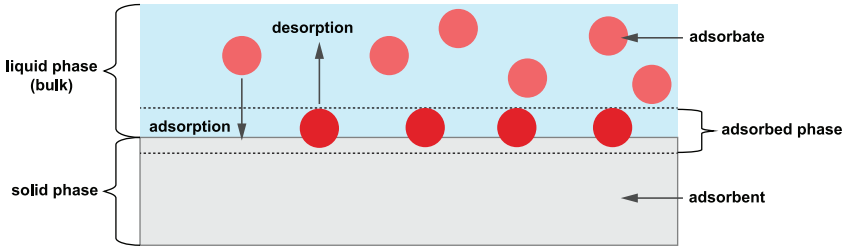


Figure 1.3. Basic terms of adsorption. Adopted from Worch (2012)

In the literature, the term sorption is sometimes used instead of adsorption.[33] Adsorption refers specifically to the enrichment of molecules at the surface of a solid material, whereas absorption describes the transfer of a substance into the bulk of another phase. In some systems, however, these processes occur simultaneously, and the term sorption is preferred. This is often the case for soils, sediments, and aquifer materials, where solutes can adsorb to mineral surfaces and absorb into organic matter fractions located in the interior of the material. For this reason, environmental chemistry literature commonly uses the more general term sorption,[34] which encompasses both adsorption and absorption. Since this thesis focuses on engineered adsorption processes in porous solids used for PFAS removal, the term adsorption is used throughout, as it is the commonly used terminology in engineering and water treatment textbooks.[30]

1.4.2. What is activated carbon?

The most common used adsorbent in water purification is activated carbon (AC). AC is widely applied in drinking water treatment due to its high internal surface area arising from its porous structure, its ability to non-selectively remove a broad range of organic micropollutants and natural organic matter, and its relatively low cost.[30] Because AC was already an established technology for the removal of organic contaminants, many drinking water utilities adopted AC for PFAS removal during the last decade.[22,35–37] In particular, AC has shown good performance for long-chain PFAS, which were historically of greatest regulatory concern.

Two key properties govern the adsorption behaviour of AC: pore size distribution and surface chemistry, both of which are determined by the choice of feedstock and the activation method. Feedstock selection strongly influences pore structure. Coal- and coconut-shell-based ACs generally produce predominately microporous materials, with coconut-shell ACs being particularly rich in micropores. These structures provide large internal surface areas suitable for the adsorption of small organic molecules. In contrast, wood-based activated ACs typically contain a higher fraction of mesopores and macropores, which enhance pore accessibility and facilitate the adsorption of larger molecules.[30,38]

The activation method significantly determines surface chemistry. Thermal (physical) activation, typically performed with steam or carbon dioxide at high temperatures, produces Acs with relatively few oxygen-containing surface groups and therefore a more neutral and hydrophobic surface character. Chemical activation, commonly performed using agents such as phosphoric acid or potassium hydroxide, introduces a higher density of surface functional groups, often resulting in more negatively charged and more hydrophilic ACs.[39,40]

The pore structure of AC is commonly described according to the IUPAC pore size classification: micropores (<2 nm), mesopores (2–50 nm), and macropores (>50 nm).[41] For many solutes, micropores provide most of the internal surface area and therefore dominate

adsorption capacity, while mesopores and macropores act primarily as transport pathways that facilitate diffusion toward smaller internal pores.[42–44]

The internal surfaces of AC contain energetically heterogeneous adsorption sites that interact with solutes in the surrounding aqueous phase through their electronic and spatial characteristics. Because these sites span a range of adsorption energies, the AC surface exhibits an intrinsic heterogeneity that results in a distribution of adsorption affinities. Adsorption on AC is governed primarily by weak intermolecular forces, particularly van der Waals dispersion interactions, enabling the non-selective adsorption of a wide range of organic compounds. Depending on solute properties, additional interactions may contribute, including π–π interactions between the delocalized π-electron system of the carbon structure and aromatic molecules, as well as electrostatic interactions between surface functional groups and ionic species.[38]

ACs are used in two main forms: granular activated carbon (GAC), with particle sizes typically between 0.5 and 4 mm, and powdered activated carbon (PAC), with particle sizes below 40 μm (Figure 1.4).[30] Regardless of particle size, the adsorptive capacity of AC is gradually exhausted as its surface becomes saturated with pollutants. For GAC, this depletion requires reactivation, a process in which the spent carbon is typically thermally treated at high temperatures to remove adsorbed contaminants and restore its adsorption capacity, enabling multiple cycles of reuse. In contrast, PAC cannot be practically reactivated due to its fine particle size and is instead disposed of after use.[45,46]

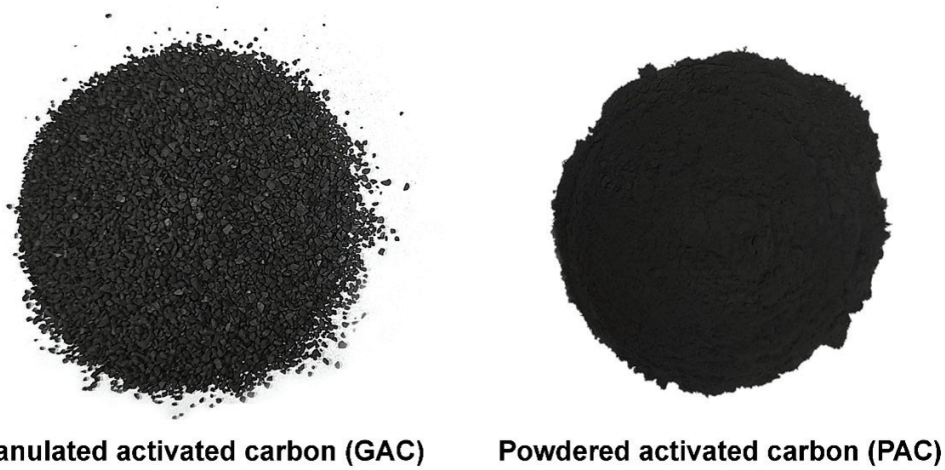


Figure 1.4. Pictures of typical commercial granular activated carbon (left) and powdered activated carbon (right)

1.4.3. Evaluating the performance of activated carbon

The performance of AC in water treatment is typically evaluated through adsorption isotherm and kinetic experiments (Figure 1.5).[30,47] These two types of experiments provide complementary and essential information: isotherms describe how a solute distributes between the aqueous phase and the AC surface at equilibrium (Figure 1.5C), while kinetic tests describe the rate at which adsorption proceeds (Figure 1.5D). Together, they form the basis for understanding, comparing, and modelling adsorption processes in engineered systems.

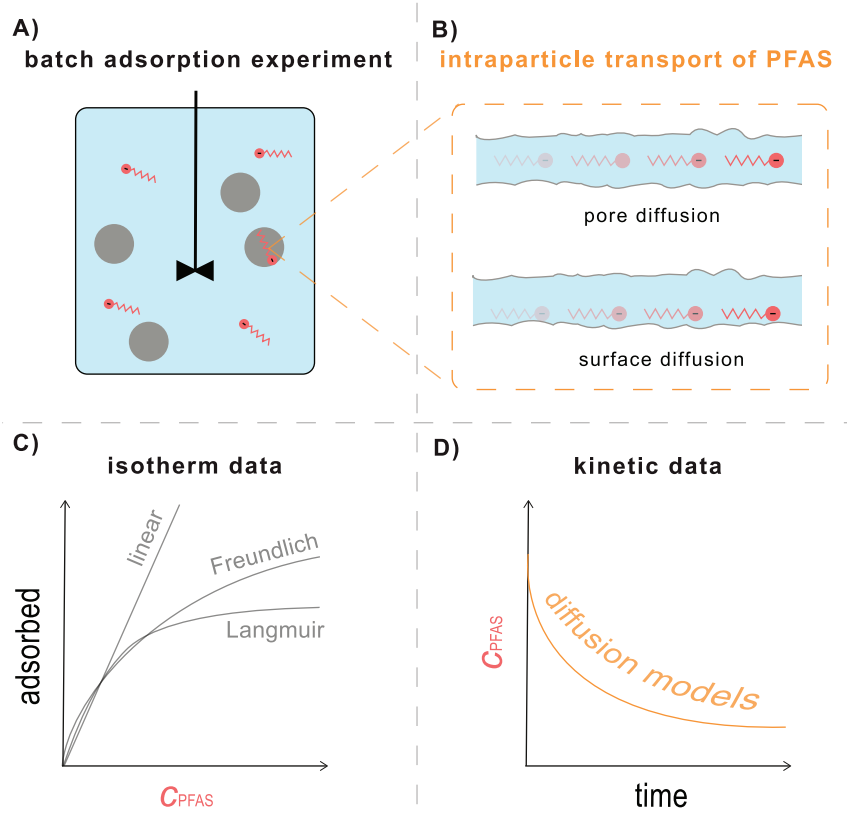


Figure 1.5. Evaluation of activated carbon (AC) performance using batch adsorption experiments. (A) Batch bottle containing PFAS solution and AC. (B) Schematic of mass transport processes within an AC particle, including pore diffusion and surface diffusion. (C) Adsorption isotherm showing the equilibrium relationship between bulk PFAS concentration and the amount adsorbed. (D) Adsorption kinetics illustrating the decrease of PFAS concentration in the bulk solution over time.

Adsorption isotherms characterize the equilibrium relationship between the concentration of a solute in solution and the amount adsorbed onto the adsorbent at constant temperature. From these data, key parameters describing adsorption affinity and adsorption capacity can be derived, reflecting how strongly and how much a solute binds to the adsorbent. Empirical and mechanistic models, such as the Freundlich and Langmuir isotherm respectively, are commonly used to describe equilibrium adsorption behaviour (Figure 1.5C).[48] Isotherm parameters are widely applied to compare ACs, assess the influence of operating conditions or water matrix components, and provide equilibrium inputs for adsorption column models.[44]

Kinetic experiments describe the rate at which a solute is taken up by AC and are governed by a sequence of mass-transfer steps. These include external mass transfer from the bulk solution to the particle surface and intraparticle diffusion within the pore structure. Intraparticle transport may occur via pore diffusion, where molecules migrate through water-filled pores, or via surface diffusion, where molecules move along the internal carbon surface (Figure 1.5B).[30,49] By fitting kinetic data with mechanistic intraparticle diffusion models, diffusion coefficients can be obtained. These coefficients quantify solute mobility within the carbon particle and are essential for predicting the dynamic performance of adsorption columns, such as breakthrough behaviour in GAC filter.[50]

1.4.4. Activated carbon as adsorbent for PFAS removal

AC has been studied as an adsorbent for PFAS removal for nearly two decades (2005–2025), with research efforts intensifying as awareness of PFAS contamination increased. One of the earliest widely cited studies is that of Ochoa-Herrera and Sierra-Alvarez (2008), who compared the removal of PFOS, PFOA, and PFBS using GAC, zeolite, and anaerobic sludge.[51] They reported clearly superior performance of GAC and observed increasing adsorption capacity with increasing PFAS chain length (PFOS > PFOA > PFBS). A similar trend was reported by Qiu et al. (2007), who investigated eleven PFAS and likewise found adsorption capacity to increase with hydrophobic chain length. That study also showed that the presence of natural organic matter (NOM) reduced PFAS adsorption and that coal-based GAC outperformed coconut-shell-based GAC.[52] Importantly, both studies were conducted at PFAS concentrations in the mg/L range, which are orders of magnitude higher than the ng/L–µg/L concentrations relevant to drinking water treatment applications.

Already in the mid-2000s, monitoring studies made it clear that PFAS concentrations in raw and treated drinking water are typically very low. For example, Takagi et al. (2008) reported PFOS and PFOA concentrations in tap water of 0.16–22 ng/L and 2.3–84 ng/L, respectively, and noted that utilities that replaced GAC more frequently achieved lower PFAS levels.[53] Similarly, Skutlarek et al. (2006) found total PFAS concentrations in drinking water of 77–598 ng/L in the Ruhr region of Germany, which reflected highly contaminated surface water sources (up to 4385 ng/L).[21] Despite these early observations, laboratory studies on PFAS adsorption continued for many years to rely almost exclusively on mg/L or even g/L

concentration ranges. This practice was largely driven by analytical limitations and experimental convenience, as higher concentrations are easier to measure with and associated with fewer experimental artefacts.

The first influential review summarizing PFAS adsorption studies on AC was published by Du et al. (2014). This work summarized proposed adsorption mechanisms (Figure 1.6) and concluded that ACs, being largely non-polar materials with limited surface charge, exhibit strong affinity for hydrophobic long-chain PFAS such as PFOS and PFOA, whereas electrostatic interactions become more important for charged adsorbent surfaces.[54] However, because nearly all studies available at the time focused on long-chain PFAS and were conducted at relatively high concentrations, the mechanisms identified primarily reflected the behaviour of these compounds and did not capture the adsorption characteristics of shorter and more hydrophilic PFAS.

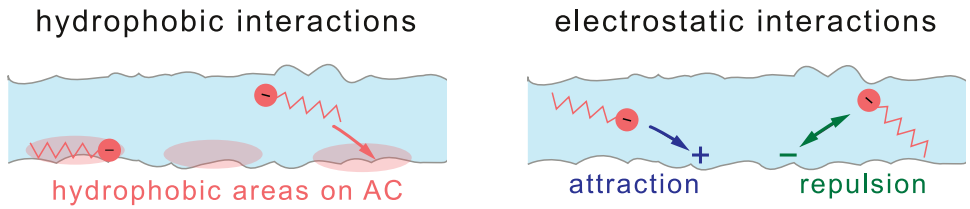


Figure 1.6. Mechanisms of PFAS adsorption on activated carbon, illustrating hydrophobic interactions with the carbon surface (left) and electrostatic attraction or repulsion between PFAS headgroups and charged surfaces (right).

Du et al. (2014) further emphasized the surfactant nature of PFAS and the potential for aggregate formation within adsorbent pores. They reported that hemimicelles or micelles may form on carbon surfaces at concentrations as low as 0.001–0.01 times the critical micelle concentration (CMC). For PFOS and PFOA, this corresponds to concentrations in the mg/L range. While such concentrations are far above environmentally relevant ng/L levels, they are representative of many laboratory studies conducted over the past two decades. Under these conditions, surface aggregation can increase apparent adsorption capacity, potentially leading to results that are not representative of PFAS behaviour under realistic drinking water conditions

As regulatory pressure increased, long-chain PFAS such as PFOS and PFOA were phased out and replaced by shorter-chain analogues, for example GenX in The Netherlands.[16] These shorter-chain PFAS are more hydrophilic and display weaker hydrophobic interactions with GAC. Their adsorption behaviour is therefore governed to a greater extent by electrostatic interactions involving the anionic headgroup and the surface charge of the carbon. Because typical GAC has limited surface charge and is relatively hydrophobic, adsorption of short-chain PFAS is consistently lower than that of long-chain PFAS.

The shift in industrial practice created a need to understand short-chain PFAS removal mechanisms, prompting the first review focused specifically on short-chain PFAS by Ateia et al. (2019). The authors noted that short-chain PFAS had been largely neglected in the literature and identified only thirteen adsorption studies, of which seven involved carbon-based adsorbents.[55] They further highlighted that short-chain PFAS are more sensitive to competition for adsorption sites by NOM and other dissolved solutes. Because their adsorption relies more strongly on access to available surface sites and less on non-specific hydrophobic interactions, short-chain PFAS are readily outcompeted by long-chain PFAS, which bind more strongly to AC. Consequently, the presence of long-chain PFAS or NOM suppresses short-chain PFAS adsorption, making their removal substantially more challenging under realistic water quality conditions.

In the period of 2010-2020 several studies examined PFAS removal at environmentally relevant ng/L concentrations using adsorption columns. Appleman et al. (2013) examined the removal of both short- and long-chain PFAS in column experiments using three types of GACs at an influent concentration of 1000 ng/L. They found that GAC was substantially more effective in low-NOM water, whereas the presence of NOM significantly reduced PFAS removal.[56] These results highlighted the importance of understanding how NOM concentration and composition influence PFAS adsorption, particularly for short-chain PFAS that are more readily outcompeted. Another study by McCleaf et al. (2017) evaluated GAC and anion-exchange resins for a mixture of 14 PFAS at initial concentrations of 100 ng/L each. They observed early desorption and weak retention for short-chain PFAS, while long-chain PFAS continued to accumulate in the bed toward the end of the experiment; the authors suggested that this behaviour may be related to PFAS–PFAS interactions at the AC surface, such as aggregation phenomena.[57]

A comprehensive synthesis of PFAS adsorption literature was provided by Gagliano et al. (2020). Their central conclusion was that most published studies had been conducted under conditions that are not representative of drinking water treatment, including high adsorbent doses, long empty bed contact times, and PFAS concentrations several orders of magnitude above environmental levels.[24] The authors further noted that the role of NOM remained poorly resolved, with contradictory findings on whether NOM suppresses, enhances, or has little effect on PFAS adsorption. The review identified fourteen isotherm studies conducted in the μg/L to mg/L concentration range, nearly all focused on long-chain PFAS, whereas only a single isotherm study, by Hansen et al. (2010), investigated adsorption from real contaminated waters at ng/L concentrations.[58] This disparity highlighted a major knowledge gap, as adsorption behaviour at trace concentrations may differ fundamentally from that observed under elevated experimental conditions. In particular, the review emphasized that experiments performed at high PFAS concentrations may overestimate adsorption capacity, because aggregation and steep concentration gradients can artificially enhance apparent adsorption.

Recent advances in analytical techniques and stricter regulations have driven a shift toward examining PFAS adsorption under realistic conditions. In the last five years, several studies have reported PFAS removal using ng/L concentration ranges, primarily through full-scale monitoring or column experiments.[22,36,59,60] While such studies provide essential insight into breakthrough behaviour, residence time effects, and the influence of water matrices, these studies generally do not allow mechanistic interpretation of adsorption at equilibrium or within carbon particles. To clarify PFAS adsorption mechanisms at low concentrations; especially intraparticle diffusion, pore accessibility, competitive adsorption, and the absence or presence of aggregation; dedicated kinetic and isotherm experiments are necessary. Reliable isotherm and kinetic parameters are essential inputs for predicting PFAS removal in the full-scale treatment plants.

1.4.5. Reactivation of exhausted GAC filters

Tightening PFAS regulations have direct consequences for the operation of GAC filters. In the EU, utilities must currently comply with a total PFAS limit of 100 ng/L,[11] while in The USA the limit is only 4–10 ng/L depending on specific PFAS,[17] and in The Netherlands a non-enforceable guideline recommends a limit of 4.4 ng PEQ/L. To achieve PFAS concentrations in the low ng/L range in treated water, GAC filters must be operated with more frequent regeneration or replacement of the carbon. This increased regeneration frequency significantly raises treatment costs and amplifies the environmental footprint of PFAS treatment due to higher energy demand, associated CO_2 emissions, and the continued production and transport of fresh GAC.[18] Consequently, the management and regeneration of exhausted GAC has become a central technical, economic, and environmental challenge in modern PFAS treatment.

The most widely applied method for restoring exhausted GAC is thermal reactivation. In this process, spent carbon is transported to specialized facilities and subjected to a sequence of drying, pyrolysis in an inert atmosphere, and controlled oxidation at up to 1000 °C to remove residual organic matter and reopen blocked pores. Thermal reactivation can desorb and degrade a broad range of contaminants, including PFAS, and benefits from mature industrial infrastructure, making it the current standard for GAC reuse.[61,62]

Despite these advantages, thermal reactivation has important limitations. Maintaining high temperatures demands considerable energy input, resulting in substantial CO_2 emissions. Each regeneration cycle leads to 10–20% carbon loss due to burn-off, necessitating continuous replacement with newly produced GAC, which is typically coal-based and therefore associated with additional environmental impacts. From an operational perspective, GAC filters must be taken offline and spent carbon transported to external regeneration facilities, further increasing costs and resource use.[46]

To reduce reliance on frequent, energy intensive thermal reactivation of GAC filters, chemical regeneration has been explored as an alternative. Chemical regeneration involves the application of regenerant solutions such as acids, bases, salts, organic solvents, or their combinations to weaken PFAS-carbon interactions and promote desorption. Regenerants containing organic solvents, such as methanol, can desorb a large fraction of PFAS from exhausted carbon, often achieving removal efficiencies exceeding 80–90%. However, this approach generates a concentrated liquid waste stream that requires further treatment or destruction, and repeated chemical exposure may alter the pore structure or surface chemistry of the carbon.[46] Economic assessments further indicate that chemical regeneration is generally more costly than thermal reactivation, particularly when the handling and disposal of spent regenerants are considered.[63]

An emerging approach to extend filter lifetime is electrochemical regeneration, in which the exhausted AC is integrated into an electrochemical cell and used as an electrode.[64–66] When a negative potential is applied to the carbon, the surface becomes negatively charged. Because PFAS exist predominantly as anions in water, this imposed surface charge creates strong electrostatic repulsion that promotes PFAS desorption. Electroregeneration could be implemented on-site and powered by renewable electricity, thereby reducing reliance on energy-intensive thermal reactivation and lowering associated CO_2 emissions. However, the technology remains at an early stage of development. Key uncertainties include the dominant desorption mechanisms, the influence of pore structure and carbon saturation, the role of water matrix components such as NOM and competing ions, and the long-term effects of electrochemical operation on carbon stability and adsorption performance.

1.5. Knowledge gaps

The PFAS literature reviewed in Section 1.4 highlights several key knowledge gaps in the understanding of PFAS adsorption onto AC, which are summarized below.

Lack of isotherm and kinetic data under environmentally relevant conditions

Most PFAS adsorption studies have been conducted at µg/L–mg/L concentrations, while PFAS typically occur at ng/L levels in drinking water. Experiments at elevated concentrations may induce aggregation and high surface coverage, resulting in adsorption capacities that overestimate performance under realistic conditions. In addition, kinetic and equilibrium data obtained in the presence of NOM or at temperatures representative of full-scale systems remain scarce. This lack of mechanistic data at trace concentrations limits the ability to model PFAS adsorption, quantify mass-transfer limitations, and reliably predict breakthrough in GAC filters.

Unclear role of natural organic matter (NOM)

Although NOM is widely recognized as a key factor impacting PFAS adsorption, mechanisms of PFAS-NOM interactions remain unclear. NOM is chemically heterogeneous, and reported effects range from strong suppression to negligible or even enhanced PFAS adsorption. It is therefore uncertain which NOM fractions most strongly affect adsorption, whether competition, pore blockage, or PFAS–NOM interactions dominate, and how these mechanisms differ between short- and long-chain PFAS. Resolving these uncertainties is essential for predicting GAC performance in real water matrices.

Limited understanding of activated carbon properties governing PFAS adsorption

While pore size distribution and surface chemistry are known to influence PFAS adsorption, their relative importance at ng/L concentrations remains poorly defined. Most existing data originate from high-concentration experiments where aggregation and non-representative mass-transfer conditions dominate. Consequently, key questions remain unresolved, including the effective contribution of micropores at trace concentrations, the role of mesopores in PFAS transport and adsorption, the importance of electrostatic interactions for short-chain PFAS, and the influence of operating conditions such as adsorbent dose and temperature. These gaps limit the selection and design of ACs optimized for PFAS removal in drinking water treatment.

Need for sustainable and effective regeneration strategies for short-chain PFAS

Stricter PFAS regulations have increased the frequency of GAC regeneration, particularly because of early short-chain PFAS breakthrough. Frequent thermal reactivation is energy-intensive, causes significant CO_2 emissions, and results in 10–20% carbon loss per cycle. These drawbacks underscore the need for alternative regeneration strategies that can extend GAC service life and reduce reliance on high-temperature processes. Electroregeneration has emerged as a potential option, but its effectiveness for short-chain PFAS under environmentally relevant conditions remains largely unexplored.

1.6. Thesis objectives and outline

Based on the identified research gaps, this Thesis is organised around four research objectives, each addressed in one or more of the five experimental chapters. Figure 1.7 presents the graphical outline of the experimental Chapters 2-6. These chapters are followed by an integrated discussion and outlook in Chapter 7.

Objective 1. Determine and model PFAS adsorption on activated carbon under environmentally relevant conditions.

Addressed in Chapters 2 and 4

The first objective is to obtain adsorption isotherms and intraparticle diffusion parameters for short- and long-chain PFAS at ng/L concentrations under realistic operating conditions. This includes quantifying equilibrium behaviour and mass transfer in different types of AC, and assessing how operating variables such as temperature and the presence of natural organic matter (NOM) affect PFAS adsorption and transport.

- **Chapter 2** presents the first systematic isotherm and kinetic dataset for nine PFAS at environmentally relevant concentrations (0.1–100 ng/L). Chapter 2 quantifies equilibrium adsorption behavior, evaluates differences between micro- and mesoporous ACs, and determines intraparticle diffusion coefficients using mechanistic surface-diffusion models. The chapter establishes how PFAS adsorption and transport behave under realistic drinking-water conditions.

- **Chapter 4** expands this objective by examining how temperature influences PFAS adsorption and intraparticle diffusion. Isotherms and diffusion parameters are determined at 10, 20 and 30 °C, enabling prediction of temperature-dependent breakthrough curves. Together, Chapters 2 and 4 provide a mechanistic description of PFAS adsorption and mass transfer under environmentally relevant conditions.

Objective 2. Identify activated carbon properties that limit PFAS adsorption

Addressed in Chapters 3

Pore size distribution and surface chemistry are thought to govern PFAS adsorption, but their individual and combined roles are not well resolved. The third objective is to establish a framework that links measurable GAC properties, such as micro- and mesopore volumes and surface functional groups, to PFAS adsorption behavior, in a way that is independent of situational experimental choices like GAC dose or initial PFAS concentration.

- **Chapter 3** introduces the total PFAS isotherm methodology, a framework that normalizes adsorption data obtained under different experimental conditions onto a unified curve. By normalizing for situational factors, this approach isolates the intrinsic influence of GAC properties. The chapter demonstrates how micropore and mesopore volumes, as well as the density of acidic surface groups, govern PFAS adsorption, and provides a tool for comparing carbons across studies in a consistent way.

Objective 3. Identify NOM components that limit PFAS adsorption

Addressed in Chapters 5

NOM is known to interfere with PFAS removal, but the specific fractions responsible and their mechanisms of competition have remained unclear. The third objective is therefore to develop an experimental approach that can identify which molecular size and chemical fractions of NOM most strongly reduce PFAS adsorption.

- **Chapter 5** applies membrane and resin fractionation to separate NOM into chemically and size-defined fractions. Through batch and column adsorption experiments, the chapter identifies which specific fractions inhibit adsorption of short- and long-chain PFAS, revealing distinct competition mechanisms. This provides a practical methodology for linking NOM composition to PFAS removal performance and informs strategies for pretreatment to remove competing fractions.

Objective 4. Assess whether electroregeneration is a suitable regeneration strategy for PFAS-laden activated carbon.

Frequent thermal regeneration of GAC filters is costly and has a substantial environmental footprint. The fourth objective is to evaluate whether electroregeneration can effectively desorb PFAS, especially short-chain compounds, under environmentally relevant conditions.

Objective 4 is addressed in Chapter 6

- **Chapter 6** evaluates electroregeneration as an lower environmental impact alternative to thermal reactivation. Using PFAS mixtures at ng/L levels and high ionic strength representative of surface water, Chapter 6 examines the desorption of short-chain PFAS, the role of electrode charging, and how carbon surface modification affects regeneration efficiency. The chapter demonstrates the potential of electroregeneration to concentrate PFAS and regenerate AC, viding the first assessment under realistic treatment conditions.

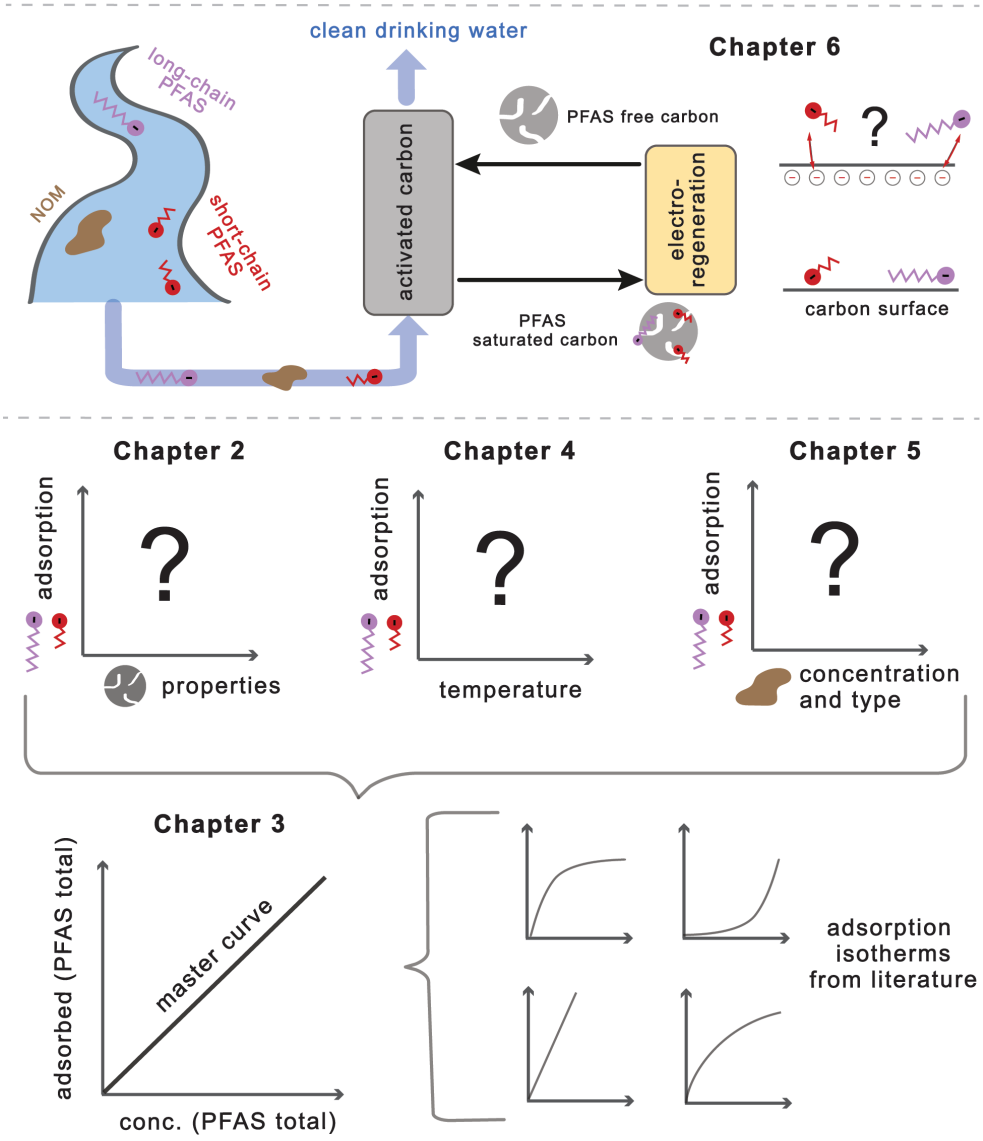


Figure 1.7. Graphical outline of the experimental chapters in this Thesis

Integrative discussion, practical implications, and outlook

Addressed in Chapter 7

Chapter 7 synthesizes the findings from Chapters 2–6 to describe the mechanisms governing PFAS adsorption AC in drinking water application.

- **Section 7.1** summarize main findings of experimental chapters in reference to Objectives of this Thesis

- **Section 7.2** identifies the main factors limiting PFAS adsorption (low concentrations, slow intraparticle diffusion, PFAS–PFAS competition, pore-size distribution, surface charge, NOM, and temperature), discusses mechanisms underlying these limitations, and strategies to reduce their negative impact on PFAS adsorption.

- **Section 7.3** translates these insights into practical recommendations for treatment design, including desirable AC properties, NOM pretreatment strategies (e.g. BAC/O_3–BAC), and modelling approaches for predicting breakthrough in full-scale GAC filters.

- **Section 7.4** formulates future research priorities directly linked to the thesis objectives, such as confirming multilayer adsorption at trace concentrations, extending NOM–PFAS interaction studies to other water matrices and PFAS classes, and further developing electroregeneration and concentrate management.

- **Section 7.5** places these technical findings in an economic context by analyzing how NOM removal, operational time, and regeneration strategy influence the cost of PFAS treatment under increasingly strict regulatory limits.

Chapter 7 thus serves as an integrative chapter and provides a perspective, connecting the detailed experimental work to practical implementation, costs, and future research needs.

1.7. PFAS investigated in this thesis

The experimental planning for this PhD Thesis, including the development of analytical methods for PFAS quantification in drinking water and the initiation of batch and column studies, began in late 2021 and early 2022. At that time, regulatory and scientific attention in Europe and The Netherlands was primarily focused on short- and long-chain PFSAs and PFCAs, as these were the compounds explicitly covered by the existing EU Drinking Water Directive.

Based on this regulatory context, nine PFAS were selected for investigation. Their physicochemical properties are summarized in Table 1.1. The selected compounds include both short- and long-chain homologues and comprise sulfonic acids (PFSAs), carboxylic acids (PFCAs), GenX as a representative long-chain replacement compound, and one sulfonamide (FOSA) to probe the influence of functional-group chemistry on adsorption. Most PFAS were selected due to their regulatory relevance, while FOSA was added specifically to explore the effect of structural differences on removal performance.

Table 1.1. Properties of PFAS investigated in this Thesis

PFAS	# of fluorinated carbons	functional group	M_w (g/mol)	LogKow	pKa	CMC mmol/L	D_L (m^2/s) $*10^{-10}$	Stokes radius (nm)	RPF
PFBS	4	SO3-	299	1.82	3.31	22	6.97	0.57	0.001
PFHxS	6	SO3-	399	3.16	0.14	12	5.85	0.68	0.6
PFOS	8	SO3-	499	4.49	<1.0	3.1 – 8.0	5.11	0.77	2
PFDS*	10	SO3-	599	6.83	3.24	n.a.	4.58	0.86	2
PFPeA	4	COO-	264	3.01	0.34	200 - 700	7.17	0.55	0.05
PFOA	7	COO-	414	4.81	<4.2	9.12	5.55	0.71	1
PFNA	8	COO-	464	5.48	0.21	2.63-9.1	5.20	0.76	10
GenX	5	COO-	329	4.00	3.8	150	6.37	0.62	0.06
FOSA	8	SO2NH2	499	5.80	3.37	0.039	5.10	0.78	2

Molecular weight, M_w, $LogK_{ow}$ and pK_a values for GenX were taken from Vakili et al.[67]; corresponding properties for all other PFAS were obtained from Gagliano et al. (2020).[13] The minimum critical micelle concentration (CMC) values in this table were taken from Kancharla et al. (2022),[68] except for FOSA, for which values were obtained from Niarchos et al. (2023); maximum CMC values for all PFAS were taken from Niarchos et al. (2023).[69] Relative potency factors (RPFs) were taken from the Proposal for an EU Directive 2022/0344 (COD).[19] The Stokes radius was calculated for all PFAS using the Stokes–Einstein equation, and liquid-phase diffusion coefficients (D_L) were estimated using the Wilke–Chang equation, which was identified as suitable for PFAS based on Endo (2025).[70]

*PFDS was investigated only in Chapter 2

CHAPTER 2

Kinetic and Isotherm Study for the Adsorption of PFAS on Activated Carbon in the Low ng/L Range



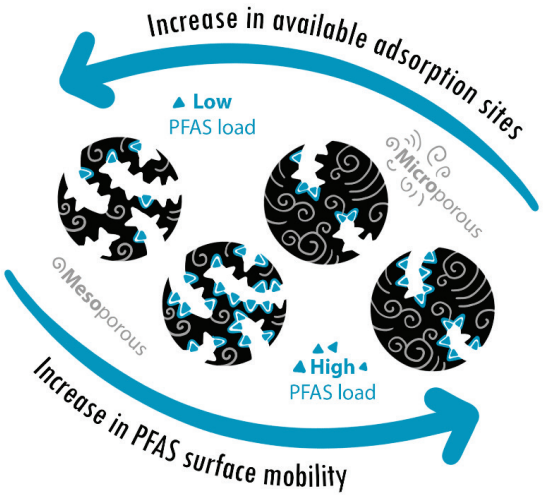
This chapter has been published as:

Pranić, M.; Carlucci, L.; van der Wal, A.; Dykstra, J. E. Kinetic and Isotherm Study for the Adsorption of Per- and Polyfluoroalkyl Substances (PFAS) on Activated Carbon in the Low Ng/L Range. Chemosphere 2025, 370. https://doi.org/10.1016/j.chemosphere.2024.143889

Abstract

Activated carbon adsorption is a widely used technology for the removal of per- and polyfluoroalkyl substances (PFAS). However, the rapid breakthrough of PFAS in activated carbon filters poses a challenge to meet the very low allowable PFAS concentrations in drinking water, leading to high operational costs. In this study, we conducted batch isotherm and kinetic adsorption experiments using nine different types of PFAS molecules at concentrations typically found in water sources used for drinking water production (0.1 – 100 ng/L). The isotherm experiments at these low concentrations reveal that the maximum adsorption capacity of several PFAS is much lower than reported in literature. The estimated isotherms were included in a dynamic model that includes mass transport based on surface diffusion. This model effectively describes the experimental kinetic data, and the obtained surface diffusion coefficients indicate a very slow PFAS surface mobility. Additionally, our findings indicate that PFAS surface mobility decreases in scenarios with more available adsorption sites. Notably, mesoporous activated carbon, with its higher adsorption capacity, exhibits lower PFAS surface mobility than microporous carbon with lower PFAS adsorption capacity. Moreover, for both carbons, we observed a decrease in PFAS surface mobility at higher carbon loadings when the surface is less saturated with PFAS. Our findings suggest a potential inherent limitations in activated carbon technology for PFAS removal under environmentally relevant conditions, as we observed lower adsorption capacities than previously reported at higher concentrations, and a decrease in PFAS surface mobility with more available adsorption sites.

Graphical Abstract



Keywords: PFAS, adsorption, drinking water treatment, surface diffusion

2.1. Introduction

Per- and polyfluoroalkyl substances (PFAS) are persistent organic micropollutants of industrial origin that raise significant concerns due to their suspected toxicity at relatively low concentrations found in the environment.[1,7,71] In sources used for drinking water production, the sum of measured concentrations of PFAS commonly ranges from less than 1 ng/L to approximately 1 µg/L.[16,37] The current EU directive set a total maximum concentration of 100 ng/L in drinking water for a selected group of PFAS of concern.[11] A report by the European Food Safety Authority recommends that the total concentration of four listed PFAS components should not exceed 4.4 ng/L in drinking water,[1] which has been adapted in a recent proposal for a new EU directive.[19] Furthermore, the US EPA has recently announced new regulations for five PFAS of concern, with allowable concentrations ranging from 4 to 10 ng/L depending on the specific PFAS.[17]

Adsorption technology has been proven in reducing PFAS concentrations to acceptable levels in drinking water.[13,26] Several studies demonstrated effective removal of PFAS using adsorptive media.[36,42,72] However, these studies also reported relatively rapid breakthrough of PFAS in adsorption columns, meaning frequent adsorbent regeneration is needed to maintain performance. Considering that adsorbent regeneration significantly contributes to the total treatment costs, there is an economic interest to minimize the frequency of regeneration.[36]

Activated carbon (AC) is the primary adsorbent used in drinking water treatment, due to its cost-effectiveness, high affinity for various compounds, and large adsorption surface area.[30] Sörengård et al.[73] tested 44 different adsorbents for PFAS removal and found that ACs exhibited the highest performance. However, understanding which AC properties impact PFAS removal is crucial. A review by Liu et al.[74] showed that PFAS removal improves with carbon materials that have fewer oxygen surface groups. Positively charged AC materials also delay PFAS breakthrough compared to neutral or negatively charged materials.[75,76] Furthermore, pore size distribution significantly impacts PFAS adsorption. Kancharla et al.[68] reported that micropores (diameter <2 nm) enhance the adsorption of short-chain PFAS, while mesopores (>2 nm) are more crucial for the adsorption of long-chain PFAS. According to Du et al.,[54] mesopores provide sufficient space for the diffusion of relatively large long-chain PFAS that cannot easily enter the micropores.

Empirical kinetic models, such as the pseudo-first or pseudo-second order models, are frequently employed to describe the dynamics of PFAS adsorption.[77–79] However, these models offer limited predictive value and lack physical interpretation. In contrast, mechanistic intraparticle diffusion models provide a more detailed description of mass transfer within AC granules. One example of such a model is the pore and surface diffusion model (PSDM).[80,81] The PSDM offers the advantage of obtaining diffusion coefficients that can be used to predict PFAS breakthrough curves, and can thereby support the design of AC filters for PFAS

removal in pilot and full-scale treatment plants.[82] Additionally, diffusion coefficients can be correlated with molecular properties, further enhancing the understanding of the adsorption process.[44]

To investigate the interactions between PFAS and adsorbents, adsorption experiments are often conducted using high PFAS concentrations and large adsorbent quantities. However, these conditions do not accurately represent realistic conditions in drinking water treatment.[13] Furthermore, the mechanisms responsible for adsorption of micropollutants can vary with concentration.[83,84] Specifically, for surfactants such as PFAS, high concentrations (>20 mg/L) can lead to the formation of (hemi-)micelles.[79] A study by Zaggia et al.[85] demonstrated the possible formation of molecular aggregates for long-chain PFAS at a concentration of 1 mg/L, a level not typically observed in drinking water treatment. Several studies conducting PFAS experiments at concentration <100 ng/L were conducted in pilot or full-scale systems, focusing solely on obtaining breakthrough curves.[36,59,60,82] Adsorption isotherms for PFAS in the 0.1-100 ng/L concentration range have not been systematically reported in experimental studies. Consequently, drawing conclusions regarding adsorption mechanisms and capacities at such low concentrations is challenging. Furthermore, the lack of isotherm data significantly limits modelling of adsorption systems using mechanistic models.

In this study, batch adsorption experiments are performed to investigate the mechanisms of PFAS adsorption within concentration ranges relevant to drinking water treatment. To our knowledge, this is the first study to report isotherm and kinetic data for PFAS adsorption in the 0.1 – 100 ng/L range. We obtain isotherm parameters and intraparticle diffusion coefficients for nine PFAS compounds using two types of AC with distinct pore size distributions. The selected ACs have similar surface charge properties, allowing us to isolate and clarify the effects of pore size distribution on PFAS adsorption. The PFAS compounds are selected for their relevance to drinking water treatment regulations and their molecular properties, to provide insight into their interactions with microporous and mesoporous AC. This study aims to asses whether there are significant differences between the isotherm and kinetic parameters derived from our novel low-concentration data and those widely reported in the literature, which are based on higher concentrations. Accurate isotherm and kinetic parameters are essential for predicting and designing effective adsorption filters. To ensure that any deviations between our results in the 0.1 – 100 ng/L range and the higher concentrations reported in the literature are not due to experimental artifacts, we conducted additional experiments on perfluorooctanoic acid (PFOA) within the 1-1000 μg/L range commonly studied.

2.2. Materials and methods

2.2.1 Activated carbons

Two granular activated carbons (GAC) with distinct pore size distributions were selected for this study. The carbon selected for its higher micropore volume and micropore surface area is AcquasorbTM K-CS from Jacobi (CS), which is a thermally activated coconut shell-based activated carbon. The carbon selected for its higher mesopore volume and mesopore surface area is SRD from Chemviron, which is a reagglomerated bituminous-based activated carbon. According to the supplier, SRD possesses similar properties to the commonly used Filtrasorb F400, but with higher mesopore volume, which was also confirmed by our N_2 physisorption analysis (see Figure S.2.1). The GAC particles were sieved to obtain a diameter range of 0.60 – 0.85 mm, which aligns with the dominant particle sizes used in some activated carbon filters.[75] A narrow particle size distribution was selected to ensure particles homogeneity. After sieving, the particles were thoroughly washed with demineralized water, and were then dried and stored. Prior to the adsorption experiments, the GAC was dried at 105 °C for 24 h to eliminate moisture. The GAC was then weighed, boiled to remove entrapped air, and subsequently cooled down to room temperature. Several well-established methods were performed to determine the properties of GAC,[47] and the results are summarized in Table S.2.1.

2.2.2. PFAS

Nine PFAS compounds were selected for this study. Molecular properties of these PFAS can be found in Table 2.1. The selected PFAS represent a combination of short-chain and long-chain compounds, encompassing PFAS with either sulfonic or carboxylic functional groups, as well as perfluorooctane sulfonamide acid (FOSA), which possesses an amide functional group. Most of the selected PFAS compounds were included due to their regulatory maximum concentrations limits, while FOSA was selected to explore the impact of functional groups on adsorption.

2.2.3. Adsorption experiments

Isotherm and kinetic adsorption experiments started by adding a specific quantity of activated carbons to a 1 L solutions containing mixture of 9 PFAS compounds dissolved in Mili-Q water, buffered at pH 7.2 using a 10 mM phosphate buffer (5 mM of Na_2HPO_4 + 5 mM KH_2PO_4). This was the minimum buffer concentration required to maintain a constant pH throughout the experiment in all bottles. The initial concentration of the PFAS compounds was similar in all experiments, ranging from ~70 to ~100 ng/L depending on the specific PFAS. The experiments were conducted in polypropylene copolymer (PPCO) bottles, which were placed horizontally on an orbital shaker and agitated at 150 rpm at a temperature of ~20 °C. Each reported datapoint was obtained by sacrificing the entire batch volume, taking a ~ 350 mL water sample that was stored at 4 °C in PP bottles for a maximum of two weeks before analysis. Notably, a batch volume of 1 L was used, which exceeds the typical volumes

for batch adsorption experiments, to minimize experimental errors in the ng/L concentration range.

In the kinetic experiments, PFAS concentrations in solution were monitored for up to 40 days for both types of GAC, using loadings of 5 mg/L, which is a typical carbon loading in drinking water treatment,[47] and of 100 mg/L, which reflects a scenario with an excess of adsorption sites. Adsorption equilibrium was reached for all PFAS compounds. Initially, during the period of most rapid kinetic changes, samples were taken at shorter intervals (every few hours), and subsequently at longer intervals (every few days). To evaluate PFAS adsorption onto the experimental PPCO and storage PP bottle, a kinetic control experiment was conducted without GAC. No significant PFAS adsorption, onto the bottles was observed, and the resulting kinetic curves are shown in Figure S.2.3.

To obtain adsorption isotherms, GAC loading was varied between 2 and 500 mg/L. These doses were chosen based on recommendations in Worch[30] to reduce experimental errors in isotherm determination. All samples were collected after 40 days, once adsorption equilibrium had been reached. The adsorbent loading is evaluated by

$$q_{eq} = \frac{V_l}{m_a}\left(c_0 - c_{eq}\right) \tag{1.1}$$

in which q_{eq} is the adsorbent loading in equilibrium (ng_{PFAS}/mg_{GAC}), V_l is the volume of the bulk solution (L), m_a is the mass of dry GAC, c_0 is the starting PFAS concentration in the bulk solution, and c_{eq} is the concentration in equilibrium.

Our study aims to identify potential differences between high-concentration PFAS adsorption data reported in the literature and our novel low ng/L data. To ensure, these differences are not due to experimental artifacts, we conducted isotherm experiments with PFOA at higher concentrations. PFOA was selected because it is one of the most extensively studied PFAS compounds. The isotherm experiments at elevated starting concentrations (1–1000 µg/L) followed the same procedures as described earlier in this section. Detailed experimental are provided in Section 2.5.2.

2.2.4. Determination of PFAS concentrations

The PFAS samples, obtained from experiments with starting concentrations up to 100 ng/L, were analysed at the certified analytical lab AquaLab Zuid B.V. (The Netherlands) using the Xevo TQ-XS LC-MS coupled with an Acquity UPLC CSH Phenyl-Hexyl column. The quantification limits for the analysed PFAS ranged from 0.1 to 0.5 ng/L. For the PFOA isotherm experiments, which had starting concentrations between 1 and 1000 µg/L, analysis was carried out using the SCIEX 5500+ LC-AD30 system, with a Phenomenex Kinetex C18 column. The quantification limit for PFOA was 0.5 ng/L. Additional details on PFAS detection and analysis methodologies are provided in Section 2.5.3.

2.3. Results and discussion

Equilibrium adsorption data for nine different PFAS at environmentally relevant concentrations (0.1 – 100 ng/L) were collected using two granular activated carbons (GACs) with contrasting pore size distributions: the more microporous CS and the more mesoporous SRD (Table S.2.1) To describe and analyse the PFAS equilibrium data, three widely used isotherm models, i.e., the linear, Langmuir and Freundlich models (Table S.2.7), were applied and the results are discussed in Section 2.3.1. Isotherm parameters were estimated based on non-linear regression. The fitting results of the isotherm parameters were evaluated using least squares fit statistical analysis.

2.3.1. Adsorption isotherms

Our findings indicate that, for an initial PFAS concentration of ~100 ng/L, the adsorption equilibrium of the PFAS compounds included in this study can be accurately described by linear isotherms for mesoporous GAC such as SRD. Conversely, the adsorption equilibrium of PFAS on microporous GAC, such as CS, is better described by Langmuir isotherms. In addition to linear isotherms, Langmuir isotherms can also effectively capture the adsorption of short-chain PFAS on SRD (Figure 2.1). The Freundlich isotherm model also describes adsorption on both types of GAC, but because of its empirical nature, these results are not in detail discussed in this manuscript.

The estimated isotherm parameters are provided in Table 2.1. Figure 2.1 shows the isotherm curves for selected PFAS compounds, while the isotherm curves for other components can be found in Figure S.2.5, and S.2.6.

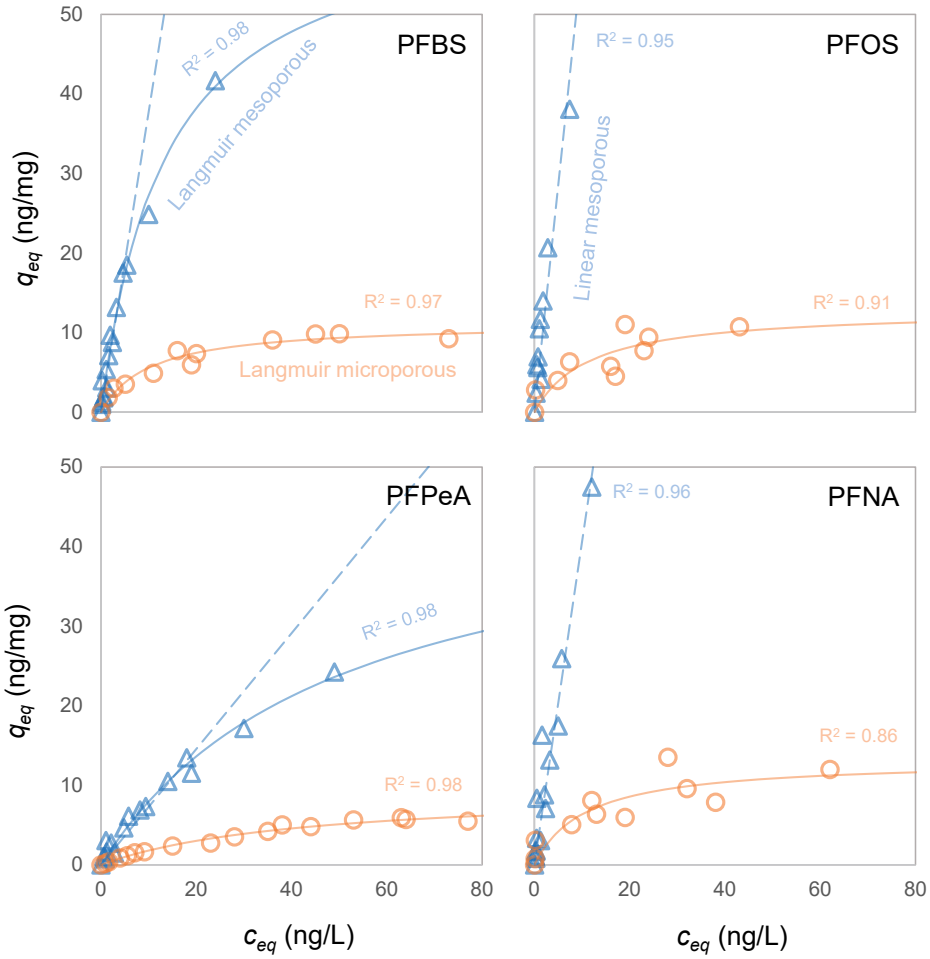


Figure 2.1. Experimental data for the adsorption of PFBS, PFOS, PFPeA and PFNA on two activated carbons, SRD (blue triangles) and CS (orange circles), described with Langmuir (full line) and linear (dashed line) isotherms.

Table 2.1. PFAS properties and estimated values of isotherm parameters for granular activated carbons used in this study

			PFBS	PFHxS	PFOS	PFDS	PFPeA	PFOA	PFNA	FOSA	GenX
PFAS properties	Chain length		4	6	8	10	4	8	9	8	5
	Functional group		SO_3^-	SO_3^-	SO_3^-	SO_3^-	COO^-	COO^-	COO^-	SO_2NH_2	COO^-
	Mw (g/mol)		299	399	499	599	264	414	464	499	329
	LogK_{ow} *1		1.82	3.16	4.49	6.83	3.01	4.81	5.48	5.8	4
	pK_a *1		-3.31	0.14	< 1.0	-3.24	0.34	< 4.2	-0.21	3.37	3.8
GAC	Isotherm	Parameter*2									
SRD (mesoporous)	Linear	a	3.77	4.54	5.07	8.23	0.73	3.86	4.06	10.72	1.21
	Langmuir	q_{max}	63.93	not available			47.67	not available		96.77	63.61
		K_L	0.074				0.020			0.137	0.024
	Freundlich	K_f	5.71	6.50	8.42	10.27	1.57	5.06	5.04	11.46	2.36
		n	0.63	0.86	0.76	0.84	0.70	0.87	0.90	0.75	0.70
CS (microporous)	Langmuir	q_{max}	11.23	11.30	12.93	7.09	9.48	10.35	13.19	16.07	8.27
		K_L	0.099	0.157	0.086	0.401	0.023	0.251	0.093	0.089	0.075
	Freundlich	K_f	1.92	3.48	2.70	1.34	0.47	3.10	2.60	2.46	1.29
		n	0.41	0.25	0.36	0.53	0.60	0.31	0.38	0.46	0.40

*1 For GenX information obtained from Vakili et al.[67], and for other PFAS from Gagliano et al.[13]
*2 units of parameters are: a (L/mg); q_{max} (ng/mg); K_L (L/ng); K_f (ng/mg)/(ng/L)$^{1/n}$; R^2 for estimated isotherms ranges from 0.86 – 0.99 and can be found in the Table S.2.8.

2.3.1.1. Comparison of 0.1 – 100 ng/L PFAS isotherm parameters with literature values

For mesoporous SRD, the adsorption data can be described with a linear isotherm (Figure 2.1), most likely, because of the high adsorption capacity. Consequently, for the low initial PFAS concentrations used in our experiments, the carbon surface was not nearing saturation, allowing the linear isotherm to accurately describe the data. For experiments at higher PFAS concentrations (0.1 mg/L and 1 mg/L) Langmuir maximum loadings were observed for SRD (see Section 2.3.3), similar to the findings of Ochoa-Herrera & Sierra-Alvarez[51], who reported results using mesoporous F400, a carbon with a comparable pore size distribution to SRD. Notably, Ochoa-Herrera & Sierra-Alvarez[51] conducted their experiments in the mg/L range. Additionally, a literature review conducted by Gagliano et al.[13] reported 12 studies where Langmuir adsorption isotherms were observed for GAC adsorption of PFAS at starting concentrations in the µg/L or mg/L range.

For microporous CS, the adsorption can be described with a Langmuir isotherm (Figure 2.1), and it is worth noting that the K_L and q_{max} values reported in this study for PFAS adsorption on GAC are significantly different from those reported in other studies that use Langmuir isotherms. In our study, K_L values range from 0.02 to 0.25 L/ng, while q_{max} values range from 8 to 97 ng/mg. High values of K_L and low values of q_{max} indicate a specific and localized adsorption. In contrast, Ochoa-Herrera & Sierra-Alvarez[51] reported K_L values ranging from

$3 \cdot 10^{-8}$ to $1.3 \cdot 10^{-7}$ L/ng and q_{max} values ranging from $99 \cdot 10^{3}$ to $2.36 \cdot 10^{5}$ ng/mg. Similarly, Inyang & Dickenson[86] reported K_L values ranging from $3.1 \cdot 10^{-7}$ to $5.2 \cdot 10^{-7}$ L/ng, and q_{max} ranging from $28 \cdot 10^{3}$ to $41 \cdot 10^{3}$ ng/mg, while Du et al.[87] reported K_L values ranging from $3.2 \cdot 10^{-4}$ to $1.6 \cdot 10^{-3}$ L/ng, and q_{max} values ranging from $18 \cdot 10^{3}$ to $4.26 \cdot 10^{5}$ ng/mg.

The significant discrepancies between our isotherm data and literature values can largely be attributed to the differing concentration ranges used in the experiments. Our study employed a lower PFAS concentration to carbon ratio than other studies, raising the question of which isotherm parameters are most practical and valuable for designing activated carbon filters, particularly in predicting breakthrough curves. To predict these breakthrough curves, diffusion coefficients are also required,[30,82] and these values vary significantly between high and low PFAS concentrations. These findings are discussed in detail in Section 2.3.3. For drinking water systems with PFAS concentrations <100 ng/L, as examined in this study, our isotherms are likely more relevant and practical. Conversely, for systems treating water with higher PFAS concentrations, such as industrial wastewaters, the isotherms reported in literature may be more applicable.

2.3.1.2. Impact of pore size distribution on 0.1 – 100 ng/L PFAS isotherm parameters

In the case of PFAS adsorption on mesoporous SRD, we have observed a linear relationship between the parameter *a* (L/mg) (also known as distribution coefficient, K_D[47]) of the linear isotherm and the number of fluorinated carbons present in the PFAS chain, as depicted in Figure 2.2. This correlation demonstrates that PFAS adsorption increases with chain length, indicating that longer-chain PFAS exhibit higher affinity for adsorption. Numerous studies have reported better adsorption of long-chain PFAS compared to short-chain PFAS,[52,73,88,89] attributing this observation to hydrophobic effects. These effects intensify with increasing chain length, leading to enhanced interaction between PFAS and the hydrophobic carbon surface. In addition to chain length, the functional group of PFAS also exhibits an influence on the adsorption on SRD. Figure 2.2 illustrates that PFAS compounds with sulfonic functional groups (PFSAs) demonstrate higher adsorption compared to those with carboxylic functional groups (PFCAs), for the same number of fluorinated carbons. The difference in adsorption between PFSAs and PFCA, consistently reported in literature,[13] is attributed to the larger and less soluble sulfonic group in PFSAs, compared to the carboxylic group in PFCAs, for the same number of fluorinated carbons. [90] Furthermore, Figure 2.2 shows that FOSA, which has the lowest water solubility of the studied PFAS, because of its uncharged sulphonamide head group,[91] exhibited the highest adsorption on SRD. A study by Sörengård et al.[73] on 44 adsorbents also observed a decreasing trend in adsorption as follows: FOSA > PFSAs > PFCAs.

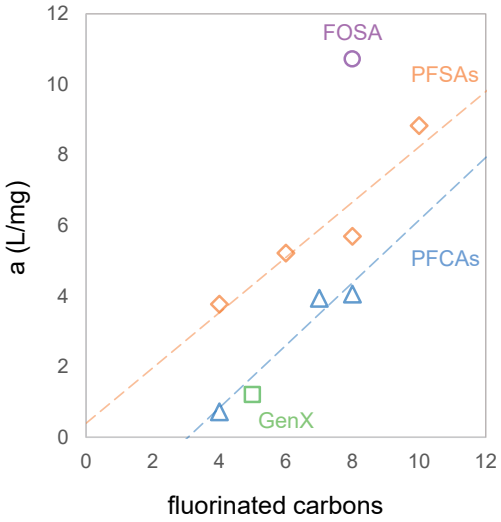


Figure 2.2. Relationship between the linear isotherm parameter *a* (L/mg) and the number of fluorinated carbons in the PFAS chain for adsorption on SRD activated carbon. The datapoints in the figure represent carboxylic PFAS (blue triangles), sulfonic PFAS (orange diamonds), GenX (green square), and FOSA (purple circle)

As discussed in the previous paragraph, we observed the influence of functional groups and carbon chain length on PFAS adsorption on mesoporous GAC at low ng/L concentrations, which is consistent with findings from existing studies at higher concentrations. Contrary to findings reported in literature, this correlation was not observed for microporous CS. The adsorption of PFAS on CS can be described using the Langmuir isotherm model (Figure 2.1). However, we did not observe a pronounced dependence of the Langmuir parameters on the specific properties of PFAS. This can be explained by the fact that long-chain PFAS, with the Stokes radius of ~ 0.4–0.6 nm,[92] cannot easily enter the micropores (< 1 nm radius) of GAC. Therefore, increasing the fluorinated carbon chain length does not necessarily enhance adsorption, contrary to observations for mesoporous SRD (Figure 2.2). Furthermore, nanobubbles have been suggested as a mechanism that may facilitate the transport of hydrophobic PFAS towards the carbon surface.[93] Since nanobubbles at the surface are typically 10 – 80 nm in height,[94] carbon materials with more mesopores could potentially accommodate a greater number of nanobubbles, thereby improving the adsorption process. At low PFAS concentrations, micropores in CS may pose a limiting factor for adsorption, whereas mesopores in SRD provide sufficient space, making PFAS characteristics more significant in determining the adsorption equilibrium.

Further evidence highlighting the crucial role of mesopores in PFAS adsorption in the ng/L range is based on comparing the Langmuir parameters between CS and SRD. The Langmuir parameter K_L, which represents the adsorbate's affinity for the adsorbent, shows comparable

values for PFBS, PFPeA, FOSA, and GenX, while the maximum adsorption capacity (q_{max}) is consistently higher for SRD compared to CS (see Table 2.1). This intriguing finding suggests, despite having similar affinities, SRD has a higher capacity to adsorb PFAS than CS. SRD's enhanced PFAS adsorption capacity is likely not due to electrostatic interactions, given the low concentration of acidic surface groups, and minimal positive charge at the experimental pH of ~ 7 for both GACs (see Table S.2.1). Instead it can be attributed to SRD's larger mesopore surface area (142 m^2/g for SRD vs 48 m^2/g for CS). Our findings are in agreement with previous studies demonstrating that mesoporous adsorbents exhibit better removal of larger PFAS molecules compared to microporous adsorbents.[56,85,87] Contrary to previous speculation that PFAS adsorption on GAC could be hindered by competition with organic matter or other PFAS, our study conducted in a 10 mM phosphate buffer matrix resembling the conductivity of drinking water (~800 µs/cm), demonstrate that, PFAS adsorption is inherently limited on microporous GAC, even in simplified matrices.

2.3.2. Kinetic experiments

Kinetic adsorption experiments were conducted using two types of GAC, namely mesoporous SRD and microporous CS, at two different GAC loadings (5 mg/L and 100 mg/L), with a mixture of 9 PFAS with initial concentration of ~ 70 – 100 ng/L. The kinetic data were described using diffusion models, which are detailed in Section 2.5. The kinetic data showed good agreement with the homogenous surface diffusion model (HSDM) and the pore diffusion model (PDM). For both models, fitting was performed with and without considering film diffusion, and the effect of film diffusion was negligible, see Section 2.5.7.1. Since linear isotherms were able to describe the adsorption on SRD, and the Langmuir isotherm was suitable for CS, their respective parameters were used as input for the diffusion models. The results obtained from the HSDM model are presented and discussed in Section 2.3.2.1. The results obtained from the PDM model are discussed in Section 2.5.7.2 as estimated values of pore diffusion coefficients were mostly found unrealistic.

2.3.2.1. Surface diffusion

The experimental kinetic data was analysed using the HSDM, with the surface diffusion coefficient, D_s, as fitting parameter. The data was described very well, and R^2 was in most cases higher than 0.93 as reported in Table S.2.14. Since for PFDS low values of R^2 were obtained, PFDS data is reported in S.I. but not discussed in manuscript. The results of the fitting procedure for PFPeA and PFNA is presented in Figure 2.3, while the other results are in Figures S.2.10, and S.2.11. The estimated values of D_s for all PFAS are reported in Table S.2.14.

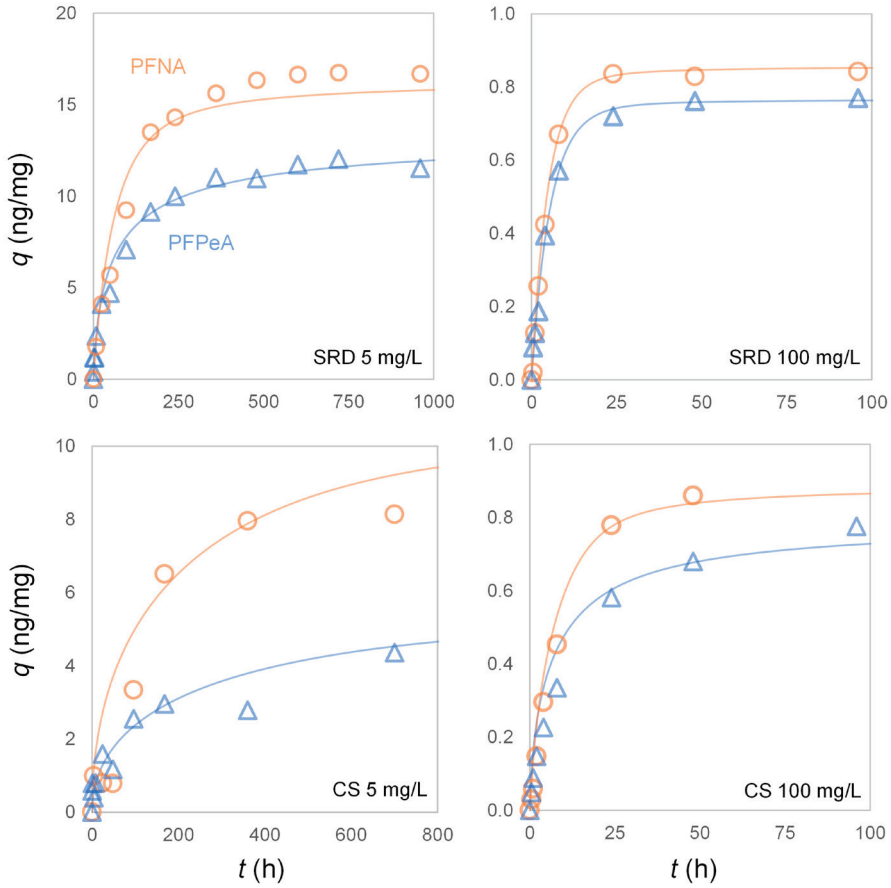


Figure 2.3. Adsorbate loading, q (ng/mg), of PFNA and PFPeA as a function of time for different loadings of mesoporous SRD (5 and 100 mg/L) and microporous CS (5 and 100 mg/L). Experimental data is represented by blue triangles for PFPeA and orange circles for PFNA. Theoretical predictions, based on the HSDM model, are depicted by solid lines, with blue indicating PFPeA, and orange PFNA.

The surface diffusion model describes the mechanism through which adsorbates, in their adsorbed state, are transported along the internal surface of adsorbent particles.[95] The diffusion process is governed by the surface diffusion coefficient, D_s, which is influenced by adsorption strength between the surface and adsorbent, concentration of adsorbate in adsorbed state, the temperature, and the molecular weight of the adsorbate.[30] As explained by Worch,[30] a higher adsorption strength leads to reduced adsorbate mobility, i.e., more strongly adsorbed molecules are less mobile. The adsorption strength can be characterized by the Freundlich coefficient, K_f, listed in Table 2.1. Higher K_f values correspond to stronger adsorption, which in turn leads to increased adsorbent loadings.[30]

Figure 2.4a highlights the significance of adsorption strength on diffusion. It is evident that, at a GAC loading of 5 mg/L, the values of D_s (surface mobility) for PFAS adsorption on CS are consistently higher than those for SRD. This observation indicates that CS exhibits faster PFAS surface mobility compared to SRD, which can be attributed to the lower adsorption strength of PFAS towards CS, as supported by the K_f values (Table 2.1), which are several times lower for CS compared to SRD. The only exception is that for a carbon loading of 100 mg/L, D_s of short-chain PFAS is higher for SRD than for CS (Figure 4b). This can be explained by the occurrence of pore diffusion in addition to surface diffusion. As discussed in Section 2.5.7.2 the pore diffusion model yielded realistic values for PFAS adsorption on SRD at a carbon loading of 100 mg/L, while it was not effective for other cases. The pore diffusion model is known to accurately describe the transport of hydrophilic compounds,[44] and short-chain PFAS are considered hydrophilic in nature.

The dependence of D_s on surface concentration can occur in the case of heterogenous adsorbents like AC that have adsorption sites of different energy.[30,95] During the adsorption process, there is a progressive filling of adsorption sites, beginning with those of higher energy and gradually moving to sites with lower energy.[96] Consequently, there is a decrease in adsorption energy, and an increase in adsorbate mobility as the concentration of adsorbed species increases.[97] From the results in this study, the dependence of D_s on surface adsorbent concentration follows from Figure 2.4, when comparing the values of D_s for 5 mg/L and 100 mg/L carbon loadings, for the same AC. For most cases in Figure 2.4, the surface diffusion coefficient is higher at a lower carbon loading, when the surface is more saturated with PFAS, i.e., when the surface interactions during intraparticle transport are considered to be weaker. Previous studies have demonstrated a relation between adsorption energy, surface adsorbent concentration, and adsorbent mobility, with higher D_s values observed when the surface is more saturated with adsorbent.[95–100] It is important to note that while the surface diffusion coefficient may be higher at lower carbon loadings, overall PFAS removal is still faster at higher carbon loadings due the greater total adsorption capacity of the activated carbon.

It has been observed that the molecular weight of adsorbates affects D_s with higher molecular weights resulting in lower D_s values.[30] From our results this trend is most clear in conditions with a lower PFAS surface saturation, as seen in Figure 2.4. For instance, the impact of chain length on D_s is significantly more pronounced for SRD, which is less saturated with PFAS, than for CS at a carbon loading of 100 mg/L. Conditions of lower saturation may facilitate increased hydrophobic effects between the carbon surface and PFAS, and consequently have a stronger impact on the diffusion of longer-chain PFAS compared to conditions of higher saturation (e.g., CS at 100 mg/L). Moreover, at a lower carbon loading of 5 mg/L, the dependency of D_s on PFAS chain length for adsorption on CS 5 mg/L is not evident (Figure 2.4a), likely due to the surface being fully saturated with PFAS, which minimizes PFAS-carbon interactions responsible for differentiation between long and short-chain PFAS.

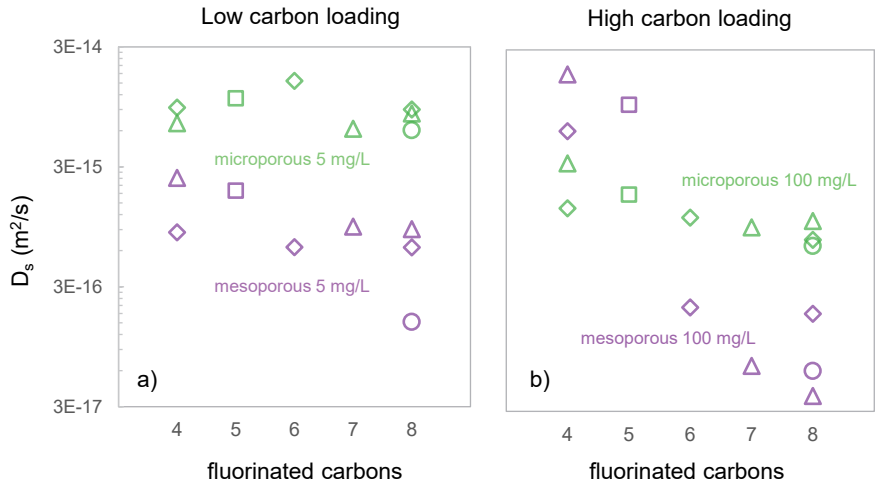


Figure 2.4. Comparison of the estimated values of D_s for mesoporous SRD and microporous CS at a carbon dosage of 5 mg/L (a) and 100 mg/L (b), as a function of the PFAS chain length. The datapoints in the figure represent carboxylic PFAS (triangles), sulfonic PFAS (diamonds), GenX (squares), and FOSA (circles)

To summarize this section, here D_s represents PFAS mobility on carbon surfaces, and is significantly influenced by interactions between PFAS molecules and the carbon material. Stronger interactions lead to a lower D_s. These interactions are more pronounced in mesoporous carbon compared to microporous carbon, as indicated by isotherm data, resulting in a lower D_s for mesoporous carbon. Additionally, higher saturation of the carbon surface with PFAS reduces these interactions, leading to an increase in D_s at lower carbon loadings. This observed behaviour, consistent with previous reports for other adsorbent/adsorbate systems,[30,95–100] supports the conclusion that PFAS are likely transported by the mechanism of surface diffusion, even at low ng/L concentrations.

The estimated values of D_s for PFAS in this study, ranging from 10^{-14} to 10^{-17} m^2/s, are considerably lower than the commonly reported D_s values in literature, which typically range from 10^{-11} m^2/s for small molecules to 10^{-15} m^2/s for large molecules.[30] A recent study by Dixit et al.[77] reported high D_s values of ~10^{-9} m^2/s for PFAS adsorption on ion exchange resin in demineralized water at starting concentrations of PFAS of ~ 10 µg/L. However, similar values of D_s to ours were obtained in a study by Burkhardt et al.,[82] by fitting isotherm parameters to model pilot-scale breakthrough curves. In our study and in Burkhardt et al., the lower values of D_s can probably by explained by the low PFAS concentrations in the ng/L range. The comparison with the study by Burkhardt et al.[82] suggests that our experimentally based isotherm parameters can be used to accurately compute D_s values that can effectively predict the breakthrough curves in Burkhardt et al.[82]

2.3.3. Impact of isotherms at higher concentration on predicting PFAS adsorption at environmentally relevant concentration

To evaluate the impact of isotherm parameters on the prediction of the surface diffusion coefficient (D_s), we obtained several isotherms for PFOA, at different initial concentrations, as shown in Figure 2.5. Interestingly, Figure 2.5 shows a strong dependence of the initial concentration on the amount of PFOA adsorbed (q_{eq}), at equivalent equilibrium concentrations (c_{eq}). For example, with microporous carbon at equilibrium concentrations between 10-20 ng/L, the adsorbed amount ranges from approximately 10 ng/L at a low initial PFOA concentration (~100 ng/L) to as much as 1000 ng/L at a higher initial concentration (~0.1 mg/L). This enhanced adsorption at higher starting concentrations could be attributed to multilayer adsorption involving PFAS aggregates, hemi-micelles or micelles.[54,85,101] Based on Figure 2.5, it is clear that much of the isotherm data reported for PFOA in the literature should be interpreted with caution, as it may not accurately reflect PFOA behaviour at concentrations below 100 ng/L.

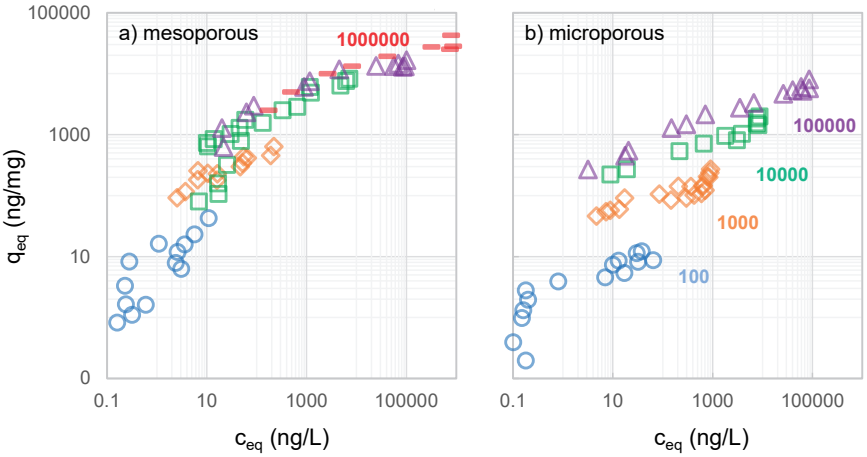


Figure 2.5. PFOA adsorption equilibrium experimental data for SRD a) and CS b) carbon obtained for multiple concentration ranges. c_0 ~ 100 ng/L (blue circles), c_0 ~ 1000 ng/L (orange diamonds), c_0 ~ 10 µg/L (green squares), c_0 ~ 100 µg/L (purple triangles) c_0 ~ 1000 µg/L (red dashes)

Several studies have conducted column experiments to investigate PFAS removal in the ng/L concentration range.[36,59,60] It would be valuable to describe the experimental data from those studies using a mechanistic column model that accounts for PFAS transport within the granule and adsorption.[30] To utilize such model isotherm parameters and diffusion coefficients obtained from this study are needed. Using isotherm parameters derived from high concentration experiments is an alternative, but these parameters fail to predict adsorption at low concentrations, as shown in Figure 2.5. Moreover, high concentration-derived parameters cannot accurately determine diffusion coefficients at lower concentrations, as shown in

Figure 2.6. In this analysis, Freundlich parameters obtained at varying initial concentrations of PFOA were used to characterize the dynamics of an experiment with an initial concentration of 100 ng/L. For example, when isotherm parameters derived from an experiment at 100 µg/L were applied to describe adsorption dynamics in the 100 ng/L range, the resulting calculated diffusion coefficient was over a factor of 1000 lower compared to using parameters determined within the 100 ng/L range. Thus, for accurate prediction in column experiments, it is essential to determine isotherm parameters and diffusion coefficients within the same concentration range as the experiment.

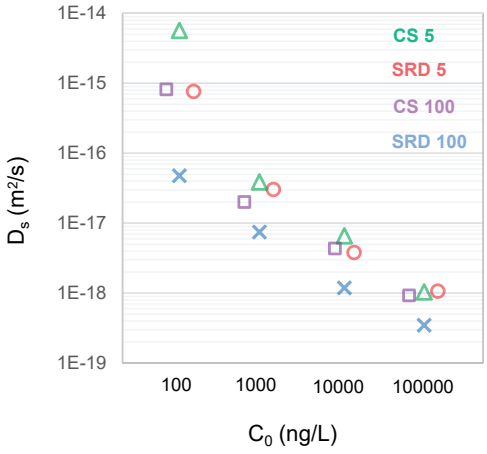


Figure 2.6. Comparison of the estimated values of D_s (m^2/s) for mesoporous SRD and microporous CS at a carbon dosage of 5 mg/L and 100 mg/L for starting concentrations for which Freundlich isotherms were obtained and used to predict D_s

2.4. Conclusion

We investigated the adsorption of nine distinct PFAS molecules at environmentally relevant concentrations of 0.1 – 100 ng/L onto two activated carbons with different pore size distributions. PFAS adsorption on microporous carbon exhibited saturation and was well described by the Langmuir isotherm, while adsorption on mesoporous carbon did not reach saturation and was better characterized by a linear isotherm. The unexpected saturation in microporous carbon at low PFAS concentrations suggests that micropores may play a less significant role in adsorbing both short- and long-chain PFAS compared to mesopores. When we compared our isotherm parameters with those reported in literature, we found that the Langmuir isotherm's maximum adsorption capacities were several orders of magnitude lower than previously reported. Our study focused on the low ng/L concentration range, whereas other studies were conducted at µg/L and mg/L levels. This discrepancy suggests that different PFAS adsorption mechanisms may operate at different concentrations, which requires further investigation. This hypothesis is further supported by our PFOA isotherm obtained at higher concentrations which showed a dependency on initial concentrations. Our findings also indicate that widely available adsorption data from high-concentration studies should be interpreted with caution, as our PFOA isotherms at high concentrations failed to accurately predict adsorption and kinetic behaviour at much lower concentrations of 0.1 – 100 ng/L.

To describe the intraparticle transport of PFAS, we coupled the estimated isotherms with surface and pore diffusion models. The experiments were conducted with both carbons at carbon dosages of 5 mg/L and 100 mg/L. Higher values of the surface diffusion coefficients (surface mobility) were observed for lower carbon loading when the surface was more saturated with PFAS, and when interactions between PFAS and carbon are expected to be weaker. Additionally, PFAS surface mobility in the more microporous carbon with lower adsorption capacity (higher PFAS surface saturation) were higher than in the more mesoporous carbon with higher adsorption capacity (lower PFAS surface saturation). These findings indicate that PFAS intraparticle mobility is a function of interactions between PFAS and carbon surface, where mobility decreases as the number or strength of interactions increases. Overall, the obtained PFAS surface diffusion coefficients in this study are lower compared to the literature. Low values of the PFAS surface diffusion coefficients, which become more hindered with increase in number of active sites for adsorption, might be an inherent limit of heterogenous adsorbents like activated carbon, and deserve further investigation.

2.5. Supplementary information for Chapter 2

2.5.1. Activated carbon characterization

Results of activated carbons characterization for mesoporous (SRD) and microporous (CS) activated carbon are summarized in Table S.2.1. The descriptions of the characterization methods are in Sections 2.5.1.1 – 2.5.1.4.

Table S.2.1. Textural and surface charge properties of activated carbons used in this study

Method	Activated carbon	CS	SRD
N_2 physisorption	Micropore surface area (m^2/g_{GAC})	1248	822
	Mesopore surface area (m^2/g_{GAC})	48	142
	Micropore volume (cm^3/g_{GAC})	0.51	0.36
	Mesopore volume (cm^3/g_{GAC})	0.04	0.23
Water Pycnometry	Particle porosity (%)	47	58
Boehm Titration	pKa* (phenols) ~ 10-13 (μmol/g_{GAC})	1.25	0.19
	pKa (lactons and lactols) ~ 6-10 (μmol/g_{GAC})	1.62	0.15
	pKa (carboxylic acids) ~ 3-6 (μmol/g_{GAC})	10.55	10.12
	pKa (total acidity) ~ 3-13 (μmol/g_{GAC})	13.42	10.47
pH drift	pH_{PZC}	8.8	8.0

* pKa values of functional groups on the surface of GAC

2.5.1.1. Textural properties

Several textural properties were determined for SRD activated carbon by measuring N_2 adsorption-desorption isotherms at 77K on Micrometrics Tristar 3000. From the isotherms, the carbon surface area was determined by the BET method, the micropore surface area and volume were determined with the T-plot method, and the mesopore surface area, volume and mesopore pore size distribution with the BJH method. To show that SRD has similar pore size distribution as F400, the pore characterization of F400 was also performed, and similar properties were found (Figure S.1). For CS, the pore characterization was reported in Piai et al.[44], for which the same equipment and data analysis methods were used. The mesopore pore size distribution for the tested GACs is presented in Figure S.2.1.

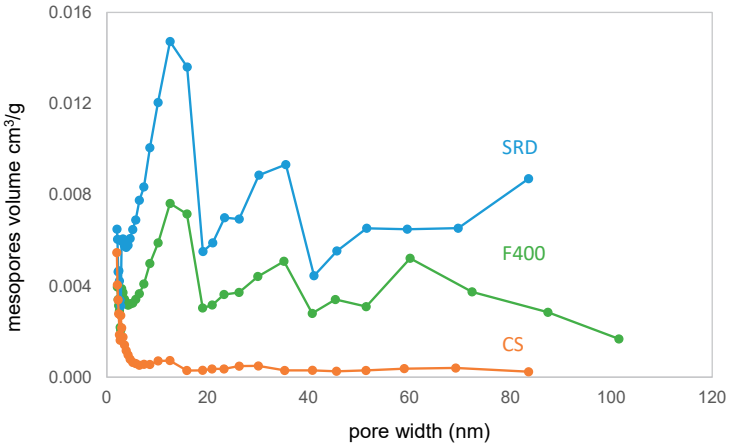


Figure S.2.1. Mesopores pore size distribution for SRD (blue marks), F400 (green marks) and CS (orange marks) obtained by BJH method

2.5.1.2. Activated carbon density measurements

The granular activated carbon (GAC) skeletal (material) and particle (apparent) densities were measured with the pycnometer with water as pycnometer liquid, as described in detail in Sontheimer et al.[31] With this method only the pores that are accessible to water are considered in density measurements. Around 3 g of dry GAC was weighted and submerged in water, which was then boiled to ensure complete wetting of GAC. The wet GAC was removed from boiling water and rolled on cellulose tissues to remove the excess water, i.e., water that is present on the external surface of the particles. The mass of the GAC particles with water-filled pores was measured in a pre-weighted pycnometer. After that, the pycnometer was filled with water and weighted again. From the obtained mass, and known pycnometer volume, the material and particle density were calculated according to equations reported in Sontheimer et al.[31] The particle porosity was calculated using the following equation:

$$\varepsilon_p = 1 - \frac{\rho_p}{\rho_m} \tag{S.2.1}$$

where ε_p (dimensionless) is particle porosity, ρ_P (g/L) is particle density and ρ_m (g/L).is material density. Calculated porosities are shown in Table S.2.1.

2.5.1.3. Boehm titration

Accurate quantification of acidic oxygen-containing groups on carbon surfaces was obtained following the protocol for indirect Boehm titration described by Schonher et al.[102]. The amounts of carboxylic, phenolic, and lactonic surface groups were determined, and the total acidity, defined as the summation of the aforementioned concentrations, was calculated. In short, the following protocol was used. Around 1.05 g of dry carbon was weighted and equilibrated with 50 ml of 0.01 N NaOH, NaHCO3, or Na_2HCO_3 for 5 days. After that, aliquots of 10 ml were taken, and to each 20 ml of 0.01 N HCl was added, which was then titrated with $NaHCO_3$ using a titrator. From the required volume to reach the titration equilibrium point, the amount of a certain oxygen group (mmol/g_{GAC}) was calculated with equations reported in Schonher et al[102]. Experiments were conducted in triplicates, and 4 aliquots of each sample were taken and titrated to calculate the standard deviation. Titrations were performed on an 888 Titrando (Metrohm) automatic titrator. Results are shown in Table S.2.1.

2.5.1.4. pH drift method

The pH drift method was used to determine the pH point (pH_{PZC}) at which the carbon surface contains equal amounts of positively and negatively charged functional groups, i.e., the surface is nett charge neutral.[47] With this method, activated carbons were equilibrated with NaCl solutions at different starting pH. Because of the protonation and deprotonation of activated carbon functional groups, the pH of the solution will change, and, in equilibrium it will be constant. Experiments were performed in glass bottles containing 0.5 L of 0.01 M NaCl. The starting pH was adjusted with the addition of HCl or NaOH to be between 2-11. After adjustment, around 1.0 g of GAC was added, and the system was stirred on a magnetic stirrer for 48 h. After 48 h the system was in equilibrium, and longer experiments showed no significant change in the final pH. During each step of the experiment, the NaCl solution was sparged with N_2 to remove the impact of CO_2 on the solution pH. The pH_{PZC} was obtained by plotting the initial vs final pH, and the resulting graph is shown in Figure S.2.2. The point where initial vs final pH curve crosses y = x line is the pH_{PZC}. For the pH below the $pH_{PZC,}$ the surface is positively charged, and negatively charged beyond.

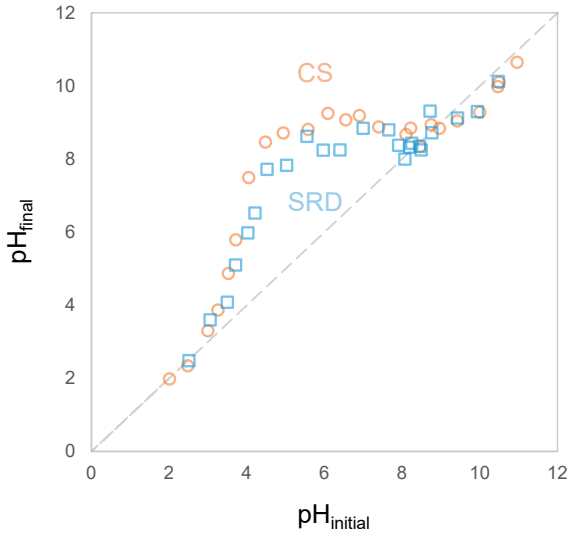


Figure S.2.2. Final vs. initial pH obtained from pH drift method for CS (orange circles) and SRD (blue squares) granular activated carbon.

2.5.2. PFOA isotherm experiments at starting concentration 1-1000 µg/L

Experiments to determine PFOA isotherms at elevated starting concentrations were conducted similarly to those described in the manuscript, which used a starting concentration of 100 ng/L. However, there were several differences: the PFAS mixture did not include PFDS due to its limited availability in large quantities; a 0.5L PPCO bottle was used instead of a 1L bottle; and samples were collected by taking approximately 3 ml of solution, filtering it, transferring it to 2 ml Eppendorf tubes, and immediately freezing it. Repeated freezing and thawing cycles did not significantly affect the PFOA concentrations.

For the mesoporous SRD activated carbon, experiments were conducted at starting concentrations of 1, 10, 100, and 1000 µg/L. For the microporous CS activated carbon, concentrations of 1, 10, and 100 µg/L were used. Isotherm data were obtained for eight PFAS compounds, but detailed analysis focused solely on PFOA, as investigations into the other compounds are planned for future work.

2.5.3. Measuring PFAS concentrations

2.5.3.1. Concentration range of 0.1 – 100 ng/L

The PFAS sample analysis was performed at AquaLab Zuid B.V. (The Netherlands). Samples of 350 ml were provided from which an aliquot was taken and diluted in a 1:1 ratio with methanol. Labelled compounds were added as internal standards, as well as HCl to acidify the mixture. Then, 100 µl of the mixture was injected into the Xevo TQ-XS LCMS system

(Waters Corporation, USA) with the Acquity UPLC CSH Pheynl-Hexyl column (Waters Corporation, USA) at 45 °C, and Acquity UPLC HSS T3 VanGuard as a pre-column (Waters Corporation, USA). The mobile phases were (A) 2 mM ammonium acetate in a mixture of Mili-Q / methanol (95% / 5%) and (B) 2 mM ammonium acetate in a mixture of Methanol / Acetonitrile (80% / 20%). UniSpray (Waters Corporation, USA) was used as an ionization source. The information about the MS parameters and the gradient can be found in Tables S.2.2, and S.2.3. The lower quantification limit of monitored PFAS was between 0.1 – 0.5 ng/L depending on the PFAS and are found in Table S.4. The upper quantification limit was 20 ng/l, and samples were diluted with Mili-Q water when necessary. Each analysing sequence consisted of measuring calibration lines with the calibration standards between 0 and 20 ng/l. A control standard of 10 ng/L was injected at the beginning, end, and after every ten samples. In the quality control, correlation coefficients for all analytes were greater than 99%.

Table S.2.2. Values of the LC-MS/MS parameters

Mass spectrometer parameter	Value
Source temperature	100 C
Capilar Voltage	1.0 kV
Desolvation temperature	300 C
Desolvation gasflow	1100 L/hr
Cone gasflow	150 L/hr
Nebuliser pressure	7 bar

Table S.2.3. LC-MS/MS method for the PFAS detection

Time (min)	Flow (ml/min)	Mobile phase A (%)	Mobile phase B (%)	Curve
0	0.3	100	0	Initial
0.50	0.3	100	0	6
2.50	0.3	60	40	6
9.50	0.3	10	90	7
15.00	0.3	0	100	1
16.50	0.3	100	0	1

Table S.2.4. Lower quantification limits (LOQ) for the studied PFAS

PFAS	LOQ (ng/L)
PFBS	0.5
PFHxS	0.2
PFOS	0.2
PFDS	0.2
PFPA	0.5
PFOA	0.1
PFNA	0.2
FOSA	0.5
GenX	0.1

2.5.3.2. Detection of PFOA at higher concentrations

The PFOA measurement was performed by an ultra-high performance liquid chromatograph (ExionLC AD-30 System) equipped with a tandem mass spectrometer (Triple Quad™ 5500$_+$ System) from SCIEX. The separation of PFOA was performed using a C18 based analytical column and water and acetonitrile based eluents, both buffered with ammonium acetate and acetic acid. In order to prevent contamination of PFAS-like components from machine parts, two precautions were implemented:

1. All tubing and valves have been replaced with PFAS-free alternatives;
2. Between the UHPLC pump and the autosampler, a so called "delay column" (Luna® 5 µm C18(2) 100 Å, LC Column 30 x 2 mm) was installed, so that any peak originated from possible PFAS leaching, was chromatographically separated from the peak used for quantification.

The Triple Quad™ 5500+ worked in negative ionisation mode, achieved by Electro Spray Ionisation (ESI) and detection of the target fragments took place by High Energy Dynode (HED). The specific MS parameters can be found in Table S.2.5.

PFOA was quantified with a calibration curve in the range of 10 to 1000 ng/l and processed with SCIEX OS 2.0 software. Two control standards at respectively 1 and 5 ng/l were measured in each run to check the performances of the system at lower concentrations. Prior to analysis, each sample was prepared by filtration through a 1 µm glass fibre filters (Glass Filter Acrodisc Syringe Filter, 25 mm, 1.0 µm, from WATERS), previously tested for not adsorbing PFOA. The filtered water samples were diluted when necessary and then mixed with methanol in a ratio 95% H_2O – 5% methanol, to reduce sorption phenomena within the analysis vials or UHPLC parts. Internal standards were also added and used to correct for ionisation enhancement or suppression. While in the manuscript only PFOA was discussed, the detection method was also developed for some other PFAS. The complete list of MS parameters for PFAS and their respective internal standards can be found in the Table S.2.5.

The LOQ for PFOA of 2.5 ng/L was determined by injecting a PFOA standard at 0.5 ng/L and obtaining RSD <30% and 50% < recovery < 150%.

2.5.3.2.a Additional information on LC method

The ExionLC AD-30, configurated as a low pressure gradient system, used eluent C (UPLC-MS quality water buffered with 2.5 mM ammonium acetate and 2.5 mM of acetic acid) and eluent D (95% in volume of UPLC-MS quality acetonitrile with 5% UPLC-MS quality water, buffered in exact same way as eluent C) to apply the following gradient, where T_0 is considered the time of injection:

a) T_0 – 1 min. constant at 95% C 5% D;
b) 1 – 14 min linear to 100% D;
c) 14 – 16 min 100% D is kept;
d) 16 – 16.1 min linear to the initial condition (95% C, 5% D);
e) 16.1 – 20 min the same condition is kept constant in order to stabilize the system for the following run.

The flow and the temperature of the column oven were kept constant respectively at 0.3 ml/min and 30°C. The used analytical column is a Phenomenex Kinetex 2.6 µm EVO C18 100 Ä, 150 mm; the guard column SecurityGuard™ ULTRA UHPLC C18 2.1mm ID from Phenomenex was used to delay the deterioration of the stationary phase. The autosampler temperature was kept at 5°C to prevent sample degradation; injection volume was 10 µl.

2.5.3.2.b Additional information on MS method

The Triple Quad™ 5500+ system was operated in scheduled mass reaction monitoring mode (S-MRM): in this mode, specific transitions are monitored only at the retention times in which the related target components are expected: this is done to keep the dwell time (directly linked to the sensitivity of the system) as high as possible, without compromising too much with the number of points per peak. The negative ionisation mode was used during the whole run with an ion spray voltage of -4500 V and a temperature of 350 °C.

In Table S.2.5 all component specific parameters are listed; here follows a short description of each parameter.

Target ion (m/z):	mass over charge ratio of ion formed after ionisation of the target molecule;
Fragment ion (m/z):	mass over charge ratio of ion formed after fragmentation in the collision cell;
De-clustering potential (DP):	voltage applied at the orifice to minimize solvent cluster;
Entrance Potential (EP):	voltage difference between the so called Q_0 region and the ground, to focus ions in the first quadrupole;

Collision Energy (CE): voltage difference between Q_0 region and the collision cell, to accelerate the ions against the collision gas for fragmentation;

Collision gas exit potential (CXP): voltage applied to guide the fragmented ions in the last quadrupole (Q_3).

Collision activated Gas (CAD): pressure of the gas in the collision cell for ion fragmentation: this is set constant at 9 psi for all the transitions.

Retention Time (RT): centre of a 30 second time window in which the specific transition was monitored, and the retention time of the target component, expected.

Table S.2.5. MS parameters for PFAS components

Component	Target ion (m/z)	Fragment ion (m/z)	DP (V)	EP (V)	CE (V)	CXP (V)	RT
PFBS 01	298.9	79.9	-90	-10	-60	-10	8.48
PFBS 02	298.9	98.9	-90	-10	-39	-12.5	8.48
PFBS D3	301.8	98.9	-90	-10	-39	-13	8.46
PFHxS 01	389.9	80	-110	-10	-72.5	-12.5	9.87
PFHxS 02	389.9	98.9	-110	-10	-85	-12.5	9.87
PFHxS D3	401.8	79.9	-125	-10	-92	-9	9.86
PFOS 01	498.9	80	-80	-5	-80	-15	10.95
PFOS 02	498.9	80	-80	-5	-120	-10	10.95
PFOS D4	502.8	80	-75	-10	-120	-9	10.94
PFOA 01	412.9	169	-30	-5	-25	-15	9.67
PFOA 02	412.9	369.1	-30	-5	-15	-18	9.67
PFOA D4	416.9	371.9	-40	-15	-24	-19	9.66
PFNA 01	462.9	419.1	-75	-10	-15	-19	10.23
PFNA 02	462.9	169	-75	-10	-27	-15	10.23
PFNA D5	468	423	-75	-10	-15	-19	10.22
PFPeA 01	262.9	219	-30	-10	-12	-17.5	7.48
PFPeA 02	262.9	262.9	-30	-10	-5	-15	7.48
PFPeA D5	267.9	22.9	-45	-10	-12	-29	7.47
GenX 01	328.9	169.1	-5	-10	-18	-13	8.63
GenX 02	328.9	285	-5	-10	-9	-20	8.63
GenX D3	332.1	286.9	-25	-10	-10	-25	8.62
PFOSA 01	498	78.1	-120	-3.5	-85	-12	13.17
PFOSA 02	498	169	-120	-3.5	-37.5	-20	13.17
PFOSA D8	506	78.1	-120	-3.5	-85	-12	13.16

For each component, two fragments are monitored: the first used for quantification and the second for confirmation through the evaluation of the ion ratio.

The concentrations of the components for which in Table S.2.5 a deuterated internal standard is available, have been corrected for internal standard response. Each internal standard was present both in calibration standards and in samples at the concentration of 500 ng/l. As response factors in the calibration line, the ratio between the response of the target component and the one of the respective deuterated internal standard is used, instead of the response of the target component only. This allows to minimize the effect of matrix on quantification (so called ion suppression or ion enhancement).

2.5.4. Kinetic concentration data for experimental blank at low ng/L

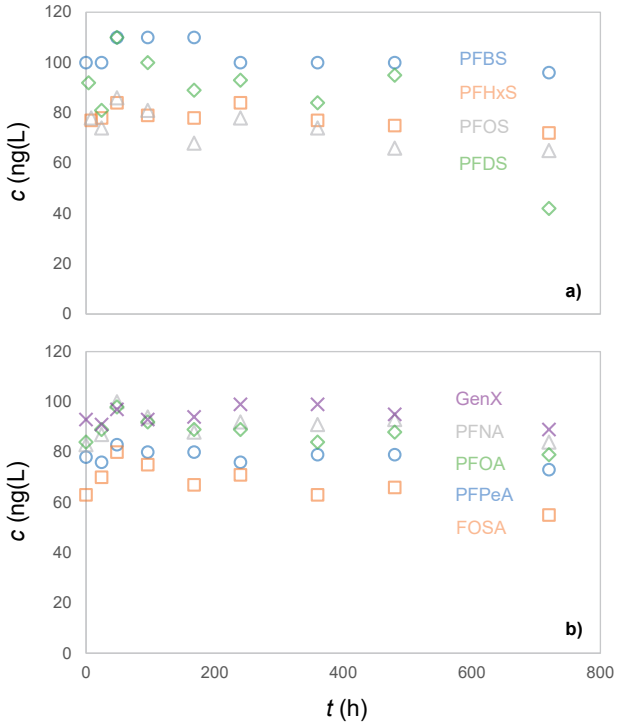


Figure S.2.3. Change of concentration over time for the experimental blank without activated carbon. a) Concentrations of PFBS (blue circles), PFHxS (orange square), PFOS (grey triangles) and PFDS (green diamonds). b) Concentrations of GenX (purple x), PFNA (grey triangles), PFOA (green diamonds), PFPeA (blue circles) and FOSA (orange squares)

2.5.5. Diffusion models

2.5.5.1. Pore and surface diffusion model

During adsorption, intraparticle mass transport can be explained by two distinct mechanisms, with one mechanism typically prevailing over the other. One mechanism is pore diffusion, which involves the movement of the adsorbate through the liquid within the adsorbent pores. The other mechanism is surface diffusion, which pertains to the transport of the adsorbate along the internal surface of the adsorbent particle. In this study, we consider both transport mechanisms and employ a mechanistic intraparticle transport model known as the pore and surface diffusion model (PSDM). The PSDM model has been extensively documented in the literature.[30,80,103]

The governing equation of the PSDM model is

$$\varepsilon_p \frac{\partial c_p}{\partial t} + \rho_p \frac{\partial q_p}{\partial t} = \frac{1}{r^2} \frac{\partial}{\partial r} \left(r^2 \left(D_p \frac{\partial c_p}{\partial r} + \rho_p D_s \frac{\partial q_p}{\partial r} \right) \right) \quad \text{(S.2.2)}$$

where ε_p (dimensionless) is the particle porosity, c_p (ng/L) is the adsorbate concentration inside the particle pores, t (s) is the time, ρ_p (g/L) is the particle apparent density, q_p (ng/mg) is the amount of molecules adsorbed per mass of adsorbent, i.e. adsorbent loading, r (m) is the radiant coordinate, D_p (m^2/s) is the pore diffusion coefficient, and D_s (m^2/s) is the surface diffusion coefficient. The initial and boundary conditions, assumptions of the model, and the solving method can be found in the Section 2.5.5.2.

In our study, we use two simplified models, namely the homogeneous surface diffusion model (HSDM) and the pore diffusion model (PDM), to describe the dynamics of PFAS adsorption. These models are derived from the PSDM by considering only one transport mechanism.[104] We employed both HSDM and PDM to determine the most suitable parameter values for describing the data, and we discuss the rationality of these values.

For both models, an adsorption isotherm is required. When surface diffusion dominates ($D_s \neq 0$, $D_p = 0$), the adsorption isotherm relates the adsorbent loading on position $r = r_p$ to the concentration in solution at the solution – adsorbent interface. When pore diffusion dominates ($D_s = 0$, $D_p \neq 0$), we assume local equilibrium between the concentration in the pore liquid and the adsorbent loading at each position within the pores. The adsorption equilibrium in our study was characterized using the isotherms presented in Table S.2.7. The isotherm fitting procedure is explained in the Section 2.5.5.3.

2.5.5.2. Assumptions, initial and boundary conditions

In our study we employ homogenous surface diffusion model (HSDM) and pore diffusion model (PDM) to describe the experimental kinetic data for adsorption of PFAS on activated carbon. These two models are derived from pore and surface diffusion model (PSDM) by

considering only one transport mechanism. The PSDM, and consequently HSDM and PDM, are based on the following assumptions: (1) the adsorbent particle is spherical, rigid, homogenous, and isotropic; (2) the distribution of adsorption sites is homogenous; (3) the bulk solution is well-mixed; (4) adsorption onto the active site occurs rapidly compared to other processes; and (5) convective mass transport is negligible in comparison to diffusion.

The initial conditions of diffusion models are

$$q = 0,\ c_p = 0 \text{ at } t = 0,\ 0 \le r \le r_p \tag{S.2.3}$$

$$c_l = c_0 \text{ at } t = 0 \tag{S.2.4}$$

where c_l (ng/L) is the concentration of adsorbate in the bulk, c_0 (ng/L) is the initial concentration of adsorbate in the bulk, and r_p (m) is the radius of the particle, for which the arithmetic average of particle size distribution is taken. The PSDM has two boundary conditions that are defined for the radial coordinate. The first boundary condition is for the outer edge of the particle, where $r = r_p$, and where we can either consider or neglect film diffusion. If we consider film diffusion, we use

$$D_p \frac{\partial c_p}{\partial r} + \rho_p D_s \frac{\partial q_p}{\partial r} = k_F \left(c_l - c_s \right) \tag{S.2.5}$$

where k_F is the film diffusion coefficient (m/s) and c_S is the concentration of adsorbate on the external particle surface. If we neglect film diffusion, we use

$$D_p \frac{\partial c_p}{\partial r} + \rho_p D_s \frac{\partial q_p}{\partial r} = -\frac{\varepsilon_b}{a_{vr}} \frac{\partial c}{\partial t} \tag{S.2.6}$$

where ε_p (dimensionless) is bulk porosity and a_{vr} (m^2) is the external surface area of particle related to the reactor volume. The second boundary condition is defined for the core of the particle where we assume that the flux of adsorbate is zero, which is given by

$$\frac{\partial q_p}{\partial r} = 0,\ \frac{\partial c_p}{\partial r} = 0 \text{ at } t > 0,\ r = 0 \tag{S.2.7}$$

The boundary conditions for HSDM and PDM can easily be derived from equations S.2.4 and S.2.5 by assuming that $D_p = 0$ (for HSDM) or $D_s = 0$ (for PDM).

2.5.5.3. Solving method

To solve diffusion models, we considered a mass balance for a batch system that relates the total amount of adsorbent in the system to the concentrations in the different phases, i.e., the bulk, pores and carbon surface, given by

$$m_{total} = \varepsilon_b v_r c_l + (1 - \varepsilon_b)\, v_r \left(\rho_p \overline{q} + \varepsilon_p \overline{c}_p \right) \tag{S.2.8}$$

where m_{total} (ng) is the total amount of adsorbent in the batch system, ε_b (dimensionless) is the bulk porosity, which is defined as the volume of liquid in the system over the reactor volume, v_r (L). Variable $\overline{q}$ is the average adsorbent loading and $\overline{c}_p$ is the average pore concentration.

The following steps were taken to describe our experimental adsorption kinetic data with intraparticle diffusion models:

- By assuming that surface diffusion coefficient, $Ds \neq 0$, and pore diffusion coefficient, $Dp = 0$, the pore and surface diffusion model (PSDM) represented by Eq. S2 was simplified to the homogeneous surface diffusion model (HSDM), or by assuming that $D_S = 0$, and $D_P \neq 0$, the PSDM model was simplified to the pore diffusion model (PDM)
- A numerical Runge-Kutta method was applied to solve the system of differential and algebraic equations over time for both models, using MATLAB code. The fitting parameter was D_s or D_p, and the fitting procedure is described in Section 2.5.5.4.
- The Method of Lines was used to discretize the mass balance equation (Eq. S.2.7). Average adsorbent loading, $\bar{q}$, and average pore concentration, $\bar{c}_{p,}$ were calculated from the mass balance.
- For the evaluation of film diffusion, the values of D_s or D_p were kept constant as determined without considering film diffusion, after which k_F was used as a fitting parameter. Impact of film diffusion on intraparticle diffusion and fitting results is discussed in Section 2.5.7.1.

The values of parameters used as input to solve HSDM and PDM are given in the Table S.2.6. The method to estimate the porosities and particle density is explained in Section 2.5.1.2.

Table S.2.6. Parameters used to solve the HSDM and PDM

Parameter	CS		SRD	
	5 mg	100 mg	5 mg	100 mg
ε_b (-)	$5.78 \cdot 10^{-6}$	$1.16 \cdot 10^{-4}$	$6.74 \cdot 10^{-6}$	$1.35 \cdot 10^{-4}$
ρ_p (g/L)	878		753	
ε_p (-)	0.464		0.575	
r_p (m)	$3.625 \cdot 10^{-4}$		$3.625 \cdot 10^{-4}$	
v_r (L)	0.985		0.985	

2.5.5.4. Fitting procedure

In this study, we determined the isotherm parameters (Section 2.3.1) and diffusion coefficients (Section 2.3.2) for the adsorption of 9 PFAS on two activated carbons. We fitted several isotherm models, including Freundlich, Langmuir, and linear to the experimental data of PFAS adsorption. Additionally, we applied a surface diffusion model to the kinetic adsorption data to estimate the diffusion coefficients.

A common approach to fitting theoretical models to experimental data is maximizing the coefficient of determination ('the R^2-value'). R^2 often used as a measure of the model's goodness-of-fit, and is calculated as follows

$$R^2 = 1 - \frac{\sum_i (y_i - f_i)^2}{\sum_i (y_i - \overline{y})^2} \tag{S.2.9}$$

where y_i is the measured value of a datapoint, f_i is the corresponding theoretical value, and $\overline{y}$ is the mean of y over all datapoints.

We demonstrate that R^2 is not a reliable metric for assessing goodness-of-fit. Additionally, we propose an alternative metric that yields a significantly better fit. In Figure S.2.4, we compare two theoretical descriptions of experimental adsorption data, each with a different value of the surface diffusion coefficient, D_s. In Figure S.2.4a, the theory is fitted using our own procedure, resulting in R^2=0.9884. In Figure S.2.4b, the theory is fitted by maximizing R^2, resulting in R^2=0.9940. Although the theoretical description in Figure S.2.4a appears to be a better fit, its R^2 value is lower.

In our own fitting procedure, we calculate the error between the data and theory and multiple this error by a weighing factor based on the domain in which each datapoint is considered relevant. For all datapoints, except for the first and last, the weighing factor for each datapoint i is calculated as follows

$$W_i = \frac{1/2(x_{i+1} - x_{i-1})}{x_{max} - x_{min}} \tag{S.2.10}$$

where x is the value of the independent variable, and "max" refers to the maximum value of x among the datapoints, and "min" to the minimum. For the first datapoint (at x_{min}) W is calculated using Eq. S.2.10, with x_{i-1} replaced by x_i. For the last datapoint (at x_{max}), W is calculated by replacing x_{i+1} with x_i.

In this fitting procedure, we minimize the total error, defined as

$$error = \sum_i W_i \, |y_i - f_i| \tag{S.2.11}$$

Figure S.2.4 clearly demonstrates that fitting based on Eq. S.2.9 and S.2.10 (a) provides a much better visual fit compared to fitting by maximizing R^2 (b). This discrepancy arises because the early hours of the experiment have relatively more data points, while the latter part has fewer, leading to an overemphasis on the first part in the fitting process.

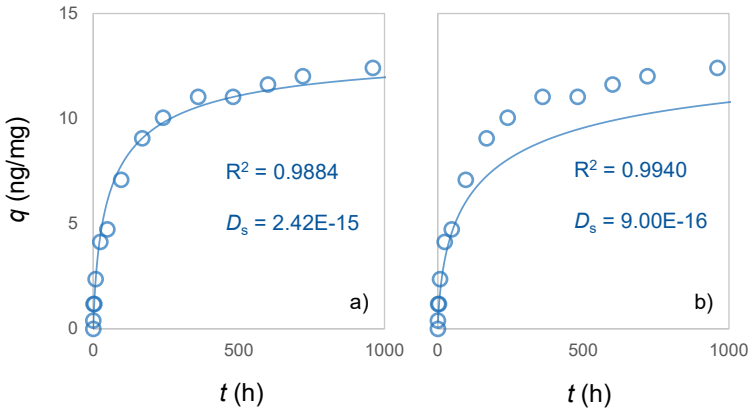


Figure S.2.4. Experimental data for PFPeA adsorption on mesoporous SRD activated carbon as function of time. The data is described using the surface diffusion model (discussed in Section 2.5.5), with the surface diffusion coefficient D_s determined by fitting the theory. a) Fitting is performed using our custom algorithm (Eq. S.2.10 and S.2.11), resulting in a lower R^2 value but a visually better fit. b) Fitting is performed by maximizing R^2, resulting in a higher R^2 but a visually poorer fit.

2.5.6. PFAS isotherms

In order to estimate the parameters associated with the Linear, Langmuir, and Freundlich isotherm models (Table S.2.7) from adsorption equilibrium data, we employed a MATLAB code based on non-linear regression. The fitting results of the isotherm parameters were evaluated using a least square fit statistical analysis. The experimental data is given in Tables S.2.9, and S.2.10, and fitted curves are presented in the Figures S.2.5, and S.2.6. The estimated isotherm parameters are reported in the Table 2.1, and Table S.2.8.

Table S.2.7. Isotherms used in this study

Isotherm	Equation	Parameters
Linear	$q_{eq} = ac_{l,eq}$	a – linear slope [L/mg]
Langmuir	$q_{eq} = \frac{q_{max}K_L c_{l,eq}}{1+K_L c_{l,eq}}$	q_{max} – maximum adsorption capacity [ng/mg] K_L – Langmuir constant [L/ng]
Freundlich	$q_{eq} = K_f {c_{l,eq}}^n$	K_f – adsorption coefficient (ng/mg)/(ng/L)^n n – adsorption intensity (-)

q_{eq} – adsorbent loading in equilibrium [ng/mg]; $c_{l,eq}$ – concentration of adsorbate in bulk in equilibrium [ng/L]

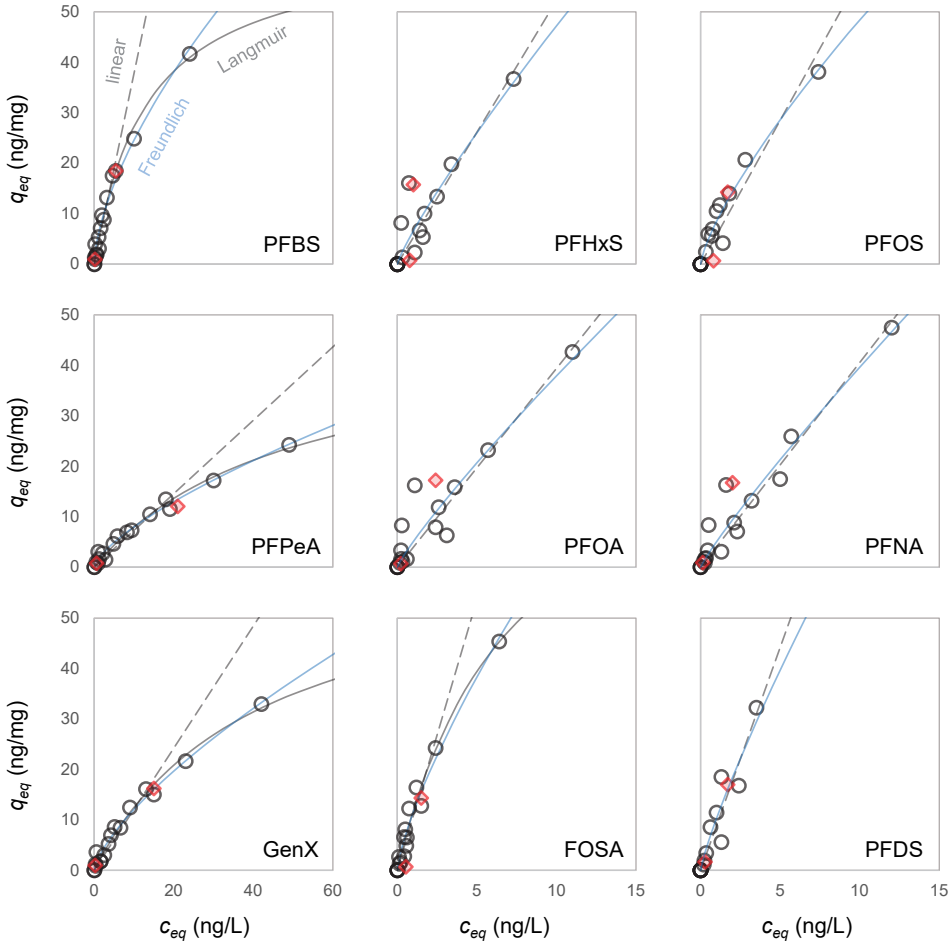


Figure S.2.5. Experimental data (markers) and linear (dotted grey line), Langmuir (full grey line) and Freundlich (blue line) isotherms for the adsorption of PFAS on SRD activated carbon. Red diamonds represent the equilibrium conditions in the kinetic experiments.

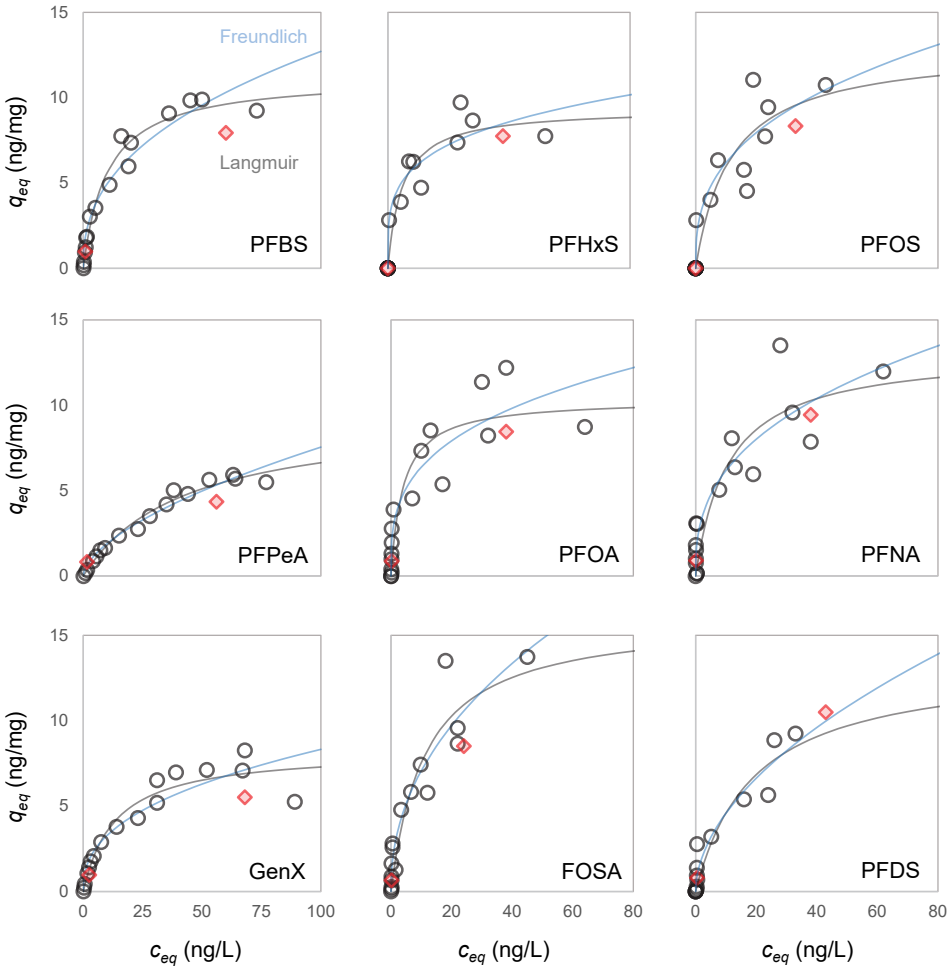


Figure S.2.6. Experimental data (circles) and fitted Langmuir (full grey line) and Freundlich (blue line) isotherms for the adsorption of PFAS on the CS activated carbon. The red diamonds represent the equilibrium condition in the kinetics experiments.

Table S.2.8. Estimated values of isotherm parameters for granular activated carbons used in this study

GAC	SRD (mesoporous activated carbon)								CS (microporous activated carbon)					
Iso-therm	Linear		Langmuir			Freundlich			Langmuir			Freundlich		
PFAS	a^1	R^2	q_{max}	K_L	R^2	K_f	n	R^2	q_{max}	K_L	R^2	K_f	n	R^2
PFBS	3.77	0.98	63.93	0.074	0.98	5.71	0.63	0.98	11.23	0.099	0.97	1.92	0.41	0.96
PFHxS	5.22	0.91	non avaliable			6.50	0.86	0.87	9.36	0.217	0.94	3.48	0.25	0.95
PFOS	5.70	0.95				8.42	0.76	0.96	12.93	0.086	0.89	2.70	0.36	0.91
PFDS	8.83	0.94				10.27	0.84	0.89	13.43	0.052	0.92	1.34	0.53	0.94
PFPeA	0.73	0.97	47.67	0.020	0.98	1.57	0.70	0.99	9.48	0.023	0.98	0.47	0.60	0.97
PFOA	3.94	0.92	non avaliable			5.06	0.87	0.89	10.35	0.251	0.87	3.10	0.31	0.88
PFNA	4.06	0.96				5.04	0.90	0.94	13.19	0.093	0.86	2.60	0.38	0.87
FOSA	10.72	0.95	96.77	0.137	0.97	11.46	0.75	0.97	16.07	0.089	0.90	2.46	0.46	0.91
GenX	1.21	0.96	63.61	0.024	0.98	2.36	0.70	0.99	8.27	0.075	0.94	1.29	0.40	0.90

1 – units of parameters are reported in Table S.2.7.

Table S.2.9. The experimental equilibrium data for adsorption of PFAS on the SRD activated carbon

PFBS		PFHxS		PFOS		PFDS		PFPeA		PFOA		PFNA		FOSA		GenX	
c^1	q	c	q	c	q	c	q	c	q	c	q	c	q	c	q	c	q
0.12	1.32	0.24	8.18	0.32	2.41	0.2	1.15	0.55	1.02	0.16	0.83	0.18	1.119	0.1	2.65	0.33	1.21
0.16	0.99	0.32	1.36	0.48	5.98	0.24	1.96	0.94	0.76	0.23	3.32	0.26	0.84	0.14	1.32	0.4	0.91
0.23	3.95	0.72	16.07	0.69	5.61	0.35	3.43	1	3.05	0.24	1.65	0.28	1.67	0.2	1.64	0.54	3.62
0.55	1.80	1.1	2.31	0.74	6.97	0.62	8.56	1.2	1.61	0.28	8.27	0.34	1.80	0.42	6.58	1.6	1.79
0.59	1.96	1.4	6.67	1	10.48	1	11.46	2.1	2.73	0.32	1.10	0.44	3.35	0.43	2.80	1.6	1.78
1.1	5.36	1.6	5.35	1.2	11.68	1.3	18.50	2.8	1.49	0.6	1.62	0.5	8.35	0.49	8.13	2.5	3.03
1.2	3.06	1.7	10.03	1.4	4.16	1.3	5.61	4.8	4.63	1.1	16.19	1.3	3.06	0.56	4.89	3.6	5.23
1.6	7.13	2.5	13.37	1.8	13.99	2.4	16.81	5.8	6.13	2.4	7.89	1.6	16.29	0.6	6.54	4.2	6.96
1.9	9.69	3.4	19.79	2.8	20.69	3.5	32.22	8.2	6.90	2.6	11.89	2.1	8.81	0.74	12.24	5.1	8.59
2.4	8.79	7.3	36.68	7.4	38.08			9.4	7.32	3.1	6.31	2.3	7.08	1.2	16.41	6.6	8.45
3.2	13.17							14	10.48	3.6	15.85	3.2	13.17	1.5	12.79	9	12.46
4.6	17.51							18	13.45	5.7	23.20	5	17.44	2.4	24.27	13	16.11
5.4	18.48							19	11.52	11	42.63	5.7	25.93	6.4	45.35	15	15.04
10	24.86							30	17.16			12	47.48			23	21.63
24	41.67							49	24.22							42	32.94

[1] c – concentration in equilibrium (ng/L), q – adsorbent loading in equilibrium (ng/mg)

Table S.2.10. The experimental equilibrium data for adsorption of PFAS on the CS activated carbon

PFBS		PFHxS		PFOS		PFDS		PFPeA		PFOA		PFNA		FOSA		GenX	
c[1]	*q*	*c*	*q*	*c*	*q*	*c*	*q*	*c*	*q*	*c*	*q*	*c*	*q*	*c*	*q*	*c*	*q*
0.12	0.18	0.38	2.82	0.24	2.82	0.37	0.14	0.88	0.18	0.1	0.39	0.12	0.77	0.14	0.26	0.27	0.22
0.25	0.37	4.3	3.89	4.9	4.01	0.39	0.28	1.6	0.36	0.15	0.98	0.13	1.02	0.14	1.64	0.58	0.43
0.62	0.93	7	6.26	7.4	6.34	0.41	0.93	4	0.85	0.16	1.31	0.13	1.81	0.15	0.13	1.7	1.07
0.96	1.24	8.4	6.24	16	5.77	0.42	1.39	5.5	1.15	0.18	0.20	0.19	1.53	0.16	0.87	2.4	1.41
1.2	1.79	11	4.72	17	4.53	0.51	2.77	7.1	1.51	0.18	2.78	0.2	3.09	0.17	0.65	3.1	1.76
1.5	1.84	23	7.37	19	11.04	0.6	0.69	9.1	1.65	0.2	1.96	0.43	3.05	0.46	2.80	4.4	2.08
2.7	3.02	24	9.72	23	7.73	5.2	3.20	15	2.37	0.8	3.90	0.44	0.15	0.5	2.58	7.5	2.89
5.1	3.54	28	8.66	24	9.45	16	5.40	23	2.75	7	4.55	0.44	0.15	1.5	1.27	14	3.78
11	4.90	52	7.74	43	10.74	24	5.65	28	3.51	10	7.33	7.8	5.05	3.3	4.78	23	4.30
16	7.75					26	8.85	35	4.20	13	8.54	12	8.08	6.6	5.83	31	6.51
19	5.97					33	9.24	38	5.03	17	5.38	13	6.38	9.8	7.43	31	5.18
20	7.36							44	4.81	30	11.37	19	5.97	12	5.77	39	6.97
36	9.08							53	5.65	32	8.22	28	13.51	18	13.51	52	7.12
45	9.84							63	5.93	38	12.20	32	9.58	22	8.66	67	7.09
50	9.89							64	5.71	64	8.74	38	7.87	22	9.58	68	8.27
73	9.24							77	5.50			62	11.99	45	13.74	89	5.24

[1] *c* – concentration in equilibrium (ng/L), *q* – adsorbent loading in equilibrium (ng/mg)

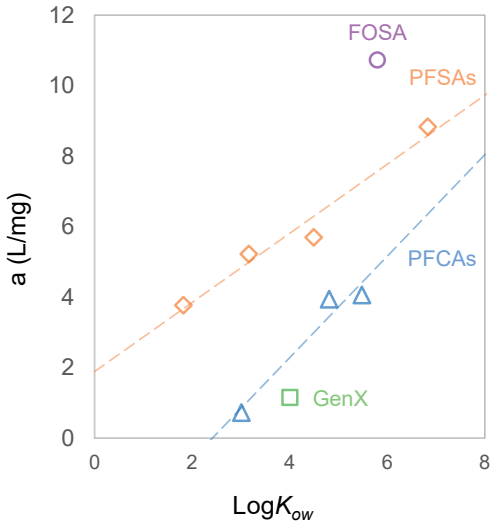


Figure S.2.7. Relationship between the linear isotherm parameter *a* (L/mg) and the PFAS LogK_{OW} values for adsorption on SRD activated carbon. The datapoints in the figure represent carboxylic PFAS (blue triangles), sulfonic PFAS (orange diamonds), GenX (green square), and FOSA (purple circle)

2.5.7. PFAS kinetics

2.5.7.1. Evaluation of film diffusion mechanism

With the homogenous surface diffusion model (HSDM) and pore diffusion model (PDM) PFAS adsorption kinetic data on microporous CS could be fitted without considering film diffusion. For SRD 5 mg/l and SRD 100 mg/l, an overprediction of the adsorbed amount was predicted by both HSDM and PDM at the start of the kinetic curve (Figure S.2.8). After including film diffusion, we observed no overprediction, and a good fit between experimental and predicted kinetic data for both models. To evaluate to which extent film or interparticle diffusion was dominant for the transport of PFAS in the case of adsorption on SRD a common approach of calculating Biot number (Bi) was applied.[105] The Biot number is a dimensionless mass transfer number that represents the ratio of external mass transfer (film diffusion) over internal mass transfer (pore or surface diffusion) resistances according to the following equation

$$Bi = \frac{k_F R_p}{D} \qquad \text{(S.2.12)}$$

where D is either D_s or D_p. For Bi < 1, film diffusion is the dominant mechanism, while for 1 < Bi < 30 pore diffusion is dominant, and for Bi > 30 surface diffusion is dominant.[77] Table S.11 shows high values of Bi (~ 10^6 - 10^8) for the HSDM model, which indicates that film diffusion is negligible compared to the surface diffusion. For the PDM model, the values of Bi > 1 indicate that interparticle diffusion is dominant. Since values of Bi show that film

diffusion is likely negligible compared to the interparticle diffusion, the better fitting of PFAS kinetic data for the adsorption on SRD in a model with film diffusion added was likely not the consequence of a better explanation of PFAS transport mechanisms; instead it was the consequence of the addition of another fitting parameter k_f. By adding the film diffusion resistance, the overprediction of the adsorbed amount at the start of adsorption could be compensated, i.e., the kinetics could be slowed down.

Table S.2.11. Values of Biot number for the case of SRD 5 mg/l for pore and surface diffusion

PFAS	5 mg/l		100 mg/l	
	Bi_{pore}	$Bi_{surface}$	Bi_{pore}	$Bi_{surface}$
PFBS	9.22	3.2E+07	51.61	2.7E+06
PFHxS	11.07	4.8E+07	169.46	1.0E+08
PFOS	5.49	5.8E+07	169.56	1.3E+08
PFDS	20.80	3.4E+08	179.35	1.2E+08
PFPeA	8.90	3.1E+07	7.91	8.9E+05
PFOA	6.07	3.4E+07	167.32	3.4E+08
PFNA	4.78	3.3E+07	168.36	5.0E+08
FOSA	22.94	2.7E+08	172.00	3.8E+08
GenX	7.67	2.0E+07	17.41	1.5E+06

The HSDM and PDM model may overpredict the adsorbed amounts at the start of adsorption kinetics because of incomplete linear isotherms. Both HSDM and PDM evaluate locally an adsorption isotherm for the duration of a full kinetic curve. The estimated PFAS linear isotherms for SRD are valid in the range of c_{eq} ~ 0.1-20 ng/L, while the concentrations at the start of the adsorption kinetic experiments are as high as 100 ng/L, i.e., the isotherm is out of range. For the adsorption on CS, Langmuir isotherms were used, and no overprediction was observed. Decreased overprediction at the start of kinetic curve can be shown for adsorption on SRD by running HSDM or PDM with a Langmuir isotherm instead of the linear isotherm (Figure S.2.8). However, we could only obtain a Langmuir isotherm for 4/9 PFAS for adsorption on SRD. Furthermore, the linear isotherm explains the adsorption on SRD better. Therefore, we used the linear isotherm in HSDM and PDM combined with film diffusion for each PFAS kinetics on SRD.

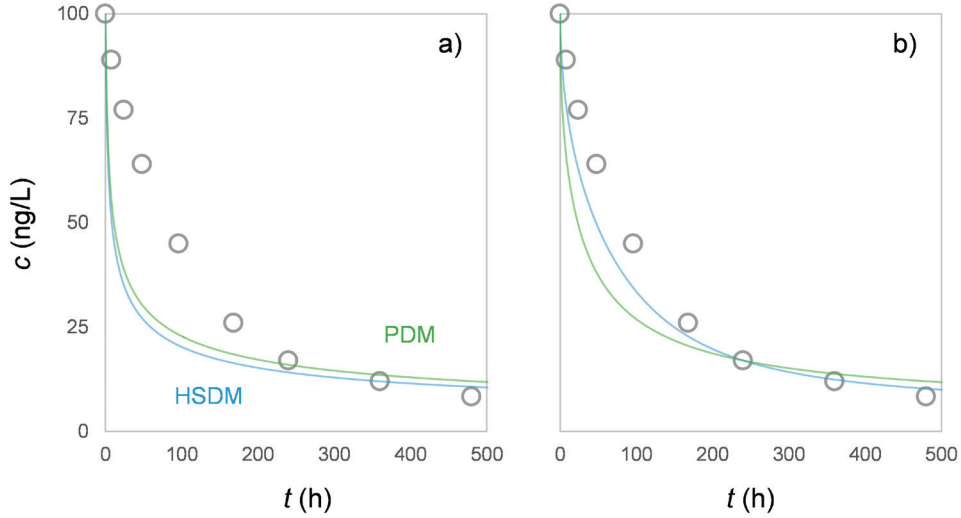


Figure S.2.8. a) Discrepancy between experimental data (circles) and model predictions by HSDM (blue line) and PDM (green line) at the start of PFAS adsorption kinetics for the case of SRD 5 mg/L. b) Discrepancy is reduced by coupling the Langmuir isotherm with diffusion models instead of the linear isotherm.

2.5.7.2. Pore diffusion

In this study, both the pore diffusion model (PDM) and the homogenous surface diffusion model (HSDM) were found to effectively describe the kinetic data. The kinetic curves obtained using PDM closely resemble those obtained with HSDM (Figure 2.3), and a comparison can be found in Figure S.2.9. However, the two models yielded different values for the diffusion coefficients of PFAS. While the values of surface diffusion coefficients, D_s, were lower than typical values reported for PFAS, as discussed in the main paper, the values of the pore diffusion coefficient, D_p, were estimated to be in the range of D_p ~$1{\cdot}10^{-8}$ - $1{\cdot}10^{-11}$ m^2/s (Table S.2.12). These D_p values align with those reported for the transport of other molecules[30,44] and are the first reported values for PFAS. The conventional modelling framework for intraparticle transport of PFAS is based solely on surface diffusion, but our study demonstrates that the pore diffusion model can effectively describe the kinetic data as well.

However, the estimated values of D_p for most kinetics in this paper are not realistic if we take into account the predicted values of the diffusion coefficient in solution, D_l (m^2/s), according to the following commonly used equation[106]

$$D_l = \frac{7.4{\cdot}10^{8}(\phi M)^{0.5}T}{\eta_b V_A^{0.6}} \qquad \text{(S.2.13)}$$

where ϕ is the association factor representing the effective molecular weight of water, for which we consider ϕ = 2.6, M (g/mol) is the molecular weight of the solvent (PFAS), T (K) is temperature, η_b (cp) is the solution viscosity, and V_A is the adsorbate molecular volume

(cm^3/mol) that for each PFAS was determined with ChemSketch software. In Table S.2.12. the estimated values of D_l and D_p are reported. In most cases the values of D_l ~ $4 \cdot 10^{-10}$ - $7 \cdot 10^{-10}$ m^2/s were lower than the values of D_p, which suggests that PFAS would diffuse faster inside the pores than in solution, which is unlikely.

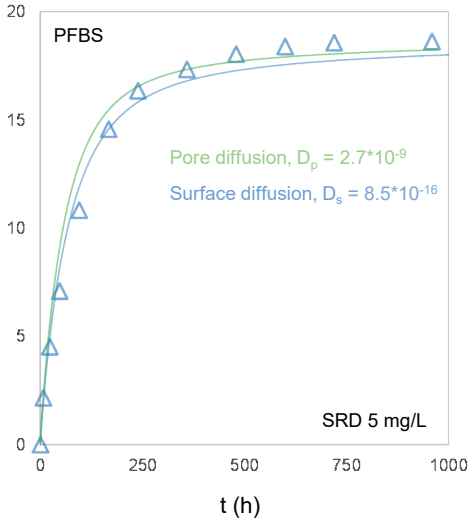


Figure S.2.9. Comparison of fitting results of HSDM (blue line) and PDM (green line) on experimental kinetic data (blue triangles)

Table S.2.12. The estimated values of D_p (m^2/s) from PDM model for different kinetic cases, and D_L based on the Chemsketch software and equation S13

PFAS	SRD 5 mg/L	SRD 100 mg/L	CS 5 mg/L	CS 100 mg/L	D_L
PFBS	1.74E-09	3.38E-10	7.09E-10	4.42E-10	6.97E-10
PFHxS	1.75E-09	1.19E-10	1.41E-09	2.46E-10	5.85E-10
PFOS	3.44E-09	1.25E-10	1.17E-09	2.36E-10	5.11E-10
PFDS	1.07E-09	1.37E-10	2.64E-09	8.58E-10	4.58E-10
PFPeA	1.14E-09	1.94E-09	3.21E-10	3.26E-10	7.17E-10
PFOA	2.76E-09	8.47E-11	5.48E-10	1.82E-10	5.55E-10
PFNA	3.19E-09	1.13E-10	9.28E-10	5.74E-10	5.20E-10
FOSA	8.47E-09	1.15E-10	1.05E-09	1.10E-09	5.10E-10
GenX	1.43E-09	8.52E-10	5.61E-10	2.39E-10	6.37E-10

With the estimated values of D_l and D_p one can calculate the tortuosity, τ (dimensionless), according to equation

$$D_p = \frac{D_l \varepsilon_p}{\tau} \qquad \text{(S.2.14)}$$

where τ is a parameter that describes the hindrance of molecular transport inside a porous medium caused by the curvatures of the pores.[30] Values of τ above 1 are considered realistic. However, most of the values of τ reported in Table S.13 are lower than 1 which means that considering only pore diffusion is not appropriate when describing intraparticle transport of PFAS. A similar conclusion was obtained in a study by Raul Ocampo-Perez et al.[104] that showed that for the adsorption of phenol both pore and surface diffusion models could describe experimental kinetic data well, but unrealistic values of D_p higher than D_l were obtained. Nevertheless, it is important to note that experimental determination of PFAS D_l at low concentrations is challenging and has not yet been conducted, making it difficult to draw clear conclusions about the values of τ that are reported in Table S.2.13.

Table S.2.13. The calculated values of tortuosity, τ, for SRD and CS at carbon loadings of 5 mg/L and 100 mg/L

PFAS	SRD 5 mg/L	SRD 100 mg/L	CS 5 mg/L	CS 100 mg/L
PFBS	0.23	1.19	0.46	0.73
PFHxS	0.19	2.83	0.19	1.11
PFOS	0.09	2.35	0.20	1.00
PFDS	0.25	1.92	0.08	0.25
PFPeA	0.36	0.21	1.04	1.02
PFOA	0.12	3.77	0.47	1.42
PFNA	0.09	2.65	0.26	0.42
FOSA	0.03	2.55	0.23	0.21
GenX	0.26	0.43	0.53	1.24

Table S.13 shows that the most realistic values of τ were obtained for the transport of PFAS in mesoporous SRD 100 mg/L, where τ values were found to be between 2-4 for the long chain PFAS. Only in the specific case of adsorption on mesoporous SRD carbon, when the surface was less saturated (100 mg/L of carbon dose), the realistic values of τ indicate the relevance of pore diffusion. At the higher carbon dosages more mesopores are available for PFAS diffusion compared to the lower dosages and at the same PFAS concentration. In reality, both pore and surface diffusion contribute to the intraparticle transport of molecules within a porous medium like GAC, with one mechanism often dominating the other. In this study, it was not possible to determine the percentage of pore and surface diffusion responsible for PFAS transport. However, the realistic values of D_S suggest that surface diffusion primarily governs the transport process, while pore diffusion becomes more relevant in some specific cases, such as when there are sufficient mesopores available.

2.5.7.3. Kinetic experimental data and results of fitting by HSDM

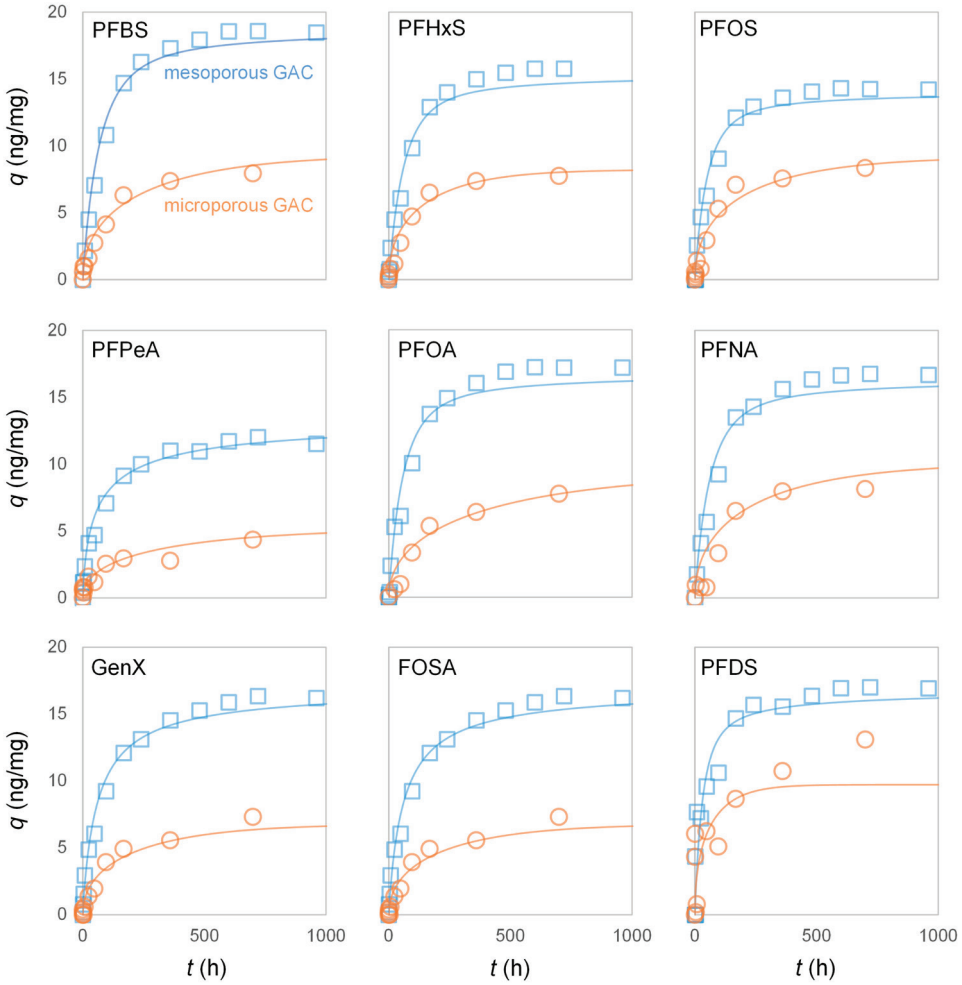


Figure S.2.10. Adsorbate loading, q (ng/mg), of PFAS as a function of time for SRD (5 mg/L) and CS (5 mg/L) activated carbon. Experimental data is represented by blue squares for SRD and orange circles for CS. Theoretical predictions, based on the HSDM model, are depicted by solid lines, with blue indicating SRD, and orange CS.

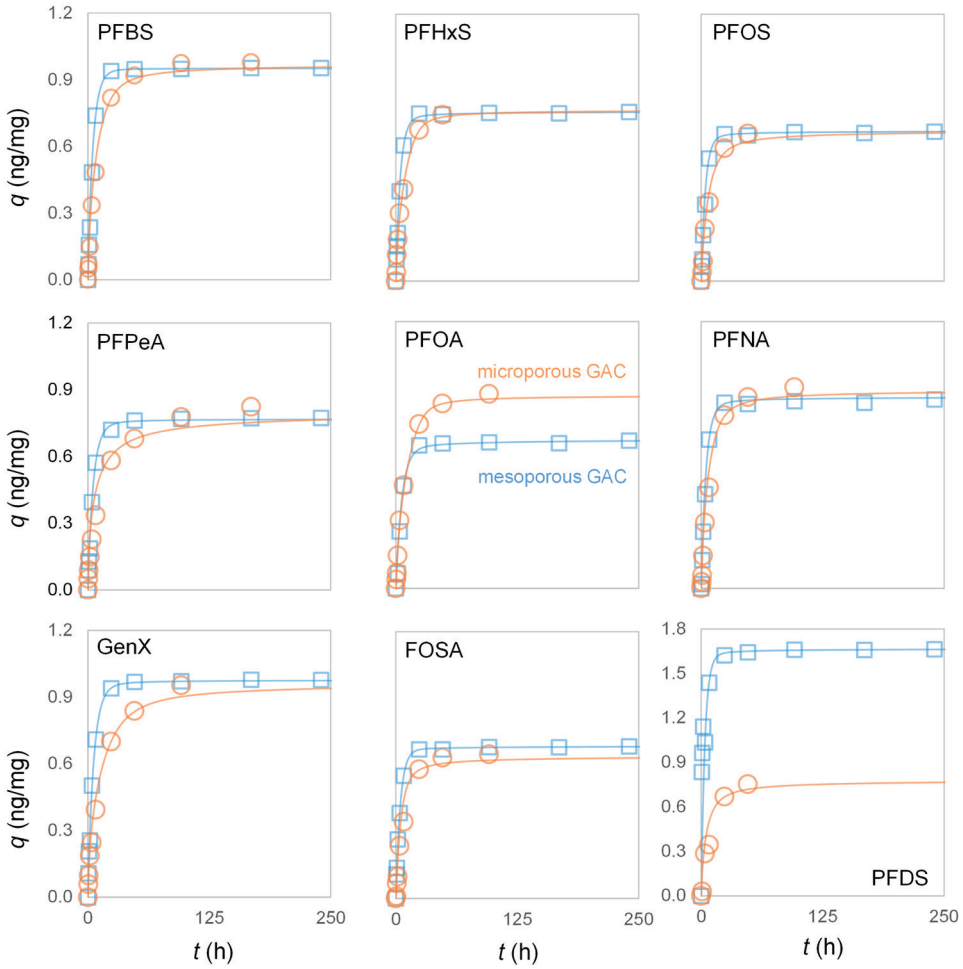


Figure S.2.11. Adsorbate loading, q (ng/mg), of PFAS as a function of time for SRD (100 mg/L) and CS (100 mg/L) activated carbon. Experimental data is represented by blue squares for SRD and orange circles for CS. Theoretical predictions, based on the HSDM model, are depicted by solid lines, with blue indicating SRD, and orange CS.

Table S.2.14. Estimated values of the surface diffusion coefficient, D_s (m^2/s).

PFAS	SRD 5 mg/L	R^2	SRD 100 mg/L	R^2	CS 5 mg/L	R^2	CS 100 mg/L	R^2
PFBS	8.53E-16	0.994	6.34E-15	0.998	9.35E-15	0.970	1.45E-15	0.993
PFHxS	6.43E-16	0.992	2.18E-16	0.997	1.56E-14	0.957	1.22E-15	0.998
PFOS	6.41E-16	0.988	1.93E-16	0.997	9.04E-15	0.951	7.92E-16	0.984
PFDS	1.95E-16	0.929	2.20E-16	0.887	3.15E-14	0.565	1.40E-15	0.750
PFPeA	2.42E-15	0.990	1.87E-14	0.998	6.92E-15	0.928	3.42E-15	0.971
PFOA	9.54E-16	0.988	7.13E-17	0.980	6.24E-15	0.938	1.01E-15	0.998
PFNA	9.07E-16	0.987	4.03E-17	0.997	8.36E-15	0.912	1.14E-15	0.989
FOSA	1.53E-16	0.983	6.49E-17	0.998	6.07E-15	0.879	7.07E-16	0.978
GenX	1.90E-15	0.992	1.05E-14	0.998	1.12E-14	0.971	1.89E-15	0.995

Table S.2.15. The experimental kinetic data for adsorption of PFAS on the SRD activated carbon at 5 mg/L

Time	PFBS		PFHxS		PFOS		PFDS		PFPeA		PFOA		PFNA		FOSA		GenX	
(h)	c[1]	q	c	q	c	q	c	q	c	q	c	q	c	q	c	q	c	q
0	100	0	81	0	74	0	88	0	82	0	89	0	87	0	75	0	98	0
0.5	110	n.a.	80	0.20	77	n.a.	66	4.36	80	0.40	92	n.a.	93	n.a.	68	1.39	97	0.20
1	100	n.a.	78	0.59	81	n.a.	96	n.a.	76	1.18	88	0.20	93	n.a.	74	0.20	94	0.78
4	100	n.a.	77	0.78	77	n.a.	89	n.a.	76	1.18	87	0.39	92	n.a.	72	0.59	90	1.57
8	89	2.17	69	2.37	61	2.56	49	7.69	70	2.37	77	2.37	78	1.78	59	3.16	83	2.96
24	77	4.49	58	4.49	50	4.68	51	7.22	61	4.10	62	5.27	66	4.10	50	4.88	73	4.88
48	64	7.06	50	6.08	42	6.27	39	9.60	58	4.70	58	6.08	58	5.69	42	6.47	67	6.08
96	45	10.82	31	9.83	28	9.05	34	10.62	46	7.08	38	10.03	40	9.24	30	8.85	51	9.24
168	26	14.69	16	12.90	13	12.11	14	14.69	36	9.13	20	13.70	19	13.50	12	12.51	37	12.11
240	17	16.27	9.5	14.01	8	12.94	7.9	15.70	31	10.00	13	14.90	14	14.31	8.3	13.07	31	13.13
360	12	17.30	4.7	15.00	4.8	13.60	8.8	15.57	26	11.01	7.5	16.02	7.5	15.62	4.6	13.84	24	14.54
480	8.4	17.94	2	15.47	2.2	14.06	4.4	16.37	26	10.97	2.9	16.86	3.6	16.33	2.1	14.28	20	15.28
600	6.6	18.56	1.6	15.78	2	14.31	2.7	16.95	23	11.72	2.4	17.21	3.2	16.65	1.7	14.57	18	15.90
720	5.7	18.59	1	15.77	1.7	14.25	1.7	17.01	21	12.02	1.9	17.17	2	16.75	1.6	14.47	15	16.36
960	24	41.67	n.a.	n.a.	n.a.	n.a.	n.a.	n.a.	49	24.22	n.a.	n.a.	n.a.	n.a.	n.a.	n.a.	42	32.94

[1] c – concentration (ng/L), q – adsorbent loading (ng/mg)

Table S.2.16. The experimental kinetic data for adsorption of PFAS on the SRD activated carbon at 100 mg/L

Time	PFBS		PFHxS		PFOS		PFDS		PFPeA		PFOA		PFNA		FOSA		GenX	
(h)	c^1	q	c	q	c	q	c	q	c	q	c	q	c	q	c	q	c	q
0	97	0	78	0.000	69	0.000	170	0.000	79	0.000	69	0.000	88	0.000	70	0.000	100	0.000
0.5	90	0.069	68	0.098	62	0.069	85	0.837	70	0.089	82	-0.128	86	0.020	59	0.108	89	0.108
1	81	0.158	62	0.158	59	0.098	72	0.965	66	0.128	71	-0.020	75	0.128	56	0.138	79	0.207
2	73	0.236	56	0.217	48	0.207	54	1.142	60	0.187	62	0.069	62	0.256	43	0.266	74	0.256
4	48	0.483	37	0.404	34	0.345	65	1.035	39	0.394	43	0.256	45	0.424	31	0.384	49	0.503
8	22	0.739	16	0.611	13	0.552	24	1.438	21	0.571	22	0.463	20	0.670	14	0.552	28	0.709
24	1.6	0.939	1.4	0.754	1.8	0.661	5	1.624	5.8	0.720	3.6	0.644	3.1	0.836	1.9	0.670	4.5	0.940
48	0.78	0.948	1.8	0.750	2.4	0.656	3.1	1.644	1.7	0.761	2.8	0.652	3.8	0.829	1.9	0.671	1.6	0.969
96	0.8	0.948	1.2	0.757	1	0.670	1.5	1.661	0.98	0.769	2.3	0.658	2.6	0.842	0.87	0.682	1.4	0.972
168	0.34	0.953	1.4	0.755	1.4	0.666	1.6	1.660	0.67	0.772	2.7	0.653	3.2	0.836	1.0	0.680	0.73	0.978
240	0.34	0.953	0.77	0.761	0.81	0.672	1.1	1.664	0.59	0.773	1.5	0.665	1.8	0.849	0.54	0.685	0.78	0.978

[1] c – concentration (ng/L), q – adsorbent loading (ng/mg)

Table S.2.17. The experimental kinetic data for adsorption of PFAS on the CS activated carbon at 5 mg/L

Time	PFBS		PFHxS		PFOS		PFDS		PFPeA		PFOA		PFNA		FOSA		GenX	
(h)	c^1	q	c	q	c	q	c	q	c	q	c	q	c	q	c	q	c	q
0	97	0	75	0.	75	0.	100	0.	79	0.	81	0.	86	0	75	0.00	96	0
0.5	98	n.a.	74	0.20	74	0.20	69	6.05	76	0.59	82	n.a.	91	n.a.	67	1.56	94	0.39
1	94	0.59	73	0.39	72	0.59	78	4.33	75	0.79	83	n.a.	93	n.a.	63	2.36	95	0.20
4	92	0.99	76	0.00	73	0.40	99	0.20	77	0.40	84	n.a.	81	0.99	73	0.40	96	n.a.
8	92	0.99	71	0.79	68	1.39	96	0.79	75	0.79	82	n.a.	86	n.a.	76	n.a.	93	0.60
24	89	1.59	69	1.19	71	0.79	110	0.00	71	1.59	78	0.60	82	0.79	72	0.60	89	1.39
48	83	2.73	61	2.73	60	2.93	68	6.25	73	1.17	76	0.98	82	0.78	62	2.54	86	1.95
96	76	4.12	51	4.71	48	5.30	74	5.11	66	2.55	64	3.34	69	3.34	51	4.71	76	3.93
168	65	6.31	42	6.50	39	7.09	56	8.67	64	2.96	54	5.32	53	6.50	35	7.88	71	4.93
360	60	7.36	38	7.36	37	7.56	46	10.74	65	2.79	49	6.37	46	7.96	34	8.16	68	5.57
700	60	7.94	38	7.74	33	8.34	30	13.10	56	4.36	45	7.74	44	8.14	24	8.51	59	7.33

[1] c – concentration (ng/L), q – adsorbent loading (ng/mg)

Table S.2.18. The experimental kinetic data for adsorption of PFAS on the CS activated carbon at 100 mg/L

Time	PFBS		PFHxS		PFOS		PFDS		PFPeA		PFOA		PFNA		FOSA		GenX	
(h)	c^1	q	c	q	c	q	c	q	c	q	c	q	c	q	c	q	c	q
0	100	0	79	0	70	0	81	0	85	0	89	0	92	0	66	0	100	0
0.5	95	0.049	75	0.039	71	n.a.	81	n.a.	80	0.049	85	0.039	89	0.030	65	0.010	94	0.059
1	93	0.069	67	0.118	66	0.039	78	0.030	76	0.089	82	0.069	86	0.059	59	0.069	90	0.099
2	85	0.148	60	0.187	61	0.089	130	n.a.	70	0.148	74	0.148	77	0.148	56	0.099	81	0.187
4	66	0.335	48	0.305	46	0.236	52	0.286	62	0.227	58	0.305	62	0.296	42	0.236	75	0.246
8	51	0.483	37	0.414	34	0.355	46	0.345	51	0.335	42	0.463	46	0.454	31	0.345	60	0.394
24	17	0.818	10	0.680	9.3	0.598	13	0.670	26	0.582	14	0.739	13	0.779	7.1	0.581	29	0.700
48	6.8	0.918	3.1	0.748	2.7	0.663	4.5	0.754	16	0.680	4.6	0.832	4.7	0.860	1.8	0.633	15	0.838
96	1.1	0.974	n.a.	n.a.	n.a.	n.a.	0.64	0.792	6.2	0.776	0.18	0.875	0.14	0.905	0.18	0.649	3.2	0.954
168	0.8	0.978	n.a.	n.a.	n.a.	n.a.	0.51	0.794	1.5	0.823	n.a.	n.a.	0.15	0.906	0.13	0.649	2.5	0.961

[1] c – concentration (ng/L), q – adsorbent loading (ng/mg)

2.5.8. PFOA isotherm experimental and modelling data at varying starting concentrations

Table S.2.19. Experimental equilibrium data for adsorption of PFOA on the SRD activated carbon at varying starting concentrations.

c_0 ~ 100 ng/L		c_0 ~ 1000 ng/L		c_0 ~ 10000 ng/L		c_0 ~ 100000 ng/L		c_0 ~ 1000000 ng/L	
c^1	q	c	q	c	q	c	q	c	q
0.16	0.83	2.6	92.3	7.0	79.9	20.2	1282	174.6	2484
0.23	3.32	3.7	115.9	10.1	731.9	21.8	626.3	491.5	4962
0.24	1.65	6.6	182.0	10.6	641.7	62.3	2332	2658	9904
0.28	8.27	6.6	254.1	13.8	847.2	87.2	2981	8171	13114
0.32	1.10	10.5	231.2	16.8	159.0	888.7	6038	41719	19057
0.6	1.62	16.0	179.5	17.3	106.3	1163	7527	319984	27112
1.1	16.19	16.4	227.7	25.5	318.9	4550	11749	752628	24940
2.4	7.89	47.1	297.0	30.2	1023	24894	13377	791121	42164
2.6	11.89	52.0	341.9	45.5	1288	56313	13245	864372	27972
3.1	6.31	55.3	435.7	48.3	788.9	68866	14602		
3.6	15.85	65.0	414.7	59.0	1753	85087	12934		
5.7	23.20	191.0	453.5	132.1	1561	94175	13135		
11	42.63	221.7	636.1	330.0	2510	100455	16618		
				650.1	2860				
				1167	6056				
				1225	4869				
				4768	6357				
				6212	7593				
				7205	8259				

[1] c – concentration (ng/L), q – adsorbent loading (ng/mg)

Table S.2.20. Experimental equilibrium data for adsorption of PFOA on the CS activated carbon at varying starting concentrations.

c_0 ~ 100 ng/L		c_0 ~ 1000 ng/L		c_0 ~ 10000 ng/L		c_0 ~ 100000 ng/L	
c[1]	q	c	q	c	q	c	q
0.1	0.39	4.7	46.0	8.9	221.3	3.2	269.1
0.15	0.98	7.2	54.2	19.0	269.5	17.6	450.2
0.16	1.31	8.9	57.2	215.5	534.0	20.5	543.7
0.18	0.20	13.4	60.0	659.0	711.4	148.6	1282
0.18	2.78	17.1	91.4	1787	954.3	295.5	1485
0.2	1.96	85.5	105.6	3053	811.3	712.2	2143
0.8	3.90	145.7	84.7	3841	1029	3506	2751
7	4.55	205.2	142.2	7608	1541	6624	3307
10	7.33	297.2	91.2	7736	1840	26040	4654
13	8.53	365.3	140.0	8233	1437	40207	5376
17	5.38	424.8	101.8	8682	1986	59086	6047
30	11.37	595.9	108.4	9839	2599	63273	5243
32	8.22	636.8	147.3			85340	8031
38	12.20	638.5	142.8			85370	5740
64	8.74	699.6	122.5				
		782.2	203.2				
		831.2	200.6				
		873.1	237.8				
		904.0	271.7				

[1] c – concentration (ng/L), q – adsorbent loading (ng/mg)

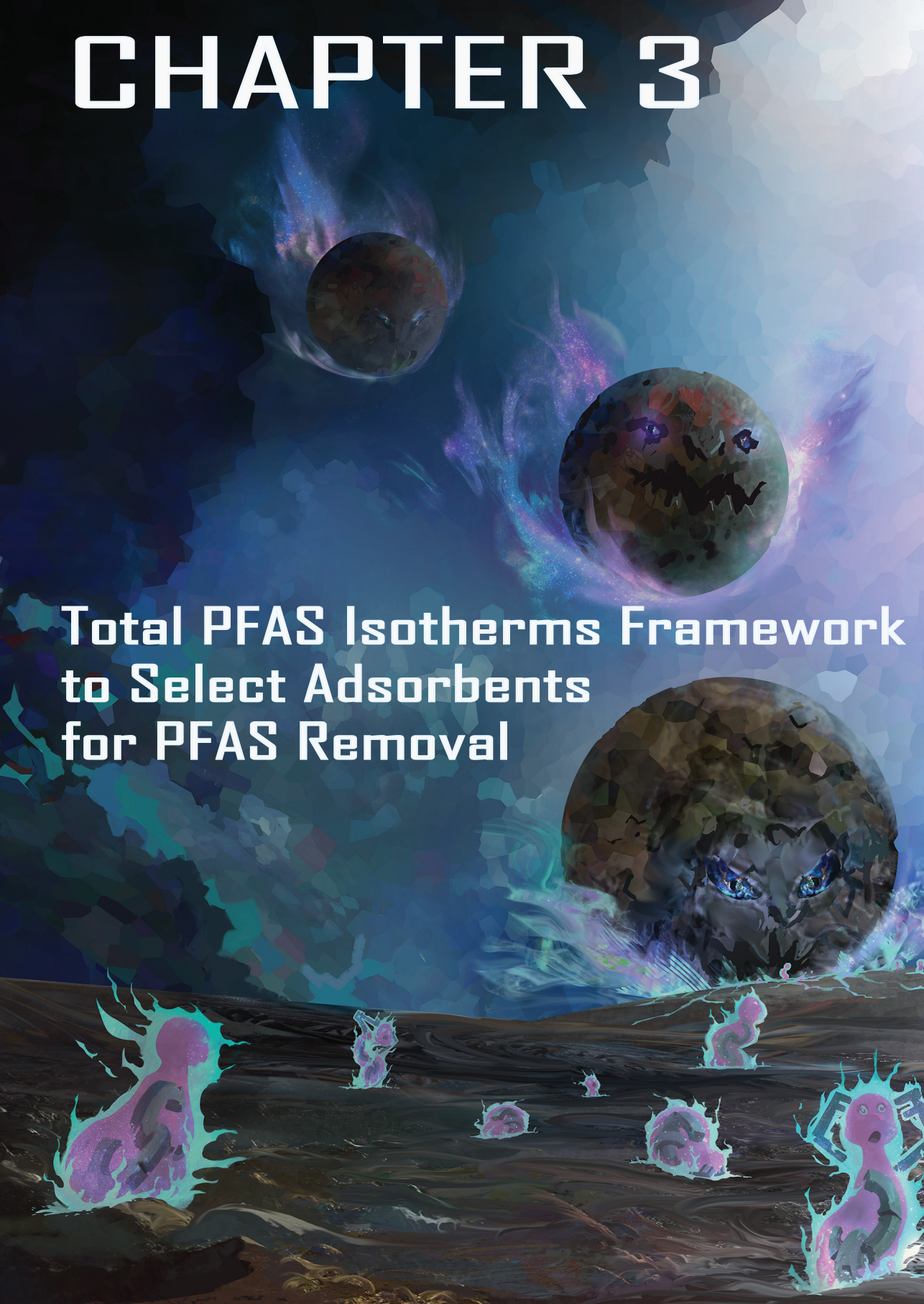
Table S.2.21. Estimated Freundlich isotherm parameters for adsorption of PFOA on SRD and CS activated carbon under different starting PFAS concentrations.

GAC	c_0 ~ (ng/L)	K_f (ng/mg)/(ng/L)^n	n	R^2
Mesoporous (SRD)	1000	94.03	0.33	0.95
	10000	278	0.38	0.95
	100000	1558	0.20	0.95
	1000000	1746	0.21	0.94
Microporous (CS)	1000	43.92	0.17	0.92
	10000	52.60	0.38	0.96
	100000	303	0.27	0.97

Table S.2.22. Estimated values of surface diffusion coefficient, D_s obtained with HSDM by using isotherm parameters from various concentrations on predicting PFAS kinetics at 100 ng/L.

c_0 ~ (ng/L)	D_s (m^2/s)			
	SRD 5 mg/L	SRD 100 mg/L	CS 5 mg/L	CS 100 mg/L
100	9.54E-16	7.13E-17	6.24E-15	1.01E-15
1000	4.64E-17	1.26E-17	5.90E-17	3.16E-17
10000	6.69E-18	2.25E-18	1.12E-17	7.60E-18
100000	2.07E-18	7.18E-19	2.00E-18	1.79E-18

CHAPTER 3



Total PFAS Isotherms Framework to Select Adsorbents for PFAS Removal

This chapter is in preparation for submission as:

Pranić, M.; Sigmund, G.; Martin, P.; Hofmann, T.; van der Wal, A.; Dykstra, J. E. Total PFAS isotherms as a framework to select adsorbents for PFAS removal

Abstract:

Per- and polyfluoroalkyl substances (PFAS) are organic micropollutants regulated at very low concentrations and are commonly removed from water by adsorption onto activated carbon. A major challenge in comparing PFAS adsorption data across studies is that results are strongly influenced by experimental conditions such as carbon particle size, initial PFAS concentration, and applied adsorbent dose. Here, we propose the use of total isotherms, where the total adsorbed PFAS is plotted against the total PFAS concentration in solution at equilibrium, as a framework for evaluating adsorption. Using experiments with mixtures of short- and long-chain PFAS across a wide range of concentrations and carbon doses, supported by literature data, we demonstrate that total PFAS isotherms are independent of initial PFAS concentration and adsorbent dose. Furthermore, we show that when adsorption-governing factors such as pore size distribution and surface charge are accounted for, total PFAS isotherms fall onto a single curve. Mesopores are identified as the limiting factor for adsorption when the micropore volume exceeds ~0.3 cm^3/g, while carbons with fewer acidic surface groups exhibit higher adsorption capacities. Overall, the total isotherm framework provides a robust tool for comparison of PFAS adsorption across studies and can be used for selecting and optimizing activated carbons for PFAS removal.

Keywords: PFAS, adsorption, activated carbon, pore size distribution

3.1. Introduction

Per- and polyfluoroalkyl substances (PFAS) are synthetic industrial chemicals whose extensive use resulted in their widespread presence in the environment. Because of their persistence, potential toxicity, and bioaccumulation potential, PFAS are recognized as substances of concern, leading to strict limits for their concentrations in drinking water.[1,19] Adsorption is widely applied technology for PFAS removal from drinking water,[24,26] and activated carbon (AC) filters are commonly employed in such systems. However, the specific AC properties that drive PFAS removal remain unclear. Moreover, different experimental conditions across studies complicate direct comparison of adsorption results.

Pore size distribution is one of the key properties of AC governing PFAS adsorption. Adsorbent pores are commonly classified by diameter as micropores (<2 nm), mesopores (2–50 nm), and macropores (>50 nm).[30] However, studies have reported conflicting conclusions regarding the pore size range determining PFAS removal. Several studies have indicated that micropores play a dominant role in PFAS adsorption onto AC. For example, Saeidi et al. (2020) reported that increasing the micropore fraction (1–2 nm) of AC felts enhanced long-chain PFAS removal.[107] Molecular dynamics simulations by Schutta et al. (2025) further suggested that micropores of 0.8–1 nm favor adsorption of short-chain over long-chain PFAS.[108] Other studies also discuss that micropores are the main adsorption sites for both short- and long-chain PFAS adsorption, while mesopores act primarily as transport pathways toward micropores.[75,76,109] In contrast, several reports suggest that micropores are not accessible to long-chain PFAS and that their adsorption predominantly occurs within mesopores and macropores.[54,68] Two adsorption mechanisms have been proposed for long-chain PFAS that cannot occur within micropores due to spatial constraints: (i) adsorption assisted by nanobubbles,[93] which typically have dimensions of 10–80 nm,[94] and (ii) multilayer adsorption in the form of PFAS aggregates.[85] In a study by Zhang et al. (2023), pre-equilibration of AC with short-chain PFAS followed by exposure to long-chain PFAS resulted in complete desorption of the short-chain species from AC.[110] The authors concluded that if short-chain PFAS had been adsorbed in the micropores, such displacement would not have occurred, suggesting that mesopores can also act as adsorption sites for short-chain PFAS.

As highlighted in the previous paragraph, it remains unclear which pore sizes are most critical for PFAS adsorption in a given scenario. Several factors complicate the comparison of adsorption data across studies. The first is the limited characterization of ACs. While reporting the specific surface area (BET) is relatively common, detailed information on mesopore and micropore areas and volumes is often missing.[111] In addition, many studies do not include surface charge characterization, despite its known influence on PFAS adsorption.[112] Adsorbents with a higher density of positive surface charge and fewer acidic (negatively charged) functional groups generally exhibit better PFAS removal performance.[113] Moreover, defunctionalization of AC surfaces has been shown to enhance adsorption by reducing the

concentration of acidic groups and increasing surface hydrophobicity.[74,109,114] Meaningful comparison of adsorption performance is therefore only possible when both pore structure and surface chemistry are well characterized. Finally, experimental conditions, such as initial PFAS concentration, carbon dose, and particle size, must also be considered, as these can significantly influence experimental outcomes.

Batch adsorption experiments are most commonly used to obtain adsorption isotherms, which describe the equilibrium relationship between bulk solute concentration and the amount adsorbed, providing valuable insight into adsorption capacity and affinity.[34] When designing isotherm experiments, several parameters can be controlled, including the initial PFAS concentration, the applied adsorbent dose, and the particle size of the carbon. However, the shape and position of adsorption isotherms can depend strongly on these experimental conditions. In our previous work, we observed a pronounced dependence of PFAS isotherm results on both initial concentration and carbon dose, with multiple adsorption plateaus appearing for the same equilibrium PFAS concentration as a result of varying these parameters.[115]

According to Worch,[30] isotherms obtained by varying both the initial concentration and the adsorbent dose will overlap only in the absence of interactions between adsorbing molecules. In practice, however, competition among PFAS species for adsorption sites is frequently reported. In particular, short-chain PFAS are often displaced by long-chain PFAS during adsorption onto AC.[110,116] Furthermore, PFAS are surfactant-like compounds that, under appropriate conditions, typically at high concentrations, can form multilayers, which may also contribute to the multiple adsorption plateaus observed at equilibrium. Adsorbent particle size additionally influences adsorption behaviour: smaller particles enhance mass transfer and adsorption kinetics, and several studies have reported higher apparent adsorption capacities for carbons with smaller particle sizes.[117–119]

We hypothesize that different experimental conditions can make either micropores or mesopores the limiting factor for PFAS adsorption. Meaningful comparison of adsorption data across studies therefore requires a standardized framework that treats adsorption consistently and accounts for variability in experimental parameters. The aim of this study is to develop and demonstrate such a framework.

We will show that an effective way to standardize PFAS adsorption data is by constructing a total isotherm, where the summed equilibrium concentration of all PFAS in solution is plotted against the total amount adsorbed onto AC. Total isotherms are traditionally used to describe adsorption of multicomponent mixtures with unknown compositions, such as natural organic matter (NOM), where adsorption is commonly expressed in terms of dissolved organic carbon, since only the sum of all components can be measured.[30] Sontheimer et al. (1988) demonstrated a strong influence of initial concentration and carbon dose on

total DOC isotherms of industrial wastewater,[31] while Summers and Roberts (1988) showed that DOC isotherms obtained at different adsorbent doses and initial concentrations of soil humic and fulvic acids align to a single master curve when normalized for adsorbent dose.[120]

Building on this concept, we hypothesized that expressing multicomponent PFAS adsorption data as a summed quantity would similarly yield a master curve, that is independent of experimental artifacts such as concentration and adsorbent dose, and therefore more representative of the intrinsic adsorption behaviour. By subsequently applying corrections for adsorption-limiting carbon properties (e.g., pore size distribution, surface charge) data from different ACs could also be fall on the same curve. For instance, normalizing adsorption capacity (adsorbent loading) or distribution coefficients (adsorption affinity) by specific surface area or pore volume allows identification of which pore sizes govern PFAS adsorption. Additionally, expressing adsorption as total PFAS isotherms aligns with regulatory practice, since PFAS drinking-water guidelines are often defined as sum parameters.[11,19] To our knowledge, this study represents the first systematic application of total isotherms for evaluating PFAS adsorption.

In this study, we apply the total isotherm approach to describe the adsorption of PFAS mixtures across a wide range of concentrations and AC doses. We distinguish between situational adsorption factors inherent to experimental design (e.g., initial concentration, carbon dose, particle size) and adsorption governing factors, which reflect the intrinsic properties of the adsorption system (e.g., pore size distribution, surface charge, temperature, matrix composition), which fundamentally determine adsorption behaviour. A broad range of experimental conditions was examined with several ACs, combining laboratory data generated within our group with data compiled from the literature. Our goal is to provide a unified framework for comparing adsorption performance across studies.

3.2. Materials and methods

3.2.1. Activated carbon

Adsorption experiments were performed using two ACs with similar surface charge properties but distinctly different pore size distributions. The more mesoporous carbon, SRD (Chemviron), is a reagglomerated coal-based carbon with properties comparable to the widely used Filtrasorb 400 (F400). SRD was selected due to its relatively high mesoporosity, which is associated with enhanced PFAS removal. As a more microporous counterpart, AquaSorb™ K-CS (Jacobi; hereafter referred to as CS) was chosen. The key physicochemical properties of both carbons are summarized in Table 3.1.

For both carbons particles were sieved to obtain a size fraction between 0.60 and 0.85 mm, which corresponds to dominant size fraction in some granular activated carbon (GAC)

fitlers. The particles were thoroughly rinsed with deionized water, dried, and stored in airtight containers. Prior to adsorption experiments, the carbons were dried at 105 °C for 24 h to remove residual moisture. The dried GAC was weighed, boiled in deionized water to remove entrapped air, cooled to room temperature, and subsequently added to the batch bottles for adsorption experiments.

3.2.2. PFAS

Eight PFAS compounds with varying chain lengths and functional groups were selected for this study. The short-chain PFAS included PFBS, PFPeA, and GenX, while the long-chain PFAS comprised PFHxS, PFOS, PFOA, PFNA, and FOSA. The physicochemical properties of these compounds are provided in Table S.3.1. For all experiments, regardless of the initial PFAS concentration, the mixtures were prepared to contain equimolar proportions of short- and long-chain PFAS. For example, at an initial individual PFAS concentration of 1000 ng/L, the mixture contained approximately 10 nmol/L of short-chain PFAS and 10 nmol/L of long-chain PFAS.

3.2.3. Adsorption experiments

Isotherm experiments were conducted in 0.5 L polypropylene copolymer (PPCO) bottles (Thermo Scientific, USA) at 20 °C. Each bottle contained a mixture of eight PFAS compounds at initial concentrations of approximately 1000, 10000, or 100000 ng/L, a specified amount of GAC (0.5–500 mg/L), and Milli-Q water buffered to pH ~7.2 using a 5 mM Na_2HPO_4 / 5 mM KH_2PO_4 phosphate buffer. The buffer was selected to maintain a stable pH during the experiment and to achieve a conductivity (~800 µS/cm) similar to that of typical tap water.

The bottles were placed horizontally on an orbital shaker and agitated at 120 rpm for 52 days. Kinetic control experiments confirmed that this duration was sufficient to achieve equilibrium (Figure S.3.1). After sampling, solutions were transferred to 2 mL polypropylene Eppendorf tubes and stored at -20 °C. Multiple freeze–thaw cycles were tested and found to have no measurable effect on PFAS concentrations.

3.2.4. Masurement of PFAS concentration

PFAS concentrations were quantified using a SCIEX 5500+ LC–MS/MS system equipped with a Phenomenex Kinetex C18 column. The analytical method provided quantification limits of 2.5 ng/L for all measured PFAS. Specific analytical details, including instrument settings and method validation, are provided in Pranić et al. (2025).[115]

3.2.5. Construction of total PFAS isotherms

Equilibrium adsorption isotherms describe the relationship between the amount of solute adsorbed onto an adsorbent and the remaining concentration of that solute in solution at equilibrium. For individual PFAS compounds, the equilibrium adsorbent loading, $q_{eq,PFAS}$, is calculated as:

$$q_{eq,PFAS} = \frac{V_l}{m_a}\left(c_{0,PFAS} - c_{eq,PFAS}\right) \quad (3.1)$$

where $q_{eq,PFAS}$ is in $nmol_{PFAS}/mg_{GAC}$ or ng_{PFAS}/mg_{GAC}, V_l is the solution volume (L), m_a is the mass of dry AC (mg), c_0 is the initial PFAS concentration, and c_{eq} is the equilibrium PFAS concentration.

Eq. 3.1 shows that adsorbent loading as a function of equilibrium concentration can be obtained either by varying initial PFAS concentration or by varying the adsorbent dose (m_a/V_l). In this study, both approaches were used. Isotherm data were generated at four initial concentrations (100, 1000, 10,000, and 100,000 ng/L), using GAC doses ranging from 0.5 to 500 mg/L. The 100 ng/L obtained under same experimental conditions as described in Section 3.2.3 were taken from Chapter 2.

Accurate determination of adsorbent loading requires a sufficiently large difference between initial and equilibrium concentrations. When removal is very low, e.g., at low adsorbent doses for weakly adsorbing short-chain PFAS, small concentration differences result in high uncertainty in calculated adsorbent loadings. Therefore, PFAS adsorbent loadings were only calculated when the equilibrium concentration decreased by at least 10% relative to the initial concentration. The 10% threshold corresponds to the uncertainty of the analytical method.

To construct total PFAS isotherms, the c_{eq} of individual PFAS in solution were summed to obtain $c_{eq,PFAS\ total}$, and the individual q_{eq} were summed to obtain $q_{eq,PFAS\ total}$.This summation is performed on a molar basis; therefore, all concentrations and loadings were converted to molar units prior to summation. Each batch bottle (experiment) provides one point on the total isotherm, corresponding to a specific initial PFAS mixture and carbon dose.

Total PFAS isotherms were expressed in several ways:
1. per mass of carbon, where unit of $q_{eq,PFAS\ total}$ is nmol/mg,
2. normalized to mesopore volume where unit of $q_{eq,PFAS\ total}$ is $nmol/cm^3$,
3. normalized to mesopore surface area where unit of $q_{eq,PFAS\ total}$ is $nmol/m^2$,
4. normalized for charge of surface groups by multiplying $q_{eq,PFAS\ total}$ with γ, which is the ratio of negative and positive surface charge groups.

By applying different normalization approaches, we evaluated which AC properties enable adsorption data from different carbons and conditions to be represented by a single isotherm curve.

3.2.6. Literature data extraction

The total PFAS isotherm obtained in this study for an eight-component PFAS mixture, evaluated across four initial concentrations and in a simple matrix without NOM, was compared

with adsorption data from previous studies performed within our group as well as with representative isotherm data from other scientific studies.

Two internal studies with SRD carbon were included in this comparison. In Chapter 4, individual PFAS isotherms were measured at three different temperatures (10, 20, and 30 °C), and total PFAS isotherms were reconstructed from those data.[121] In Chapter 5, isotherms were generated using a smaller GAC particle size (~0.125 mm) and under both NOM-free conditions and varying NOM compositions. In both studies, experimental procedures and analytical methods were consistent with those described in Section 3.2.3 – 3.2.4.

For comparison of our data with literature, we selected studies reported in the review by Gagliano et al. (2020) that conducted experiments in DI water (same as in this study), including both single-solute and multi-solute PFAS systems.[13] Table 3.1 provides information on the ACs used in the literature studies, while Table 3.2 summarizes the experimental conditions. For studies in which only single-solute data were available, the shortest- and the longest-chain PFAS isotherm data were selected for comparison.

Most studies listed in Table 3.2 do not report the raw experimental inputs required to directly construct total PFAS isotherms; namely (i) the carbon dose corresponding to each data point, and (ii) the exact initial and equilibrium concentrations of each PFAS in solution. Instead, data points are typically presented graphically as isotherms (c_{eq} vs. q_{eq}), which we extracted from the published figures. However, this approach yields only pairs of (c_{eq}, q_{eq}) for individual PFAS and does not provide the associated carbon dose or initial concentration. Constructing total PFAS isotherms requires summing the c_{eq} values of all PFAS from the same batch experiment, as well as the q_{eq} values. The published figures, however, do not indicate which data points correspond to the same batch experiment. To address this limitation, we made a practical assumption: adjacent data points (from right to left) across individual graphical isotherms correspond to the same batch experiment, i.e., to the same adsorbent dose and initial PFAS concentration. Although this assumption introduces some uncertainty, it represents the only feasible approach in the absence of raw experimental inputs.

Table 3.1. Activated carbon properties evaluated in this study compared with carbons reported in the literature

Activated carbon	Total pore volume	Micropores volume cm^3/g	Mesopores volume cm^3/g	Total surface area m^2/g	Micropores area m^2/g	Mesopores area m^2/g	γ (total acidity/total basicity)	Ref.
Jacobi CS (CS)	0.55	0.51	0.04	966	822	144	~0.91*	This
SRD	0.59	0.36	0.23	1296	1248	48	~0.91*	This
Filtrasorb 400 (F400)	0.44	0.32	0.12	862	786	76	0.91**	This
Aquasorb CX (ACS)	0.625	0.618	0.007	1056	n.r.	n.r.	n.r.	[122]
Filtrasorb 200 (F200)	0.415	0.34	0.075	840	n.r.	n.r.	n.r.	[122]
Hydro-darco 4000 (HD4000)	0.613	0.1605	0.4525	628.5	n.r.	n.r.	n.r.	[122]
Norit GAC 400 (N400)	0.212	0.0405	0.1715	866.5	n.r.	n.r.	n.r.	[122]
1240C	0.64	0.54	0.1***	1428	n.r.	n.r.	0.21**	[113]

*γ values for CS, SRD, and F400 are assumed to be similar based on previously reported similarity in surface charge between CS and SRD, and the known similarity in manufacturing between SRD and F400[115]

**surface charge data reported in Zhi et al. (2015)[113]

***for normalization in Figures 3.5E. and 3.5F, a γ value of 0.04 was used for 1240C instead of the reported 0.1. This correction was derived from the ratio of mesopore volumes measured for F400 in Zhi et al. (2015) and in this study, ensuring consistent normalization across datasets

Table 3.2. Summary of experimental conditions in literature studies

AC	PFAS	$c_{0,PFAS}$ µg/L	carbon dose mg/L	particle diameter mm	study
		Multi solute			
Bituminous coal*	PFPeA, PFHxA, PFOA, PFBA	6	0.5-150	powder	Ref. 123
F400	PFOA, PFOS	0.5 - 5	500	0.4-1.7	Ref. 52
F400, ACX, F200, HD4000, CN400	PFBA, PFPeA, PFHpA, GenX, PFOA, PFNA, PFDA, PFBS, PFHxS, PFOS	~ 3000 - 20 000	400 - 20 000	not reported	Ref. 122
		Single solute			
F400	PFNA	3	0.5 - 12	0.56 - 1,7	Ref. 124
F400	PFBS, PFOS	15000 – 150 000	1000	0.85-1.7	Ref. 51
F400	PFBA, PFOA	10 - 5000	n.r.	<1 mm	Ref. 125
F400	PFOS	1000	100 - 2600	0.4-1.7	Ref. 52
F400	PFOS	5 – 5000	100	0.85 - 1	Ref. 113
1240C	PFOS	5 – 5000	100	0.85 - 1	Ref. 113
F400	PFOA	0-100000	1000	0.55-0.75	Ref. 126

*Assumed to be F400

3.3. Results and discussion

In this study, we demonstrate that the total isotherm approach can be used to distinguish between situational experimental factors and adsorption-governing factors. When PFAS adsorption data are expressed as total isotherms, the resulting curves become linear for each carbon, and situational factors no longer affect the observed adsorption. We first discuss the formation of the total PFAS isotherm and the observed regions in which either short- or long-chain PFAS preferentially adsorb. We then compare total isotherms across multiple studies and show that, when all relevant adsorption-limiting factors are considered, PFAS total isotherms fall onto a single curve.

3.3.1. Formation and Regions of Total PFAS Isotherms

Adsorption isotherm data over a wide concentration range and carbon dose were obtained for a mixture of eight PFAS compounds onto two ACs that primarily differ in their pore size distribution: the more mesoporous SRD and the more microporous CS (Table 3.1). Calculated total PFAS isotherms are presented in Figure 3.1.

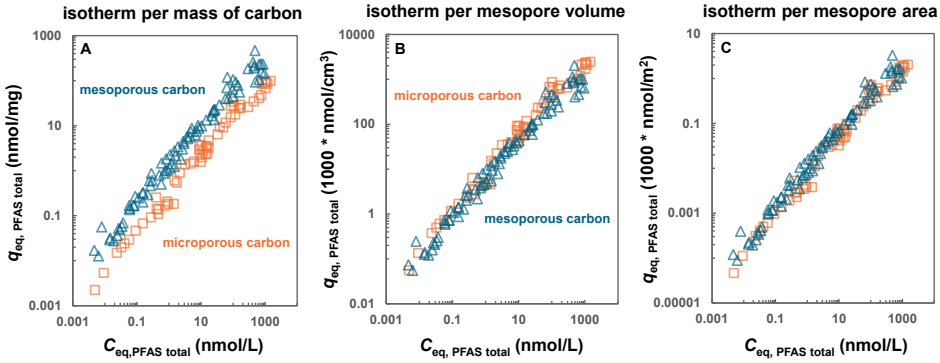


Figure 3.1. Total isotherms for PFAS adsorption constructed from a mixture of eight single PFAS isotherms in a multicomponent system. The isotherms are presented as a function of (A) carbon mass, (B) mesopore volume, and (C) mesopore surface area.

Figure 3.1A shows that SRD exhibits a higher adsorption capacity for PFAS than CS, both at low (nmol/L) and high (μmol/L) equilibrium concentrations. Because these two carbons have comparable total pore volumes and specific surface areas (Table 3.1) and similar surface charge properties (Table 3.1) the higher adsorption on SRD can be attributed to the larger mesoporous space (volume and/or area) for adsorption. Better performance of mesoporous adsorbents in PFAS removal has been reported before.[56,85,87] Additional evidence that mesopores govern PFAS adsorption in the case of SRD and CS was obtained by normalizing the adsorbent loading (q_{eq}) by either mesopore volume (Figure 3.1B) or mesopore surface area (Figure 3.1C). After this normalization, the total isotherms of two different carbons fall on a single line, yielding a PFAS total-isotherm *master curve* – defined here as a single, unified

relationship between total equilibrium PFAS concentration in solution and total adsorbed PFAS that is shared across different ACs once the relevant adsorption-governing properties (e.g., pore-size distribution and surface charge) are accounted for.

Data could be normalized to either mesopore volume (Figure 3.1B) or mesopore area (Figure 3.1C), and both yielded a master curve, likely because pore volume and pore area are typically linearly correlated. In principle, the chosen normalization should correspond to the factor that limits adsorption. For our system, mesopore volume is more appropriate, as multilayer PFAS adsorption (indicated by S-shaped isotherms) was observed (Figure 3.2C). Additionally, most studies summarized in Table 3.1 report only pore volume, not mesopore or micropore area. For these reasons, all subsequent master curves are presented over mesopore volume. If adsorption were governed primarily by monolayer coverage, normalization to mesopore area would be more suitable.

The total isotherms in Figure 3.1 were constructed from experiments at four different initial concentrations (~100, ~1000, ~10,000 and ~100,000 ng/L), with data points obtained by varying the carbon dose (0.3 – 200 mg/L). We observed that the relative contributions of short- and long-chain PFAS to the total isotherm strongly depend on the carbon dose (i.e., the available adsorption space). To illustrate this dependence, Figure 3.2 presents total and individual PFAS isotherms at an initial concentration of 1000 ng/L for adsorption on mesoporous SRD.

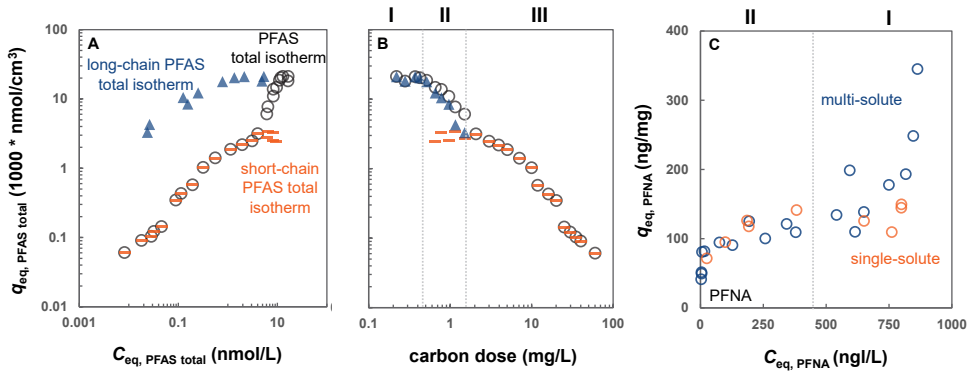


Figure 3.2. (A, B) Total PFAS isotherms for a mesoporous carbon at an initial concentration of 1000 ng/L, with contributions from short- and long-chain PFAS on the total isotherm. The isotherms are expressed as (A) adsorbent PFAS loading, q_{eq} vs equilibrium PFAS concentration, c_{eq} and (B) q_{eq} vs carbon dose. (C) Adsorption isotherms for long-chain PFNA in a multi-solute and single-solute system. Three distinct regions are highlighted: (I) adsorption dominated by long-chain PFAS, where multilayer adsorption occurs in multi-solute solutions as shown in C, (II) adsorption influenced by both short- and long-chain PFAS; and (III) adsorption dominated by short-chain PFAS.

Figure 3.2A and 3.2B show the influence of short-chain PFAS and long-chain PFAS on the total PFAS isotherm. Long-chain PFAS adsorption is higher than that of short-chain PFAS, which is in agreement with previous studies comparing PFAS adsorption onto AC[52,73,88,89]. We observed that three regions can be distinguished based on the competition between short- and long-chain PFAS.

Region I represents conditions of low carbon doses where adsorption sites are limited and primarily occupied by the more strongly adsorbing long-chain PFAS. As a result, the total isotherm of all PFAS approaches that of the long-chain PFAS alone (Figure 3.2A and 3.2B). Region II represents conditions of medium carbon dose where both long- and short-chain PFAS contribute to the total isotherm. The adsorption capacity for short-chain PFAS remains nearly constant, while increasing the carbon dose primarily enhances the removal of long-chain PFAS. This means that in systems containing both long- and short-chain PFAS, simply increasing the carbon dose may not be sufficient to remove short-chain PFAS. In other words, long-chain PFAS must be removed first before significant removal of short-chain PFAS can occur. Region III represents conditions of high carbon doses, where long-chain PFAS are largely removed from solution (under the detection limit), allowing short-chain PFAS to adsorb onto AC without competition. In this region, the total isotherm is determined solely by the adsorption of short-chain PFAS. While Figure 3.2 illustrates adsorption on mesoporous SRD carbon at an initial concentration of 1000 ng/L, the same three regions are observed across all concentrations, for both granular and powdered carbon, for microporous carbon, and also in the presence of NOM. With NOM, however, these regions shift toward higher carbon doses because of competition between PFAS and NOM for adsorption sites.

At conditions of limited adsorption space (Region I), S-shaped isotherms are observed for individual long-chain PFAS adsorbing onto microporous CS carbon (Figure 3.2C). This behavior was observed under multi-solute adsorption conditions but was absent in single solute experiments. In single solute adsorption, the isotherm approaches saturation, whereas in multi-solute systems the adsorption capacity continues to increase at lower carbon doses, resulting in an S-shaped curve indicative of multilayer adsorption. In multi-solute systems, the adsorption surface is more saturated with a mixture of PFAS molecules than in single-solute systems, reducing the number of available sites and promoting multilayer adsorption.

PFAS multilayer adsorption has been reported previously, but not at the low concentrations relevant for drinking water treatment covered in our study. Zaggia et al. (2016) visualized long-chain PFAS molecular aggregates at concentrations around 1 mg/L (resin dose of 1000 mg/L) with transmission electron microscopy,[85] Yu et al. (2009) inferred the formation of hemi-micelles and micelles from kinetic and isotherm data at PFAS concentrations above 20 mg/L,[79] and Dunmyer et al. (2024) observed multilayer adsorption on quartz-crystal microbalance surfaces at 5 mg/L.[127] These studies confirm that PFAS, as surfactants, can adsorb in multilayers under sufficiently high experimental concentrations.

The novelty of our findings is that multilayer adsorption can occur even at environmentally relevant PFAS concentrations when adsorption space is limited (Region I). The S-shaped isotherm observed for the carbon with limited mesoporosity (CS) in multicomponent systems at low carbon doses indicates PFAS aggregation within mesopores, likely arising from competition between PFAS species for a restricted adsorption space and the resulting local accumulation of PFAS within the pores. These locally elevated concentrations drive aggregation and multilayer adsorption even though bulk solution concentrations remain low. Furthermore, at realistic drinking water treatment scenarios, the effective adsorption space will be further reduced by the presence of NOM. This is in line with McCleaf et al. (2017) who reported that long-chain PFAS removal increased as NOM accumulated in a GAC column. They speculated that progressive site blockage by NOM promoted PFAS aggregation and enhanced adsorption.[57]

3.3.2. Comparison of Total PFAS Isotherms Across Multiple Studies

In Section 3.3.1, we showed that normalizing total PFAS isotherms by mesoporous adsorption space (either pore area or pore volume) yields a single master curve, confirming that mesopores govern adsorption for the two carbons tested. To further evaluate the applicability of the total isotherm framework for describing PFAS adsorption, we compared this master curve with additional data obtained from our group under varying experimental conditions (particle size, temperature, and the presence or absence of NOM) as well as with adsorption data reported in the literature (see Table 3.2).

3.3.2.1. Comparison of PFAS master curve with our data at different conditions

Figure 3.3A shows that total PFAS isotherms for two different granule sizes coincide onto the same master curve, even though individual isotherms, especially for long-chain PFAS, exhibit higher adsorption capacities for smaller particles (Figure 3.3B). This apparent discrepancy is explained by the impact of carbon dose (solid to liquid ratio) on adsorption. The higher adsorbent loading values observed for smaller particles were obtained at lower carbon doses than those used for larger particles (Figure 3.3C). Therefore, the increased PFAS adsorption observed for smaller particles reflects the influence of adsorbent dose rather than an intrinsic particle-size effect. In other words, PFAS removal cannot be meaningfully compared across particle sizes unless the same adsorbent dose is used.

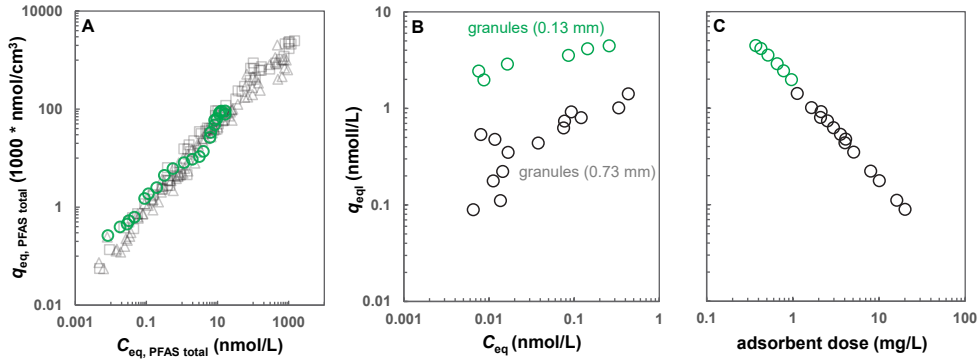


Figure 3.3. Impact of granule size on PFAS adsorption for two activated carbon particle sizes 0.13 mm, (green) and 0.73 mm (grey). (A) Total PFAS isotherms for the two particle sizes, showing alignment onto the same master curve. (B) Individual isotherms for long-chain PFAS, illustrating higher apparent adsorption for the smaller particles. (C) Adsorbent loading (q_{eq}) as a function of carbon dose for both particle sizes, highlighting the dose differences that underline the trends in panel B.

Several studies have reported enhanced PFAS adsorption with smaller granules, attributing this to increased external surface area and improved intraparticle diffusion, which can lead to higher apparent adsorption.[117–119] For such conclusions to be valid, individual isotherms must be compared at the same carbon dose. The influence of the solid to liquid ratio (adsorbent dose) on adsorption isotherms is well documented and one of the main reasons why cross-study comparisons are often inconsistent.[128] Alternatively, the total PFAS isotherm can be used to remove the influence of dose entirely. When adsorption is expressed as a total PFAS isotherm (Figure 3.3A), the effect of carbon dose disappears because the total isotherm integrates the contributions of all PFAS species within the same experiment, making the comparison independent of the applied carbon dose.

In this study, we classify carbon dose as a situational experimental factor determining adsorption results, rather than a property that reflects intrinsic adsorption behavior. A similar situational factor is also seen for individual PFAS isotherms, where multiple adsorbent loading values can occur at the same equilibrium concentration across different combinations of PFAS concentration and carbon dose (Figure S.3.2). This variability also vanishes when data are expressed as total PFAS isotherms. Overall, total PFAS isotherms are independent of situational experimental factors such as PFAS concentration and carbon dose (solid to liquid ratio), which commonly differ across studies and complicate data interpretation. Once these situational experimental factors are eliminated, it is easier to compare data and make conclusions about adsorption governing factors. Contrary to several previous studies that indicated PFAS adsorption is higher on smaller particles[58,129]

In this study, by using total isotherms we determined that PFAS equilibrium adsorption is not higher on smaller particles, and is thus not a governing factor for adsorption, but rather a situational experimental artifact. In contrast, temperature and the presence of NOM are universally governing factors for adsorption (Figure 3.4).

Figure 3.4A shows that total PFAS isotherms obtained at different temperatures do not coincide onto the same master curve. In our previous work, we discuss that increasing temperature enhances negative lateral interactions between adsorbed molecules, thereby reducing adsorption capacity.[121] This temperature dependence reflects a true mechanistic effect and therefore does not disappear when data are expressed as total PFAS isotherms.

Figure 3.4B shows the influence of NOM on total PFAS isotherms. Because the isotherms are expressed relative to mesoporous adsorption space, the lower adsorption values observed in the presence of NOM indicate that NOM occupies or blocks a portion of the mesopore volume. In other words, NOM alters the effective adsorption space and thus represents another adsorption-governing factor.

Together, temperature and matrix composition (e.g., NOM type and concentration) represent mechanistic drivers of PFAS adsorption, and their influence appears in Figure 3.4 as systematic deviations from the mesopore-normalized master curve. Similarly to the pore size distribution (Figure 3.1), isotherms obtained under different temperatures and matrix, will not coincide onto the master curve unless temperatures and matrix effects are explicitly normalized for.

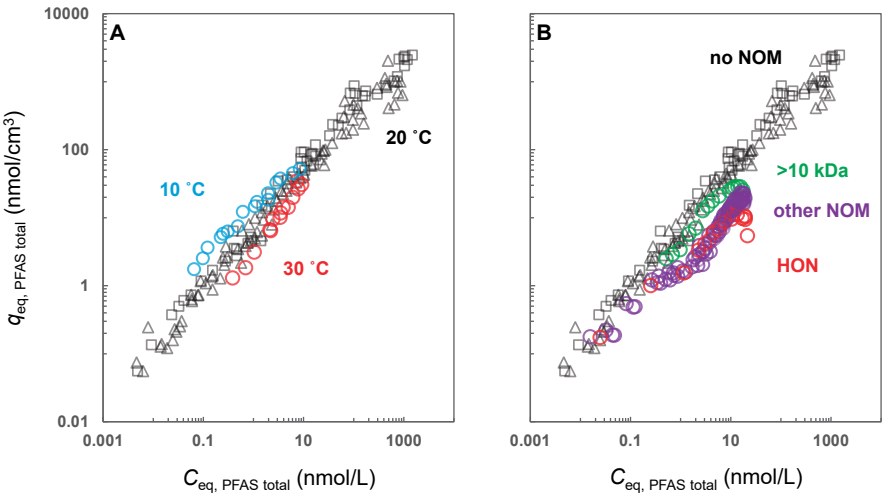


Figure 3.4. Comparison of total PFAS isotherms normalized for mesopore volume obtained under different experimental conditions: (A) varying temperatures (B), different fractions of natural organic matter

In conclusion, the total isotherm approach effectively removes the influence of situational experimental factors while retaining mechanistic differences arising from adsorption-governing factors. To assess the broader applicability of this approach, we next evaluate how published PFAS adsorption data compare to the total PFAS master curve.

3.3.2.2. Comparison of PFAS master curve with literature data

Most PFAS adsorption data available in the literature were generated using Filtrasorb 400 (F400) activated carbon. In our comparison, we also included several other microporous carbons and one carbon (1240C) with a significantly different surface charge (Table 3.1). Unfortunately, surface charge is rarely reported in adsorption studies, which limited the number of carbons with well-characterized surface chemistry that could be included here. Our primary goal was to compare our results with multi-solute data from other studies, since PFAS in natural environments typically occur as mixtures. However, because multi-solute datasets including both short- and long-chain PFAS are limited, single-solute data were also included (Table 3.2). The comparison between our PFAS master curve and literature data is presented in Figure 3.5.

Figures 3.5A (multi-solute) and 3.5D (single-solute) present total PFAS isotherms from the literature compared to our data for SRD and CS carbons, without any normalization. When adsorption capacities are normalized by mesoporous volume (Figures 3.5B and 3.5E), most data fall onto a single master curve. This outcome is expected, as the majority of the selected publications used Filtrasorb 400 (F400) AC, which shares similar properties with the mesoporous SRD carbon used to construct our master curve (Table 3.1). The total PFAS isotherms for F400 align well with the master curve in both multi-solute systems (Figure 3.5B) and for long-chain PFAS in single-solute systems (Figure 3.5E). However, normalization by mesoporous volume did not result in convergence into a single line (Figure 3.5E) for short-chain PFAS, suggesting that PFAS can adsorb in the micropores. A recent study by Schutt et al. (2025) identified critical pore diameters for PFAS binding and transport, at 0.9 – 1 nm for short-chain PFAS.[130] We hypothesize that normalizing single-solute short-chain PFAS adsorption data to microporous adsorption space within the critical pore size range would lead to alignment with our master curve. However, data on pore volume or surface area specific to these micropores are not yet available, as such characterization requires CO_2 physisorption analysis, which is rarely done and reported.

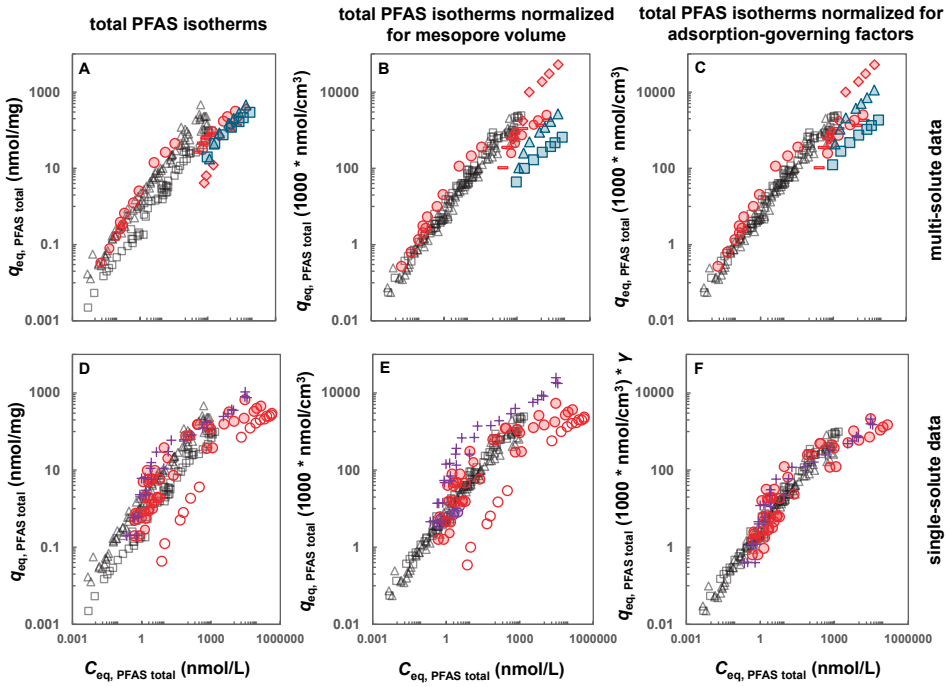


Figure 3.5. Comparison of total PFAS isotherms (black markers) obtained in this study with literature data from seven additional studies (Table 3.2). Panels A–C show multi-solute data; Panels D–F show single-solute data. Panels A and D present total isotherms without normalization for carbon properties. Circles denote F400 data: solid red circles represent long-chain PFAS and open red circles represent short-chain PFAS. Blue points correspond to two carbons that fall below the mesopore-normalized master curve (B) but align closer when normalized by micropore volume instead (C). Purple points correspond to carbon 1240C, which does not align with the mesopore-normalized master curve (E) but coincides onto the curve once adsorption is normalized by both mesopore volume and the surface-charge ratio γ (ratio of negative to positive surface functional groups) (F). Short-chain PFAS data (open red circles) are omitted from Panel F for clarity, as they do not coincide onto the master curve

Two more examples on Figure 3.5 show that once relevant carbon properties are accounted for, total PFAS isotherms converge onto the same master curve. The first example involves multi-solute data for two carbons from Sun et al. (2023),[122] shown as blue data points in Figure 5B (H4000 and N400). These points fall below the master curve, indicating lower PFAS adsorption capacity when normalized by mesopore volume. When expressed conventionally per unit carbon mass (Figure 3.5A), both ACs also exhibit reduced PFAS removal capacity. Notably, H4000 and N400 contain substantially less micropore volume (0.16 cm^3/g and 0.04 cm^3/g, respectively) than the other carbons included in this study, all of which exceed ~0.3 cm^3/g (Table 3.1). When H4000 and N400 total PFAS isotherms are normalized by micropore volume (Figure 3.5C), the data shift upward and align much more closely with the master

curve. This indicates that, unlike most carbons for which mesopores govern adsorption, PFAS adsorption in H4000 and N400 is limited by their restricted microporosity, although both carbons possess abundant mesopores (Table 1.1). Similarly, Saeidi et al. (2020)[112] reported that PFAS adsorption on AC felts is determined by micropore volume, with increased maximum adsorption capacity observed for felts with more pores in the 1–2 nm range.

Thus, both micropores and mesopores can be essential for PFAS adsorption, with different conditions determining which pore domain becomes limiting. Micropores are particularly important for short-chain PFAS, which are small enough to enter these narrow structures. Long-chain PFAS, by contrast, experience stronger steric constraints and interact more extensively with mesopores, where they can accumulate at higher local concentrations and form aggregates or multilayers, as observed in Figure 3.1C. These mechanistic differences align with reported diffusion behavior: short-chain PFAS exhibit higher intraparticle diffusion coefficients and therefore face fewer kinetic limitations in accessing microporous regions, whereas long-chain PFAS diffuse more slowly along carbon surfaces, increasing their residence time within mesopores and promoting multilayer adsorption.[115] Overall, our data and literature review suggest that a micropore volume of at least ~0.3 cm^3/g is required to avoid micropore limitation at drinking water treatment conditions. Beyond this threshold, increased mesopore volume is associated with enhanced adsorption capacity

The second example concerns single-solute long-chain PFAS adsorption data for 1240C AC, shown as purple data points in Figure 3.5E from the study by Zhi et al. (2015).[113] These data are above the PFAS master curve, indicating better adsorption performance compared to F400 AC after normalization for mesopore volume. To understand this enhanced performance, the surface chemistry of the ACs must be considered. Among the ACs shown in Figure 3.4E, 1240C contains roughly four times fewer acidic functional groups than the others (Table 3.1). When this difference is accounted for, by normalizing adsorption capacity to the concentration of surface functional groups in addition to mesopore volume, the 1240C data align with the master curve (Figure 3.4F). Although 1240C contains relatively few mesopores, its low negative surface charge facilitates PFAS adsorption. This observation aligns with previous studies showing that a lower negative surface charge enhances PFAS affinity for AC surfaces.[74,107]

In conclusion, Figure 3.5 shows that PFAS total isotherms from this study and the literature coincide onto a single master curve once all adsorption-governing factors are accounted for. For the SRD and CS carbons used to establish the curve, mesopores act as the adsorption-limiting factor because both carbons already contain sufficient microporosity and have similar surface charge, meaning neither of these properties restricts PFAS adsorption. Carbons that lack one of these prerequisites, such as H4000 and N400 with low microporosity or 1240C with distinct surface charge, deviate from the curve until the relevant adsorption-governing factor is included in the normalization.

3.4. Conclusions

This study demonstrates that expressing PFAS adsorption data as total PFAS isotherms provides a robust framework for evaluating and comparing adsorption behaviour across different experimental conditions and activated carbons (ACs). Presenting data in this form eliminates the influence of situational experimental factors, such as adsorbent dose or initial PFAS concentration, that typically complicate cross-study comparisons. Using this approach, we found that the commonly reported increase in PFAS adsorption capacity for smaller AC particles does not persist once the effect of carbon dose is removed. This indicates that the apparent particle-size dependence observed in conventional isotherms can arise from situational experimental factors rather than intrinsic adsorption behaviour.

Using the total isotherm approach, we identified several adsorption-governing properties that control PFAS adsorption. Both micropores and mesopores are important. Our analysis suggests that a micropore volume of roughly 0.3 cm^3/g is required to avoid micropore limitation drinking-water treatment conditions. Beyond this threshold, mesopores become the dominant factor determining adsorption capacity. Mesopores provide the pore space in which PFAS can accumulate at high local concentrations and adsorb in multilayers when adsorption space is limited. Surface chemistry also plays a key role: carbons with fewer acidic (negatively charged) functional groups exhibit higher adsorption capacities, indicating that low negative surface charge favours PFAS adsorption. Together, these findings suggest that ACs optimized for PFAS removal should combine sufficient microporosity, high mesopore volume, and a low density of acidic surface groups. The total isotherm framework further reveals how competition and matrix effects, such as the presence of NOM, act as adsorption-governing factors that can systematically reduce PFAS adsorption.

Further work is needed to quantify and normalize the effects of NOM and other matrix constituents on total PFAS isotherms, thereby extending this framework to other water systems such as wastewater effluents. With continued development, the total PFAS isotherm framework can serve as a standardized tool for comparing adsorption performance, identifying adsorption-limiting mechanisms, and guiding the rational design of next-generation ACs for PFAS removal.

3.5. Supplementary information for Chapter 3

Table S.3.1. Properties of PFAS used in this study[a]

Compound name	Abbreviation	Formula	Mw (g/mol)	pK_a	$Log_{Ko}w$
Perfluorobutane sulfonic acid	PFBS	$C_4F_9SO_3H$	300.10	-3.31	1.82
Perfluorohexane sulfonic acid	PFHxS	$C_6F_{13}SO_3H$	400.11	0.14	3.16
Perfluorooctane sulfonic acid	PFOS	$C_8F_{17}SO_3H$	500.13	< 1.0	4.49
Perfluoropentanoic acid	PFPeA	C_4F_9COOH	264.05	0.34	3.01
Perfluorooctanoic acid	PFOA	$C_7F_{15}COOH$	414.07	-0.5 - 4.2	4.81
Perfluorononanoic acid	PFNA	$C_8F_{17}COOH$	464.08	-0.21	5.48
Perfluorooctane sulfonamide	FOSA	$C_8H_2F_{17}NO_2S$	499.14	3.37	5.8
Hexafluoropropylene oxide dimer acid	GenX	$C_6HF_{11}O_3$	330.05	2.82	2.58

[a] For GenX information obtained from Vakili et al. (2021)[67], and for other PFAS from Gagliano et al. (2020)[13]

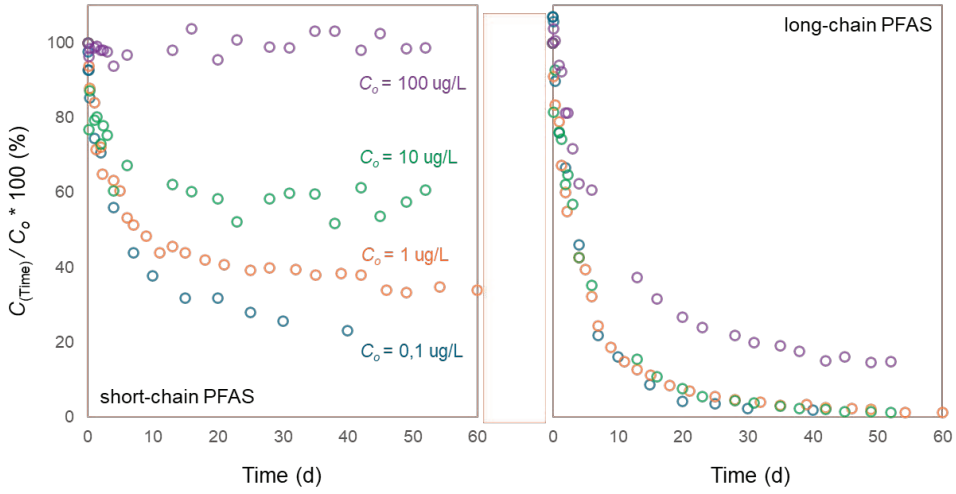


Figure S.3.1. PFAS kinetic curves at different initial PFAS concentrations for SRD activated carbon

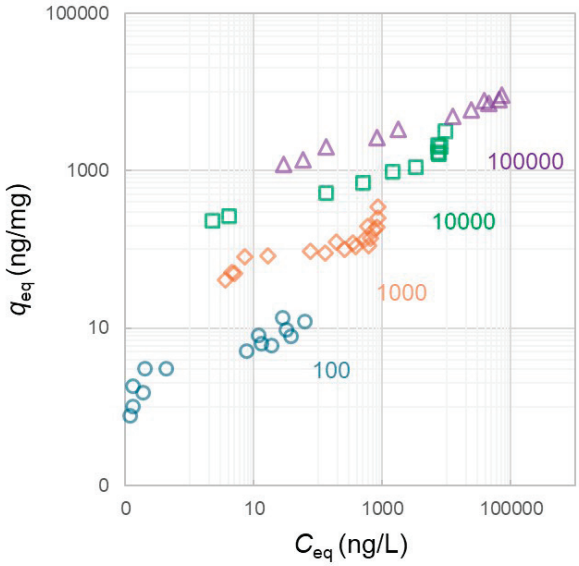
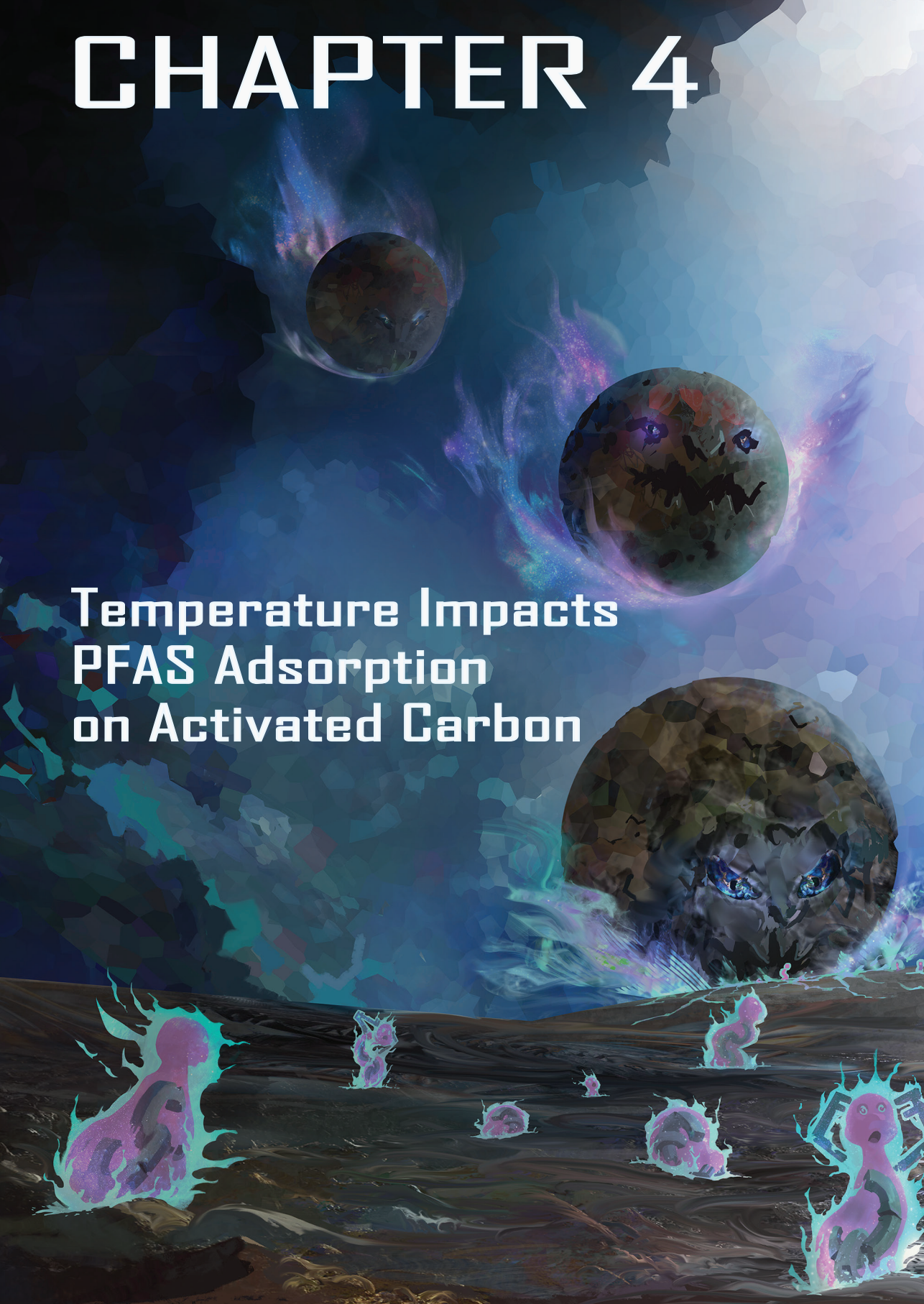


Figure S.3.2. Long-chain PFAS adsorption equilibrium on CS carbon. Experimental data obtained for several concentration ranges with an initial concentration c_0 of ~ 100 ng/L (blue circles), c_0 ~ 1000 ng/L (orange diamonds), c_0 ~ 10 µg/L (green squares), c_0 ~ 100 µg/L (purple triangles)

CHAPTER 4

Temperature Impacts PFAS Adsorption on Activated Carbon



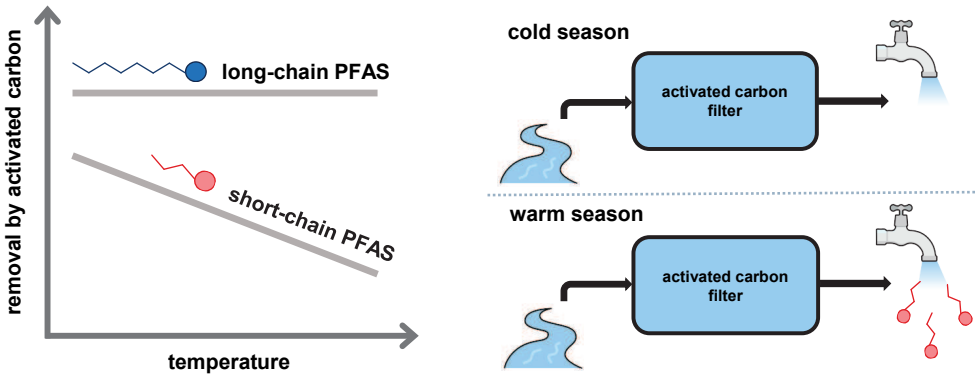
This chapter has been published as:

Pranić, M.; Zhou, K.; Biesheuvel, P. M.; van der Wal, A.; Dykstra, J. E. Temperature Impacts PFAS Adsorption on Activated Carbon. ACS ES&T Water 2025. https://doi.org/10.1021/acsestwater.5c00343.

Abstract:

While PFAS adsorption on activated carbon has been widely studied, the effect of temperature at environmentally relevant concentrations remains unclear. This study investigated the adsorption of eight PFAS at 10, 20, and 30 °C. Short-chain PFAS adsorption decreased up to fourfold by a temperature increase from 10 to 30 °C, whereas long-chain PFAS were minimally affected. The Freundlich isotherm described all equilibrium adsorption data with a single parameter value of n = 0.5. The Langmuir model provided a good fit for all short-chain PFAS, but failed to yield a consistent maximum adsorption capacity (q_{max}) at different temperatures. Extending Langmuir to the Frumkin isotherm provided a constant q_{max} and revealed that reduced short-chain PFAS adsorption at higher temperatures is due to increased lateral interactions between adsorbed molecules. Kinetic analysis showed that intraparticle diffusion coefficients increased with temperature, with stronger effects for short-chain PFAS. Using isotherm and kinetic parameters breakthrough curves predictions showed that for short-chain PFAS, an increase in temperature from 10 to 30 °C reduced the number of treated bed volumes before breakthrough by a factor of three, whereas long-chain PFAS remained unaffected. These findings highlight the importance of considering temperature effects in PFAS removal using activated carbon.

Graphical abstract:



Keywords: PFAS adsorption, temperature effects, drinking water treatment, breakthrough curves

4.1. Introduction

Per- and polyfluoroalkyl substances (PFAS) are persistent organic molecules that are increasingly subject to stringent regulatory limits regarding their presence in drinking water. The proposed EU drinking water directive is expected to set a maximum allowable concentration of 4.4 ng/L for the sum of PFAS,[19] while the US EPA has established limits ranging from 4 to 10 ng/L, depending on the specific compound.[17] To meet these strict standards, drinking water treatment facilities primarily rely on adsorption using activated carbon (AC).[25,131] However, early PFAS breakthrough at concentrations exceeding regulatory limits necessitates frequent regeneration of the adsorbent bed, significantly increasing treatment costs.[36] Strategies such as extending residence time or reducing the concentration of competing organic matter have been implemented to enhance PFAS removal.[36,88] However, a fundamental understanding of PFAS adsorption mechanisms at environmentally relevant ng/L concentrations remains limited, while advancing this understanding could lead to other strategies to improve removal efficiency.

The most fundamental way to describe adsorption is through adsorption isotherms, which represent the equilibrium relationship between the concentration of a solute in a liquid and on an adsorbent.[30,34] Temperature can significantly affect the adsorption equilibrium.[132,133] Although numerous adsorption isotherms for different PFAS molecules on various materials, such as activated carbon, have been reported,[13] the effect of temperature on PFAS adsorption has rarely been addressed, and existing results remain inconsistent. Some studies indicate a decrease in adsorption with increasing temperature, suggesting that PFAS adsorption is an exothermic process. For instance, Qian et al. reported that PFOS adsorption on boehmite decreased as temperature increased from 20 °C to 40 °C.[134] Similarly, Omo-Okoro et al. observed a reduction in PFOS and PFOA adsorption on chemically activated corn tassel biochar as the temperature rose from 25 °C to 45 °C.[135] In contrast, other studies have reported an increase in adsorption with temperature. Guo et al. found that increasing the temperature from 15 °C to 35 °C enhanced PFOS adsorption on corn straw biochar.[136] Qian et al. showed that PFOS adsorption on powdered AC increased as water temperature rose from 20 °C to 40 °C,[137] and Xu et al. demonstrated that PFOS and PFOA adsorption on polyaniline nanotubes increased for the 15 - 55 °C range.[138]

There are significant challenges in applying findings from these studies to drinking water treatment. Importantly, experiments were conducted at PFAS concentrations in the µg/L or mg/L range, which are representative of industrial wastewater. A previous study has shown that data from high-concentration studies cannot be extrapolated to the low ng/L concentrations relevant to drinking water.[115] Moreover, studies have focused exclusively on PFOS and PFOA, leaving the effects of temperature on short-chain PFAS largely unknown. Lastly, studies have not explored the use of granular activated carbon (GAC) types, such as coal-based carbon, which are commonly applied in drinking water treatment for PFAS removal. Given

the conflicting findings, with some studies reporting an increase in adsorption with temperature and other a decrease, it remains challenging to draw definitive conclusions regarding the effects of temperature on PFAS adsorption in drinking water treatment.

Understanding the effects of temperature on PFAS adsorption provides valuable insights for both theory, and practice. Determining the temperature dependence of isotherm parameters can provide insights into the nature of adsorption interactions and whether they are strengthened or weakened by temperature variations.[139,140] Additionally, kinetic studies can provide valuable information on the influence of temperature on intraparticle diffusion.[98,104] The intraparticle diffusion coefficients, which are temperature dependent, are essential for predicting full-scale breakthrough curves and designing efficient adsorbent bed filters.[30,82] For drinking water utilities, anticipating reduced PFAS removal due to temperature fluctuations is important. It remains unclear whether seasonal variations can significantly impact adsorption efficiency. For instance, in Spain, the temperature of treated surface water ranges from 10 to 29 °C throughout the year.[141] A better understanding of the temperature dependence of PFAS adsorption would enable drinking water utilities to anticipate periods of reduced removal efficiency and implement proactive measures to mitigate breakthrough risks.

In this study, we conducted experiments to investigate the impact of temperature on PFAS adsorption onto GAC. Unlike previous studies that typically examine temperature effects at PFAS concentrations representative of industrial wastewater, our experiments were performed in the ng/L levels, reflecting conditions in drinking water treatment. We generated adsorption isotherms and kinetic data at 10 °C, 20 °C, and 30 °C for eight distinct PFAS compounds, both short- and long-chain. We applied several isotherm models to describe the PFAS adsorption data, including the widely used Freundlich and Langmuir models, as well as the less commonly applied Frumkin isotherm, which accounts for interactions between adsorbed PFAS molecules.[142] The resulting isotherm parameters are discussed in terms of their practical and theoretical implications. Also, we used a homogeneous surface diffusion model to describe the kinetic data and quantify the temperature dependence of surface diffusion coefficients.[30] Finally, we used the isotherm and kinetic data to estimate PFAS breakthrough curves, discussing the implications of temperature variations on PFAS removal during drinking water treatment.

4.2. Materials and methods

4.2.1. Activated carbon

In this study, thermally activated and reagglomerated bituminous-based granular activated carbon (SRD) from Chemviron was used. This carbon has properties similar to the frequently applied Filtrasorb 400 (F400).[143] The SRD particles were sieved to obtain a diameter range of 0.60 – 0.85 mm. The particles were thoroughly washed with demineralized water, dried, and stored. Prior to the adsorption experiments, the particles were dried at 105 °C for 24 hours to eliminate any moisture. The dried GAC was weighed, boiled to remove entrapped air, cooled to room temperature, and then added to the batch bottles.

4.2.2. PFAS

Eight PFAS compounds with varying chain lengths and functional groups were selected for this study. The short-chain PFAS included PFBS, PFPeA, and GenX, while the long-chain PFAS comprised PFHxS, PFOS, PFOA, PFNA, and FOSA. The properties of these selected PFAS are detailed in Table S.4.1.

4.2.3. Adsorption experiments

Isotherm and kinetic batch experiments were conducted in 0.5 L polypropylene copolymer (PPCO) bottles (Thermo Scientific, USA). The adsorption system in each bottle consisted of a mixture of eight PFAS compounds with an initial concentration of ~ 1000 ng/L, a certain amount of GAC (1-30 mg/L), and Milli-Q water buffered at pH ~ 7.2 with phosphate buffer (5 mM Na_2HPO_4 + 5 mM KH_2PO_4) to have a conductivity similar to tap water (~800 µS/cm), and to keep pH constant during the experiment.

Adsorption experiments were conducted in temperature-controlled incubators (Innova44, New Brunswick) to keep the temperature of the solution inside the bottles at 10 °C, 20 °C, or 30 °C. The incubators were operated at 150 rpm for 60 days to ensure the adsorption process reached equilibrium. To obtain isotherms, samples were taken at the start (before GAC addition) and after 60 days. Samples were filtered (1000 µm Glass Fiber, Acrodisc) and stored in 2 mL polypropylene Eppendorf tubes at -20°C. Multiple freezing and thawing cycles did not impact the concentration of PFAS. Kinetic experiments were conducted at GAC loadings of 5 and 20 mg/L under all temperatures, with samples taken periodically over 60 days. The blank control showed no significant PFAS losses due to adsorption on the bottle walls.[115]

4.2.4. Determination of PFAS concentration

Measurements of PFAS concentrations were performed with the SCIEX 5500+ LC-AD30 system, equipped with a Phenomenex Kinetex C18 column. Quantification limits for measured PFAS were determined at 2.5 ng/L. Details about the analysis can be found in Pranic et al., 2025.[115]

4.2.5. Data analysis

4.2.5.1. Isotherms

The amount of PFAS adsorbed onto activated carbon is determined using the mass balance

$$q_{eq} = \frac{V_l}{m_{GAC}}\left(c_0 - c_{eq}\right) \tag{4.1}$$

where q_{eq} is the adsorbent loading in equilibrium (ng_{PFAS}/mg_{GAC}), V_l is the volume of the bulk solution (L), m_{GAC} is the mass of dry activated carbon, c_0 is the starting concentration of PFAS in the bulk solution, and c_{eq} is the concentration of PFAS in equilibrium.

The adsorption equilibrium data were described using three isotherm models: Freundlich, Langmuir and Frumkin (Table 4.1). These models were selected because they are widely applied and provided a good fit to the experimental data (Section 4.3.1). Non-linear regression was employed to estimate the isotherm model parameters from the equilibrium data.

Table 4.1. Isotherms used in this study

Isotherm	Equation	Parameters
Freundlich[48,144]	$q_{eq} = K_f {c_{l,eq}}^n$	K_f – adsorption coefficient (ng/mg)/(ng/L)^n n – adsorption intensity (-)
Langmuir[48,144]	$q_{eq} = \frac{q_{max} K_L c_{l,eq}}{1+K_L c_{l,eq}}$	q_{max} – maximum adsorption capacity [ng/mg] K_L – Langmuir constant [L/ng]
Frumkin[145]	$q_{eq} = \frac{q_{max} K_L c_{l,eq} e^{-\alpha\theta}}{1+K_L c_{l,eq} e^{-\alpha\theta}}$	α – lateral interaction parameter (-) θ – surface saturation (-)

q_{eq} – adsorbent loading in equilibrium [ng/mg]; $c_{l,eq}$ – concentration of adsorbate in bulk in equilibrium [ng/L]

To facilitate the estimation of Frumkin isotherm parameters, the Frumkin equation can be formulated as

$$c_{l,eq} = \frac{1}{K_L}\ \frac{q_{eq}}{q_{max} - q_{eq}} e^{\alpha\theta} \tag{4.2}$$

where surface saturation, θ, is defined as

$$\theta = \frac{q_{eq}}{q_{max}} \tag{4.3}$$

4.2.5.2. Kinetic model

The intraparticle mass transport can be explained by two distinct mechanisms, with one mechanism typically prevailing over the other. One mechanism is pore diffusion, which involves the movement of the adsorbate through the liquid within the adsorbent pores. The other mechanism is surface diffusion, which pertains to the transport of the adsorbate along the internal surface of the adsorbent particle.[30] Our previous study showed that the homogenous surface diffusion model (HSDM) can provide a good description of PFAS intraparticle transport.[115] The governing equation of HSDM is

$$\frac{\partial q_p}{\partial t} = \frac{1}{r^2}\frac{\partial}{\partial r}\left(r^2 D_s \frac{\partial q_p}{\partial r}\right) \tag{4.4}$$

where q_p (ng/mg) is the amount of molecules adsorbed per mass of adsorbent, i.e., the adsorbent loading, t (s) is the time, r (m) is the radiant coordinate, D_s (m^2/s) is the surface diffusion coefficient, which we treat as a fitting parameter. The initial and boundary conditions, the assumptions of the model, and the numerical method used to solve these equations can be found in Pranic et al., 2025.[115] In the HSDM, the adsorption equilibrium, i.e., the isotherm, is evaluated at the particle's outer boundary.

The surface diffusion coefficient D_s is typically temperature-dependent.[30,98,104,146] Because D_s is a critical parameter in the design of activated carbon filters, understanding the impact of temperature on D_s provides valuable insights for optimizing adsorption processes.

4.3. Results and discussion

4.3.1. Impact of temperature on PFAS isotherms

Adsorption isotherms for a mixture of eight PFAS compounds, with starting concentrations of ~ 1000 ng/L, were obtained for granular activated carbon (GAC) at temperatures of 10 °C, 20 °C, and 30 °C. The experimental equilibrium data, fitted using the Freundlich isotherm, are shown in Figure 4.1. The exact values of experimental data points are provided in Section 4.5.5.

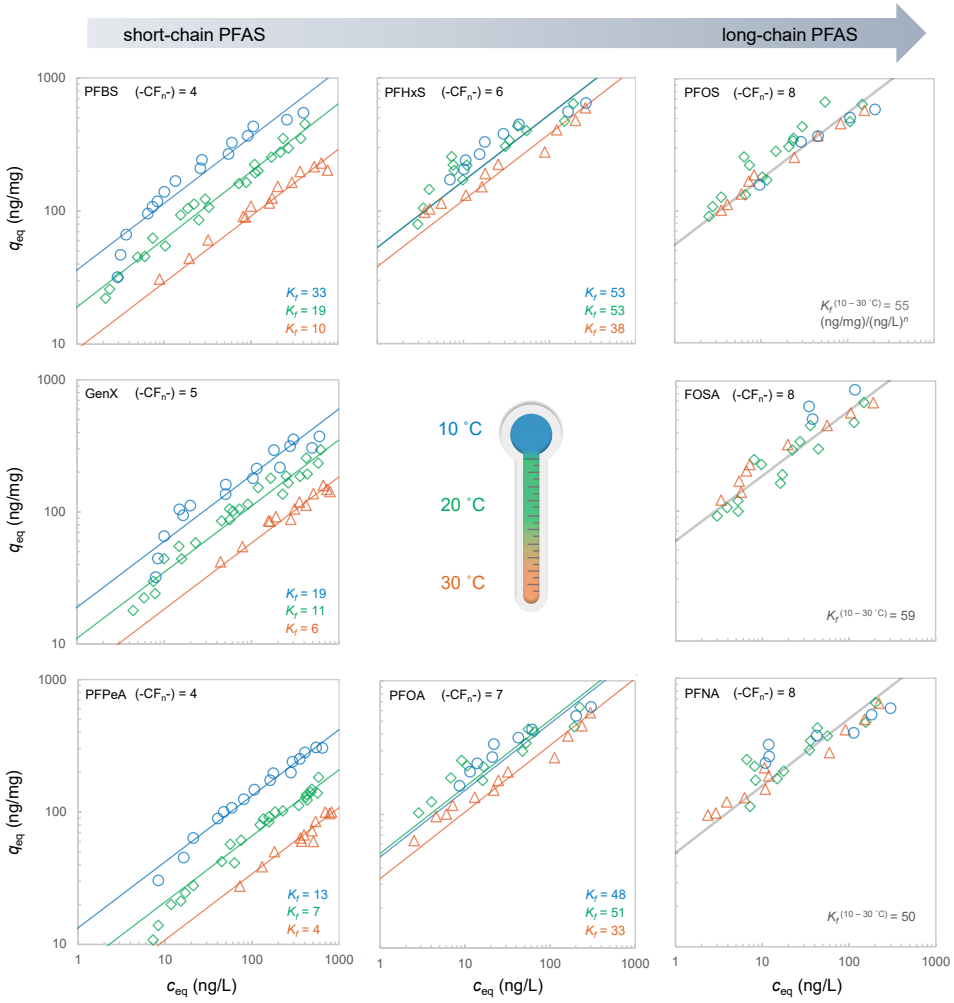


Figure 4.1. Adsorption of PFAS on granular activated carbon at different temperatures. Equilibrium data at 10 (blue circles), 20 (green diamonds), and 30 ˚C (brown triangles), described with the Freundlich isotherm (full lines). All data sets were fitted with an adsorption intensity of $n = 0.5$.

Figure 4.1 shows that temperature significantly affects the isotherms of short-chain PFAS. As the temperature increases from 10 °C to 30 °C, the adsorption capacity of PFBS, PFPeA, and GenX decreases at the same equilibrium concentration in solution, resulting in a 3- to 4-fold reduction in the Freundlich K_f values. This reduction indicates that the adsorption of short-chain PFAS on reagglomerated coal-based GAC is an exothermic process. In contrast, the adsorption of long-chain PFAS is less affected by temperature changes. Adsorption of PFAS with 6 (PFHxS) and 7 (PFOA) fluorinated carbons remains unchanged between 10 °C and 20 °C, with only a slight reduction at 30 °C. For PFAS with 8 fluorinated carbons (PFNA, PFOS, FOSA), adsorption remains the same for all tested temperatures. The relative temperature insensitivity of hydrophobic long-chain PFAS may be attributed to entropic effects, which have been reported to dominate in hydrophobically driven adsorption processes.[133] The clear dependence of temperature sensitivity on chain length suggests that ultra short-chain PFAS, such as trifluoroacetic acid, with only 1 fluorinated carbon, may be highly sensitive to temperature fluctuations. Although these compounds are highly mobile and challenging to remove with GAC,[55] our findings suggest that temperature can be used as an operational parameter to enhance their removal. In summary, within the 10 - 30 °C range, short-chain PFAS show significant temperature sensitivity, whereas long-chain PFAS show only minor or no adsorption changes.

Importantly, the experiments in this study were conducted at relatively low, environmentally relevant, concentrations. Under these conditions, the carbon surface is unlikely to be saturated, particularly with strongly adsorbing long-chain PFAS that have high adsorption capacities on GAC.[13,147] This abundance of available adsorption sites for long-chain PFAS likely minimizes the impact of temperature changes on their adsorption. In contrast, short-chain PFAS, with fewer available adsorption sites, are more prone to exhibit greater sensitivity to temperature variations.

In Figure 4.1, the empirical Freundlich isotherm was applied to describe the equilibrium PFAS adsorption data. This widely used model describes data well using a single value of the Freundlich parameter, $n = 0.5$. This finding is significant, as it implies that for PFAS adsorption on activated carbon, only one parameter, K_f, needs to be fitted, simplifying the process – particularly for datasets with limited data points. Furthermore, setting $n = 0.5$ simplifies the unit conversion between ng/L concentrations, relevant for drinking water treatment, and mg/L, commonly used in wastewater applications. Specifically, with $n = 0.5$, the same values of K_f are obtained for both $(ng/mg)/(ng/L)^n$ and $(mg/g)/(mg/L)^n$ units, which is not possible with other values of n (see Section 4.5.2 for derivation). Additionally, with the same value of n, comparing K_f, i.e., the adsorption strength, between different PFAS, becomes straightforward.[30] Long-chain PFAS exhibit higher K_f values than short-chain PFAS, and among compounds with the same number of fluorinated carbons, sulfonic PFAS have higher K_f values than carboxylic PFAS (e.g., PFOS > PFNA; PFBS > PFPeA). These trends align with previous studies and are well-documented in the literature.[52,73,88–90] While the Freundlich

equation with n = 0.5 describes most of the data in Figure 4.1 reasonably well, deviations are observed for short-chain PFAS at low concentrations (<10 ng/L). Under these conditions, where adsorption sites are abundant and competitive effects are minimal, a linear isotherm may provide a more valid description of adsorption behaviour. Although the use of Freundlich equation with n = 0.5 offers several practical advantages, its empirical nature remains a limitation, providing limited insight into the underlying mechanisms of PFAS adsorption.

To better understand the mechanisms underlying the temperature dependency of short-chain PFAS adsorption, we applied the mechanistic two-parameter Langmuir isotherm and the three-parameter Frumkin isotherm models to fit the adsorption data. The resulting fits for PFPeA are shown in Figure 4.2A (Langmuir) and Figure 4.2B (Frumkin), while similar fits for other short-chain PFAS are provided in Figure S.4.1.

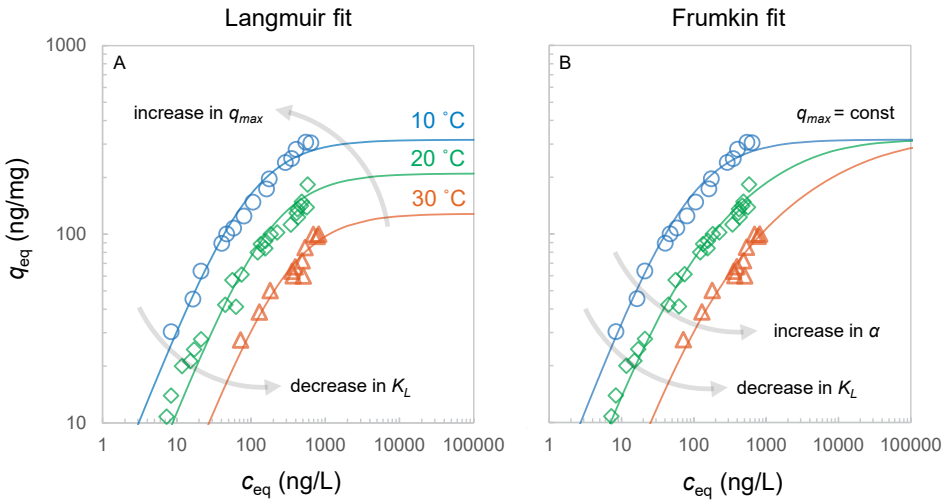


Figure 4.2. Adsorption equilibrium data at 10 (blue circles), 20 (green diamonds) and 30 ˚C (brown triangles), described with (A) Langmuir and (B) Frumkin isotherm (full lines) for adsorption of short-chain PFPeA on granular activated carbon. For two other short-chain PFAS, the fits are shown in Figure S.4.1. The values of fitted parameters, q_{max}, K_L, and α are in Table S.4.3.

Figure 4.2 shows that both the Langmuir and Frumkin isotherm models effectively describe the adsorption of short-chain PFAS. The simpler two-parameter Langmuir model provides a good fit only when both the maximum adsorption capacity, q_{max}, and the Langmuir constant, $K_{L,}$ decrease with increasing temperature (Figure 4.2A). The decrease in K_L value, which represents the ratio of adsorption to desorption rates, indicates a reduced adsorption affinity of short-chain PFAS at higher temperatures. It is widely accepted that K_L depends on temperature, while the temperature dependence of q_{max}, the other Langmuir parameter, remains debated.[132] According to Langmuir isotherm theory, q_{max} represents the fixed number of

adsorption sites on the adsorbent. Some studies argue that q_{max} is temperature-independent, reasoning that a change in the number of maximum adsorption sites with temperature lacks physical significance.[148,149] First, we kept q_{max} constant at all temperatures while fitting K_L for specific PFAS, but this approach was unsuccessful, as shown in Figure S.4.2. Instead, the Langmuir model only provided a good fit at different temperatures (Figure 4.2A) when q_{max} was treated as temperature-dependent. This aligns with findings from several other studies that also consider q_{max} to vary with temperature.[139,150,151]

To determine whether q_{max} in the Langmuir model should be temperature-dependent for short-chain PFAS adsorption, it is essential to consider the interactions between short-chain PFAS and GAC that impact q_{max}. Several interactions influence PFAS adsorption on activated carbon, including electrostatic interactions, the hydrophobic effect, ion exchange, and hydrogen bonding[13,54]. For short-chain PFAS, electrostatic interactions between the negatively charged PFAS head groups and charged sites on the carbon surface are the most significant.[13] While non-specific hydrophobic interactions between the adsorbate and adsorbent may cause q_{max} to depend on temperature,[152] the total number of charged sites on the adsorbent is unlikely to change within the 10 - 30 °C range. This suggests that if short-chain PFAS adsorption is primarily driven by electrostatic interactions, q_{max} should remain constant regardless of temperature. To enforce a constant q_{max}, we revisited a key assumption of the Langmuir isotherm - that adsorbed molecules do not interact with one another - and extended the Langmuir model to the three-parameter Frumkin equation.

The Frumkin isotherm model extends the Langmuir isotherm by introducing an additional fitting parameter, α, which accounts for lateral interactions between adsorbed molecules.[142,145] These kind of interactions have been experimentally observed in other studies.[127,153,154] When α equals 0, there are no lateral interactions, and the Frumkin equation simplifies to the Langmuir equation. As shown in Table S.4.3, for short-chain PFPeA, α is close to $\alpha = 0$ at 10 °C, but increases to approximately $\alpha = 4$ at 30 °C. This trend indicates that elevated temperatures enhance lateral interactions among adsorbed PFAS molecules. Lateral interactions can be attractive, driven by hydrophobic associations between PFAS tails, or repulsive, resulting from electrostatic repulsion between charged head groups.[142] At higher temperatures, increased molecular kinetic energy is expected to amplify these interactions. For short-chain PFAS, which typically exhibit weaker hydrophobic interactions, the dominant effect may be an increase in repulsive electrostatic forces, explaining reduction in short-chain PFAS adsorption with temperature increase. At sufficiently high equilibrium concentration (Figure 4.2B), the Frumkin isotherm can predict the same q_{max} across different temperatures, something that the Langmuir model cannot (Figure 4.2A). However, because three-parameter isotherm models allow multiple parameter combinations to fit the data, the Frumkin equation can also yield varying q_{max} values for the same dataset. This flexibility necessitates caution when interpreting the q_{max} values reported in this study. Further uncertainty in the exact value of q_{max} arises from the fact that real saturation is not observed in experimental data points

(Figure 4.2). Nevertheless, the observed increase in lateral interactions (α) with temperature remains consistent, even when different q_{max} values are used to fit the data in Figure 4.2B (see Figure S.4.3). Future studies on the temperature dependence of short- and long-chain PFAS adsorption should include single-compound systems to allow for more detailed mechanistic interpretation.

Besides q_{max} and α, K_L is the third parameter in the Frumkin equation. It has the same physical meaning as in the Langmuir model, representing the ratio of adsorption to desorption rates. In this study, the estimated K_L values from the Langmuir and Frumkin models are very similar. For short-chain PFAS, the observed K_L trend at a given temperature follows PFBS > GenX > PFPeA, consistent with previous findings.[115] The higher adsorption affinity of GenX compared to PFPeA can be attributed to its additional fluorinated carbon atom and branched structure, which enhance hydrophobic interactions with the carbon surface. The highest K_L value for PFBS is likely due to its sulfonic functional group, which is larger and less soluble than the carboxyl groups in GenX and PFPeA.[90]

4.3.2. Impact of temperature on PFAS kinetics

The adsorption kinetics of PFAS on granular activated carbon (GAC) were monitored over 60 days at carbon loadings of 5 mg/L and 20 mg/L to confirm equilibrium and assess the impact of temperature on adsorption kinetics. Figure 4.3 shows the concentration changes over time for (A) short-chain PFPeA and (B) long-chain PFNA at a carbon loading of 5 mg/L, while data for other PFAS at both loadings are presented in Figure S.4.4 – S.4.6.

During the first 8 days, no significant differences were observed in the kinetic curves at different temperatures for short-chain PFAS (Figure 4.3A). This can be attributed to the large number of available active sites on the GAC, enabling rapid adsorption with minimal temperature dependence. After 8 days, the kinetic curves for short-chain PFAS began to level off at different plateaus (Figure S.4.4), with higher adsorption observed at lower temperatures, consistent with the isotherm data (Figure 4.1). In contrast, the kinetic curves for long-chain PFAS showed only minor differences between temperature conditions (Figure 4.3B), in line with the trends observed in the isotherm data (Figure 4.1). To describe the intraparticle mobility of PFAS, we applied the homogeneous surface diffusion model (HSDM) to the kinetic data (see Eq. 4.4). As shown in Figure 4.3, the HSDM provides a good fit (R^2>0.95). The estimated PFAS surface diffusion coefficients, D_s, for all temperatures and carbon loadings are presented in Table S.4.4.

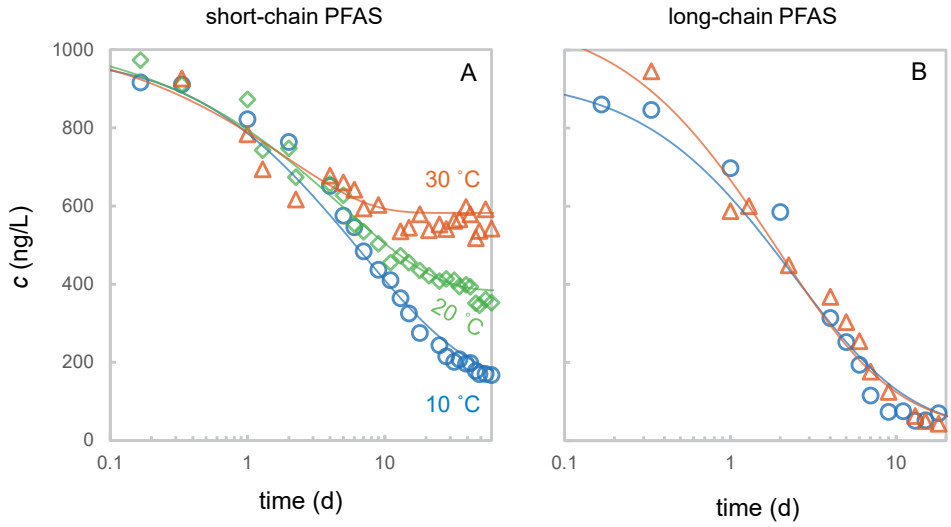


Figure 4.3 Concentration, *c* (ng/L), over time (d) for (A) short-chain PFPeA, and (B) long-chain PFNA at 10 (blue circles), 20 (green diamonds) and 30 ˚C (brown triangles), for a carbon dose of 5 mg/L. The data are described using homogenous surface diffusion model with a Freundlich isotherm (full lines). To improve clarity and avoid overlap, data for long-chain PFAS adsorption at 20 °C are omitted in panel (B)

Figure 4.4 shows that the surface mobility of PFAS molecules (D_s) increases with temperature. This mobility depends on the interaction strength between diffusing molecules and the adsorbent surface.[30] Weaker interactions lead to higher intraparticle mobility (higher D_s), which, in this study, is observed at higher temperatures, as indicated by the decreasing Langmuir constant (K_L). In other words, elevated temperatures increase molecular energy, facilitating desorption and diffusion to other adsorption sites.[103]

The importance of PFAS-carbon surface interactions in determining D_s is evident from two key observations in Figure 4.4. First, the lower D_s values for long-chain PFAS compared to short-chain PFAS are likely due to stronger interactions between long-chain PFAS and the surface during intraparticle transport. Second, for a specific PFAS at the same temperature, D_s is generally higher at a carbon loading of 5 mg/L than at 20 mg/L, where the surface is lower (see also Table S.4.4). At higher surface saturation, interactions during diffusion weaken, consistent with previous studies.[97–100] Additionally, for the most hydrophobic compound, FOSA (Figure 4.4E), D_s is not significantly impacted by temperature under low carbon loading, likely due to high surface saturation. Similarly, between 10 °C and 20 °C, no significant temperature effect on D_s is observed for other long-chain PFAS (Figure 4.4A, and 4.4C). Under conditions of high surface saturation, surface interactions have a reduced impact on intraparticle transport, particularly for strongly adsorbing PFAS, compared to scenarios with lower saturation (e.g., at higher carbon loadings).

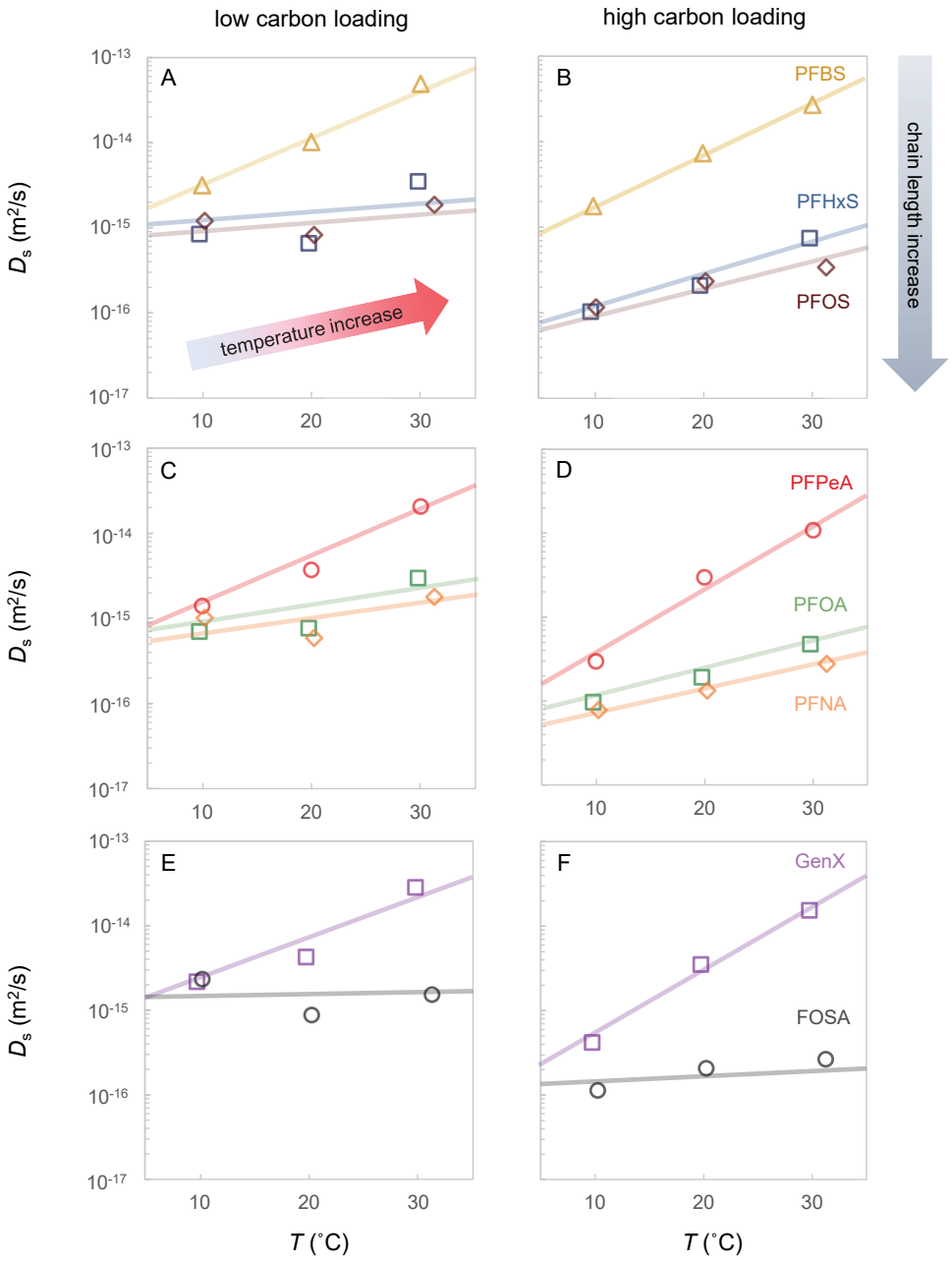


Figure 4.4. Estimated surface diffusion coefficients, D_s (m²/s), as a function of temperature at low (5 mg/L) and high (10 mg/L) carbon loadings for various PFAS. (A, B) PFAS with sulfonic functional groups: PFBS (yellow triangles), PFHxS (blue squares), and PFOS (brown diamonds). (C, D) PFAS with carboxylic functional groups: PFPeA (red circles), PFOA (green squares), and PFNA (orange diamonds). (E, F) Additional compounds: GenX (purple squares) and FOSA (black circles). Lines serve to guide the eye.

4.3.3. Implications for drinking water treatment

As discussed in previous sections, temperature significantly impacts the isotherm and kinetics for short-chain PFAS adsorption, whereas its effect on the adsorption of long-chain PFAS is less pronounced. The obtained isotherm and kinetic parameters enable the prediction of PFAS breakthrough curves. To achieve this, we integrated the homogeneous surface diffusion model (HSDM) with a mass balance equation for fixed-bed adsorbers (see Section 4.5.4).

Figure 4.5 illustrates the impact of temperature on the breakthrough of short-chain PFPeA, based on the isotherm and kinetic parameters estimated in this study. At 10 °C, breakthrough occurs at approximately 100,000 bed volumes, decreasing to about 50,000 at 20 °C and 25,000 at 30 °C. These results are primarily determined by the isotherm parameters. For instance, the Freundlich parameter K_f at 10 °C is approximately twice its value at 20 °C (Figure 4.1), allowing for twice as many bed volumes to be treated before breakthrough. While the isotherm determines the adsorption capacity (i.e., the start of breakthrough), the shape of the breakthrough curve is controlled by the surface diffusion parameter, D_s. At 30 °C, the higher D_s results in a breakthrough curve approaching the ideal case of instant intraparticle diffusion. In contrast, the lower D_s at 10 °C leads to slower diffusion and a more gradual breakthrough curve.

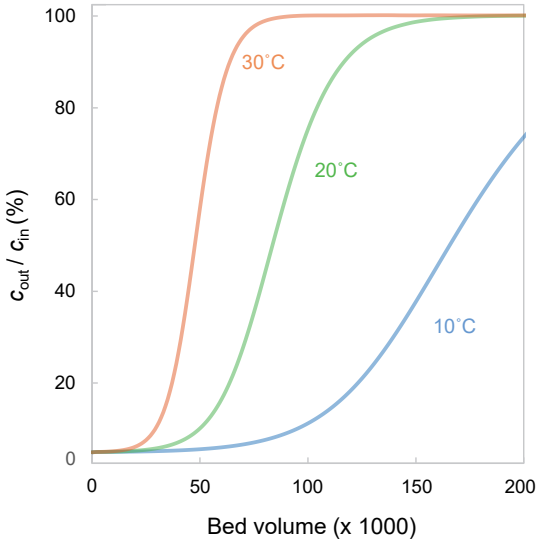


Figure 4.5. Breakthrough curves of short-chain PFAS predicted using the homogeneous surface diffusion model at 10 °C, 20 °C and 30 °C. Simulations are based on isotherm and kinetic parameters derived for PFPeA from batch experiments conducted in this study. Matrix effects and competitive adsorption between different types of PFAS are not included in the simulations.

Figure 4.5 highlights the significant influence of temperature on predicted breakthrough curves for short-chain PFAS adsorption. In contrast, for long-chain PFAS, the predicted breakthrough curves overlap (see Figure S.4.7), reflecting similar isotherm and kinetic parameters for the studied temperature range. It is important to note that PFAS competition is not accounted for in these predictions. As a result, treated bed volumes before breakthrough shown in Figure 4.5 are higher than those typically reported in the literature for short-chain PFAS, where breakthrough can occur earlier than 10,000 treated bed volumes.[57,75] Future studies could improve the HSDM model by incorporating PFAS competition. Additionally, experimental investigations of PFAS breakthrough curves at different temperatures would be valuable, as no such data are currently available. To the best of our knowledge, García-Mateos et al. (2015) and Pan et al. (2005) are the only studies examining the impact of temperature on solute breakthrough in aqueous systems. These studies reported earlier breakthrough for paracetamol when the temperature increased from 15 °C to 35 °C and for phenol from 25 °C to 40 °C, respectively.[155,156]

As mentioned, only a few studies have examined the impact of temperature on adsorbent breakthrough, likely because temperature variations are generally considered negligible in most water treatment applications. However, this assumption is often only valid for groundwater treatment. Surface water, on the other hand, shows significant seasonal temperature fluctuations.[141] For instance, Agudelo-Vera et al. (2020) reported seasonal temperature variations of 2–23 °C in The Netherlands, 2–26 °C in United Kingdom, and 10–28 °C in Spain. Such fluctuations could substantially affect the removal efficiency of short-chain PFAS, as demonstrated in Figure 4.5.

In our study, we used reagglomerated activated carbon, which has a high capacity for PFAS removal due to its high mesoporous surface area.[42,60,115] When carbons with lower adsorption capacities are used, such as microporous, coconut-based carbons, temperature effects are likely to be more pronounced. Furthermore, natural organic matter may further inhibit the adsorption of short-chain PFAS at elevated temperatures. A recent monitoring study by Nakazawa et al. (2023) reported reduced removal of short-chain PFAS in full-scale drinking water treatment plants during warmer periods, attributing this to increased competition with organic matter.[35]

Our study emphasizes the need to consider temperature effects on short-chain PFAS adsorption, particularly in areas with significant seasonal fluctuations. Conducting column studies at both the highest and lowest anticipated temperatures in drinking water treatment plants would provide valuable insights into the impact of temperature on the removal of short-chain PFAS. Such studies could help to guide the design, optimization, and risk management of treatment systems.

4.4. Conclusions

This study investigated the effect of temperature on PFAS adsorption onto activated carbon at ng/L concentration levels relevant for drinking water treatment. Isotherm and kinetic experiments were conducted at 10 °C, 20 °C, and 30 °C. For short-chain PFAS, the adsorption capacity decreased with increasing temperature, whereas for long-chain PFAS, adsorption capacity showed a slight reduction or remained unaffected. The adsorption equilibrium for all PFAS was accurately described by the Freundlich isotherm, with a constant adsorption intensity n = 0.5. For short-chain PFAS, the adsorption was also accurately described by the Langmuir and Frumkin isotherms. However, the Langmuir equation failed to yield a temperature-independent maximum adsorption capacity (q_{max}) for certain short-chain PFAS. By extending the Langmuir model to the Frumkin isotherm, we incorporated a lateral interaction parameter, α, enabling a single q_{max} value for specific PFAS. The increasing α with temperature suggests that short-chain PFAS are more sensitive to temperature due to lateral interactions. At higher temperatures, the increased α indicates that the interactions between adsorbed long-chain PFAS and short-chain PFAS molecules increased, leading possibly to a desorption of short-chain PFAS from the surface.

The intraparticle homogeneous surface diffusion model (HSDM) effectively described kinetic data across different temperatures. We found that the surface diffusion coefficient, D_s, increased with temperature for both long- and short-chain PFAS, with a stronger temperature dependency for short-chain compounds. At higher temperature, molecules have higher energy in the adsorbed state, facilitating desorption and diffusion to other adsorption sites.

The obtained isotherm parameters and D_s values were used to predict PFAS breakthrough curves at different temperatures. Increasing the temperature from 10 °C to 30 °C reduced the treated bed volumes before breakthrough by a factor of three for short-chain PFAS compounds. In contrast, temperature had no significant effect on long-chain PFAS breakthrough. The influence of temperature on breakthrough curves is often overlooked in studies; however, our findings show that this assumption is invalid for short-chain PFAS.

4.5. Supplementary Information for Chapter 4

4.5.1. PFAS properties

Table S.4.1. Properties of PFAS used in this study[a]

Compound name	Abbreviation	Formula	Mw (g/mol)	pK_a	$LogK_{ow}$
Perfluorobutane sulfonic acid	PFBS	$C_4F_9SO_3H$	300.10	-3.31	1.82
Perfluorohexane sulfonic acid	PFHxS	$C_6F_{13}SO_3H$	400.11	0.14	3.16
Perfluorooctane sulfonic acid	PFOS	$C_8F_{17}SO_3H$	500.13	< 1.0	4.49
Perfluoropentanoic acid	PFPeA	C_4F_9COOH	264.05	0.34	3.01
Perfluorooctanoic acid	PFOA	$C_7F_{15}COOH$	414.07	-0.5 - 4.2	4.81
Perfluorononanoic acid	PFNA	$C_8F_{17}COOH$	464.08	-0.21	5.48
Perfluorooctane sulfonamide	FOSA	$C_8H_2F_{17}NO_2S$	499.14	3.37	5.8
Hexafluoropropylene oxide dimer acid	GenX	$C_6HF_{11}O_3$	330.05	2.82	2.58

[a] For GenX information obtained from Vakili et al. (2021)[67], and for other PFAS from Gagliano et al. (2020)[13]

4.5.2. Isotherm data

As mentioned in the manuscript, with Freundlich parameter $n = 0.5$, the K_f value is independent of units of q_{eq} and $c_{l,eq}$. The transformation of the units of $c_{l,eq}$ from ng/L to mg/L and its impact on K_f is as follows
thus

K_{f2}	$\leftrightarrow$	K_{f1}
$\frac{\frac{ng}{mg}}{\left(\frac{ng}{L}\right)^n}$	$\leftrightarrow$	$\frac{\frac{10^6}{10^3}\frac{mg}{g}}{10^{6n}\left(\frac{mg}{L}\right)^n} = 10^{3-6n}\frac{\frac{mg}{g}}{\left(\frac{mg}{L}\right)^n}$

$$K_{f2} = 10^{3-6n} K_{f1} \quad \text{(S.4.1)}$$

or

$$K_{f1} = 10^{6n-3} K_{f2}. \quad \text{(S.4.2)}$$

According to Eq. S.4.2, when $n = 0.5$, the exponent (6n – 3) equals zero, so $K_{f1} = K_{f2}$. This explains why only for $n = 0.5$, the K_f value is independent of the concentration unit used, an outcome we also confirmed by the fitting process, which is shown in Table S.4.2. Furthermore Eq. S.4.1 and S.4.2 have also been reported in Worch [30].

Table S.4.2. Estimated K_f values in different units for different values of n. In this example, K_f was calculated from isotherm data for PFPeA at 20°C by maximizing R^2 using non-linear regression ($R^2 > 0.94$). The results show that only when $n = 0.5$ does the fitting produce the same K_f values, regardless of the unit in which adsorption data is presented.

n	K_f (ng/mg)/(ng/L)^n	K_f (mg/g)/(mg/L)^n
0.4	11.75	2.9
0.5	6.62	6.62
0.6	3.68	14.64

Table S.4.3. Estimated values of Langmuir and Frumkin isotherm parameters for short-chain PFAS adsorption at different temperatures

		Langmuir		Frumkin		
PFAS	T (°C)	Q_{max} (ng/mg)	K_L (L/ng)	Q_{max} (ng/mg)	K_L (L/ng)	α (-)
PFBS	10	528.82	0.0326	528.82	0.0360	0.8
	20	360.00	0.0222		0.0161	2.4
	30	231.74	0.0130		0.0058	4.4
GenX	10	351.93	0.0205	351.93	0.0200	0.1
	20	256.05	0.0119		0.0121	1.5
	30	186.78	0.0048		0.0036	3.1
PFPeA	10	316.50	0.0106	316.50	0.0120	0.2
	20	210.00	0.0057		0.0049	2.1
	30	128.46	0.0031		0.0014	3.1

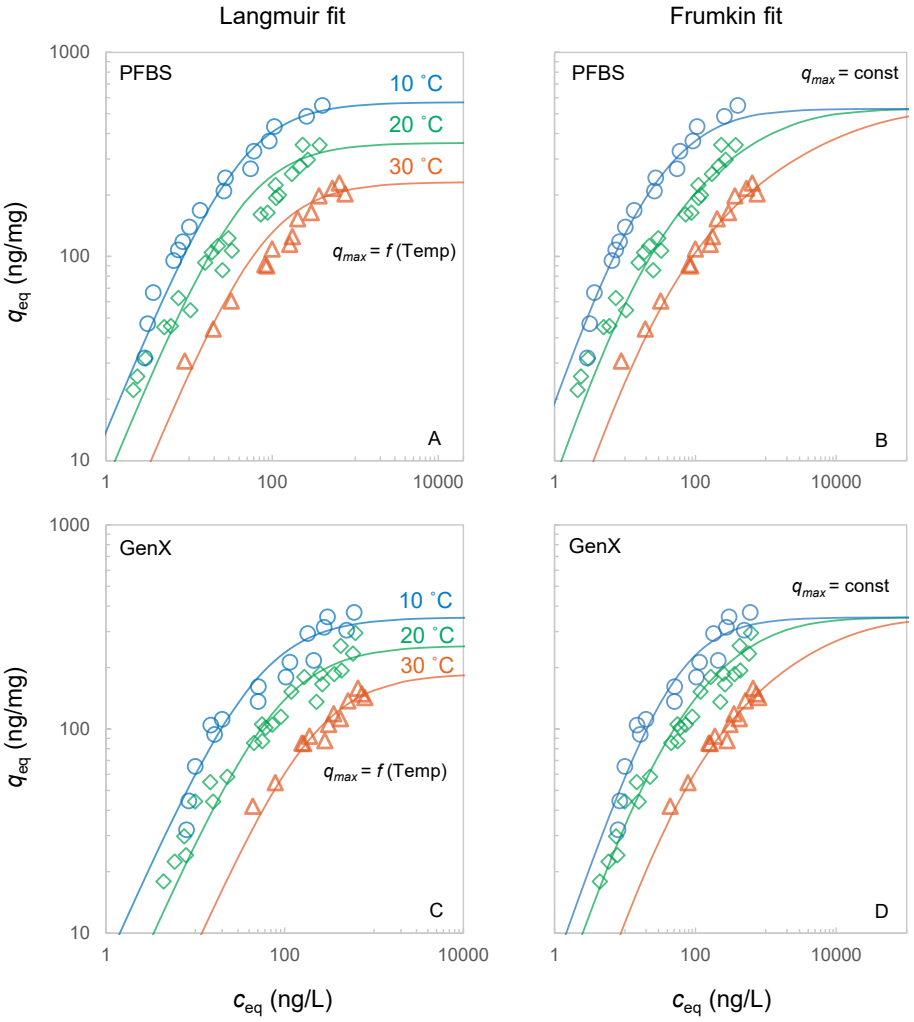


Figure S.4.1 Adsorption equilibrium data at 10 (blue circles), 20 (green diamonds) and 30 ˚C (brown triangles) are described with (A,C) Langmuir and (B,D) Frumkin isotherm (full lines) for PFBS (A,B) and GenX (C,D)

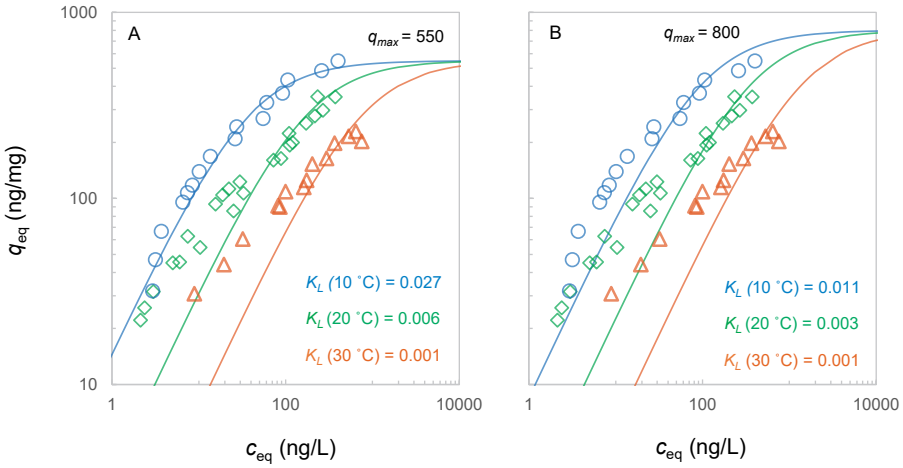


Figure S.4.2 Adsorption equilibrium data for PFBS at 10 °C (blue circles), 20 °C (green diamonds), and 30 °C (brown triangles) fitted with the Langmuir isotherm (solid lines) using two different maximum adsorption capacities (q_{max}): (A) 550 ng/mg and (B) 800 ng/mg. The Langmuir isotherm cannot fit the data at different temperatures with one value of q_{max}

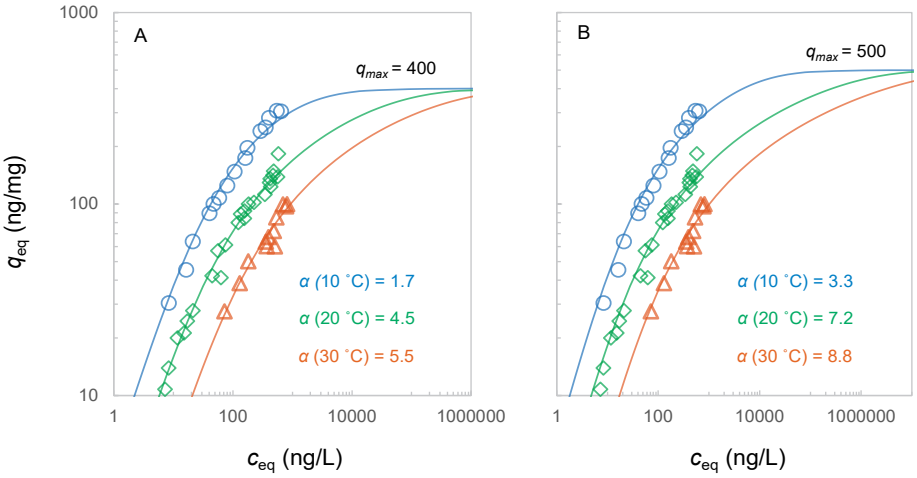


Figure S.4.3 Adsorption equilibrium data for PFPeA at 10 °C (blue circles), 20 °C (green diamonds), and 30 °C (brown triangles) fitted with the Frumkin isotherm (solid lines) using two different maximum adsorption capacities (q_{max}): (A) 400 ng/mg and (B) 500 ng/mg. The Frumkin parameter (*K*L) is kept constant for each specific temperature in both panels (*K*L10 °C =0.0120 L/ng, *K*L20 °C = 0.0049 L/ng, KL30 °C = 0.0014 L/ng). The three-parameter Frumkin isotherm can describe the data with multiple parameter combinations. However, when q_{max} is fixed, an increase in temperature consistently leads to a higher lateral interaction parameter (α) regardless of the chosen q_{max} value

4.5.3. Kinetic data

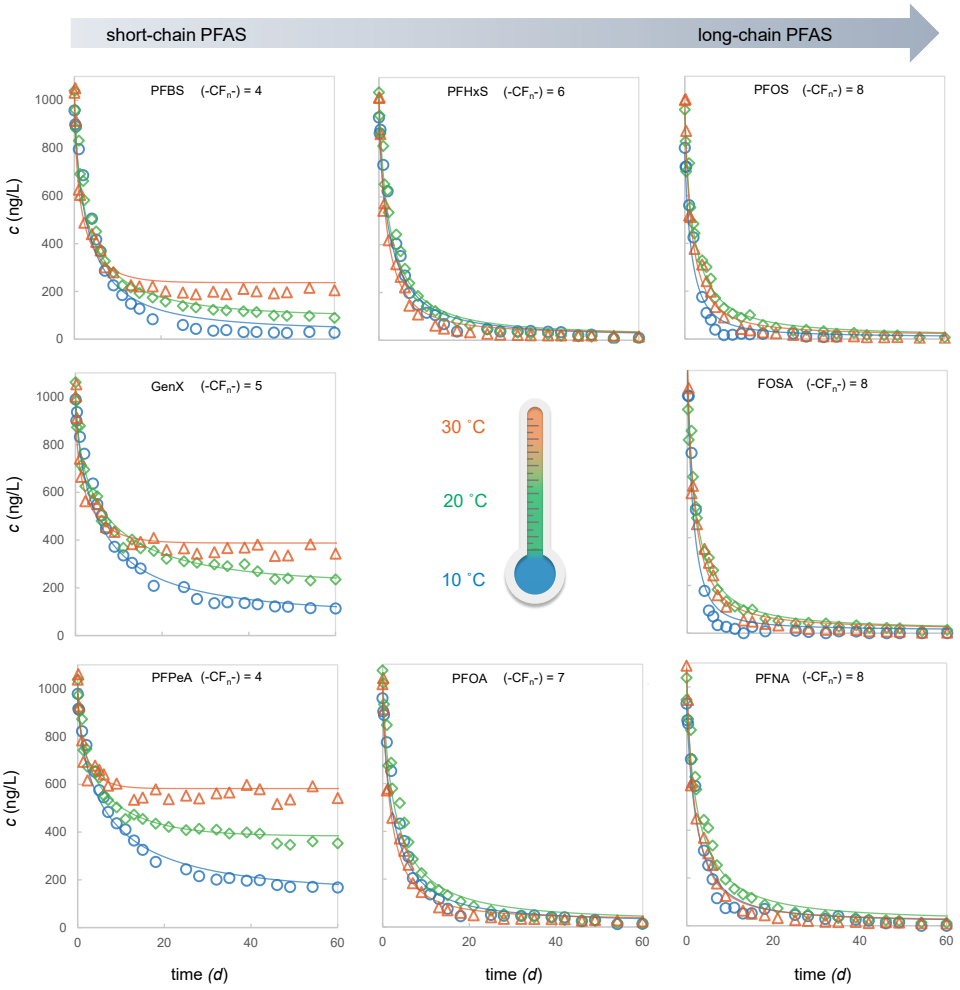


Figure S.4.4 Concentration, *c* (ng/L), over time (d) for (A) studied PFAS at 10 (blue circles), 20 (green diamonds) and 30 ˚C (brown triangles) under carbon dose of 5 mg/L, described with homogenous surface diffusion model utilizing the Freundlich isotherm (full lines). The data points in this figure are the same as those in Figure S.4.5 but are presented on a non-logarithmic x-axis to highlight the different adsorption plateaus for short-chain PFAS.

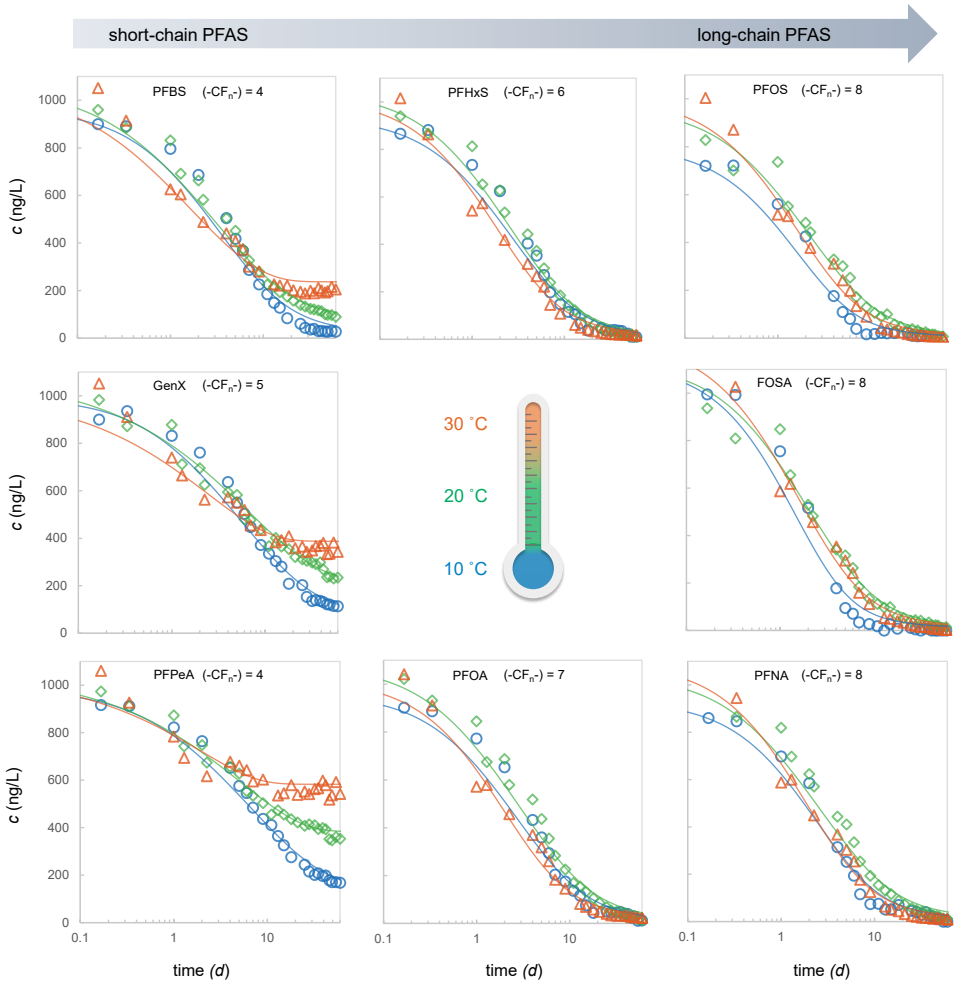


Figure S.4.5 Concentration, *c* (ng/L), over time (d) for (A) studied PFAS at 10 (blue circles), 20 (green diamonds) and 30 ˚C (brown triangles), under carbon dose of 5 mg/L described with homogenous surface diffusion model utilizing Freundlich isotherm (full lines). The data points in this figure are the same as those in Figure S.4 but are presented on a logarithmic x-axis to enhance clarity

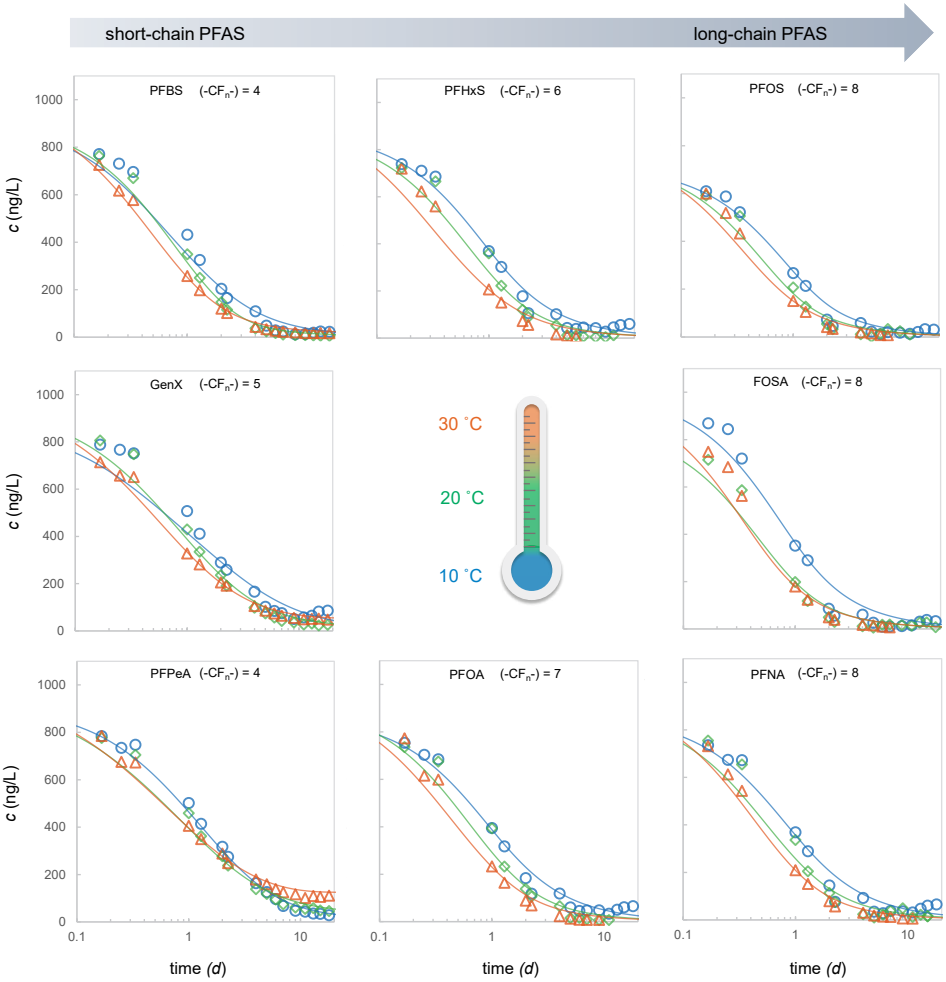


Figure S.4.6. Concentration, *c* (ng/L), over time (d) for (A) studied PFAS at 10 (blue circles), 20 (green diamonds) and 30 ˚C (brown triangles), under carbon dose of 20 mg/L described with homogenous surface diffusion model utilizing Freundlich isotherm (full lines).

Isotherm and Kinetic data points QR-Code

Table S.4.4. Estimated values of surface diffusion coefficient, D_s (m^2/s), for different experimental conditions in this study. D_s was estimated by utilizing Freundlich parameters reported in Figure 4.1.

PFAS	Experimental condition (temperature, carbon dose)					
	10 ˚C, 5 mg/L	10 ˚C, 20 mg/L	20 ˚C, 5 mg/L	20 ˚C, 20 mg/L	30 ˚C, 5 mg/L	30 ˚C, 20 mg/L
	D_s (m^2/s)					
PFBS	1.45E-15	3.03E-16	3.88E-15	2.83E-15	1.95E-14	1.11E-14
PFHxS	7.12E-16	9.69E-17	7.59E-16	1.94E-16	2.47E-15	4.81E-16
PFOS	1.41E-15	9.42E-17	7.65E-16	1.67E-16	1.25E-15	2.29E-16
PFPeA	3.57E-15	1.91E-15	8.39E-15	6.45E-15	2.82E-14	2.18E-14
PFOA	8.63E-16	1.03E-16	6.59E-16	1.89E-16	3.18E-15	7.54E-16
PFNA	1.09E-15	1.08E-16	7.45E-16	1.85E-16	1.51E-15	3.43E-16
FOSA	2.81E-15	1.13E-16	8.81E-16	2.09E-16	1.30E-15	2.68E-16
GenX	2.20E-15	3.24E-16	4.47E-15	3.80E-15	2.49E-14	1.66E-14

Table S.4.5. Parameters used to solve the HSDM and estimate values of D_s given in Table S.4.

Parameter*	Experimental condition (temperature, carbon dose)					
	10 ˚C, 5 mg/L	10 ˚C, 20 mg/L	20 ˚C, 5 mg/L	20 ˚C, 20 mg/L	30 ˚C, 5 mg/L	30 ˚C, 20 mg/L
ε_b^{batch} (-)	$6.68 \cdot 10^{-6}$	$2.70 \cdot 10^{-5}$	$6.72 \cdot 10^{-6}$	$2.70 \cdot 10^{-5}$	$6.74 \cdot 10^{-6}$	$2.70 \cdot 10^{-5}$
ρ_p (g/L)	753					
ε_p (-)	0.575					
r_p (m)	$3.625 \cdot 10^{-4}$					

*parameters used here are determined following procedure described in Pranic et al 2025[115], ε_b^{batch} is ratio of adsorbent mass and liquid mass, ρ_p is particle apparent density, ε_p is particle porosity, r_p is particle radius,

4.5.4. Breakthrough curve model for fixed bed adsorbers

To predict the PFAS breakthrough curves depicted in Figure 4.5 and Figure S.4.7, we employed the homogeneous surface diffusion model (HSDM) in combination with a fixed-bed adsorber material balance.

The differential material balance equation for the fixed-bed adsorber is

$$v_f \frac{\partial c}{\partial z} + \varepsilon_B \frac{\partial c}{\partial t} + \rho_B \frac{\partial \bar{q}}{\partial t} = 0 \qquad \text{(S.4.1)}$$

where multiplying the superficial velocity v_f (m/s) by the spatial concentration gradient $\partial c/\partial z$ gives the advection term. The accumulation term is represented by the product of the bed porosity and temporal concentration change $\partial c/\partial t$. Similarly, the adsorption term is given as a product of bed density ρ_B and the rate of change of the average adsorbed concentration $\partial \bar{q}/\partial t$. A detailed derivation of the mass balance (eq. S.4.1.) can be found in Worch.[30]

Next, we substitute $\partial \bar{q} / \partial t$ with the mass transfer equation that governs film diffusion

$$\frac{\partial \bar{q}}{\partial t} = \frac{k_F a_{VR}}{\rho_B}\left(c - c_s\right) \tag{S.4.2}$$

where k_F is film diffusion coefficient, and a_{VR} is the external surface area related to the reactor volume which for spherical particles is

$$a_{VR} = \frac{3}{r_P}\left(1 - \varepsilon_B\right) \tag{S.4.3}$$

The final differential mass balance is

$$v_f \frac{\partial c}{\partial z} + \varepsilon_B \frac{\partial c}{\partial t} + \frac{3k_F(1-\varepsilon_B)}{r_P}(c - c_s) = 0 \tag{S.4.4}$$

which when combined with surface diffusion model (Eq. 4.4) and the specific isotherm (Table 4.1) gives 3 dependent variables: the concentration in the bulk solution, c, the concentration on the surface of the particle, c_s, and the amount adsorbed q.

The initial conditions for model are defined as

$$q(t = 0, z, r) = 0 \tag{S.4.5}$$

and the boundary conditions for the model at the core of the granule (Eq. S.4.6) and at the edge of the granule (Eq. S.4.7) are

$$\left[\frac{\partial q(t,z,r)}{\partial r}\right]_{r=0} = 0 \tag{S.4.6}$$

$$\left[\frac{\partial q(t,z,r)}{\partial r}\right]_{r=0} = \frac{k_F}{\rho_P D_s}[c(t,z) - c_s(t,z)] \tag{S.4.7}$$

where ρ_P is the particle porosity.

To solve the HSDM combined with the mass balance equation for a fixed bed adsorber, we first transformed equations into its dimensionless form, as detailed in Worch [30]. The Method of Lines was then used to discretize the mass balance equation, and the resulting system was solved using a Runge-Kutta numerical algorithm implemented in MATLAB. Table S.4.6 lists the input parameters employed to generate the breakthrough curves for short-chain PFAS (Figure 4.5) and long-chain PFAS (Figure S.4.6).

Table S.4.6. Parameters used to predict PFAS breakthrough curves reported in Figure 4.5 for PFPeA and Figure S.4.6 for PFNA at 10, 20 and 30 ˚C. Surface diffusion coefficient, D_s, and Freundlich parameter K_f were estimated from kinetic and isotherm batch data respectively. To neglect the impact of film diffusion, K_f was kept constant regardless of the PFAS or temperature. Feedwater concentration, $c_{0,}$ was the same as initial concentration in batch experiments. Other parameters were selected to represent conditions in drinking water treatment

Parameter	Short-chain PFPeA			Long-chain PFNA		
Temperature (˚C)	10	20	30	10	20	30
D_s (m^2/s)	$3.57 \cdot 10^{-15}$	$8.39 \cdot 10^{-15}$	$2.82 \cdot 10^{-14}$	$1.09 \cdot 10^{-15}$	$7.45 \cdot 10^{-16}$	$1.51 \cdot 10^{-15}$
K_f (ng/mg)/(ng/L)^n	13	7	4		50	
k_F (m/s)			$4 \cdot 10^{-6}$			
n (-)			0.5			
c_0 (ng/L)			1000			
EBCT (min)			10			
r_p (m)			0.0005			
ε_b (-)			0.455			
ρ_b (g/L)			410			

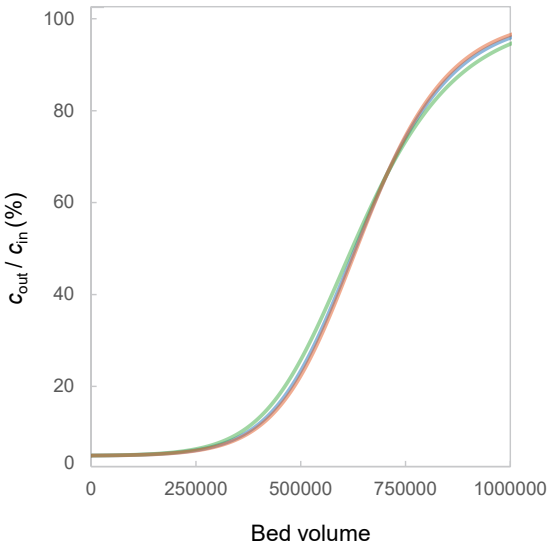


Figure S.4.7. Breakthrough curves of long-chain PFNA predicted using the homogeneous surface diffusion model at 10 °C, 20 °C and 30 °C. Simulations are based on isotherm and kinetic parameters derived for PFNA from batch experiments conducted in this study. Matrix effects or PFAS competition are not included in the simulations.

CHAPTER 5



Which Natural Organic Matter Components Limit PFAS Removal by Activated Carbon

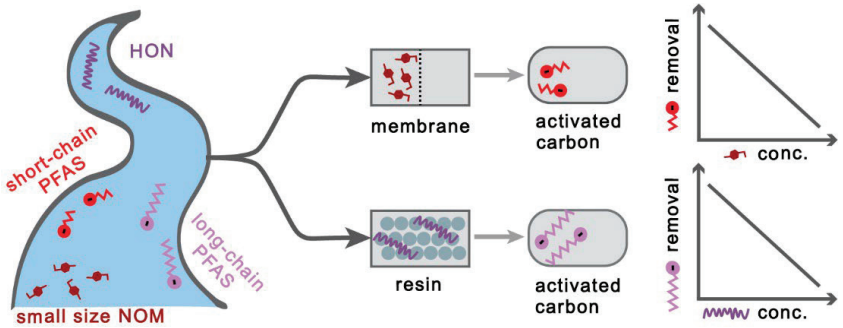
This chapter has been published as:

Pranic, M., Cantoni, B., de Ridder, D.J., Antonelli, M., Dykstra, J. E, van der Wal, A., (2026) Which natural organic matter components limit PFAS removal by activated carbon? Chem. Eng. J. doi. org/10.1016/j.cej.2026.178076

Abstract:

Per- and polyfluoroalkyl substances (PFAS) are persistent micropollutants subject to strict drinking water regulations. Although granular activated carbon treatment can effectively remove PFAS from water, early breakthrough, especially for short-chain PFAS, requires frequent regeneration and increases treatment costs. While many studies have related the presence of natural organic matter (NOM) to early breakthrough, the mechanisms affecting PFAS adsorption remain unclear. In this study, we used resin and membrane fractionation to isolate distinct NOM fractions based on chemical characteristics and molecular size. Batch isotherm, kinetic, and column experiments showed that the presence of the <3 kDa fraction significantly reduced short-chain PFAS adsorption. As low molecular weight compounds (<3 kDa) are consistently detected in source waters at concentrations comparable to or higher than those included in the present study, their removal is crucial to improving short-chain PFAS removal during drinking water treatment. Conversely, long-chain PFAS adsorption was not notably affected by molecular weight fractions but was significantly reduced in the presence of the hydrophobic neutral (HON) fraction. The HON fraction consists of compounds with similar molecular characteristics as long-chain PFAS, leading to direct competition for adsorption sites. The HON fraction is typically present at lower concentrations compared to other NOM fractions in natural waters. This low concentration of the HON fraction helps explain the delayed breakthrough observed for long-chain PFAS, in contrast to short-chain PFAS, whose breakthrough is rapid due to the high concentration of the <3 kDa fraction. We found that the presence of specific NOM fractions can indicate reduced PFAS removal, suggesting that NOM fractionation techniques could be integrated into monitoring procedures at drinking water facilities, as the presence of specific fractions can indicate reduced PFAS removal.

Graphical abstract:



Keywords: PFAS, natural organic matter, activated carbon, drinking water treatment

5.1. Introduction

Per- and polyfluoroalkyl substances (PFAS) are persistent, fluorinated micropollutants commonly detected in various water sources used for drinking water production.[7,16,37] Current European Union regulations set the maximum allowable total PFAS concentration in drinking water at 100 ng/L,[11] with a proposed revision lowering this limit to 4.4 ng/L.[19] Although numerous technologies are being explored for PFAS removal to meet these stringent standards, granular activated carbon (GAC) filtration remains the most widely implemented method in drinking water treatment plants.[42,157] While GAC filters can achieve the required low PFAS concentrations, early PFAS breakthrough, defined here as effluent concentrations exceeding regulatory limits, necessitates frequent regeneration of the GAC, significantly increasing operational costs.[24,36]

Although the mechanisms causing early breakthrough remain poorly understood, several studies have reported that competitive adsorption with natural organic matter (NOM) particularly affects the removal of short-chain, hydrophilic, PFAS. Gagliano et al. (2020) proposed two mechanisms to reduce short-chain PFAS adsorption: blockage of pore access by NOM and electrostatic repulsion from adsorbed negatively charged NOM. However, it is important to note that among the numerous experimental studies summarized in Gagliano et al. (2020), only 11 investigated PFAS removal with activated carbon in the presence of NOM, and just five of those included short-chain PFAS.[13] While these studies reported lower removal of short-chain PFAS in the presence of NOM, the mechanisms underlying the competition between short-chain PFAS and NOM remained speculative.[56,58,85,86,158]

In contrast to short-chain PFAS, the impact of NOM on the adsorption of long-chain PFAS has been studied more extensively, though findings remain inconsistent. For instance, Sgroi et al. (2018) observed similar breakthrough behaviour of PFOA, PFDA, and PFOS across varying NOM compositions and concentrations, suggesting minimal impact of NOM on adsorption.[159] Conversely, Pramanik et al. (2017) reported that both the concentration and composition of NOM significantly affected adsorption, with protein-rich NOM reducing adsorption through a combination of hydrophobic and electrostatic interactions.[160] Interestingly, McCleaf et al. (2017) observed that the removal capacity for long-chain PFAS increased as NOM accumulated in the GAC column.[57] They speculated that as NOM progressively blocked available adsorption sites, long-chain PFAS began to aggregate, resulting in enhanced removal.

As inferred from the previous two paragraphs, NOM-PFAS interactions are often speculative and highly dependent on experimental conditions. As also noted by Ateia et al. (2019),[55] studies investigating interactions between short-chain PFAS and NOM remain limited. For long-chain PFAS, NOM was found to decrease, increase or have no effect on adsorption. Consequently, there is a clear need for experimental studies to clarify the mechanisms behind

reduced short-chain PFAS adsorption in the presence of NOM and to resolve conflicting findings for long-chain PFAS. In the context of GAC-based drinking water treatment, such studies should use PFAS concentrations representative of real-world conditions, typically 1 µg/L or lower.[16,37] Maintaining low concentrations is essential, as PFAS adsorption mechanisms are concentration-dependent; higher concentrations can promote multilayer adsorption or aggregation, resulting in artificially high adsorption capacities that do not reflect actual treatment scenarios.[115] In addition, the concentration gradient itself can promote diffusion from the bulk solution to the carbon particles, which may contribute to an apparent removal that does not necessarily represent equilibrium adsorption behaviour.

The main challenge in clarifying PFAS-NOM interactions stems from the complexity of NOM, which is a heterogeneous mixture of humic substances, proteins, polysaccharides, and other organic molecules that vary widely by source.[161] An effective approach to address this complexity involves fractionation techniques that separate NOM constituents based on molecular size or chemical characteristics.[162] For instance, Yu et al. (2012) used ultrafiltration membrane fractionation to show that NOM fractions smaller than 1 kDa significantly reduced the adsorption of long-chain PFOA and PFOS.[78] However, the relevance of these findings to drinking water treatment is limited due to the high PFAS concentrations (up to 300 µg/L) and the use of wastewater-derived NOM in this study. Nonetheless, this approach is valuable, as it suggests that under such conditions, low-molecular-weight organic compounds may compete with long-chain PFAS for adsorption sites.

Besides membrane fractionation, resin fractionation is a common, cheap and widely used method to isolate NOM fractions based on charge and hydrophobicity.[162] Through a series of adsorption and elution steps, NOM is separated into hydrophobic and hydrophilic fractions, each of which can be further subdivided into acidic, basic, and neutral fractions. Although it has not yet been applied to elucidate PFAS-NOM competition, this approach has been used to study disinfection byproducts and micropollutant degradation in the presence of NOM.[163–165]

In the present study, we performed batch isotherm and column adsorption experiments utilizing environmentally relevant concentrations of PFAS and NOM. We employed NOM fractions with distinct chemical characteristics obtained by resin fractionation, as well as size-based fractions obtained through membrane fractionation. Our objective is to identify which specific NOM fractions impact the adsorption of short- and long-chain PFAS. Finally, we discuss the implications of our findings for drinking water treatment, specifically the extent to which competitive interactions may occur during the treatment of PFAS- and NOM-containing waters with GAC.

5.2. Materials and methods

5.2.1 Organic matter fractions

A stock solution of Suwannee River Natural Organic Matter (SRNOM, 2R101N) was prepared by dissolving 1 g/L of SRNOM powder in ultrapure water over the night, followed by filtration through a 0.45 μm membrane. Organic matter fractions were subsequently obtained using resin- and membrane-based fractionation methods.

For resin-based fractionation, NOM fractions differing in hydrophobicity and charge were isolated using polymeric XAD-7HP resin. Fractionation involved sequential adsorption and elution steps of NOM components from the resin with acid, base, or methanol solutions. Specific details are reported in Section 5.5.1.1. Four distinct fractions were obtained, characterized as Hydrophobic Acid (HOA), Hydrophobic Base (HOB), Hydrophobic Neutral (HON), and Hydrophilic (HI) fraction.

Membrane fractionation was performed to separate NOM fractions by molecular size, employing ultrafiltration membranes with different molecular weight cut-offs. Using the Amicon stirred-cell batch system, the SRNOM was filtered using a 10 kDa molecular weight cut-off (MWCO) ultrafiltration membrane to obtain a fraction referred to as the >10 kDa fraction. The resulting permeate step was then filtered through a 3 kDa MWCO membrane, and the final permeate is referred to as the <3 kDa fraction. The detailed membrane fractionation protocol is provided in Section 5.5.1.3.

5.2.2 PFAS

Eight PFAS compounds with varying chain lengths and functional groups were selected for this study. The short-chain included PFBS, PFPeA, and GenX, while PFHxS, PFOS, PFOA, PFNA, and FOSA represented the long-chain compounds. Their properties are summarized in Table S.5.3.

5.2.3 Activated carbon

Thermally activated, reagglomerated bituminous-based granular activated carbon (SRD, Chemviron) was used in this study. SRD has properties comparable to the widely used Filtrasorb 400 (F400).[143] The carbon was ground using a mortar and pestle and then sieved to obtain particles with an average diameter of 0.135 mm (Figure S.5.2). Particles were thoroughly washed with demineralized water, dried, and stored. Crushing did not significantly affect surface chemistry, as indicated by the similar cation exchange capacities before and after crushing (Table S.5.4). Before the adsorption experiments, the GAC was dried at 105 °C for 24 h, weighed, boiled to remove entrapped air, cooled to room temperature, and then used.

5.2.4 Adsorption experiments

5.2.4.1 Batch isotherms

Isotherm experiments were performed at 20 ˚C in 0.5 L polypropylene copolymer (PPCO) bottles (Thermo Scientific, USA), which have previously been shown to have negligible PFAS adsorption under the experimental conditions used in this study.[115] Each bottle contained a solution with eight PFAS compounds at an initial concentration of approximately 1000 ng/L, a specified amount of GAC (0.5–50 mg/L), and Milli-Q water buffered at pH ~7.2 using a 10 mM phosphate buffer (5 mM Na_2HPO_4 + 5 mM KH_2PO_4). A selected NOM fraction was added at 1 mg/L. Because the fractionation protocol involves acid and base treatment, spiking introduces additional K^+ and Cl^-. To ensure a consistent background electrolyte composition, KCl was added to have the same ionic strength in all samples. This resulted in a final conductivity comparable to that of tap water: ~800 µS/cm from the phosphate buffer and ~200 µS/cm from KCl.

The isotherm bottles were placed horizontally on an orbital shaker and agitated at 120 RPM for 36 days. Kinetic control experiments confirmed that this duration was sufficient to reach equilibrium (Figure S.5.3). Samples were stored in 2 mL polypropylene Eppendorf tubes at -20℃. Multiple freeze-thaw cycles were found to have no impact on PFAS concentrations.

5.2.4.2 Rapid small scale column tests (RSSCT)

The Rapid Small-Scale Column Test (RSSCT) method was selected for the adsorption experiments, as it enables the treatment of large numbers of bed volumes (BV) within a relatively short timeframe. This method uses small adsorption columns, 7 mm in diameter in our case, each packed with 250 mg of AC, resulting in a bed volume of 0.61 mL. By applying the constant diffusivity model, $\frac{EBCT_{RSSCT}}{EBCT_{Filter}} = \left[\frac{particle\ diamater_{RSSCT}}{particle\ diameter_{Filter}}\right]^2$, this setup allows for the simulation of full-scale adsorption filters.[75] The flow rate through each column was maintained at 2 ± 0.2 mL/min, corresponding to a full-scale filter with an empty bed contact time (EBCT) of 16.9 minutes and an average particle diameter of 1 mm.

The feedwater was prepared in a 20 L tank, matching the composition used in the batch experiments. Prior to introducing the PFAS and NOM-spiked feedwater, the columns were flushed overnight with deionized water. Feedwater samples were collected daily, both before and after refreshing the feedwater. Effluent samples were collected using an autosampler every 1000 treated bed volumes, or more frequently when breakthrough was expected.

5.2.5 Analytical methods

5.2.5.1 Natural organic matter characterization

Several well-established methods were used to characterize NOM. Total organic carbon (TOC) was measured using the non-purgeable organic carbon (NPOC) method on a TNM-L TOC analyser (Shimadzu). Since the organic matter fractions were filtered through a 0.45 µm membrane prior to analysis, TOC is reported as dissolved organic carbon (DOC). Ultraviolet absorbance at 254 nm was measured using an Infinite M200 Pro multimode plate reader (Tecan). Specific ultraviolet absorbance at 254 nm ($SUVA_{254}$) was calculated by dividing the absorbance at 254 nm by the DOC concentration. Liquid chromatography with organic carbon detection (LC-OCD) was used to quantify low molecular weight (LMW) neutrals and, LMW acids, determine the carbon content and average molecular weight of humic acids. Details regarding the LC-OCD measurements are provided in Ribero Pinela et al. (2024).[166] Fluorescence excitation-emission matrix spectroscopy was performed using a Varian Cary Eclipse spectrofluorometer (Agilent, USA), using a PMT voltage of 680 V, slit width of 5 nm, averaging time of 0.125 s and default correction factors. Both the spectrophotometer blanks and daily Raman scatter profiles were obtained using MilliQ water. The fluorescence emission-excitation matrices were used to determine the total fluorescence (TF).

5.2.5.2 PFAS detection

PFAS concentrations were measured using a SCIEX 5500+ LC-AD30 system with a Phenomenex Kinetex C18 column. The quantification limit for all PFAS was 2.5 ng/L. Analytical details are provided in Pranic et al., 2025.[115]

5.3. Results and discussion

In this study, we conducted batch isotherm and column adsorption experiments using granular activated carbon (GAC) with eight different PFAS compounds in the presence of various fractions of natural organic matter (NOM). Under environmentally relevant conditions, we found that the adsorption of long-chain PFAS was significantly inhibited by the hydrophobic neutral (HON) fraction of NOM, whereas short-chain PFAS were primarily affected by NOM fractions smaller than 3 kDa.

In the following sections, we present and interpret the PFAS adsorption results in the presence of different NOM fractions. Table 5.1 summarizes the key characteristics of these fractions. A detailed description of the fractionation protocols and the quality of the obtained NOM fractions is provided in Sections 5.5.1.1 – 5.5.1.4.

Table 5.1. Properties of SRNOM and its fractions obtained by resin and membrane fractionation. Values are normalized to a TOC concentration of 1 mg/L, reflecting the conditions used during the adsorption experiments

NOM property*	SRNOM	Resin fractions				Membrane fractions		
		HOA	HON	HOB	HI	<3 kDa	3-10 kDa	>10 kDa
$SUVA_{254}$ (L/mg/m)	3.87	4.26	3.63	2.08	2.26	3.07	5.26	6.16
TF/TOC (A.U./mg)	269	298	520	227	177	507	221	227
Average Mw (kDa)	3.9	4.0	3.8	2.6	3.0	2.9	6.0	7.7
Humic acids – C (ug/L/mg)	1258	1402	1002	812	1367	620	711	672
LMW neutrals (ug/L/mg)	102	176	233	<5.00	232	129	60	71
LMW acids (ug/L/mg)	35	39	151	13	47	16	21	9

* $SUVA_{254}$ and TF/TOC values represent averages from six fractionation replicates for the resin fractions and two replicates for the membrane fraction. The average molecular weight (MW) of humic acids, concentration of humic acids, low molecular weight (LMW) neutrals, and LMW acids were determined from measurements of composite samples

5.3.1. PFAS removal in the presence of NOM with varying chemical properties

Figure 5.1 shows PFAS removal at equilibrium as a function of applied carbon dose, conducted in the presence of SRNOM and its two resin fractions: hydrophilic (HI) and hydrophobic neutral. The corresponding isotherms derived from these data are presented in Figure S.5.4., and the estimated parameters for both the Langmuir and Freundlich models are summarized in Tables S.5.6. – S.5.13.

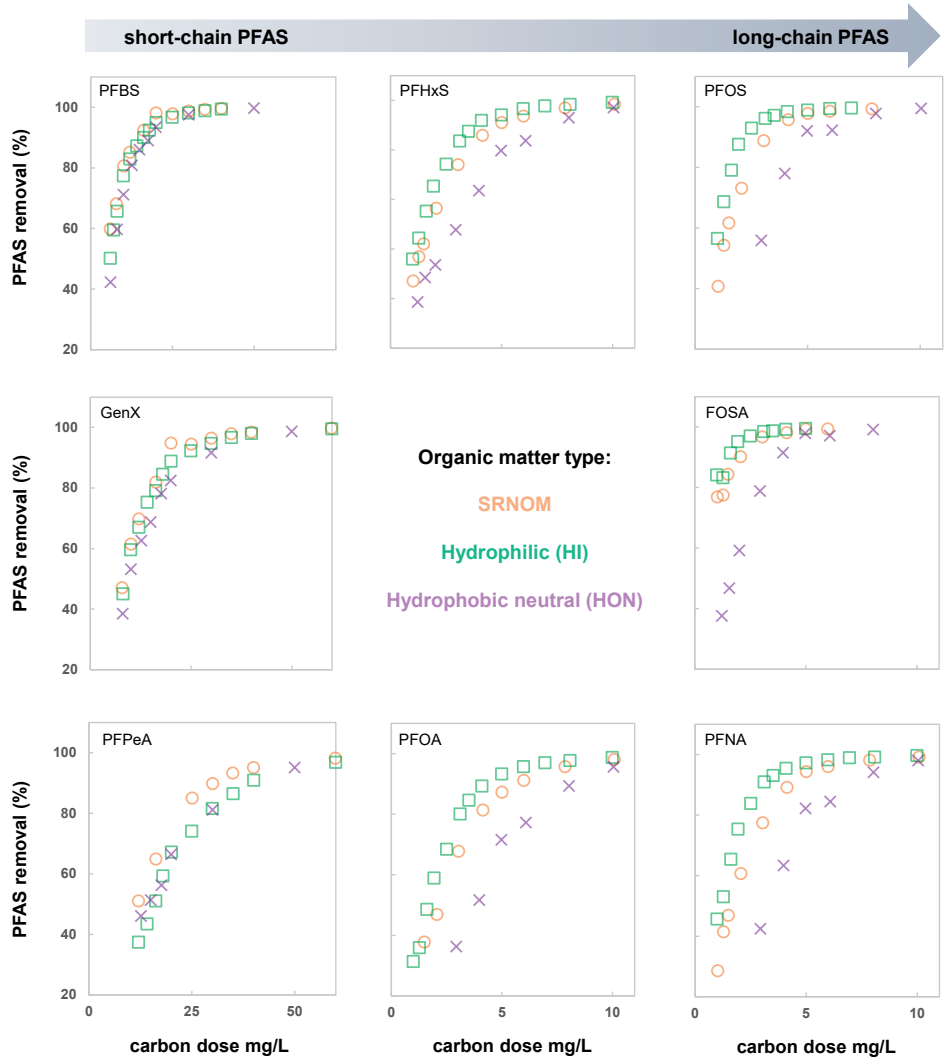


Figure 5.1. PFAS removal as function of carbon dose in the presence of SRNOM (orange circles) and two SRNOM resin fractions: hydrophilic (green squares) and hydrophobic neutral (purple X). Data for the hydrophobic acid (HOA) fraction are not shown due to overlap with the SRNOM data, which are largely composed of HOA.

Figure 5.1 illustrates that the difference in PFAS removal between the HI and HON fractions increases with PFAS chain length. For short-chain PFAS, removal is largely unaffected by the hydrophobic or hydrophilic nature of the organic matter. In contrast, the removal of long-chain PFAS is significantly lower in the presence of the HON fraction. The negative impact of HON on long-chain PFAS adsorption can be mitigated at higher carbon doses (>10 mg/L), where the increased availability of adsorption sites reduces competition. Additionally, the presence of SRNOM, which is predominantly composed of HOA (Figure S.5.1), leads to only a slight decrease in long-chain PFAS removal relative to the HI fraction. Adsorption isotherm experiments with the hydrophobic bases (HOB) fraction were not conducted due to insufficient quantities obtained during fractionation. However, a kinetic experiment conducted at 5 mg/L carbon dose in the presence of the HOB fraction showed no greater impact on PFAS removal than observed with the HI fraction (Figure S.5.3). In summary, among the resin fractions evaluated, the HON fraction has the strongest inhibitory effect on the adsorption of long-chain PFAS, whereas short-chain PFAS adsorption is largely unaffected by the type of NOM resin fraction.

We calculated the ratio of the Langmuir maximum adsorption capacities (q_{max}) for the HI/HON fractions, shown in Figure 5.2A. A linear trend is observed with increasing numbers of fluorinated carbons in the PFAS molecules. For short-chain PFAS, q_{max} values are comparable between the two fractions. However, for long-chain PFAS with eight fluorinated carbons, the q_{max} in the presence of the HI fraction is up to 2.5 times higher than in the presence of the HON fraction. This suggests that for waters with HON concentrations of 1 mg/L or higher, removal of the HON fraction could increase the adsorption capacity for long-chain PFAS by at least a factor of 2.5. Interestingly, extrapolating the trend in Figure 5.2A to shorter chain lengths suggests that the adsorption of ultra-short-chain PFAS (e.g., trifluoroacetic acid, with a single fluorinated carbon) may be substantially hindered in the presence of the HI fraction.

Figures 5.1 and 5.2A clearly demonstrate that the presence of the HON fraction significantly hinders the adsorption of long-chain PFAS. This raises a critical question: which specific constituents within the HON fraction are responsible for this reduced adsorption? LC-OCD analysis revealed that the HON fraction contains approximately three times higher concentrations of low molecular weight (LMW) acids compared to the HI fraction (Table 5.1). These LMW acids are primarily aliphatic organic acids with molecular weights under 350 Da. Additionally, a literature review by Świetlik et al. (2004) reported the presence of long-chain (>C9) aliphatic carboxylic acids and amines in HON fractions from various sources, which fall into the LMW acid category identified by LC-OCD. We hypothesize that these compounds compete directly with long-chain PFAS for adsorption sites due to their structural similarity. Specifically, a hydrophobic long-chain carbon backbone combined with a hydrophilic functional group.

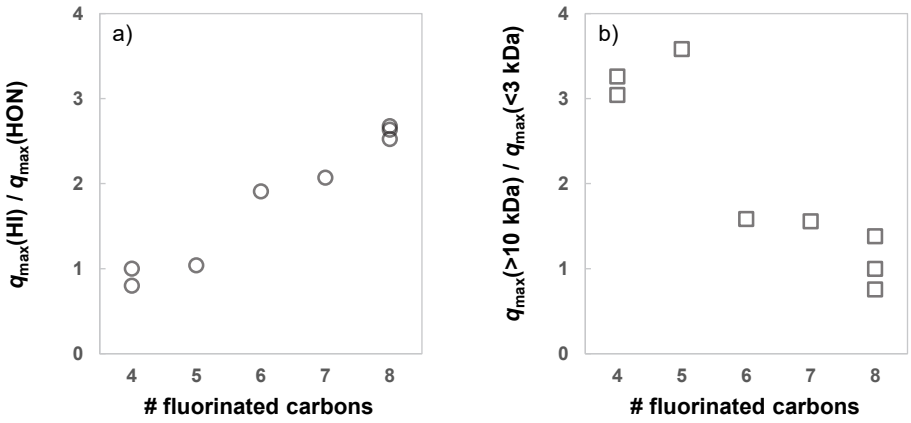


Figure 5.2 A) Ratio of Langmuir maximum adsorption capacities (q_{max}) for PFAS adsorption in the presence of hydrophilic (HI) and hydrophobic neutral (HON) fractions, as a function of the number of fluorinated carbons in the PFAS molecules. B) Ratio of q_{max} for PFAS adsorption in the presence of >10 kDa and <3 kDa ultrafiltration fractions, as a function of the number of fluorinated carbons in the PFAS molecules.

Another key difference between the HON and HI fractions is the significantly higher $SUVA_{254}$ and TF/TOC ratio observed in the HON fraction (Table 5.1), both indicative of a greater abundance of aromatic structures.[167,168] These aromatic compounds are likely >3-ring aromatic carboxylic acids and amines, as previously identified in HON fractions by Świetlik et al. (2004). Since long-chain PFAS are also adsorbed within mesopores (2–50 nm),[115,169] which can also accommodate large multi-ring aromatic molecules, direct competition between these aromatic compounds and long-chain PFAS may reduce PFAS adsorption.

Finally, it must be noted that although long-chain PFAS adsorption in the presence of the HI fraction is less inhibited than in the presence of the HON fraction, it remains lower than in the absence of organic matter (Table S.5.6-S.5.13). This suggests that certain molecules within the HI fraction inhibit PFAS adsorption, affecting both short- and long-chain compounds. As widely reported, organic matter fractionation is not completely selective; compounds characteristic of the HON fraction may be present in the HI fraction and vice versa.[162] Moreover, the presence of large humic acids across all fractions (Table 5.1) could contribute to pore blockage, further limiting PFAS access to adsorption sites.

5.3.2. PFAS removal in the presence of NOM with varying size

Figure 5.3 shows equilibrium PFAS removal as a function of carbon dose in the presence of SRNOM and its two ultrafiltration membrane fractions: <3 kDa and >10 kDa. The corresponding isotherms, fitted Langmuir and Freundlich parameters, and experimental data are provided in Section 5.5.

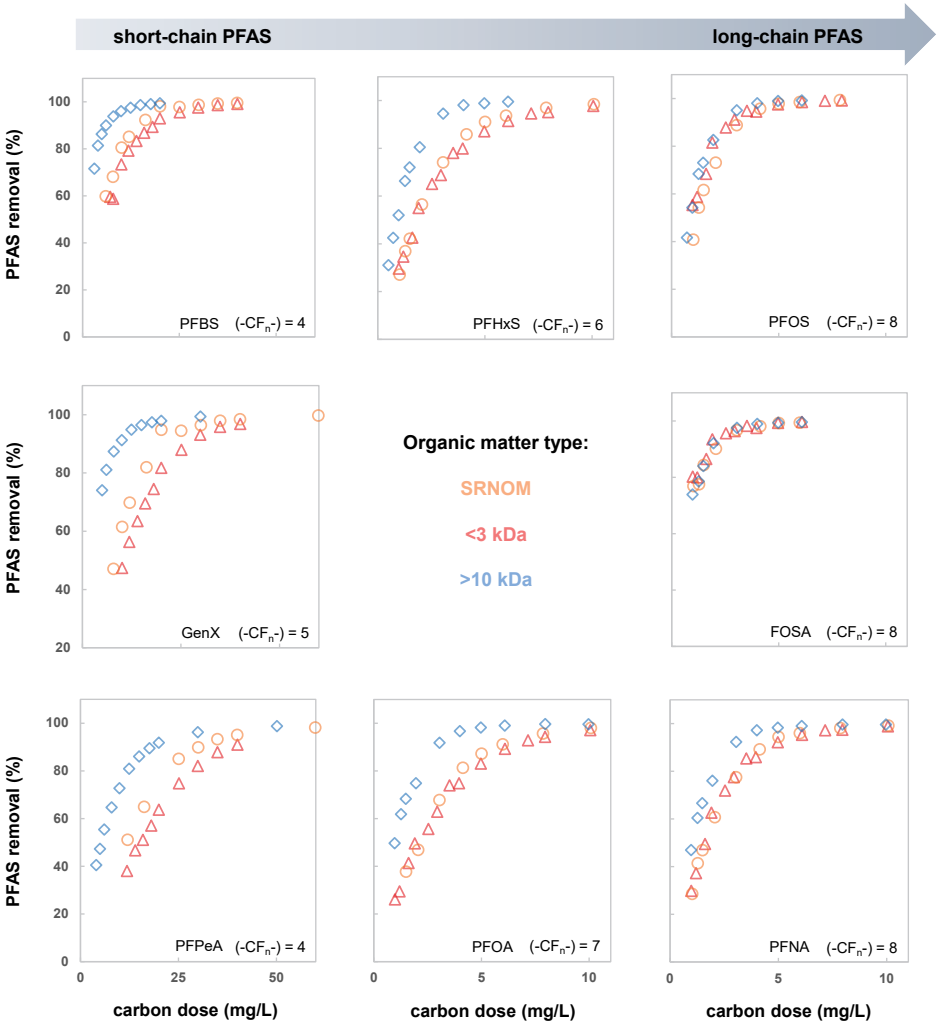


Figure 5.3. PFAS removal as function of carbon dose in the presence of SRNOM (orange circles) and two SRNOM membrane fractions: <3 kDa (red triangles) and >10 kDa (blue diamonds)

Figure 5.3 illustrates that short-chain PFAS adsorption on activated carbon is significantly reduced in the presence of the <3 kDa membrane fraction of SRNOM compared to the >10 kDa fraction. Furthermore, the removal efficiency observed with non-fractionated SRNOM closely aligns with that observed of the <3 kDa fraction, consistent with the fact that SRNOM predominantly consists of <3 kDa molecules (Figure S.5.1).

Increasing PFAS chain length reduces the influence of NOM size on PFAS removal. For the longest and most hydrophobic PFAS tested (PFOS and FOSA), removal by activated carbon remains consistent across all carbon doses, regardless of NOM size (Figure 5.3). The interaction between NOM size and PFAS chain length is further illustrated in Figure 5.2B, which shows the ratio of Langmuir maximum adsorption capacities (q_{max}) for the >10 kDa and <3 kDa fractions as a function of the number of fluorinated carbons. The data show that removing small-sized NOM molecules enhances q_{max} for short-chain PFAS by a factor of 3–3.6. However, this enhancement decreases with increasing chain length, dropping to a factor of 1.6 for PFHxS and PFOA, and becoming negligible for longer-chain PFAS. Extrapolation of the trend in Figure 5.2B suggests that adsorption of ultra-short-chain PFAS, such as TFA, may be particularly sensitive to interference from small-sized NOM components. This raises an important question: which specific constituents within the <3 kDa NOM fraction are responsible for the observed reduction in short-chain PFAS adsorption?

Table 5.1 shows that the <3 kDa fraction is enriched in smaller humic acids, with an average molecular weight of 2.9 kDa (LC-OCD), compared to 7.7 kDa for the >10 kDa fraction. The lower-than-expected molecular weight of the >10 kDa fraction reflects incomplete separation during fractionation, a common issue reported in other studies.[162] The <3 kDa fraction also has more LMW neutrals and acids than >10 kDa fraction. The abundance of small NOM molecules in the <3 kDa fraction likely contributes to competitive adsorption with short-chain PFAS, thereby reducing the removal efficiency. Additionally, the smaller NOM molecules are expected to be more hydrophilic, as indicated by the lower $SUVA_{254}$ value of 3.07 for the <3 kDa fraction, compared to 6.16 for the >10 kDa fraction. $SUVA_{254}$, which reflects the aromatic content and degree of unsaturation (double carbon bonds) in organic matter,[163] typically exceeds 4 for larger, more hydrophobic compounds. Thus, the lower $SUVA_{254}$ in the <3 kDa fraction supports the interpretation that more hydrophilic NOM components are responsible for the reduced adsorption of short-chain PFAS.

To summarize our findings from batch experiments on the impact of NOM on PFAS adsorption onto activated carbon: adsorption of long-chain PFAS was strongly affected by the HON fraction, whereas adsorption of short-chain PFAS was primarily impacted by competitive interactions with low molecular weight, hydrophilic NOM. Although batch experiments effectively elucidate competitive interactions and adsorption mechanisms, they may not fully capture the dynamics of adsorption in column systems. Therefore, column adsorption

experiments using various NOM fractions were also performed and are discussed in the next section.

5.3.3. Column experiments with PFAS and different types of NOM

Breakthrough curves for the short-chain PFPeA and the long-chain PFNA are presented in Figure 4, both with and without specific NOM fraction. In the experiments with NOM, the feedwater contained approximately 1 mg/L of NOM. Breakthrough curves and experimental data for other short and long-chain PFAS compounds are provided in Figure S.5.6.

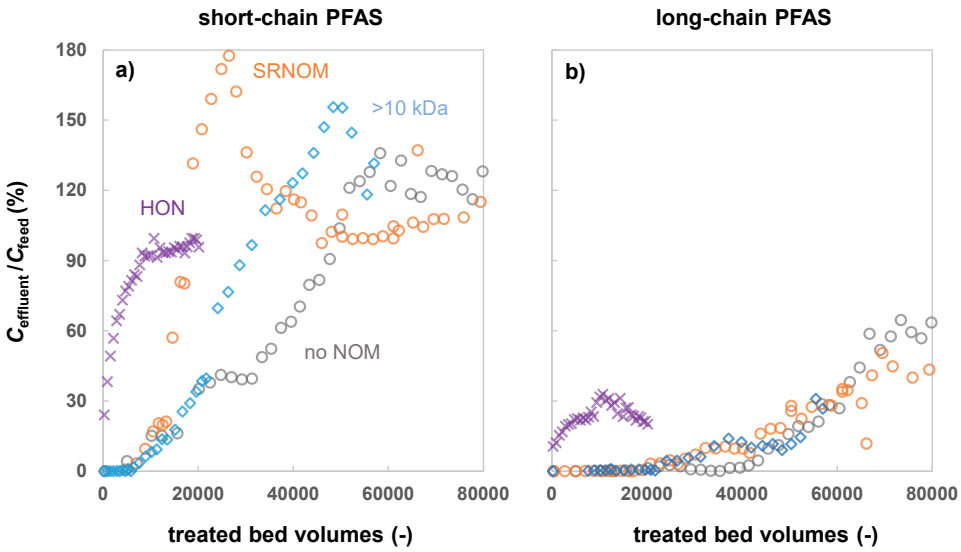


Figure 5.4. Breakthrough curves of a) short-chain PFPeA, and b) long-chain PFNA in the absence and presence of 1 mg/L SRNOM, hydrophobic neutral (HON) fraction of SRNOM, and the >10 kDa fraction of SRNOM

Figure 5.4A highlights several key trends. First, the breakthrough of short-chain PFAS occurs earlier in the presence of all NOM types. This observation is consistent with isotherm results, which showed a reduced PFPeA adsorption capacity in the presence of any form of NOM (Table S.5.9). Furthermore, when comparing breakthrough curves for short-chain PFAS in the presence of SRNOM and its >10 kDa fraction containing lower concentrations of low molecular weight compounds, breakthrough is delayed in the >10 kDa fraction. In line with the batch experiment results (Figure 5.3), these column data confirm that the removal of low molecular weight NOM enhances the adsorption of short-chain PFAS.

Secondly, the breakthrough curves for PFPeA in the presence of SRNOM, the >10 kDa fraction of SRNOM, and in the absence of NOM, exhibit a chromatographic effect, i.e., the effluent concentration of PFPeA exceeds the influent concentration. This effect is attributed to the desorption of adsorbed PFPeA by competing molecules. The onset of this effect occurs earli-

est with SRNOM (~20,000 BV), followed by >10 kDa (~40,000 BV), and lastly in the absence of NOM (~50,000 BV). Notably, the occurrence of this effect even without NOM indicates that long-chain PFAS compounds are displacing short-chain PFAS from adsorption sites. In the presence of NOM, additional competing species, likely small, hydrophilic molecules, are introduced that cause earlier start of chromatographic effect. These molecules are abundant in the SRNOM fraction and, to a lesser extent, still present in the >10 kDa fraction due to imperfect fractionation. Furthermore, an contribution to chromatographic effect observed in presence of >10 kDa fraction might be desorption of short-chain PFAS from mesopores that are accessible for large NOM molecules.

Finally, an important observation from Figure 5.4A is the immediate breakthrough of PFPeA in the presence of the HON fraction. In batch experiments, no significant differences were observed in the adsorption isotherms for short-chain PFAS in the presence of SRNOM or HON (Figure 5.1); thus immediate breakthrough in the column system is unexpected. The early breakthrough of PFPeA (Figure 5.4A) appears to be linked to the earlier breakthrough of PFNA (Figure 5.4B). As discussed previously, long-chain PFAS compete with short-chain PFAS for adsorption sites. Therefore, the early breakthrough of PFPeA in the presence of HON is likely driven by the earlier breakthrough of PFNA, resulting from competition between PFNA and HON. This raises an important question: why do long-chain PFAS in the presence of the HON fraction reduce short-chain PFAS adsorption in column systems, but not in batch experiments? We hypothesize that in column systems, mass transfer limitations, such as film diffusion or slow surface diffusion, amplify competitive effects. Modelling these interactions using the isotherm (Tables S.5.6 – S.5.13) and column data (Figures S.5.6) in mass transfer-based column models could provide valuable insights into the extent and mechanisms of PFAS competition.

Thus far, we have discussed the breakthrough curves of PFPeA (Figure 5.4A) for various NOM fractions, and of PFNA (Figure 5.4B) in the presence of the HON fraction. A final noteworthy observation in Figure 5.4B is the near overlap of PFNA breakthrough curves in the absence of NOM, and in the presence of 1 mg/L SRNOM or 1 mg/L >10 kDa fraction. During the treatment of up to 80,000 bed volumes (BV), these curves closely resemble each other. While this may seem unexpected given the substantially higher PFNA adsorption capacity in batch isotherms without NOM (Table S.11), it is important to note that the breakthrough curves for PFNA in Figure 5.4B are not yet complete. A similar overlap is observed for PFPeA within the first 18,000 BV. Another explanation for the overlapping PFNA breakthrough curves is that slower adsorption kinetics, rather than equilibrium adsorption capacity, predominantly control the breakthrough of long-chain PFAS. Previous studies have reported surface diffusion coefficients for long-chain PFAS that are several orders of magnitude lower compared to short-chain PFAS.[115]

Ultimately, removal efficiency in the adsorption process is governed by the availability of adsorption sites and mass transport towards these sites. The overlapping breakthrough curves suggest that under the experimental conditions in Figure 5.4B (1 mg/L SRNOM or 1 mg/L >10 kDa), the concentration of competing molecules was insufficient to significantly hinder long-chain PFAS adsorption during the initial 80,000 BVs. However, when column experiments were performed with a higher SRNOM concentration (5 mg/L), earlier breakthrough of long-chain PFAS was observed (Figure S.5.7). Notably, increasing the SRNOM concentration also increases the presence of the HON fraction, which, as previously established, is the primary competitor for long-chain PFAS adsorption.

5.3.4. Implications for drinking water treatment

In this study, we identified specific NOM fractions that compete with PFAS for adsorption onto a common type of activated carbon (AC) used in drinking water treatment plants. Our findings demonstrate that adsorption efficiency of short-chain PFAS is significantly reduced in the presence of small NOM molecules (<3 kDa fraction), whereas the adsorption of long-chain PFAS is primarily reduced by the hydrophobic neutral fraction (HON). These insights have important implications for PFAS removal in drinking water treatment plants (DWTPs) using AC.

To validate the relevance of our selected NOM concentration (1 mg/L), we compiled data from several studies (Table 5.2) reporting both the concentrations and relative percentages of <3 kDa and HON fractions in natural waters used as sources for DWTPs.

Table 5.2. Concentration and percentage of <3 kDa and HON fraction in different sources used for drinking water production

NOM fraction	concentration of fraction (mg/L)	percentage of total NOM (%)	type of influent to DWTP	Study
<3 kDa	6.2	78	5 geological and chemically distinct natural waters. Non specified if surface or groundwater	Ref. 170
	4.5	63		
	4.2	33		
	3.4	85		
	0.6	18		
	4.3	74	lake	Ref. 171
	2.9	27	river	
	1.9	42	lake	Ref. 167
	1.9	24	lake	
	2.4	67	surface water	Ref. 172
	2.2	39	not reported	Ref. 173
	1.1-1.43	50-65*	lake	Ref. 174

Table 5.2. Concentration and percentage of <3 kDa and HON fraction in different sources used for drinking water production (*continued*)

NOM fraction	concentration of fraction (mg/L)	percentage of total NOM (%)	type of influent to DWTP	Study
	6.2	18	river	Ref. 175
	1.3	16	river	Ref. 176
	0.45-0.78	12	groundwater	Ref. 177
HON	0.4	34	groundwater	Ref. 168
	0.3	20	lake	Ref. 178
	0.31-0.51	8	not reported	Ref. 179
	0.0	0		

As shown in Table 5.2, the concentration of the <3 kDa NOM fraction commonly found in source waters for DWTPs is typically above 2 mg/L. Conventional treatment processes prior to GAC filtration are generally ineffective at removing this LMW fraction. For example, coagulation-flocculation followed by sedimentation provides limited removal of LMW organic matter, and standard filtration methods, such as rapid or slow sand filtration, typically achieve only about 20% NOM removal.[180] According to Table 5.2, many feedwaters used in GAC filtration have background concentrations of the <3 kDa fraction comparable to or higher than those tested in our experiments. Consequently, the frequently reported rapid breakthrough of short-chain PFAS in pilot and full-scale DWTPs, documented in numerous studies,[36,59,60,75] can be attributed to competitive adsorption by this LMW NOM fraction. Notably, even at concentrations as low as 0.1 mg/L, the <3 kDa fraction exceeds typical PFAS concentrations (~1-1000 ng/L) in drinking water and is therefore a significant competitor for adsorption sites.

The removal efficiency of long-chain PFAS by AC is typically higher than that of short-chain PFAS during drinking water treatment.[24,55] Our findings indicate that higher removal is primarily due to differences in competitive adsorption mechanisms. Specifically, the primary competitor for long-chain PFAS is the HON fraction of NOM, which generally occurs at low concentrations in natural waters (Table 5.2). However, when the HON fraction is present at elevated levels (>1 mg/L), a significant reduction in long-chain PFAS adsorption can occur, as illustrated in Figure 5.1.

We strongly recommend thorough characterization of NOM to determine the presence and concentrations of fractions such as <3 kDa and HON, which significantly compete with PFAS for adsorption sites on GAC. The fractionation methods used in this study (resin- and membrane-based) are well-established and can rapidly provide representative samples, making them suitable for routine monitoring at drinking water treatment plants. Characterizing NOM composition prior to GAC treatment can greatly improve the prediction of PFAS breakthrough and removal performance.

If short-chain PFAS are a primary concern and the influent water contains elevated levels of the <3 kDa NOM fraction, several pretreatment strategies can be employed to reduce the concentration of the <3 kDa fraction. Biological pretreatment is among the most sustainable and effective approaches, as LMW molecules typically exhibit high biodegradability.[181] Biological activated carbon filters, particularly when combined with pre-oxidation methods, have demonstrated high NOM removal efficiencies, achieving up to 50-60% in TOC reduction.[182,183] In contrast, removing the HON fraction is more challenging. This is primarily because HON lacks reactive groups that readily interact with oxidants such as ozone.[163] Additionally, the HON fraction has received limited attention, likely due to its typically low concentrations and minimal impact on oxidation processes. Fortunately, because HON concentrations in natural waters are generally low, its effect on long-chain PFAS adsorption is expected to be limited under typical treatment conditions.

5.4. Conclusions

In this study, we conducted batch and column experiments with granular activated carbon (GAC) and different natural organic matter (NOM) fractions to identify the specific NOM components that inhibit the adsorption of short- and long-chain PFAS.

Adsorption of short-chain PFAS was significantly inhibited by the <3 kDa fraction obtained via ultrafiltration. This fraction, abundant in low molecular weight hydrophilic compounds, competes directly with short-chain PFAS for adsorption sites. Pre-removal of this fraction prior to GAC treatment enhanced the adsorption capacity for short-chain PFAS (4–5 fluorinated carbons) by 3–3.6 times, and potentially even more for ultra-short chain compounds such as trifluoroacetic acid (TFA). As the <3 kDa fraction is commonly found in drinking water sources, often at concentrations comparable to or higher than those tested here, its reduction should be prioritized to improve the performance of GAC filtration for short-chain PFAS, and reduce GAC filter reactivation frequencies.

Long-chain PFAS adsorption was significantly reduced in the presence of the hydrophobic neutral (HON) fraction, isolated via resin fractionation. This fraction contains molecules such as >C9 carboxylic acids and amines, which exhibit molecular characteristics similar to those of long-chain PFAS, resulting in competitive adsorption. Unlike the <3 kDa fraction, HON is typically present at lower concentrations in source waters, which explains the generally later breakthrough of long-chain PFAS compared to short-chain compounds in the presence of NOM. Nevertheless, we recommend routine monitoring of feed water prior to GAC treatment, with specific attention to both the <3 kDa and HON fractions, as their presence may indicate a risk of reduced PFAS removal.

Interestingly, in column experiments, competition from the HON fraction not only reduced long-chain PFAS adsorption but also that of short-chain PFAS, an effect not observed in batch experiments. Modeling PFAS breakthrough behavior using the isotherm, kinetic, and column data obtained here with a dynamic multi-component mass transport model could further elucidate the extent and mechanisms of these competitive interactions.

Acknowledgments

Part of this research was funded by AXA research fund "Climate change and the Water-Food Nexus: where and how acting to reduce impacts on human health" (CUP D43C23000610007).

5.5. Supporting Information for Chapter 5

5.5.1. Natural organic matter fractionation

To obtain distinct fractions of natural organic matter (NOM), standarized Suwannee River Natural Organic Matter (SRNOM) was fractionated using two approaches. Resin fractionation separated SRNOM into fractions differing in hydrophobicity and charge, while membrane fractionation produced fractions based on differences in molecular weight.[162]

5.5.1.1. Resin fractionation protocol

Resin fractionation relies on the principle that organic matter adsorbed onto a non-polar acrylic resin can be selectively eluted using solvents of varying polarity.[162,180] Historically, resins such as XAD-8 or DAX-8 have been predominantly utilized for this purpose. However, these resins are no longer commercially available, and the supplier (Supelco, Sigma-Aldritch, USA) offers XAD-7HP resin as the alternative, which was employed in this study.

Typically, resin fractionation is conducted using adsorption columns, suitable for fractionating NOM solutions with relatively low concentrations (~1–20 mg/L).[165,184] In contrast, the aim of this study was to produce sufficiently large volumes of NOM fractions at substantially higher concentrations (100–1000 mg/L) to serve as stock solutions for adsorption experiments involving PFAS. Column-based adsorption was therefore impractical due to operational challenges such as column clogging.

As an alternative to column-based fractionation, batch adsorption was utilized, allowing easier attainment of equilibrium distribution of NOM between the liquid phase and resin. The batch resin fractionation protocol applied in this study was adapted from the procedure developed by Gijn et al. (2022),[163] with full protocol detailed bellow:

- The SRNOM solution for fractionation was prepared by dissolving 1 g/L of SRNOM powder in Milli-Q water. The solution was filtered through a 0.45 μm filter, and the total organic carbon (TOC) was determined as ~450 mg/L
- Prior to fractionation, the XAD-7HP resin was purified through adsorption with 1 M KCl, Soxhlet extraction, and subsequent several washing cylcles with 0.1 M HCl, 0.1 M KOH, and Milli-Q water.
- Six fractionation replicates were prepared by mixing 36 g of XAD-7HP resin with 300 mL of the SRNOM solution.
- Four blank replicates were prepared by mixing 36 g of XAD-7HP resin with 300 mL of Milli-Q water.

- Batch bottles containing resin and liquid were placed on an orbital shaker, and each of the following adsorption/elution steps lasted at least 2 hours.
- After 2 hours of contact, the Hydrophobic Base (HOB) fraction was adsorbed onto the resin, while the remaining solution without HOB (discharge) was collected by carefully decanting for subsequent fractionation steps.
- The adsorbed HOB fraction was eluted from the resin using 300 mL of 0.1 M HCl.
- The discharge solution (without HOB) was adjusted to pH 2 with concentrated HCl and then brought into contact with the resin to adsorb the hydrophobic fraction. The Hydrophilic (HI) fraction was collected as the discharge
- Two fractions, Hydrophobic Acids (HOA) and Hydrophobic Neutrals (HON), remained adsorbed on the resin. The HOA fraction was recovered by eluting the resin with 300 mL of 0.1 M KOH.
- The HON fraction was subsequently eluted from the resin with 300 mL of methanol.
- Methanol was removed from the HON fraction by evaporation under a nitrogen stream overnight.
- The residual HON fraction was re-dissolved in 300 mL of Milli-Q water.

The protocol also included blanks for each fraction, in which Milli-Q water was treated identically to SRNOM. This allowed us to assess whether any additional organics leached from the polymer resin and to evaluate the potential impact of the fractionation process on the accuracy and quality of specific organic matter measurements (TOC, COD, UV254, and TF).

The resin dosage used in this study (120 g/L, equivalent to 36 g of resin per 300 mL of SRNOM) is significantly higher than the dosage used by Gijn et al. (15 g/L). This higher dosage was selected to ensure complete fractions separation at the higher TOC concentrations used in this study. Preliminary experiments with resin doses of 60 and 200 g/L, and extended contact times of 24 hours, showed no significant differences in quality of fractions compared to fractionation with 120 g/L at 2 h.

5.5.1.2. Quality of resin fractions

First of all, it is important to note that different organic matter characterizations indicate a closed mass balance for the fractionation process. This is demonstrated in Figure S.5.1, which compares measurements of total organic carbon (TOC), chemical oxygen demand (COD), UV254 absorbance, and total fluorescence (TF) for raw SRNOM and its corresponding resin fractions. Sum of values for the SRNOM fractions (HOA + HI + HON + HON) are slightly lower but closely align with the measurements for the non-fractionated SRNOM.

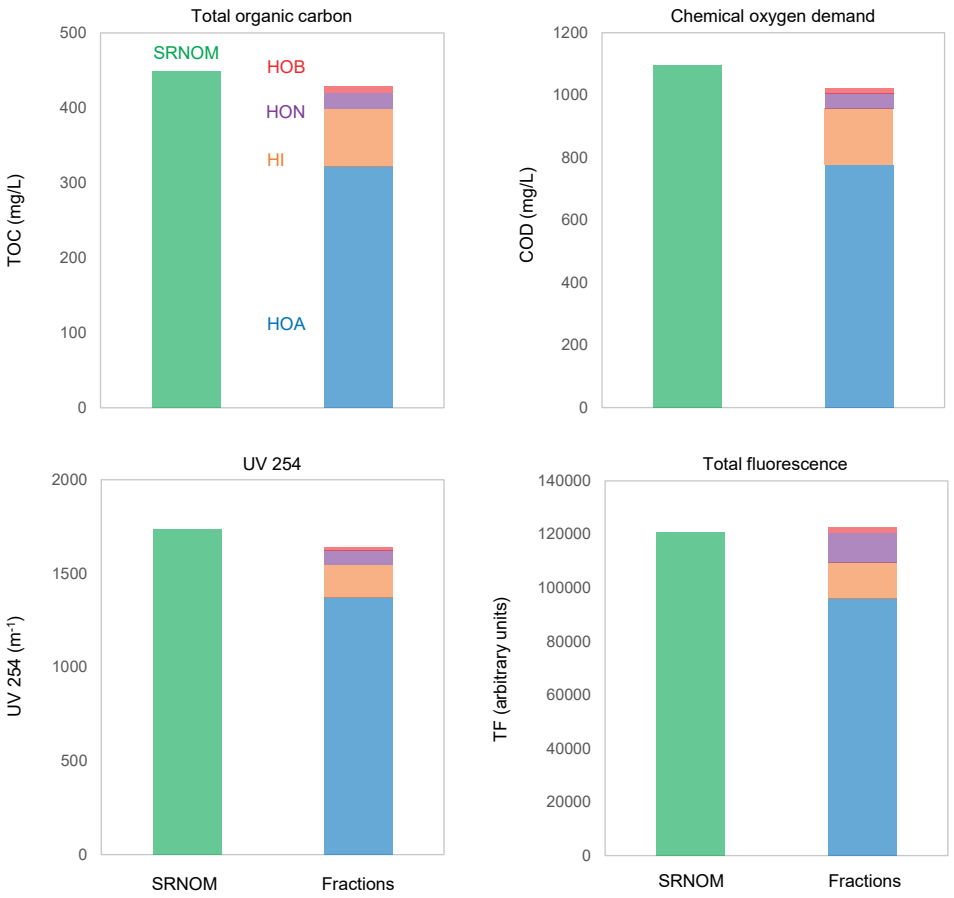


Figure S.5.1. Comparison of organic matter characterization parameters (TOC, COD, UV 254 , TF) for raw SRNOM (green) and resin-fractionated SRNOM (HOA – blue, HI – orange, HON – purple, HOB – red). The close similarity between raw SRNOM values and the summed resin fractions indicates effective fractionation with minimal organic matter loss. All values represent averages from six replicates; standard deviations are negligible. Specific numbers for values shown in Figure S.5.1 can be found in Table S.5.1.

Secondly, as we applied a modified protocol (detailed in Section 5.5.1.1) that fractionated concentrated SRNOM using batch bottles instead of the traditional column method, it is important to highlight that our results are consistent with those reported in previous studies. For example, if we look at percentage of TOC obtained of each fraction, we obtained 72% HOA, 17% HI, 4.6% HON and 1.9% HOB. Similar to us, Bai et al. (2023) reported 72% HOA, 24% HI, and 4% HON,[164] while Ratpukdi et al. (2009) reported 69% HOA, 27% HI, 3% HON, and 0.6% HOB.[176] Minor differences in composition compared to earlier studies may be attributed to our use of commercially available XAD-7HP resin, which has higher porosity and a larger surface area[162] than the now-discontinued XAD-8 resin used in those studies.

Finally, we note that organic matter measurements in the fraction blanks are generally low and negligible compared to those in the corresponding SRNOM fractions, further confirming the completeness and effectiveness of the fractionation process. The only exception was the HON blank, which showed approximately 10% of the TOC and 18% of the COD measured in blank compared to the HON fraction. This is likely due to residual methanol that did not fully evaporate. Importantly, this contribution was accounted for when dosing the HON fraction into the experimental adsorption bottles to ensure a final HON concentration of 1 mg/L.

Table S.5.1. Average values of organic matter measurments coming from 6 replicates for SRNOM, and each of SRNOM resin fractions

	SRNOM	HOA	HI	HON	HOB
TOC (mg/L)	449 ± 32	322 ± 2	76 ± 1	21 ± 1	9 ± 0
COD (mg/L)	1095 ± 54	777 ± 22	180 ± 1	49 ± 4	17 ± 0
UV_{254} (m^{-1})	1739 ± 5	1373 ± 4	172 ± 1	76 ± 1	18 ± 0
TF (A.U.)[a]	120871 ± 1341	96121 ± 2117	13487 ± 158	10915 ± 592	1956 ± 251

a – arbitrary units

5.5.1.3. Membrane fractionation protocol

Membrane fractionation of SRNOM was conducted using a dead-end stirred cell system (Amicon®), equipped with regenerated cellulose ultrafiltration membranes (Ultracel®) having molecular weight cut-offs of 10 kDa and 3 kDa. The filtration was performed at a constant pressure of 3.25 bar and a stirring speed of 1400 RPM.

Fractionation experiments were conducted in duplicate, each time starting with 1 L of SRNOM solution prepared as described in the resin fractionation section. Initially, 1 L of SRNOM solution was filtered through a 10 kDa ultrafiltration membrane until approximately 95% of the permeate volume was collected. Given the inherent limitations of ultrafiltration membranes, which do not yield perfectly sharp molecular weight separations, the retentate typically contains molecules smaller than the nominal membrane cut-off.[162]

Table S.5.2. Average values of organic matter measurments coming from 2 replicates for each of SRNOM membrane fractions

	<3 kDa	3 - 10 kDa	>10 kDa
TOC (mg/L)	262 ± 2	17 ± 0	68 ± 4
COD (mg/L)	689 ± 5	45 ± 0	199 ± 15
UV_{254} (m^{-1})	804 ± 13	88 ± 0	416 ± 12
TF (A.U.)[a]	133106 ± 542	3705 ± 79	15335 ± 3472

To improve separation efficiency, the retentate of filtering with 10 kDa membrane was cleaned by adding Milli-Q water into the filtration cell, thereby resuspending and dissolving the filtration cake layer accumulated on the membrane surface, which can include smaller molecules below the membrane cut-off. The diluted retentate was subsequently filtered again, and the permeate was discarded. This cleaning process was repeated twice. Finally, the remaining filtration cake was resuspended in 1 L of Milli-Q water and designated as the >10 kDa fraction.

The permeate from the 10 kDa filtration step was subsequently used as feed for filtration through a 3 kDa ultrafiltration membrane, following the same filtration and cleaning procedure described above. The resulting retentate from this step was designated as the 3–10 kDa fraction. The permeate obtained from the 3 kDa filtration step underwent an additional filtration through a fresh 3 kDa ultrafiltration membrane to remove molecules above the nominal cut-off, ensuring the final permeate primarily contained molecules smaller than 3 kDa. This cleaned permeate was classified as the <3 kDa fraction.

5.5.1.4. Quality of membrane fractions

The goal of the membrane fractionation was to obtain enriched fractions with distinct differences in molecular weight. To achieve this, we implemented several cleaning steps, as described in Section 5.5.1.3. For example, the permeate from the 10 kDa membrane was further filtered twice using two different 3 kDa membranes. Since the filter cake from the second filtration was not collected, a complete mass balance for the membrane fractions could not be established. Nevertheless, we can compare the amount of the <3 kDa fraction obtained with values reported in other studies. In our case, the <3 kDa fraction had a TOC of 262 mg/L, accounting for 58% of the total TOC in SRNOM. Our results are consistent with those reported by Shen et al. (2019)[185] where the <3 kDa fraction constituted 56% of SRNOM, although they differ from study Bai et al. (2023)[164] that reported only 25% of <3 kDa fraction. Given that different fractionation protocols can yield varying distributions, it is important to validate the quality of the fractions through analytical measurements. In our study, LC-OCD analysis was performed on each fraction, and results are shown in Table 5.1. Clear differences were observed, with the <3 kDa fraction showing an average molecular weight of 2.9 kDa and the >10 kDa fraction showing an average molecular weight of 7.7 kDa. These results confirm that with membrane fractionation we successfully obtained fractions of different molecular size. However, the average molecular weight of the >10 kDa fraction (7.7 kDa) suggests that smaller molecules than 10 kDa were also present. Incomplete separation is a common limitation of ultrafiltration membrane fractionation, as noted in review by Dejaeger et al. (2022). Therefore, membrane, and resin, fractions should be viewed as enriched in specific NOM characteristics, rather than as pure, isolated components.

5.5.2 PFAS properties

Table S.5.3. Properties of PFAS used in this study[a]

Compound name	Abbreviation	Formula	Mw (g/mol)	pK_a	$LogK_{ow}$
Perfluorobutane sulfonic acid	PFBS	$C_4F_9SO_3H$	300.10	-3.31	1.82
Perfluorohexane sulfonic acid	PFHxS	$C_6F_{13}SO_3H$	400.11	0.14	3.16
Perfluorooctane sulfonic acid	PFOS	$C_8F_{17}SO_3H$	500.13	< 1.0	4.49
Perfluoropentanoic acid	PFPeA	C_4F_9COOH	264.05	0.34	3.01
Perfluorooctanoic acid	PFOA	$C_7F_{15}COOH$	414.07	-0.5 - 4.2	4.81
Perfluorononanoic acid	PFNA	$C_8F_{17}COOH$	464.08	-0.21	5.48
Perfluorooctane sulfonamide	FOSA	$C_8H_2F_{17}NO_2S$	499.14	3.37	5.8
Hexafluoropropylene oxide dimer acid	GenX	$C_6HF_{11}O_3$	330.05	2.82	2.58

[a] For GenX information obtained from Vakili et al. (2021)[67], and for other PFAS from Gagliano et al. (2020)[13]

5.5.3. Activated carbon properties

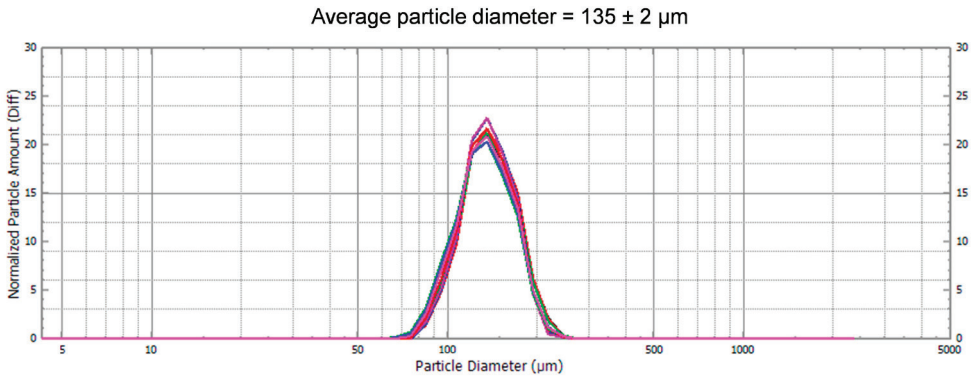


Figure S.5.2. Activated carbon particle size distribution as determined by SALD-2300 laser diffraction particle size analyzer (Shimadzu). Figure presents overlapping 9 independent measurements as obtained by measurements from which average particle diameter was calculated as 135 µm.

Table S.5.4. Cation exchange capacity before grinding (granules) and after grinding (powder) determined following protocol in Munera-Echeverri et al (2018)[186]

	Cation exchange capacity (mmol/g)	
Replicate	Granules	Powder
1	0.5762	0.6373
2	0.5705	0.5872
3	0.5707	0.6039

5.5.4. Kinetic data

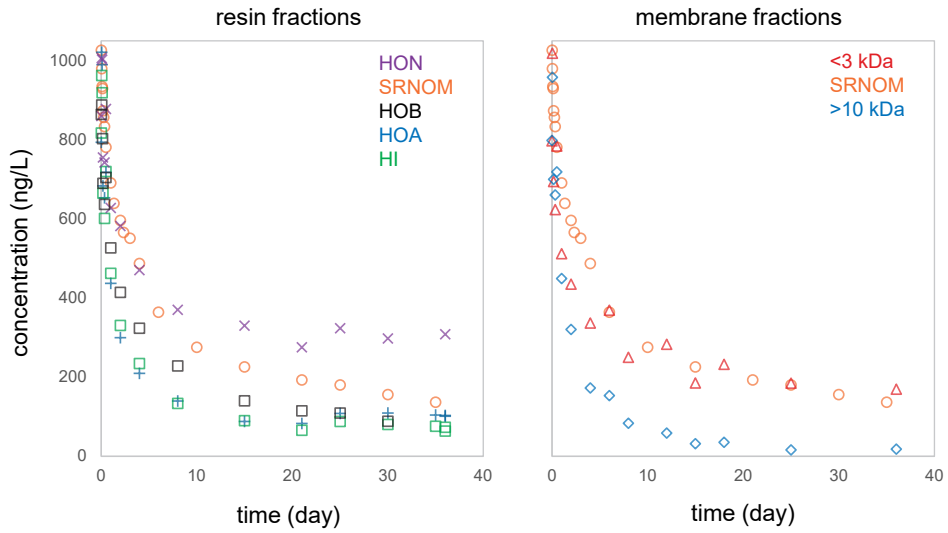


Figure S.5.3. Change of concentration (ng/L) over time (day) for adsorption of PFOA on activated carbon for different resin and membrane fractions

5.5.5. Isotherm data

The amount of PFAS adsorbed onto activated carbon is determined using the mass balance

$$q_{eq} = \frac{V_l}{m_{GAC}}\left(c_0 - c_{eq}\right) \quad \text{(S.5.1)}$$

where q_{eq} is the adsorbent loading in equilibrium (ng_{PFAS}/mg_{GAC}), V_l is the volume of the bulk solution (L), m_{GAC} is the mass of dry activated carbon, c_0 is the starting concentration of PFAS in the bulk solution, and c_{eq} is the concentration of PFAS in equilibrium. Widely applied Freundlich and Langmuir equations were used to fit equilibrium data with non-linear regression. Estimated isotherms are shown in Figures S.5.6, and S.5.7.

Table S.5.5. Isotherms used in this study

Isotherm	Equation	Parameters
Freundlich[48,144]	$q_{eq} = K_f {c_{l,eq}}^n$	K_f – adsorption coefficient (ng/mg)/(ng/L)^n n – adsorption intensity (-)
Langmuir[48,144]	$q_{eq} = \frac{q_{max} K_L c_{l,eq}}{1+K_L c_{l,eq}}$	q_{max} – maximum adsorption capacity [ng/mg] K_L – Langmuir constant [L/ng]

q_{eq} – adsorbent loading in equilibrium [ng/mg]; $c_{l,eq}$ – concentration of adsorbate in bulk in equilibrium [ng/L]

Table S.5.6. Estimated Langmuir and Freundlich isotherm parameters for adsorption of PFBS on GAC in the absence and presence of 1 mg/L of various NOM fractions

PFBS	Langmuir			Freundlich		
	Q_{max} (ng/mg)	K_L (L/ng)	R^2	K_f (ng/mg)/(ng/L)^n	n	R^2
No NOM	315.86	0.13	0.88	80.03	0.31	1.00
SRNOM	103.16	0.04	0.88	19.48	0.28	0.98
HOA	99.20	0.03	0.90	16.74	0.29	0.98
HON	90.85	0.02	0.88	19.93	0.24	0.95
HI	90.81	0.03	0.91	15.72	0.29	0.98
<3 kDa	92.46	0.02	0.88	13.53	0.31	0.98
>10 kDa	281.41	0.02	0.93	22.06	0.42	1.00

Table S.5.7. Estimated Langmuir and Freundlich isotherm parameters for adsorption of PFHxS on GAC in the absence and presence of 1 mg/L of various NOM fractions

PFHxS	Langmuir			Freundlich		
	Q_{max} (ng/mg)	K_L (L/ng)	R^2	K_f (ng/mg)/(ng/L)^n	n	R^2
No NOM	1862.13	0.16	0.80	672.89	0.20	0.93
SRNOM	320.72	0.02	0.92	59.42	0.26	0.98
HOA	335.68	0.02	0.94	55.78	0.28	0.98
HON	202.58	0.05	0.91	55.91	0.20	0.93
HI	387.00	0.02	0.94	65.98	0.28	0.99
<3 kDa	330.91	0.01	0.92	38.98	0.32	0.99
>10 kDa	524.67	0.05	0.91	122.80	0.23	0.99

Table S.5.8. Estimated Langmuir and Freundlich isotherm parameters for adsorption of PFOS on GAC in the absence and presence of 1 mg/L of various NOM fractions

PFOS	Langmuir			Freundlich		
	Q_{max} (ng/mg)	K_L (L/ng)	R^2	K_f (ng/mg)/(ng/L)^n	n	R^2
No NOM	2675.10	0.10	0.84	1066.36	0.17	0.87
SRNOM	375.47	0.05	0.92	84.28	0.25	0.98
HOA	425.07	0.05	0.88	86.28	0.28	0.98
HON	177.38	0.24	0.85	75.91	0.16	0.90
HI	467.55	0.06	0.91	103.04	0.27	0.99
<3 kDa	458.68	0.02	0.91	60.07	0.34	0.97
>10 kDa	457.96	0.05	0.94	95.73	0.26	0.99

Table S.5.9. Estimated Langmuir and Freundlich isotherm parameters for adsorption of PFPeA on GAC in the absence and presence of 1 mg/L of various NOM fractions

PFPeA	Langmuir			Freundlich		
	Q_{max} (ng/mg)	K_L (L/ng)	R^2	K_f (ng/mg)/(ng/L)^n	n	R^2
No NOM	102.48	0.05	0.95	9.98	0.52	0.99
SRNOM	45.66	0.03	0.94	8.26	0.28	0.98
HOA	35.60	0.02	0.95	6.47	0.27	0.99
HON	38.09	0.03	0.92	6.71	0.27	0.99
HI	30.44	0.04	0.94	7.62	0.22	0.91
<3 kDa	32.81	0.04	0.95	7.47	0.24	0.97
>10 kDa	106.99	0.01	0.97	7.80	0.39	1.00

Table S.5.10. Estimated Langmuir and Freundlich isotherm parameters for adsorption of PFOA on GAC in the absence and presence of 1 mg/L of various NOM fractions

PFOA	Langmuir			Freundlich		
	Q_{max} (ng/mg)	K_L (L/ng)	R^2	K_f (ng/mg)/(ng/L)^n	n	R^2
No NOM	1720.47	0.08	0.88	489.21	0.24	0.91
SRNOM	261.17	0.03	0.93	47.15	0.27	0.98
HOA	256.44	0.03	0.88	60.29	0.23	0.92
HON	143.79	0.07	0.89	47.15	0.18	0.88
HI	297.89	0.03	0.95	58.03	0.26	0.96
<3 kDa	263.19	0.02	0.92	33.54	0.32	0.99
>10 kDa	409.79	0.05	0.92	79.51	0.27	0.99

Table S.5.11. Estimated Langmuir and Freundlich isotherm parameters for adsorption of PFNA on GAC in the absence and presence of 1 mg/L of various NOM fractions

PFNA	Langmuir			Freundlich		
	Q_{max} (ng/mg)	K_L (L/ng)	R^2	K_f (ng/mg)/(ng/L)^n	n	R^2
No NOM	1996.81	0.27	0.91	827.36	0.19	0.95
SRNOM	309.02	0.03	0.93	64.51	0.25	0.96
HOA	390.38	0.03	0.89	63.19	0.29	0.97
HON	165.75	0.09	0.93	55.47	0.18	0.86
HI	418.68	0.03	0.93	73.93	0.29	0.99
<3 kDa	301.99	0.03	0.93	51.34	0.28	0.96
>10 kDa	417.13	0.05	0.94	82.24	0.27	0.99

Table S.5.12. Estimated Langmuir and Freundlich isotherm parameters for adsorption of GenX on GAC in the absence and presence of 1 mg/L of various NOM fractions

GenX	Langmuir			Freundlich		
	Q_{max} (ng/mg)	K_L (L/ng)	R^2	K_f (ng/mg)/(ng/L)^n	n	R^2
No NOM	405.60	0.03	0.90	47.07	0.38	0.98
SRNOM	69.53	0.04	0.90	16.36	0.23	0.94
HOA	70.62	0.03	0.89	13.84	0.27	0.88
HON	64.27	0.02	0.89	13.30	0.24	0.93
HI	66.75	0.02	0.91	12.93	0.26	0.96
<3 kDa	51.70	0.03	0.92	11.86	0.24	0.99
>10 kDa	185.30	0.02	0.96	14.29	0.43	1.00

Table S.5.13. Estimated Langmuir and Freundlich isotherm parameters for adsorption of FOSA on GAC in the absence and presence of 1 mg/L of various NOM fractions

FOSA	Langmuir			Freundlich		
	Q_{max} (ng/mg)	K_L (L/ng)	R^2	K_f (ng/mg)/(ng/L)^n	n	R^2
No NOM	2009.26	0.18	0.65	757.23	0.20	0.92
SRNOM	523.22	0.04	0.89	61.72	0.40	0.96
HOA	633.59	0.04	0.89	71.33	0.42	0.94
HON	301.40	0.06	0.91	96.83	0.18	0.94
HI	807.08	0.04	0.89	111.28	0.37	0.94
<3 kDa	655.74	0.03	0.88	64.38	0.42	0.94
>10 kDa	495.93	0.06	0.92	81.29	0.34	0.98

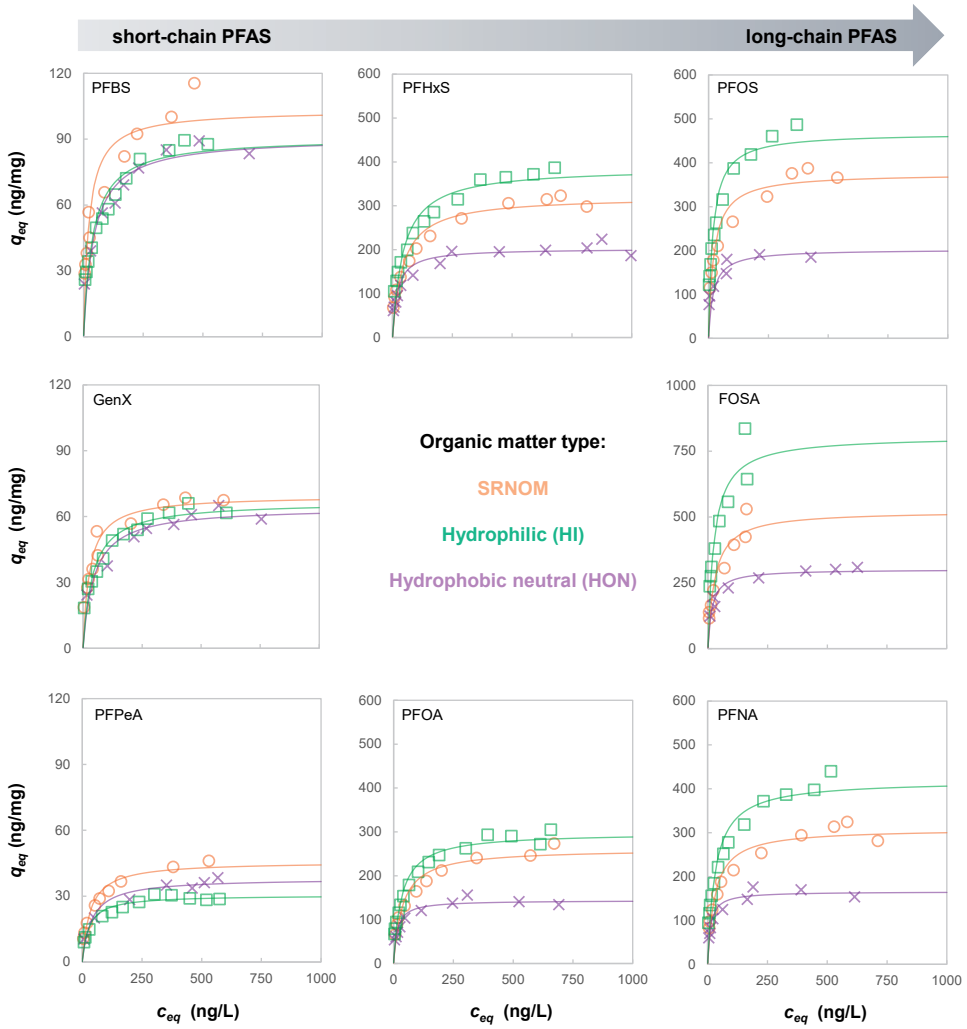


Figure S.5.4. Adsorption isotherm data of PFAS on activated carbon in the presence of SRNOM (orange circles), hydrophilic (HI) fraction of SRNOM (green squares) and hydrophobic neutral (HON) fraction of SRNOM (purple X), described with the Langmuir isotherm (full lines).

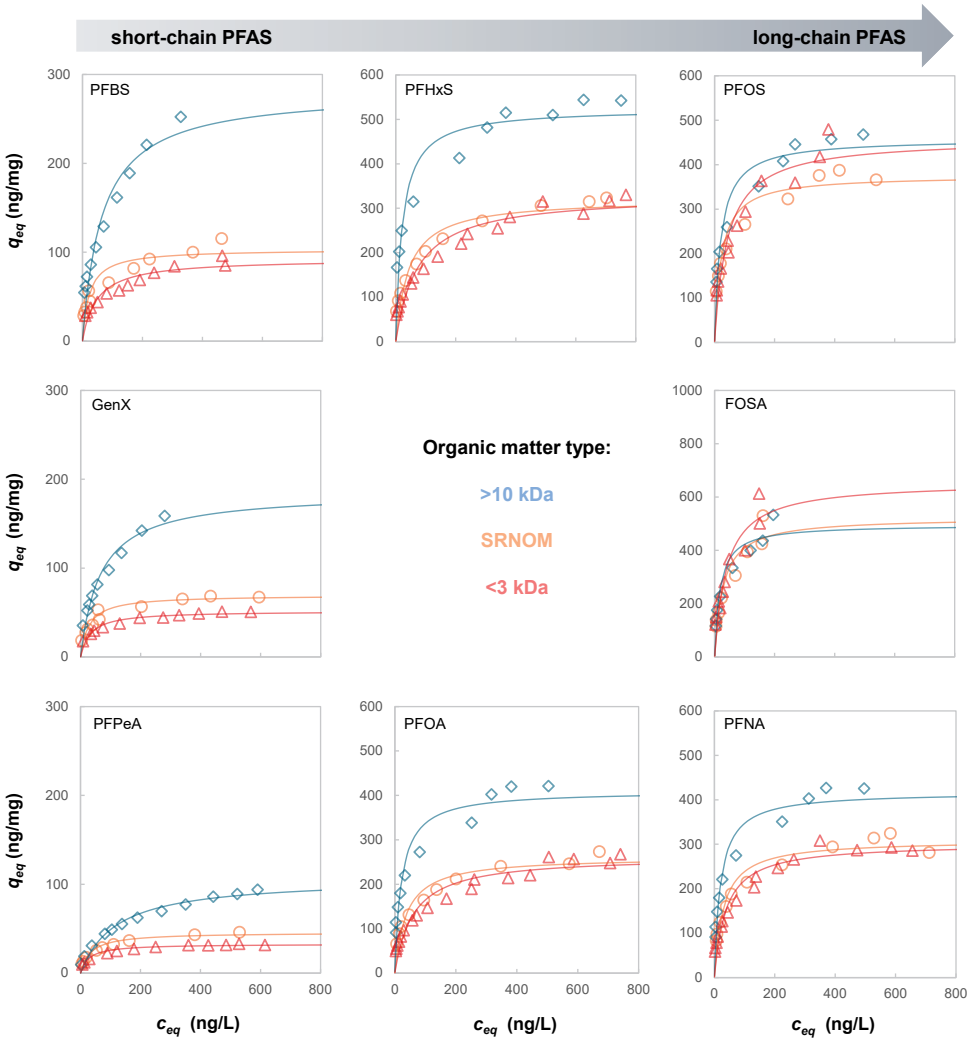


Figure S.5.5. Adsorption isotherm data of PFAS on activated carbon in the presence of SRNOM (orange circles), >10 kDa fraction of SRNOM (blue diamonds) and <3 kDa fraction of SRNOM (red triangles), described with the Langmuir isotherm (full lines).

5.5.6. Breakthrough curves

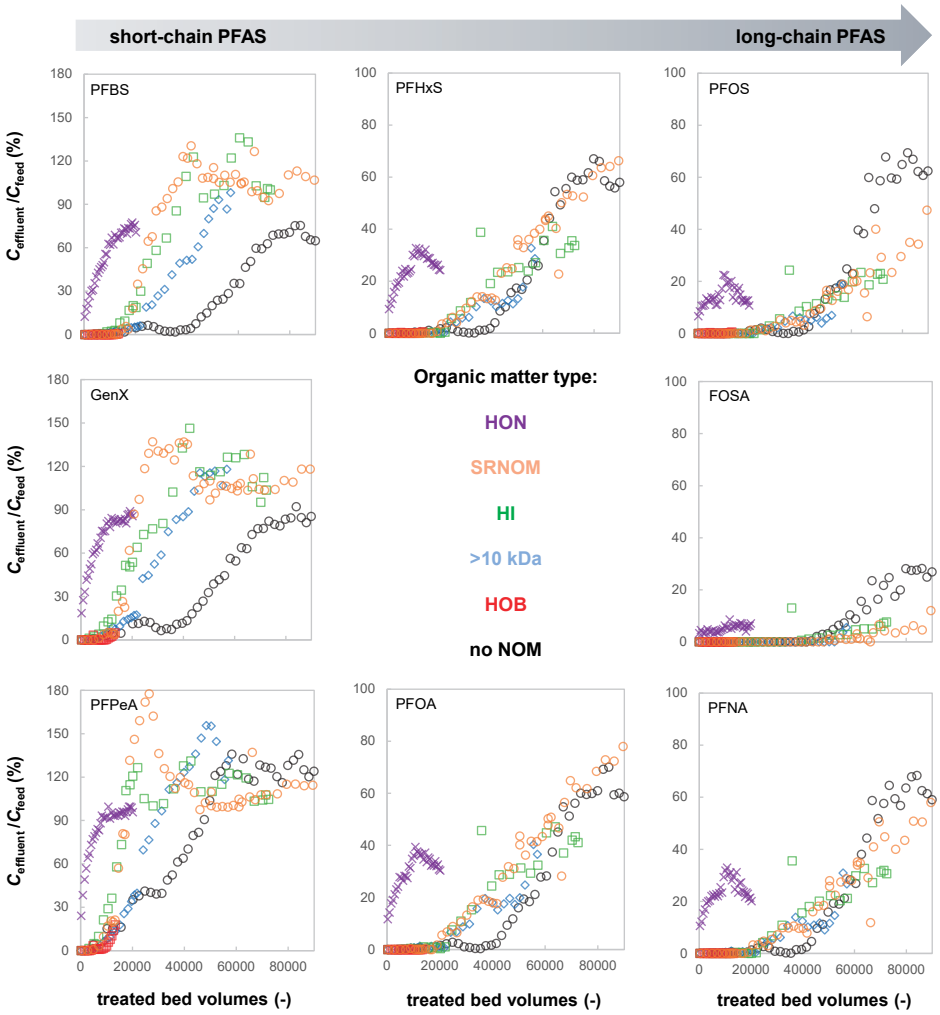


Figure S.5.6. Breakthrough curves for adsorption of PFAS on activated carbon in the absence and presence of various NOM fractions at 1 mg/L

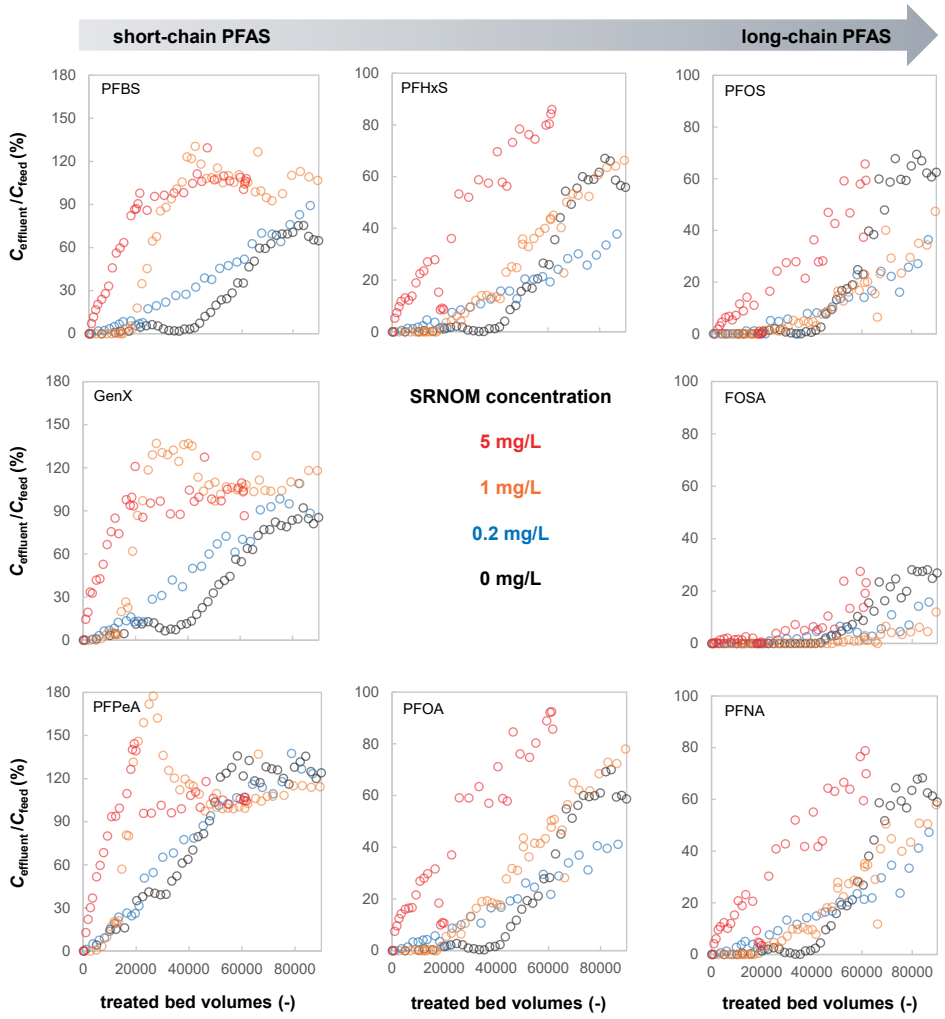
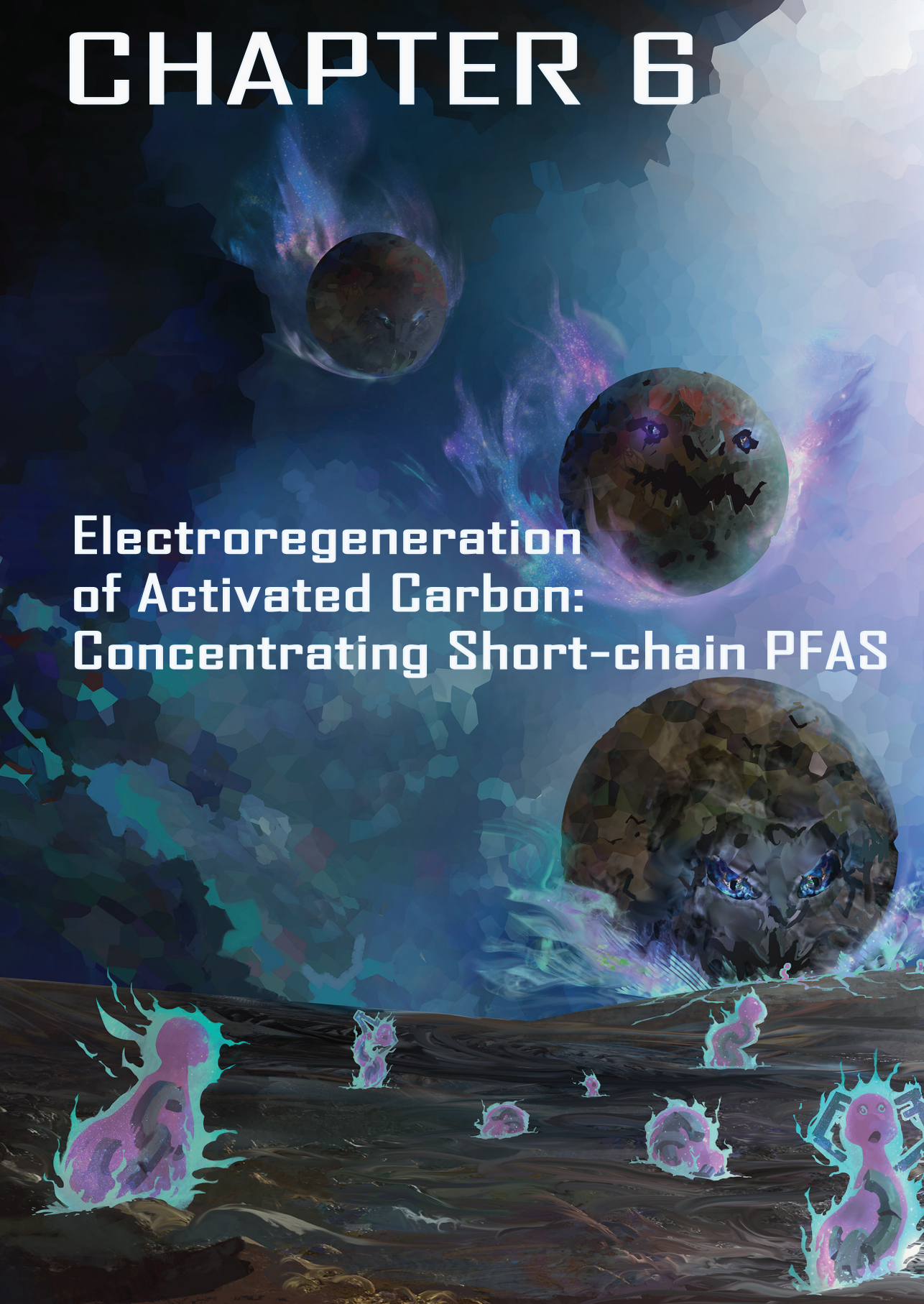


Figure S.5.7. Breakthrough curves for adsorption of PFAS on activated carbon in the presence of various concentrations of SRNOM

CHAPTER 6

Electroregeneration of Activated Carbon: Concentrating Short-chain PFAS

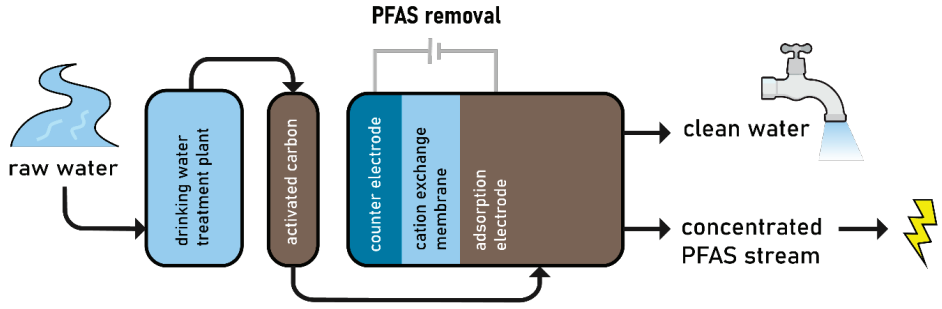


This chapter has been published as:
Zhou, K., **Pranic, M.**, Rutten, S.M., Porada, S., Post, J.W., van der Wal, A., Dykstra, J. E (2025) Electroregeneration of activated carbon filters:concentrating short-chain PFAS, ACS ES&T Water , https://doi.org/10.1021/acsestwater.5c00819

Abstract

Perfluoroalkyl and polyfluoroalkyl substances (PFAS) are persistent fluorinated micropollutants. In recent years, stringent limits have been proposed by regulatory agencies, creating significant challenges for many water utilities. Although activated carbon is widely used for the adsorption and removal of PFAS, its rapid breakthrough, particularly with short-chain PFAS, requires frequent regeneration. This study presents a novel electroregeneration technology for the potential on-site regeneration of activated carbon. PFAS are initially adsorbed onto activated carbon, which is then regenerated in an electrochemical cell with a counter-carbon electrode separated by a cation-exchange membrane. The experiments were conducted using a solution with an ionic strength comparable to surface water, implying a high concentration of competing ions. For PFPeA, a short-chain PFAS, we achieved effluent concentrations during electroregeneration 130 times higher than initial levels, with most PFPeA successfully desorbed. The method was effective for all short-chain PFAS examined (PFPeA, PFBS, GenX), which are particularly concerning due to their rapid breakthrough in activated carbon filters. We have studied the effect of electronic charge in the electrodes on PFAS adsorption, as well as the impact of electrode surface modifications on PFAS electroregeneration performance. Surface modifications increased the presence of positively charged chemical groups, which in turn influenced the efficiency of PFAS electroregeneration.

Graphical Abstract



Keywords: PFAS, granular activated carbon, regeneration, drinking water treatment, electrosorption, concentrating PFAS

6.1. Introduction

Perfluoroalkyl and polyfluoroalkyl substances (PFAS) are a class of fluorinated hydrocarbons that are difficult to remove in water treatment processes due to their distinct properties. Because of their persistence and decades of release, PFAS have become ubiquitous in the environment at ever-increasing concentrations. In recent years, these increased concentrations have raised concerns about their potential adverse effects on human health and the environment. The US EPA has provided drinking water guidelines with allowable PFAS concentrations ranging from 4 - 10 ng/L,[17] depending on the compound, while the EU directive set the maximum allowable combined concentration of PFAS of concern at 100 ng/L.[11] Many drinking water companies are unlikely to meet these stringent guidelines due to upstream industrial discharges.[22] Consequently, there is an increasing need for effective technologies for PFAS removal.

Several treatment technologies are available for PFAS removal, with granular activated carbon (GAC) being the most commonly used in water treatment plants due to its cost effectiveness and relatively high adsorption capacity for some PFAS. Adsorption of PFAS is mainly driven by electrostatic and hydrophobic interactions: the charged head interacts with the charged surface groups of the GAC, while the hydrophobic tail interacts with the hydrophobic carbon surface. GAC typically requires regeneration after processing 15,000 to 30,000 bed volumes.[36] The presence of short-chain PFAS significantly reduces the breakthrough time of GAC filters, requiring more frequent regeneration.[131] These short-chain PFAS are defined as those with fewer than eight carbon groups for PFAS with carboxylic functional groups and fewer than six for sulfonated species.[7]

Conventionally, when GAC is saturated, the material is removed from the filters and transported to external thermal regeneration facilities. To ensure that PFAS are removed from the spent GAC, regeneration occurs at temperatures ranging from 650 - 1100 °C,[62] leading to substantial energy consumption and a significant environmental burden.[18] To reduce the impact of spent activated carbon regeneration, there has been increasing interest in on-site regeneration of activated carbon at (drinking) water production facilities. Here, regeneration using solvents that alter the adsorption equilibrium has received attention in recent years.[116,187,188] Chemical regeneration can be beneficial compared to thermal methods by minimizing downtime and avoiding the removal of GAC from the filters[11,12]. However, partial recovery of activated carbon, potential changes in adsorbent stability, and the production of large volumes of hazardous chemicals are considered a significant disadvantage.[189,190]

More recently, the potential for activated carbon electroregeneration has gained traction.[64,65,191] During electroregeneration, the spent carbon is used as an electrode in an electro-chemical cell. The spent carbon at the cathodic side becomes electrically negatively charged,leading to the repulsion of contaminants and the regeneration of adsorption sites.[192]

This regeneration process does not require elevated temperatures or the use of chemicals, making it a promising emerging approach to extend the lifetime of the filter bed and overcome several techno-economic and sustainability challenges.[65,193]

Two review papers on electrochemically driven processes for regenerating spent carbons for the removal of organic micropollutants highlighted various methods.[192,194] In a proof of-principle study, electroregeneration of PFOA-laden activated carbon achieved approximately 60% regeneration efficiency after sequential adsorption and electroregeneration cycles.[195] Other studies demonstrated electro-assisted adsorption of PFAS,[196–198] and one study demonstrated the electro-assisted adsorption and regeneration of modified activated carbon for the removal of trifluoroacetic acid (TFA), an ultrashort-chain PFAS, where regeneration efficiencies of 88 to 100% could be achieved during multiple adsorption cycles.[65] Although these studies offer valuable insights into the potential of electroregeneration for the desorption of PFAS from activated carbon, the experiments were conducted with single PFAS contaminants at elevated concentrations (in the mg/L range). Therefore, there is still a lack of knowledge on the applicability of these results to actual, environmentally relevant concentrations and PFAS mixtures.

In this study, we investigate the desorption of PFAS from activated carbon through electroregeneration under environmentally relevant conditions, using a PFAS mixture at approximate concentrations of 1000 ng/L in the presence of a high concentration of competing ions (approximately 300 mg/L). We propose an alternative design of the electrochemical cell with a cation-exchange membrane between the electrodes to avoid PFAS transfer between the two oppositely charged electrodes (Figure. 6.1). The proposed process has the potential for on-site application, reducing both the economic and environmental burdens of transporting GAC to thermal regeneration facilities while extending the operational time of GAC filters. Additionally, this approach minimizes high energy costs, intensive chemical use, and capital investments associated with alternative regeneration methods for spent activated carbon.

We demonstrate that effective electroregeneration can be achieved in the presence of relevant concentrations of counterions. Furthermore, we investigate the impact of electrode surface modifications on the electroregeneration performance. Lastly, we show that a highly concentrated PFAS solution can be produced, which could be treated in subsequent PFAS destruction steps.[199]

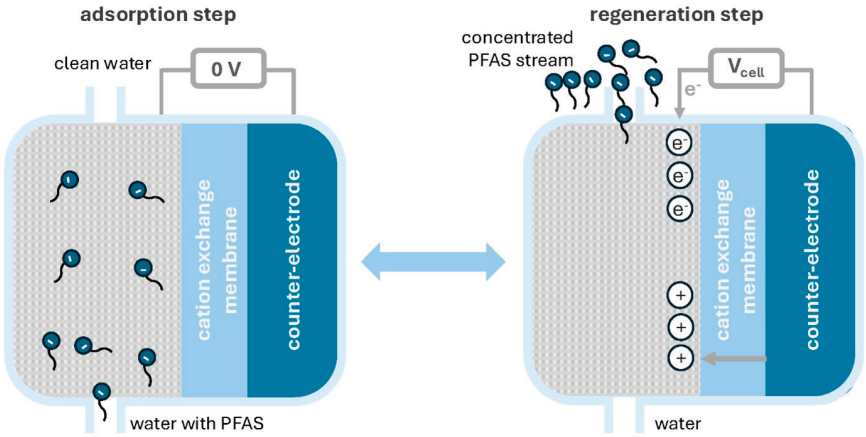


Figure 6.1. Electroregeneration of PFAS-laden activated carbon: when electrically charged, PFAS molecules are repelled from the carbon surface and desorbed from the adsorbent, exiting the activated carbon column with the effluent. This electrically-driven regeneration step can be implemented as an on-site regeneration technology. The adsorption of PFAS on the activated carbon and electroregeneration can be performed in the same device.

6.2. Materials and methods

6.2.1. Experimental setup

In this study, we employ an electrochemical cell with two carbon electrodes for electroregeneration of PFAS.[200] The experimental setup consisted of a symmetric electrochemical cell where the same type of electrode was used as both the anode and cathode, separated by a cation exchange membrane and assembled as discussed in Arulrajan et al.[201] Graphite plates served as current collectors, connecting the electrodes with external wires to a potentiostat (Ivium Technologies). The electrodes were carbon cloth electrodes purchased from Kynol Europa GmbH, and more details are reported in Table S.6.2.[202] A Type 10 cation exchange membrane (Fujifilm) was used to separate the electrode compartments in all experiments, without any spacing between the electrodes and the membrane. The properties of the electrode materials and the cation exchange membrane, as provided by the supplier, are provided in the Section 6.5. Samples were taken from the cell effluent line, and the composition of the solution was analyzed. Prior to the experiment, we investigated PFAS adsorption on the electrochemical cell components and found no adsorption to any components used in this study. Three different experiments were conducted with the objectives to: I) study the desorption of PFAS from the non-modified activated carbon upon an applied cell voltage, II) study the regeneration with surface modified activated carbons, and III) enhance the regeneration performance and enrichment of PFAS in a concentrate stream.

6.2.2. Electrically driven desorption

A solution containing 5 mM NaCl and a mixture of 7 PFAS, each at a concentration of approximately 1000 ng/L, was pumped through both electrode compartments at a flow rate of 5 mL/min per channel using Masterflex® Ismatec® Reglo Independent Channel Control (ICC) Peristaltic Pumps (Avantor). Each electrode compartment was connected to a separate solution container (Nalgene PPCO bottles), which was used for both adsorption and electroregeneration. The solution was recirculated through its respective compartment, between the cell and a container.[203] The solutions were continuously mixed using a magnetic stirrer, and the headspace of the containers was over-pressurized with nitrogen to minimize the presence of dissolved oxygen, which could otherwise lead to oxidation of the electrode material.[204] Future work should examine whether carbon oxidation occurs during electroregeneration and assess its impact on regeneration performance. Changes in the total solution volume in the cell were accounted for in the mass balances. Samples were taken from the effluent of the regeneration cell during each experiment and analyzed by LC-MS to determine PFAS concentrations. Using a mass balance equation, we calculated the PFAS concentration in the regeneration vessel.

Before the start of the electroregeneration step, an adsorption step was conducted, during which PFAS were adsorbed onto the activated carbon without applying a current. An initial, environmentally relevant concentration of approximately 1000 ng/L of each PFAS was used during the adsorption step. After the adsorption step, the PFAS concentrations, excluding PFPeA, were below the detection limits. A trace concentration of approximately 10 ng/L of PFPeA was still observed after adsorption.

6.2.3. Electrode modifications

To study the role of surface charge on the adsorption and subsequent electroregeneration of the activated carbon felt electrode, two different modifications were made. These modifications aimed at 1) an increase in positive chemical charge by functionalizing the surface with aminated groups, and 2) increasing the positive surface charge by depositing a positively charged polyelectrolyte.

Amine functional groups were introduced to the carbon surface using a silanization reaction between a silylating agent and the hydroxyl functional groups on the carbon surface. To achieve this, the unmodified carbon cloth electrodes were submerged into 150 mL of amino-silylating agent, i.e. APTES, (3-aminopropyl)triethoxysilane (99%, Sigma Aldrich, USA) in toluene (99.8%, anhydrous, Sigma Aldrich, USA) solution (30% v/v solution). The submerged electrodes were kept in an airtight container and stirred at 120 rpm for at least 24 hours to ensure maximum modification of the active carbon surface. Following the modification, the electrodes were washed several times using ultrapure water and subsequently dried at room temperature.

Polyelectrolyte modification was performed by dip-coating the carbon cloth electrodes in an ionomer solution (2.5 wt% solution of Fumion FAA-3 in 1-methyl-2-pyrrolidinone) for . Afterwards, the coated electrodes were dried at room temperature, followed by additional thermal drying at 80 °C.

The basic functional groups on the carbon surface were quantified using Boehm's titrator method on both modified and unmodified electrode materials. In this procedure, ~0.5 g of the electrode material was immersed in 30 mL of 0.05 M HCl solution for 24 hours, with occasional agitation to promote the neutralization of basic surface groups. Following this, the solution was titrated using an automatic titration (Metrohm 888 Titrando), with 50 μL aliquots of 0.05 M NaOH added at intervals of 30 to 60 seconds. The total amount of positive functional groups on the carbon surface was determined based on the difference in titrant volume to reach the equivalence of the blank titration solution and sample using $c = \frac{(V_{sample} - V_{blank}) * c_{blank}}{m_{sample}}$ with c the amount of positive functional groups on the carbon, V_{sample} the volume of titrant needed to reach the equivalence point for the sample, and V_{blanc} for the blank, c_{blank} the titrant concentration and m_{sample} the mass of the carbon material.

The chemically modified electrodes were inserted into the electrochemical cell, and adsorption/electroregeneration experiments were performed. During these experiments, the PFAS solution volume was increased to 4 L during the adsorption step. To ensure mixing during the adsorption step, the feed solution was internally recirculated using a peristaltic pump at a flow rate of 100 mL/min. Following the adsorption step, batch regeneration of the cathode was performed using a 40 mL, 5 mM NaCl solution at 1.2 V for 6 hours. During electroregeneration, the regeneration solution was continuously recirculated through the electrode compartments at a flow rate of 5 mL/min.

6.2.4. Electroregeneration of PFAS-laden carbon: enrichment and recovery

First, an adsorption step was carried out as discussed for the previous experiment. Regeneration was subsequently performed in sequential-batch mode. During each step of the regeneration experiment, a 5 mM NaCl solution was pumped into the cathode compartment of the cell (approximately 4 mL), and an electrical voltage was applied, causing PFAS desorption. After 5 minutes, the solution was ejected from the cathode compartment using high-pressure nitrogen, and the effluent was collected and analyzed. Fresh 5 mM NaCl solution was then pumped into the cell, and this sequential-batch operation was repeated for another 23 steps.

For each regeneration step, the recovery was calculated using $Recovery = \frac{V_r c_r}{V_0 c_0}$ where V_{r} and c_{r} represent the volume and concentration of the regeneration vessel, and V_0 and c_0 are the volume and concentration of the adsorption vessel, respectively. This recovery indicates which fraction of the adsorbed PFAS was desorbed into the regeneration vessel. Thus, the remaining fraction was still on the activated carbon. Alongside the recovery, an enrichment

factor was calculated in the experiment where the feed and regeneration vessel volumes differed using $Enrichment\ factor = \frac{c_r}{c_0}$.

6.2.5. PFAS solution and analysis

A solution containing 7 different PFAS components was prepared, comprising a mixture of short- and long-chain PFAS. These components were selected due to their regulatory significance. The PFAS components included in this study are listed in Table S.6.1. The initial concentration of each PFAS was around 1000 ng/L. The PFAS concentrations in the samples were determined using a SCIEX 5500+ LC-AD30 LC-MS system equipped with a Phenomenex Kinetix C18 column. The quantification limits for the targeted PFAS were determined at 2.5 ng/L. A detailed description of the analytical method is provided in Pranić et al.[115]

6.3. Results and discussion

First, we studied the desorption of both short- and long-chain PFAS during regeneration on unmodified carbon material under various cell voltages and evaluated the overall regeneration performance. Next, we studied the role of an external electronic charge on the carbon during adsorption to evaluate if the adsorption capacity can be impacted. Following this assessment, the impact of surface charge modification during electroregeneration was studied under a constant voltage. Lastly, we evaluated an alternative electroregeneration approach, namely sequential batch regeneration. In these experiments, we showed that high enrichment factors can be obtained, and we found high enrichment factors for short-chain PFAS with unmodified carbons.

6.3.1. Electrically driven desorption

In these experiments, we conducted an adsorption step followed by an electroregeneration step, with the solution volume remaining constant throughout both phases; the container was not replaced between the phases. This adsorption-regeneration process was performed consecutively twice. To ensure equilibrium, adsorption was conducted for 168 hours, after which nearly all PFAS were adsorbed onto the activated carbon, with only PFPeA detected in solution at 10 ng/L.

The regeneration of short-chain PFAS was highly effective (Figure 6.2A). In the first regeneration step, the short-chain PFAS recoveries ranged from 56 to 90%. A second adsorption-regeneration cycle was then conducted. In Figure 6.2, regeneration and adsorption efficiencies are presented as a percentage of the total amount initially removed (in adsorption 1). For all PFAS, the total amount regenerated in the second step slightly exceeded the total amount adsorbed in that step. Let us elaborate on this. For PFBS, the initial adsorption was 947 ng/L, corresponding to 947 ng given the 1 L reactor volume. During the first regeneration step, 67 % of the adsorbed PFBS (633 ng) was desorbed, leaving 314 ng on the carbon. In the

second adsorption step, 62 % of the initial adsorption (947 ng) was re-adsorbed, i.e., 586 ng, resulting in a total of 900 ng of PFBS on the carbon. In the second regeneration step, 61 % was desorbed (675 ng), leaving 272 ng on the carbon. The second regeneration step thus appeared slightly more effective than the first, although the difference was small. Future studies should include additional consecutive adsorption and electroregeneration cycles to investigate whether a dynamic steady state develops, meaning that the adsorption and regeneration of consecutive steps remain constant. Our results indicate that, over two cycles, the total amount of PFAS desorbed and the recovered adsorption capacity remained stable. These findings suggest that continuous operation of this regeneration process is feasible, even for long-chain PFAS. Following an initial adsorption–regeneration cycle, complete regeneration of adsorbed PFAS is possible in subsequent cycles.

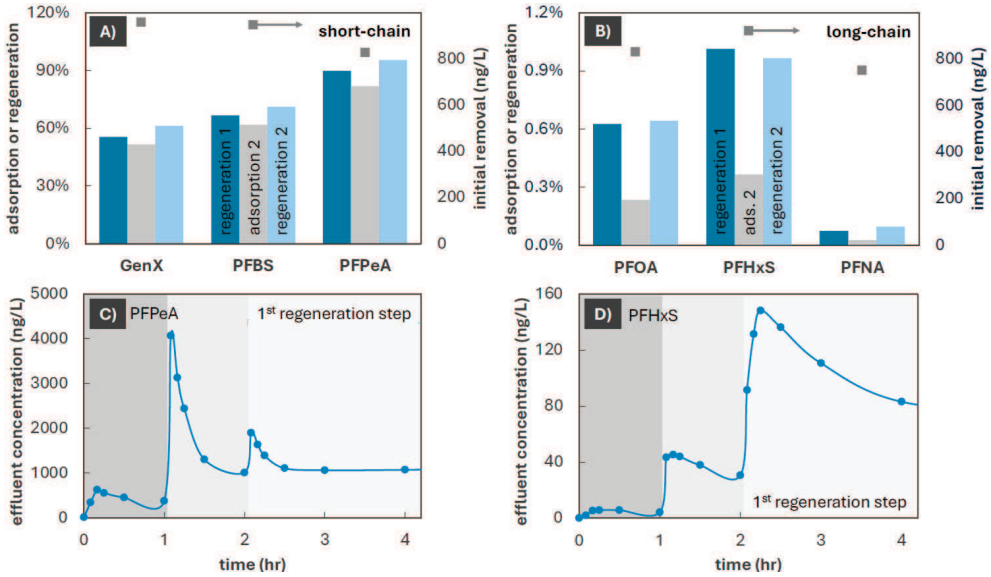


Figure 6.2. Electroregeneration of PFAS from an electrically negatively charged carbon electrode. Adsorption and electroregeneration of short-chain (A) and long-chain PFAS (B). The total initial PFAS removal in the adsorption step, which is adsorbed on the electrode (not electrically charged during adsorption), is shown with markers corresponding to the right y-axis. The regeneration efficiency in the first step, the re-adsorption efficiency (with respect to the total initial adsorption), and the regeneration efficiency in the second step are shown on the left y-axis. The effluent concentration of PFPeA (C) and PFHxS (D) as a function of time. Each regeneration step involved three sequential desorption voltages: 0.4 V for 1 hour, then 0.8 V for 1 hour, and 1.2 V for 2 hours, resulting in a total duration of 4 hours of each regeneration step. We note that the regeneration efficiencies in (A) and (B) are calculated based on desorption after a complete 4 h regeneration step. The NaCl concentration in solution was 5 mM, and the initial concentration of each PFAS before the adsorption phase was approx. 1000 ng/L. Lines serve to guide the eye. Effluent concentrations of other PFAS are reported in Figure 6.5.2.

In Figure 6.2C, we present the effluent concentration of PFPeA from the cathodic chamber as a function of time. During regeneration, the applied voltage was increased stepwise from 0 to 1.2 V, with time intervals of one hour. At a low applied voltage of 0.4 V, we observed the desorption of short-chain PFPeA from activated carbon), with a clear peak effluent concentration of 625 ng/L (Figure 6.2C). After some time, no further desorption occurred, and the concentration in solution reached an equilibrium value. Because not all adsorbed PFAS were desorbed from the activated carbon felt electrode at this low cell voltage of 0.4 V, the voltage was increased to 0.8 V, which resulted in increased PFPeA desorption and a second peak in effluent concentration, reaching values greater than 4000 ng/L. Again, after some time, no further desorption occurred, and solution concentration reached equilibrium. Increasing the cell voltage to 1.2 V after two hours resulted in a regeneration vessel concentration close to the initial PFPeA concentration of approximately 1000 ng/L. Interestingly, desorption of the long-chain PFHxS was substantially less effective (Figure 6.2D). This is most likely because its adsorption relies primarily on hydrophobic interactions between the perfluorinated tail and the carbon surface, rather than on electrostatic interactions between the charged head group and the surface charge groups. In contrast, adsorption of short-chain PFAS is governed by electrostatic interactions between the head group and the surface charge sites, which are more easily reversible upon electrically charging the carbon surface.

We demonstrated that electroregeneration can efficiently desorb short-chain PFAS from activated carbon and achieve high recoveries, even in the presence of background salts at environmentally relevant concentrations. Although successful regeneration in the presence of background salts has been demonstrated in previous studies,[65,195] our findings remain significant. In our view, the primary mechanism for electrically driven PFAS desorption is that, upon electrically charging the carbon, each electron stored in the carbon matrix leads to the desorption of one negatively charged PFAS molecule to maintain electroneutrality within the electrical double layer (EDL). However, charging the carbon with electrons may also cause the electrosorption of cations (e.g., Na^+) or the desorption of other anions (e.g., Cl^-), without leading to PFAS desorption. While the presence of ions is required to provide conductivity within the electrochemical cell, we initially expected that competition with the background salt, present at a molar concentration roughly a million times higher than that of PFAS, would hinder, or even prevent, the electrically driven desorption of PFAS.

An improved mechanistic understanding of ion interactions and competition during electroregeneration is still needed. We consider that additional mechanisms may influence PFAS desorption, such as volume-based competition with other ions.[205] In this case, when counterions like Na^+ are electrosorbed, the limited pore volume may result in competition between ions, favouring the electrosorption of ions that carry more charge per occupied volume, such as Na^+ and Cl^-. The larger ions, such as the PFAS molecules, will then be desorbed. The relative importance of these mechanisms in controlling electrically driven PFAS desorption requires further investigation.

6.3.2. Impact of external electronic charge on the PFAS adsorption

In addition to studying the adsorption and regeneration of PFAS on unmodified activated carbon felt electrodes, we investigated the influence of surface electrical charge during the adsorption of both short- and long-chain PFAS compounds (see Figure 6.3). When using unmodified carbon electrodes, we observed near-complete removal of all PFAS used in this study. Since PFAS molecules are negatively charged due to the presence of their functional groups, such as sulfonates or carboxylic acids, we hypothesized that introducing an external electronic charge to the carbon surface could influence PFAS adsorption.[196–198]

Our experiments showed that by charging the electrode negatively with a cell voltage of 1.2 V, the adsorption of short-chain PFAS was substantially reduced, while the adsorption of long-chain PFAS remained largely unaffected. The results presented in Figure 6.3 indicate that electrostatic interactions predominantly govern the adsorption of short-chain PFAS. In contrast, hydrophobic interactions appear to be the primary mechanism driving the adsorption of long-chain PFAS, which remain largely independent of the electrode's surface charge. These observations are in line with experimental data from PFAS adsorption studies. Adsorbents containing more positively charged surface functional groups and less acidic (negatively charged) groups generally show improved PFAS removal performance.[113] Furthermore, defunctionalization of activated carbon surfaces has been reported to enhance adsorption by reducing acidic surface groups and increasing surface hydrophobicity.[74,109,114]

Furthermore, we observed that, when charging the electrodes positively, the adsorption of short- and long-chain PFAS was not enhanced (results not shown). Although this finding may appear counterintuitive, it can be easily explained. The concentration of anions in solution (in this case, Cl^-) is roughly a million times higher than that of PFAS. When the activated carbon is positively charged, the positive charge is far more likely to be compensated by the electrosorption of Cl^- ions than by negatively charged PFAS molecules.

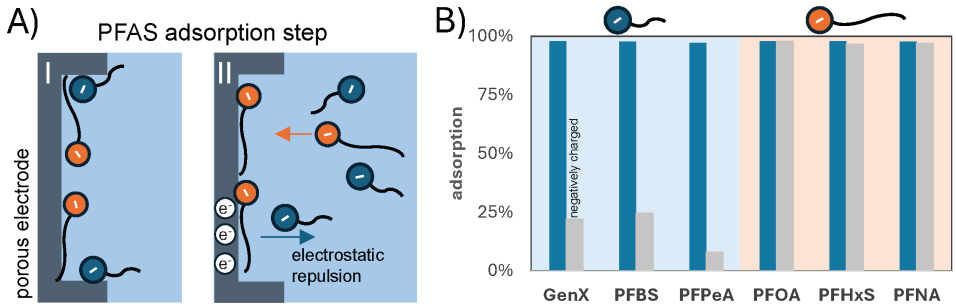


Figure 6.3. Effect of electrical charge on adsorption of PFAS on activated carbon. (A) Interactions of PFAS with an electrically charged surface (cell voltage 1.2 V). The presence of a negative electronic charge decreases the adsorption of short-chain PFAS. (B) The adsorption of short-chain and long-chain PFAS on a non-charged (blue bars) and an electrically negatively charged surface (grey bars).

6.3.3. Impact of carbon electrode modifications on PFAS electroregeneration

Next, we studied the effect of two types of surface modifications on the electroregeneration performance of PFAS. Carbon electrodes were modified with either aminated functional groups or a polyelectrolyte coating, as detailed in Section 6.2.3. Both modifications aimed to increase the density of positively charged chemical groups on the electrode surface. The titration results indicated a basic functionality of 0.29 mmol/g for the unmodified electrode material, while the polyelectrolyte and amine-modified electrodes showed values of 0.37 mmol/g and 0.42 mmol/g, respectively. These values are based on the total mass of each electrode. The polyelectrolyte-modified electrode contained 33% of polyelectrolyte by weight.

Higher enrichment factors were obtained in experiments employing electrodes with modified with aminated surface groups for two out of the three short-chain PFAS compounds studied, namely, GenX and PFBS, while the enrichment factor of PFPeA was not higher, which was most likely due to the already high enrichment factors that were achieved in the experiments with non-modified carbon felt. Simultaneously, the effect of the animated groups on long-chain PFAS remained unclear, mainly because of their generally lower electrodriven desorption (Figure 6.4). The observed enhancement in short-chain PFAS desorption was attributed to improved PFAS desorption during the electroregeneration step, which could possibly have occurred due to an increased amount of PFAS that were adsorbed onto the carbon surface via electrostatic interactions with the introduced positively charged amine groups. These observed interactions may be more easily reversed upon applying a negative charge, thereby facilitating more efficient desorption.

In contrast, in the electroregeneration experiments with polyelectrolyte modified carbon electrodes, the enrichment factors of short-chain PFAS were substantially lower (Figure 6.4). Notably, during the initial adsorption step, nearly complete removal of both short- and long-chain PFAS was achieved with the polyelectrolyte-modified electrode (Figure 6.5.3). However, during the subsequent electroregeneration step, almost no PFAS (short- or long-chain) was desorbed from the electrode surface. We hypothesize that this occurred due to the repulsive force between the negatively charged electrode and the PFAS molecules being insufficient to overcome the strong interactions of the PFAS molecules with either the positively charged polyelectrolyte coating or the carbon surface.

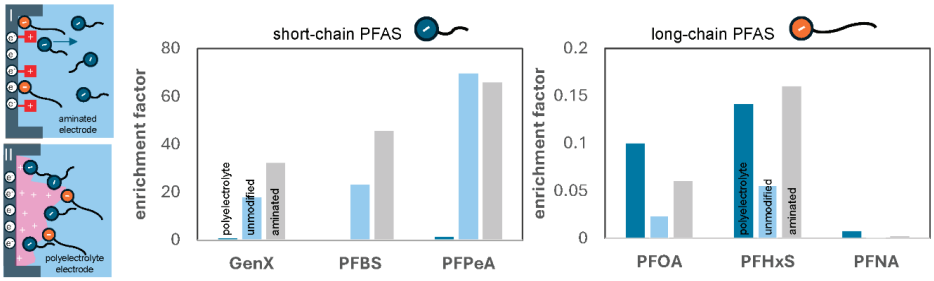


Figure 6.4. Effect of carbon electrode modifications on the electroregeneration of short- and long-chain PFAS. Compared to unmodified electrodes, in the experiments with aminated groups the enrichment of certain short-chain PFAS was enhanced, while the polyelectrolyte coating reduced the ability of the electrode for efficient electroregeneration process.

6.3.4. Electroregeneration of PFAS-laden carbon: enrichment and recovery

Next, we evaluated an alternative electroregeneration approach of non-modified carbon, namely sequential batch regeneration, to investigate if an operational change could enhance the achievable enrichment factors. After adsorption, the cathode compartment was filled with a 5 mM NaCl solution and a cell voltage of 1.2 V was applied to desorb the PFAS components. Subsequently, the cathode compartment was emptied and the solution was collected and analyzed.

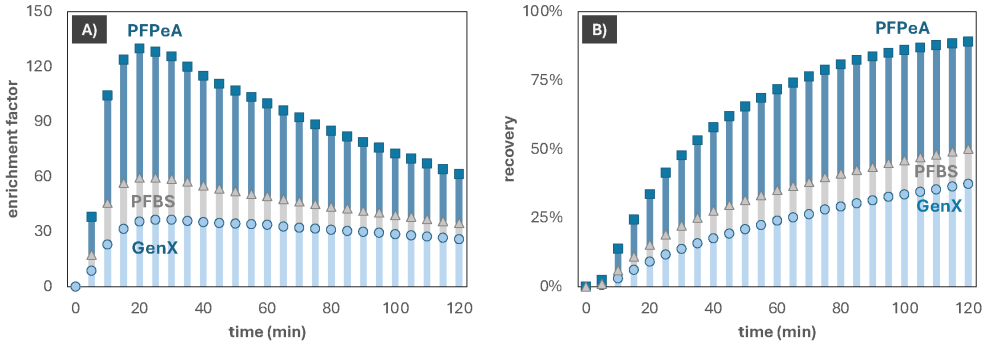


Figure 6.5. Sequential batch-mode electroregeneration of PFAS from an electrically negatively charged carbon electrode. (A) Enrichment factor of the desorption steps as a function of time. Each data point represents the concentration of PFAS for one regeneration step, i.e., the enrichment factors are not calculated based on cumulative PFAS desorption. (B) Cumulative recovery of PFAS as a function of time. Prior to regeneration, during the adsorption step, all PFAS were adsorbed onto the activated carbon electrode. For regeneration, the electrode compartment was filled with water, and the electrode was electrically negatively charged, resulting in PFAS desorption. The solution was then collected and analysed. The compartment was subsequently filled with a new batch of water, and the electrode was recharged to continue PFAS desorption.

For the short-chain PFAS, i.e. PFPeA, PFBS, and GenX, very high enrichment factors were achieved in the initial desorption steps (Figure 6.5A), with PFPeA reaching an enrichment factor of 130 in the fourth desorption step. In contrast, other commonly applied PFAS removal technologies that produce a concentrate, such as reverse osmosis[206] or nanofiltration combined with foam fractionation,[207] achieve enrichment factors of ~7 to ~41, respectively. Considering the acquired enrichment factors, the proposed electroregeneration process seems highly promising for on-site application and the coupling of the process with PFAS destruction methods seems a viable route to further investigate. Short-chain PFAS were recovered slightly less effectively compared to the initial experiment, with recoveries ranging from 37% (GenX) to 89% (PFPeA) (Figure 6.5B). However, it is important to note that the process has not yet been optimized: lower concentrations during adsorption, changes in desorption time, a different regeneration solvent, and the number of sequential batch desorption steps could yield even higher enrichment factors and improved recoveries. In contrast, the enrichment factors and recoveries for longer-chain PFAS remained below 1.1 and 1.6%, respectively. In future work, long-chain PFAS regeneration can be explored, for example, with the use of electrode materials other than activated carbon.[208]

Although not all PFAS were released back into the solution during electroregeneration, these findings do not limit the applicability of the process for short-chain PFAS desorption. In subsequent adsorption steps, the adsorption capacity may be lower for some PFAS, but a dynamic steady state will be achieved after several cycles, where the desorption of PFAS is the same as the adsorption, for the short-chain PFAS. When integrated into an on-site process, electroregeneration could potentially increase the runtimes of activated carbon filters by electrically desorbing short-chain PFAS, decreasing the environmental impact of conventional regeneration solutions of spent carbon (Figure S.6.4). For long-chain PFAS, a dynamic steady state is also reached, but under the conditions and cell design used in this study, the adsorption capacity after regeneration is likely too low to design a feasible process scheme. Since other studies have shown that regeneration of long-chain PFAS can be achieved, but at higher concentrations. For instance, a 60 % regeneration efficiency was reported for PFOA-laden activated carbon after sequential adsorption and electroregeneration cycles.[195] Further research is needed to study the factors governing the regeneration of long-chain PFAS.

6.3.5. Environmental implications

In recent years, new regulations have been proposed for the maximum allowed concentrations of PFAS in drinking water, ranging from 4 to 10 ng/L, depending on the compound.[17] According to the current EU directive, a total maximum concentration of 100 ng/L in drinking water was set for a selected group of PFAS of concern, including several short-chain components such as PFPeA, which was part of our study.[11] Many drinking water companies are unlikely to meet these stringent guidelines. Although several removal technologies are available, the removal of short-chain PFAS remains a challenge.

A viable technology for PFAS removal must satisfy several criteria. Firstly, it should efficiently remove short-chain PFAS. Preferably, its environmental impact should be minimal. The use of chemicals and the need to transport activated carbon to a regeneration facility can adversely affect this aspect. Since many technologies only remove PFAS, the resulting concentrate stream, which carries the PFAS load, requires consideration. This stream necessitates additional treatment, either thermal or electrochemical, to destruct PFAS. Thus, achieving a high concentration factor during the removal process is advantageous. Finally, treatment costs should remain low. An overview of these criteria and the technologies is provided in Figure 6.6.

	feasibility short-chain PFAS removal	chemical-free operation	on-site regeneration possible?	costs (per m3 water treated)
activated carbon electroregeneration	✓	✓	✓	not known
activated carbon thermal reg.	✓	✓	✗	$0.44 (1) / €0.02-0.10 (2)
activated carbon chemical reg.	✓	✗	✓	(3)
ion exchange	✓	✗	✓	$0.28 (4) / $0.40 (4)
foam fractionation	✗	✗	n.a. (5)	n.a. (5)
membrane filtration	large volume of concentrate			

Figure 6.6. Comparison of short-chain PFAS removal technologies based on their ability to remove short-chain PFAS, the possibilities for chemical-free regeneration and on-site application, and their costs. (1) Costs reported in Ellis et al.,[209] based on regeneration directly at breakthrough. (2) Costs reported in Belkouteb et al.,[36] based on a treatment goal of 10 ng/L ($0.10/m^3) and 85 ng/L ($0.02/m^3) for a sum of 11 PFAS, respectively. (3) Although costs per m^3 water treatment have not been reported, Larasati[63] estimated the costs of chemical regeneration to be a factor 3.5 higher than of thermal regeneration. (4) Costs reported in Ellis et al.,[209] based on regeneration directly at breakthrough. (5) Foam fractionation is not considered an effective technology for short-chain PFAS removal.[210,211]

While numerous technologies are capable of removing long-chain PFAS. Their efficiency is considerably reduced with short-chain PFAS. For example, techniques such as foam fractionation are not effective at removing short-chain PFAS.[210,211] In contrast, reverse osmosis, a membrane-based process, is capable of removing nearly all PFAS. Likewise, nanofiltration, another method involving membranes, successfully removes 70-100% of short-chain PFAS.[212] The difficulty associated with these membrane-based processes lies in generating a concentrate stream, which comprises roughly 10% of the total feed volume. The concentration of individual PFAS in this stream is about tenfold higher than in the original feed, which might prohibit direct discharge into surface water due to local regulatory constraints. Subsequently, additional treatment steps are most likely necessary to significantly up-concentrate PFAS for effective removal and destruction.

Ion exchange, a column-based technology, is highly effective for the removal of PFAS, including short-chain components.[26] The technology is, however, similar to activated carbon, not very specific to PFAS and removes many other components as well. Ion exchange resins may either be utilized for a single time or be regenerated following their use. The regeneration of ion exchange columns requires the application of chemicals, which may include an organic solvent like methanol, a base such as sodium hydroxide, an inorganic salt like sodium chloride, or a combination of these chemicals.[26,213,214] The regeneration stream, characterized by high concentrations of salts and PFAS compounds, requires additional processing. Depending on the subsequent destruction technique employed, separation of PFAS compounds from the salt solution may be required. Ellis et al.[209] calculated the costs of treatment per m^3 of water and found that single-use ion exchange resins are a cheaper alternative, see Figure 6.6.

In adsorption technologies using activated carbon, short-chain PFAS adsorption results in rapid breakthrough of the filter, necessitating frequent regeneration. Although thermal regeneration of activated carbon is feasible and has the advantage of destroying PFAS in a single step, it is energy-intensive and often requires transport to specialized treatment facilities. Ellis et al.[40] calculated that the costs of treatment with GAC are approximately $0.44-0.50 per m^3 treated. These costs have been calculated based on the assumption that the media needs replacement directly after breakthrough. Depending on the type of PFAS, between 4500-48,900 bed volumes can be treated with GAC, resulting in a regeneration frequency of approx. 2.5 months.[209] Belkouteb et al.[36] estimated the costs for GAC based on a treatment goal of 10 ng/L (sum of 11 PFAS) at $ 0.10/m^3, and of 85 ng/L at $ 0.02/m^3. The costs are dependent on the treatment objective, as this determines the necessary frequency of regeneration, which substantially affects the costs of the treatment process. The aforementioned costs are based on thermal regeneration. Although the costs per unit water treated have not been reported in the literature to the best of our knowledge, Larasati[63] estimated the costs of chemical regeneration to be a factor 3.5 higher than that of thermal regeneration.

Electroregeneration offers a sustainable alternative for the removal of short-chain PFAS. This concept can either be employed as a separate treatment step, after conventional activated carbon filters, or can be integrated in an existing carbon filter, to regenerate activated carbon granules. PFAS-laden carbon granules can be circulated to an on-site regeneration device, where these granules are electrically charged and PFAS molecules are desorbed.[215] The concentrate can be treated further by an electrochemical or thermal process. Electroregeneration allows for on-site, chemical-free, carbon regeneration, potentially reducing the costs of carbon treatment significantly. Moreover, much higher concentration factors can be achieved compared with membrane-based treatment processes.

To further develop electroregeneration as a sustainable technology for the removal of short-chain PFAS, in which carbon granules are circulated to an on-site regeneration unit, additional research is required. First, the influence of electrical resistances between carbon granules on regeneration performance and the required cell voltage should be studied.[216] Furthermore, improvements and optimization in the cell design could be explored, for example by using other membranes or by developing membraneless systems. In such membraneless configurations, particular attention should be given to potential readsorption at the counter electrode, and their performance should be compared with that of membrane-based configurations.

6.4. Conclusions

Activated carbon is widely used as an effective adsorbent to remove organic micropollutants, including PFAS. However, their rapid breakthrough, especially that of short-chain PFAS, leads to the need for frequent regeneration. In this study, we demonstrated the technical feasibility of electrogenerating PFAS-laden activated carbon under environmentally relevant ionic strengths, similar to surface water conditions, using an electrochemical cell. The results highlight that adsorbed PFAS molecules can effectively be desorbed by electrically charging the carbon. When applying a negative charge during the adsorption stage, adsorption of short-chain PFAS was inhibited, indicating that sorption of these substances most likely is dominated by electrostatic attraction. Modifying the surface charge of the carbon by introducing aminated groups improved the electro-desorption of short-chain PFAS, and resulted in an increase of the enrichment factors of GenX and PFBS. Lastly, by adapting the electroregeneration approach of non-modified carbon to a sequential-batch electroregeneration, the enrichment of short-chain PFAS was substantially increased. In our experimental configuration, for PFPeA, enrichment factors exceeding 120 were achieved across several sequential batches. By process optimization, i.e., by collecting the batches after optimal times, these factors can be increased further, making the process competitive with conventional treatment and concentrating processes. Future studies should explore novel on-site designs for regenerating activated carbon granules at drinking water treatment plants and investigate the competing effects of organics and other ions.

Acknowledgements:

This work was performed in the cooperation framework of Wetsus, European centre of Excellence for Sustainable Water Technology (www.wetsus.nl). Wetsus is co-funded by the Dutch Ministry of Economic Affairs and Ministry of Infrastructure and Environment, the Province of Fryslan, the Northern Netherlands Provinces, and The Netherlands Organization for Scientific Research. The authors like to thank the participants of the Desalination & Concentrates theme for the fruitful discussion and financial support. Jouke E. Dykstra acknowledges the support by the Netherlands Organisation for Scientific Research (NWO), Domain Applied and Engineering Science (TTW), and the Ministry of Economic Affairs (VENI grant no 19111).

6.5. Supporting Information for Chapter 6

6.5.1. Experimental setup

A schematic of the experimental setup is shown in Figure. S.6.1. The PFAS properties are reported in Table S.6.1. The activated carbon properties are reported in Table S.6.2 and the membrane properties in Table S.6.3.

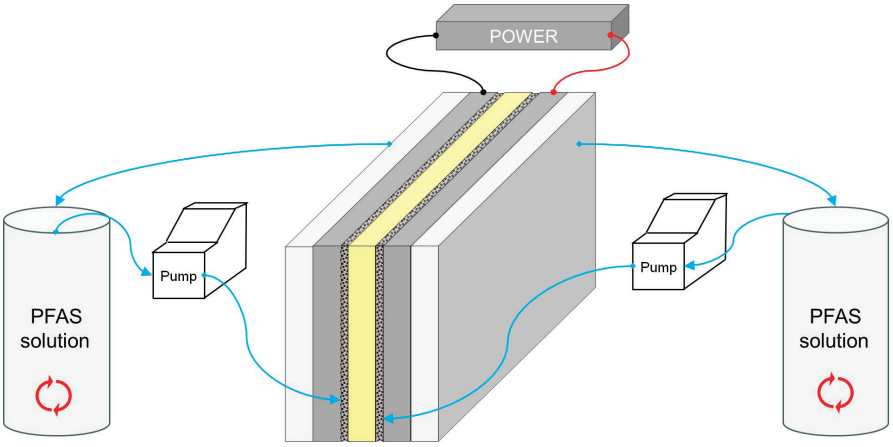


Figure S.6.1. A schematic representation of the setup. The electrochemical regeneration cell is connected to two vessels, one of which contains a PFAS solution. The solutions are recirculated through the cell, which contains two carbon electrodes. One electrode is negatively charged by the power device, causing the desorption of PFAS molecules. To prevent readsorption on the other electrode, a cation exchange membrane is placed between the two electrodes. The tubing was TYGON A-60-G (Saint-Gobain).

Table S.6.1. Properties PFAS components used in this study

PFAS	Abbreviation	Linear chain length	Functional group	Mw (g/mol)	log K_{OW}	pKa
Perfluorobutane sulfonic acid	PFBS	4	$-SO^{-3}$	299	1.82	-3.31
Perfluorohexane sulfonic acid	PFHxS	6	$-SO^{-3}$	399	3.16	0.14
Perfluorooctane sulfonic acid	PFOS	8	$-SO^{-3}$	499	4.49	<1.0
Perfluoropentanoic acid	PFPeA	4	$-COO^{-}$	264	3.01	0.34
Perfluorooctanoic acid	PFOA	8	$-COO^{-}$	414	4.81	0 – 3.8
Perfluorononanoic acid	PFNA	9	$-COO^{-}$	464	5.48	-0.21
Hexafluoropropylene oxide dimer acid	GenX	5	$-COO^{-}$	329	4.00	3.80

For GenX, values were obtained from Vakili et al.,[67] for PFOA from Musegades et al.[217] and for other PFAS from Gagliano et al.[13]

Table S.6.2. Activated carbon fabric properties. For the electrically driven desorption experiments, ACC-507-20 (Kynol Europa) activated carbon fabrics were used. In the experiments on the enrichment factor and recovery, ACC-5092-15 (Kynol Europa) activated carbon fabrics were used. For both experiments, the fabric surface area was 20 cm^2. The ACC-5092-15 electrode has a Brunauer–Emmett–Teller (BET) surface area of 1100–1478 m^2/g, a DFT pore volume of approximately 0.55 mL/g, an average pore size of 0.68 nm, and a thickness of approximately 0.8 mm. The ACC-507-20 electrode has a thickness of 0.45 mm, a BET surface area of 1800–2231 m^2/g, a DFT pore volume of approximately 0.89 mL/g, and an average pore size of 0.96 nm.[202]

		ACC-507-20	ACC-5092-15
Filter thickness	(mm)	0.45 ± 0.04	0.6 ± 0.1
Specific surface area	(mg/g)	1800 ± 15%	min. 1300
Weight	(g/m^2)	95 ± 9.5	170 ± 10
Tensile strength wrap	(kg/50 mm)	10	20
Tensile strength filling	(kg/50 mm)	8	10

Table S.6.3. Fujifilm cation exchange membrane properties

		Type 10 CEM
Dry thickness	(μm)	135
Electrical resistance	(Ω/cm^2)	2
Permselectivity	(%)	99
Ion exchange capacity	(meq/g)	1.5
Water permeation	($mL/bar.m^2.h$)	6.5
pH stability	(-)	1 - 13
Temperature stability	(°C)	60

6.5.2. Regeneration experiments

In Figure 6.2, the effluent concentration of PFPeA and PFHxS are reported, measured at the effluent of the electrochemical cell during the regeneration step. The data of the other PFAS are reported in Fig. S.6.2. The experimental conditions are the same as those in Figure 6.2.

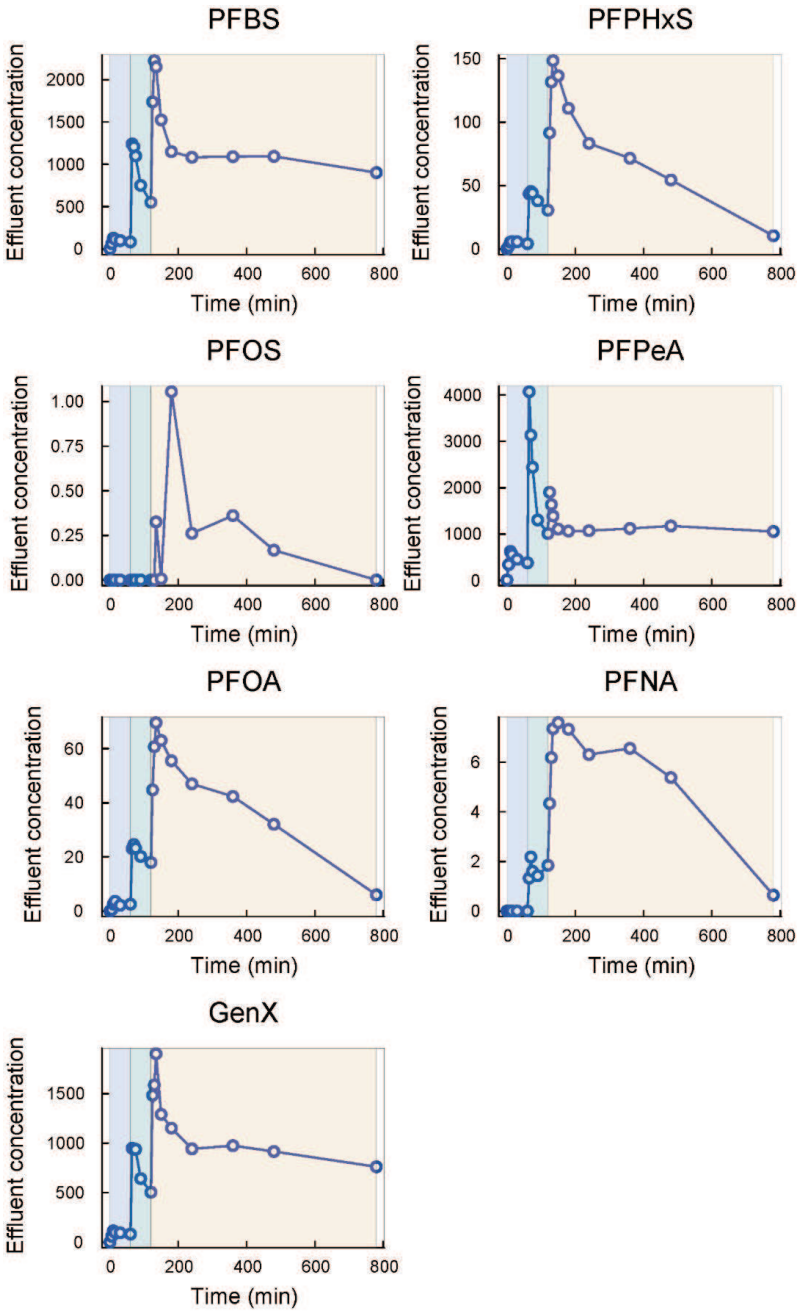


Figure S.6.2. Electroregeneration of PFAS from an electrically negatively charged carbon electrode. The effluent concentration of the different PFAS as function of time. The regeneration phase involved three sequential desorption voltages: 0.4 V, 0.8 V, and 1.2 V. The NaCl concentration in solution was 5 mM, and the initial concentration of each PFAS before the adsorption phase was approx. 1000 ng/L. Lines serve to guide the eye. The effluent concentrations of PFPeA and PFHxS are reported in the SI.

6.5.3. Impact of carbon electrode modifications on PFAS electroregeneration

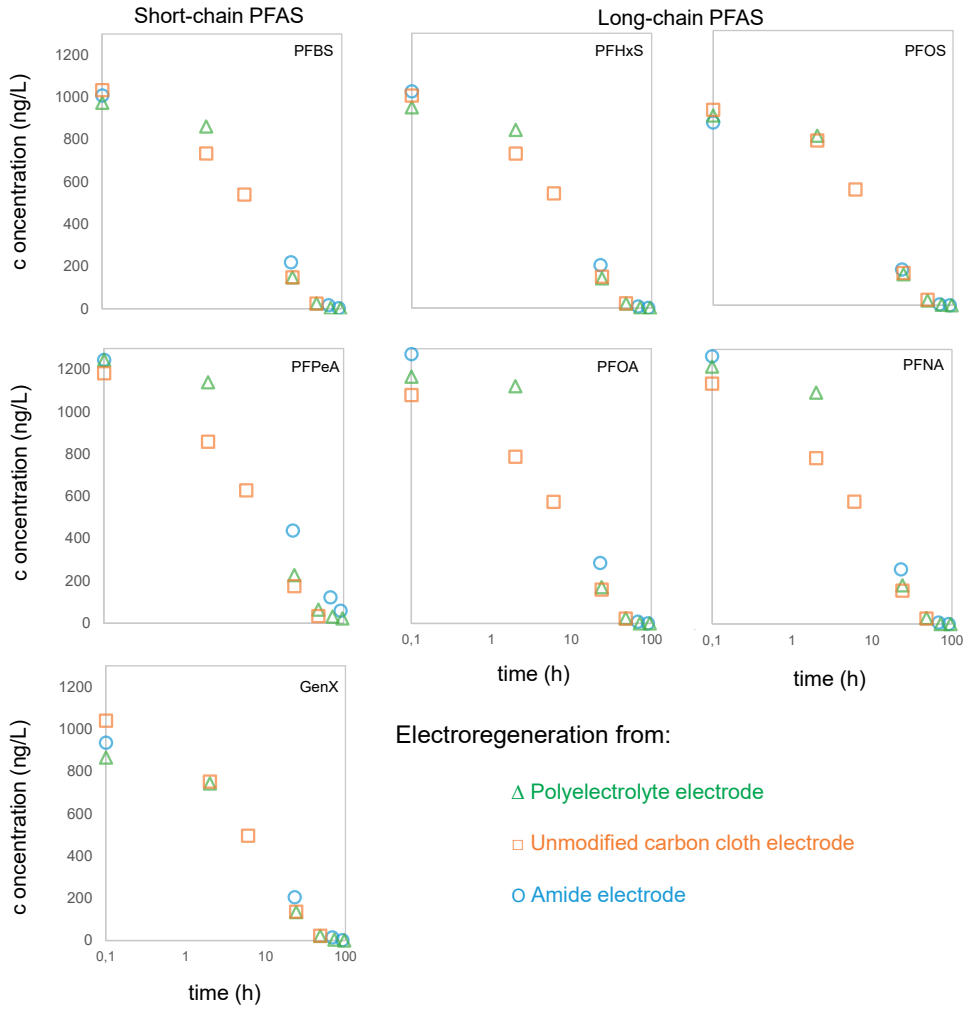


Figure S.6.3. Adsorption of PFAS over time on three different electrode materials: the polyelectrolyte electrode, the amide electrode and the unmodified carbon cloth electrode.

6.5.4. Integration of the electro-regeneration step into an on-site process

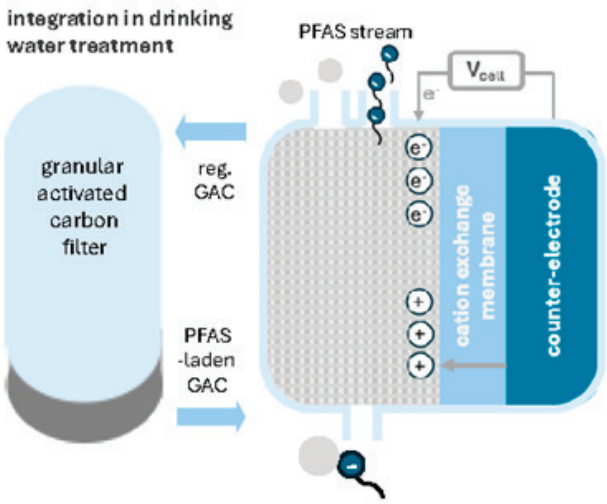


Figure S.6.4. Electroregeneration of PFAS-laden activated carbon. This electrically-driven regeneration step can be implemented as an on-site regeneration technology. The electroregeneration step can be carried out in a separate electrochemical cell, where the PFAS-laden carbon granules are transported for regeneration and then returned to the activated carbon column. This on-site process can increase the runtime of activated carbon filters, which will decrease the environmental impact of conventional regeneration solutions of spent carbon significantly.

CHAPTER 7

General Discussion



7.1. Introduction

This chapter integrates the results from experimental Chapters 2–6 to explain the mechanisms controlling PFAS adsorption on granular activated carbon (GAC) under drinking-water–relevant conditions, and to discuss how these mechanisms influence full-scale treatment performance and design.

7.1.1. Scope of discussion

The scope of this Thesis is limited to drinking water treatment applications, where PFAS typically occur at low ng/L concentrations. Experiments were conducted using GAC doses, contact times, and/or water matrices relevant to drinking water production. The work combines batch isotherm and kinetic experiments with rapid small scale column studies, supported by mechanistic models that describe adsorption equilibrium and surface-diffusion-controlled intraparticle transport. Together, this approach provides both fundamental insight into PFAS adsorption processes and a basis for translating laboratory observations to practical system design and operation.

Multiple short- and long-chain PFAS were investigated in this work. Because adsorption behaviour was found consistent within each group, in the Discussion the results are presented for one representative short-chain PFAS (PFPeA) and one representative long-chain PFAS (PFNA) to illustrate trends and mechanisms. This Thesis focuses on legacy PFAS and does not include branched isomers, ultrashort-chain PFAS, or PFAS precursors.

7.1.2. Main findings of Chapters 2-6 discussed in Chapter 7

The main findings of this Thesis are summarized below. These findings will be discussed in subsequent sections.

Objective 1: Determine and model PFAS adsorption on activated carbon under environmentally relevant conditions

PFAS adsorption at ng/L concentrations differs fundamentally from behaviour deduced from high-concentration experiments. Isotherm parameters were found to be strongly concentration-dependent, with high-concentration data overestimating adsorption capacity at drinking-water levels by orders of magnitude. PFAS adsorption kinetics were intrinsically slow at realistic GAC-to-water ratios and governed predominantly by surface-diffusion-controlled intraparticle transport. Temperature increase further reduced the adsorption capacity of short-chain PFAS.

These findings are discussed in Sections 7.2.1 (PFAS concentration), 7.2.2 (PFAS kinetics), and 7.2.7 (Temperature).

Objective 2: Identify activated carbon properties that limit PFAS adsorption

Despite being small enough to access micropores, PFAS adsorbed predominantly in the mesopores due to slow surface diffusion, making mesopore volume the effective capacity-limiting domain. Surface charge further controlled adsorption, particularly for short-chain and weakly hydrophobic PFAS, with positively charged or low-acidity carbons performing better.

These findings are discussed in Sections 7.2.4 (Pore size distribution) and 7.2.5 (Surface charge).

Objective 3: Identify NOM components that limit PFAS adsorption

Natural organic matter (NOM) was identified as a dominant factor limiting PFAS removal under realistic treatment conditions. Competitive effects intensified with increasing NOM-to-PFAS concentration ratios, leading to earlier breakthrough. Low-molecular-weight (LMW) hydrophilic NOM primarily limited short-chain PFAS adsorption, while hydrophobic neutral NOM preferentially interfered with long-chain PFAS.

These findings are discussed in Section 7.2.6 (NOM competition).

Objective 4: Assess whether electroregeneration is a suitable regeneration strategy for PFAS-laden activated carbon.

Electroregeneration demonstrated, as a proof of concept, to selectively desorb and concentrate short-chain PFAS from activated carbon under environmentally relevant conditions, indicating its potential as a low-emission alternative to frequent thermal reactivation.

These findings are discussed in Section 7.4.3 (Electroregeneration of activated carbon) and revisited in Section 7.5 (Societal costs and benefits).

The Discussion is structured as follows. Section 7.2 discusses the key factors limiting PFAS adsorption, the mechanistic reasons behind these limitations, and potential technological strategies to overcome them. Section 7.3 translates these insights into practical applications and modelling approaches for improving and predicting PFAS removal in full-scale systems. Section 7.4 outlines future research priorities to address the remaining knowledge gaps, while Section 7.5 examines the societal and economic implications of achieving increasingly strict PFAS standards in drinking water treatment.

7.2. Limitations and underlying mechanism of PFAS adsorption on activated carbon, and strategies for enhancing adsorption

7.2.1. PFAS concentration

Adsorption isotherms describe the thermodynamic equilibrium between the concentration of an adsorbate in solution (c_{eq}) and the amount adsorbed onto a solid surface (q_{eq}).[30,31] Isotherms provide parameters that give insights into adsorption mechanisms, such as whether molecules are adsorbed as individual species or in multilayers.[48] These parameters are widely used as inputs for mechanistic breakthrough models.[30,50] Because isotherm parameters are commonly treated as constant model inputs, it is essential to address one of the central findings of this Thesis: PFAS adsorption isotherm parameters are strongly dependent on the initial concentration used to reach equilibrium (Chapter 2)

Figure 7.1 qualitatively illustrates the effect of initial concentration on equilibrium adsorption behaviour for short- and long-chain PFAS on two activated carbons across four concentration ranges. For both PFAS groups, higher adsorbed amounts are observed at the same equilibrium concentration when the initial PFAS concentration is higher. Consequently, adsorption behaviour determined at elevated concentrations cannot be extrapolated to environmentally relevant ng/L levels. This effect is not caused by incomplete equilibration at low concentrations, as equilibrium was reached in all cases, as confirmed by kinetic data (Figure 7.3, Section 7.2.2). Instead, the concentration dependence reflects a fundamental shift in adsorption equilibrium associated with the concentration regime used to reach equilibrium.

The concentration dependence of PFAS adsorption is quantified in Figure 7.2 for long-chain PFAS, where the Langmuir maximum adsorption capacity (q_{max}) increases systematically with increasing initial concentration. For PFNA adsorption on microporous AC, q_{max} increased from 10 ng/mg at an initial concentration of 100 ng/L to 5545 ng/mg at 100,000 ng/L, illustrating the magnitude of this effect. A similar trend was observed for the Freundlich constant (K_f) (Table S.2.22, Chapter 2). Together, these results demonstrate that isotherm parameters derived from high-concentration experiments, under which most PFAS isotherm data in the literature have been obtained (Chapters 2 and 3), overestimate PFAS adsorption at drinking-water concentrations by several orders of magnitude and consequently lead to inaccurate predictions of PFAS breakthrough.

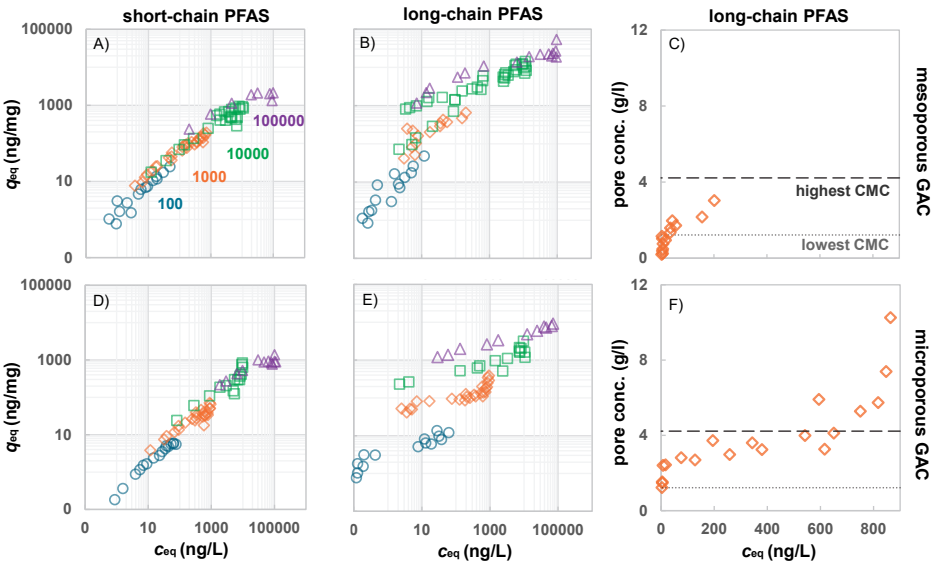


Figure 7.1. Experimental equilibrium adsorption data for short-chain PFPeA in mesoporous SRD (A) and microporous CS (D), and long-chain PFNA in mesoporous SRD (B) and microporous CS (E) at multiple initial concentrations: $C_0 \approx 100$ ng/L (blue circles), $C_0 \approx 1000$ ng/L (orange diamonds), $C_0 \approx 10$ µg/L (green squares), and $C_0 \approx 100$ µg/L (purple triangles). Data were obtained from batch adsorption experiments and are reported in detail in Chapters 2 and 3. Panels (C) and (F) show PFNA concentrations within the carbon pores, calculated by dividing the adsorbed PFNA mass by the mesopore volume of the respective carbon.

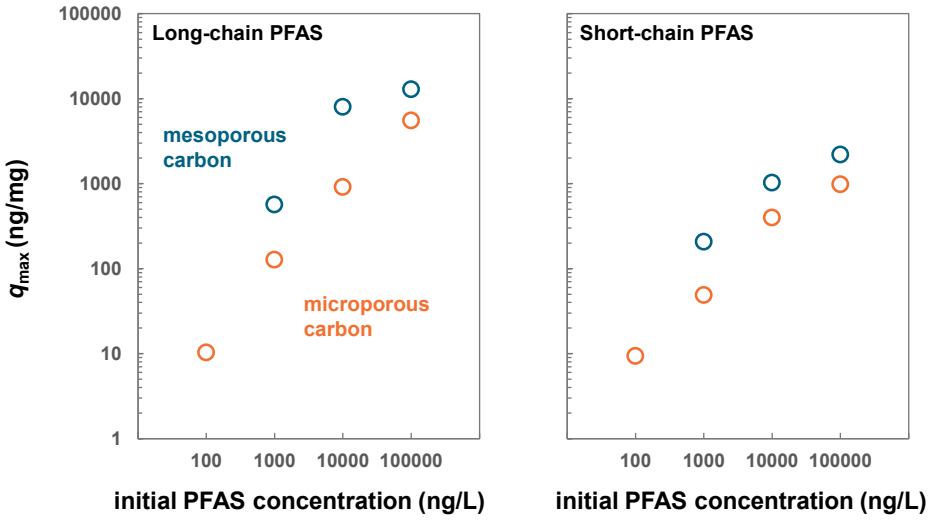


Figure 7.2. Estimated Langmuir maximum adsorption capacities (q_{max}, ng/mg) for PFAS adsorption on mesoporous SRD and microporous CS activated carbons at different initial PFAS concentrations. Values were obtained by fitting the Langmuir isotherm to the experimental data shown in Figure 7.1, excluding the part of the isotherm showing an increase after a plateau has been observed. All fits yielded $R^2 > 0.95$.

7.2.1.1. Underlying mechanism

PFAS adsorption on AC does not follow a single equilibrium isotherm but instead depends on the initial PFAS concentration used to reach equilibrium. This behaviour arises from the surfactant nature of PFAS, which are characterized by a hydrophobic fluorinated tail and a charged functional group. In aqueous systems, PFAS can self-associate and adsorb in multilayers on solid surfaces, as illustrated in Figure 1.2 in the Chapter 1.

An S-shaped isotherm is observed for the adsorption of long-chain PFNA onto microporous AC at an initial concentration of 1000 ng/L (Figure 7.1F). Although this concentration is well below the critical micelle concentration (CMC) in bulk solution, calculations show that PFNA concentrations within the carbon pores exceed the highest CMC values reported in the literature (4.2 g/L)[69] for the right-hand side of the isotherm. This indicates that local conditions within the pores are favourable for aggregation and multilayer formation. Similar behaviour has been hypothesised previously, with PFAS aggregates, hemi-micelles, or micelles reported at concentrations below the bulk CMC.[54]

Therefore, the observed increase in adsorption capacity (Figure 7.1) and q_{max} (Figure 7.2), at higher initial PFAS concentrations is attributed to multilayer adsorption arising from PFAS surfactant behaviour. At lower concentrations, cooperative adsorption is suppressed, resulting in substantially lower adsorption capacities.

7.2.1.2. Strategies to improve PFAS removal at low concentrations

Three main strategies can be considered to improve removal of PFAS occurring at low concentrations in drinking water. The most direct approach is to increase PFAS concentrations prior to adsorption, for example by applying nanofiltration or other membrane-based concentration processes upstream of GAC treatment. As shown in Figure 7.1 and discussed in Section 7.2.1.1, higher initial PFAS concentrations promote adsorption regimes associated with increased surface loading, including aggregation and multilayer adsorption within mesopores. Pre-concentration therefore shifts adsorption into a regime where GAC capacity is more effectively utilized. This effect was demonstrated by Franke et al. (2019), who reported that GAC removed approximately 2.6 times more PFAS from a nanofiltration concentrate (∑PFAS ≈ 850 ng/L) than from the corresponding influent (∑PFAS ≈ 200 ng/L).[88]

Second, there is a clear need to develop and evaluate adsorbent materials that maintain high PFAS removal efficiency at ng/L concentrations. Many emerging materials, including surface-functionalized activated carbons, ion-exchange resins, and cyclodextrin-based polymers, show excellent adsorption performance in laboratory studies conducted at elevated concentrations.[13,169,218] However, their suitability for drinking water treatment must be demonstrated under realistic low-concentration conditions.

Third, because GAC remains the dominant technology for PFAS removal, predictive modelling frameworks are required to translate high-concentration adsorption data into reliable predictions at low concentrations. Chapter 3 addresses this challenge by introducing total PFAS isotherms, which remove the effect of initial concentration and enable comparison of adsorbents based on governing properties such as mesopore volume and surface charge. While this framework aligns well with regulatory practice, where PFAS are often controlled as sum parameters,[11,19] it does not explicitly capture concentration-dependent adsorption regimes such as S-shaped isotherms, aggregation, or multilayer adsorption of individual PFAS. Mechanistic surfactant-based models, including extensions of the Langmuir framework, are therefore required in parallel to improve extrapolation across concentration ranges.[142]

7.2.2. PFAS kinetics

In addition to thermodynamic equilibrium (isotherms), mass transport parameters are critical for modelling and predicting adsorbent performance.[30,50] In this Thesis, kinetic experiments were conducted alongside all isotherm studies (Chapters 2–5), yielding kinetic data for two activated carbons across a range of initial PFAS concentrations, temperatures, and in the presence and absence of natural organic matter (NOM). Across all datasets, a consistent observation is that adsorption equilibrium is reached extremely slowly at realistic carbon loadings, indicating intrinsically slow PFAS adsorption kinetics.

As shown in Figure 7.3, at a GAC dose of 5 mg/L, at least 30 days are required to reach equilibrium across multiple concentration ranges for both short- and long-chain PFAS on

mesoporous SRD carbon, with similarly slow equilibration observed for microporous CS. Equilibration times on the order of several weeks have also been reported in previous studies.[110] Although equilibration can be accelerated by increasing the carbon dose (Chapter 2) or by using powdered activated carbon,[79] neither approach is representative of full-scale GAC filters used in drinking water treatment.[47] A carbon dose of 5 mg/L corresponds to realistic GAC-to-water ratios applied in practice, where 1 kg of GAC treats approximately 200 m^3 of water.[143]

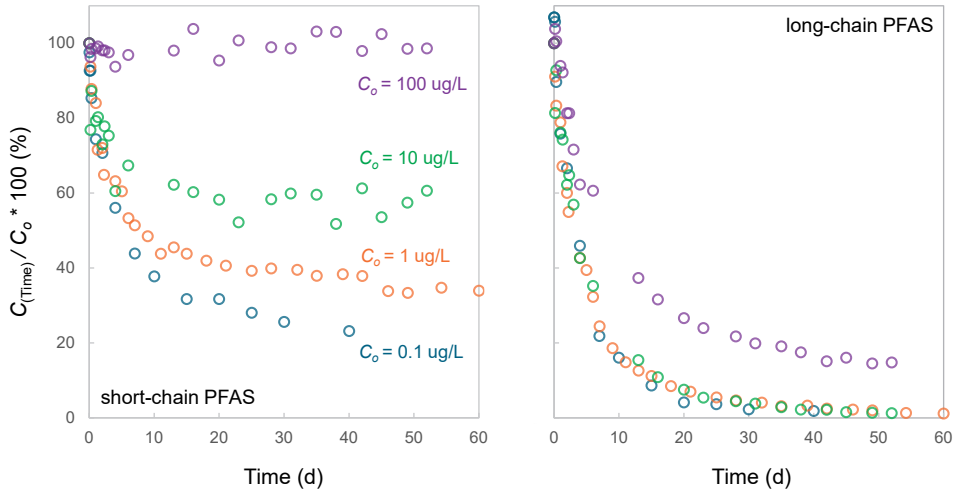


Figure 7.3. Kinetic curves for adsorption of PFAS on mesoporous GAC at different initial PFAS concentrations. Kinetic data were obtained complementary to isotherm experiments reported in Chapters 2 and 3, using a GAC dose of 5 mg/L. PFAS concentrations are normalized to the initial concentration to enable comparison across concentration ranges.

7.2.2.1. Underlying mechanism

To describe slow PFAS adsorption kinetics observed throughout this Thesis, intraparticle PFAS transport was analysed using a surface diffusion model, which describes transport along the internal surface of GAC particles.[30,80] This approach is mechanistically justified, because the hydrophobic fluorinated chains have a high affinity for carbon surface, causing intraparticle transport to occur predominantly via surface diffusion (Chapter 2). The key output of this model is the surface diffusion coefficient, D_s (m^2/s), and analysis of how D_s varies with system conditions provides direct insight into the origin of slow PFAS adsorption kinetics.

In Chapter 2, we showed that the D_s is lower (i) at higher carbon doses and (ii) in carbons with a higher mesopore volume. In addition, Figure 7.4 shows that (iii) D_s decreases by lowering initial PFAS concentrations. These three observations have in common that D_s is lower when there are more available adsorption sites. During surface diffusion, PFAS molecules

migrate along the internal AC surface while continuously adsorbing and desorbing from carbon surface. As the number of available sites increases, so does the frequency of adsorption/desorption. The consequence is decrease in intraparticle transport and characteristically slow PFAS adsorption kinetics observed in this Thesis.

The strength of PFAS–carbon interactions further controls surface diffusion behaviour. As illustrated in Figure 7.4, short-chain PFAS exhibit higher surface diffusion coefficients than long-chain PFAS, which is because of their weaker affinity towards the carbon surface. Similarly, Chapter 4 shows that the D_s increases with temperature. At higher temperatures, PFAS–GAC interactions are weakened, as evidenced by the decrease in the Langmuir affinity constant (K_l).

Taken together, these observations demonstrate that intraparticle PFAS transport in GAC is governed predominantly by surface diffusion. The systematic dependence of the intraparticle diffusion coefficient on carbon dose, initial concentration,[98,219] PFAS chain length, and temperature[30] consistently points to surface-mediated transport controlled by PFAS–carbon interactions. It should be noted that for ultrashort-chain, more hydrophilic PFAS such as trifluoroacetic acid (TFA), surface interactions are expected to be weak, and intraparticle transport is therefore likely dominated by pore diffusion.[44]

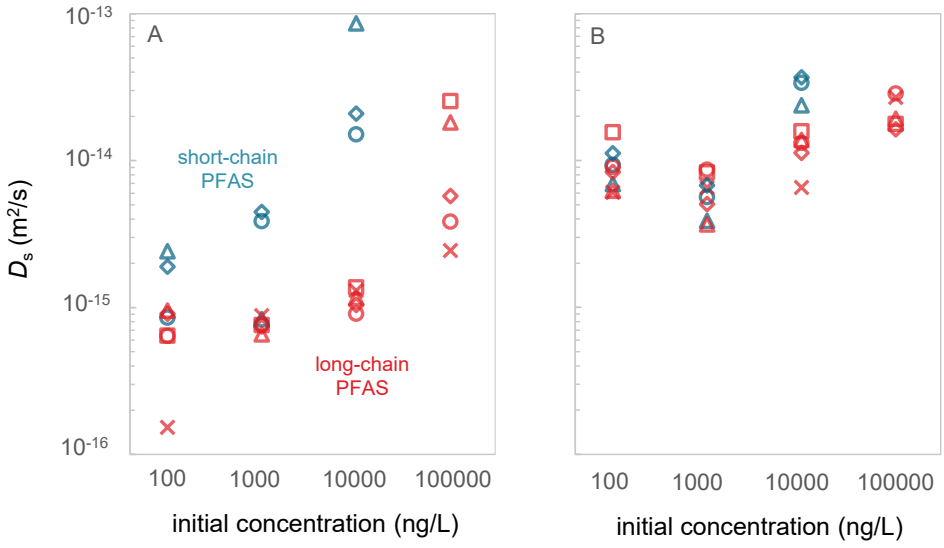


Figure 7.4. Surface diffusion coefficients D_s (m^2/s), estimated from kinetic adsorption experiments (Figure 3) at varying initial PFAS concentrations (ng/L) for (A) mesoporous and (B) microporous carbon. Blue symbols represent short-chain PFAS, while red symbols represent long-chain PFAS.

7.2.2.2. Strategies to overcome PFAS kinetic limitations

The consequence of slow surface diffusion is that adsorption equilibrium is approached only over long contact times. In batch systems, this manifests as extended equilibration periods, while in columns it necessitates longer empty bed contact time (EBCT) to achieve effective PFAS removal. Several studies have shown that longer EBCT enhances PFAS removal in both pilot- and full-scale treatment systems.[36,59]

The slow kinetics observed in this Thesis suggest that enhancing intraparticle transport within GAC could improve adsorption performance. Because PFAS transport is predominantly governed by surface diffusion, one potential strategy is to modify PFAS–carbon interactions to promote faster transport, for example by shifting the dominant mechanism toward pore diffusion. Introducing positive surface charge may alter the balance between hydrophobic and electrostatic interactions, potentially facilitating intraparticle transport. The experimental approach introduced in Chapter 6 for evaluating PFAS electroregeneration could also be applied to systematically investigate the influence of surface charge on PFAS adsorption kinetics by comparing transport behaviour under different charging conditions.

7.2.3. Competition for adsorption between PFAS molecules

A recurring observation in PFAS adsorption studies is that short-chain PFAS are outcompeted by long-chain PFAS during adsorption onto ACs.[110,220–222] A particularly important practical consequence of this behaviour is the desorption of short-chain PFAS in GAC filters. As discussed in Chapter 5, a chromatographic effect was observed in which effluent concentrations of short-chain PFAS exceeded influent concentrations. Because this behaviour occurred even in the absence of natural organic matter, it can be directly attributed to displacement of previously adsorbed short-chain PFAS by more strongly adsorbing long-chain PFAS.

7.2.3.1. Underlying mechanism

The displacement of short-chain PFAS by long-chain PFAS is governed by differences in both adsorption kinetics and adsorption affinity. Short-chain PFAS exhibit higher intraparticle diffusion coefficients (Figure 7.4) and therefore reach adsorption sites more rapidly, particularly on powdered activated carbon (PAC), where diffusion path lengths are short. As a result, PAC initially shows higher removal of short-chain PFAS than GAC (Figure 7.5A). Over time, long-chain PFAS gradually access these sites and, owing to their stronger adsorption affinity, displace the previously adsorbed short-chain PFAS. Consequently, short-chain PFAS loadings on PAC converge toward those observed for GAC. Adsorption followed by competition-induced desorption is not pronounced for GAC, because long transport pathways limit site competition.

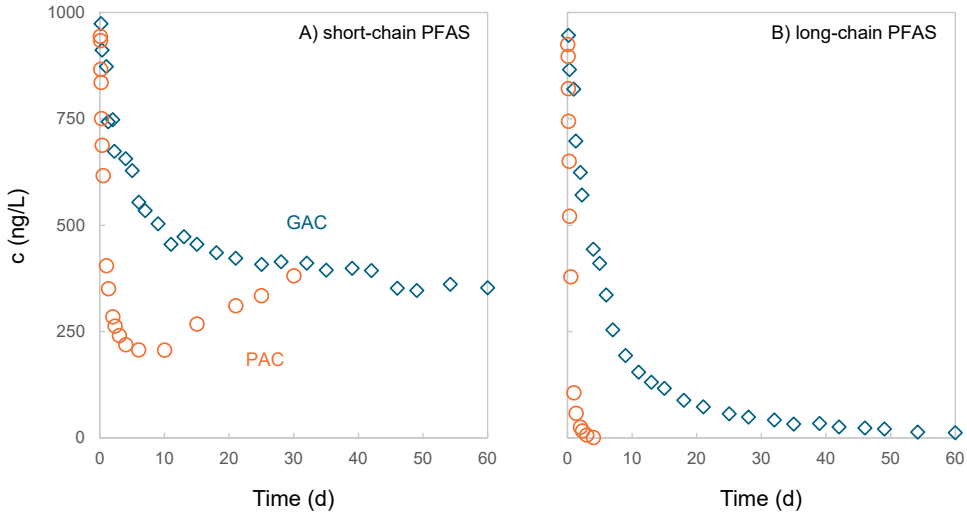


Figure 7.5. Adsorption over time of A) short- and B) long-chain PFAS onto GAC (blue diamonds) and PAC (orange circles) for mesoporous SRD carbon at dose of 5 mg/L. The data for GAC was obtained in Chapter 4 and data for PAC in Chapter 5.

PFAS competition is not governed solely by kinetic effects but is also evident under equilibrium conditions when adsorption space is limited. Figure 7.6 compares adsorption of short- and long-chain PFAS in single-solute and multi-solute systems on microporous GAC, which has limited mesopore volume identified in Chapter 3 as the primary adsorption domain for PFAS. At high initial PFAS concentrations (100 µg/L), adsorption capacities are consistently higher in single-solute systems than in multi-solute systems, indicating direct competition for adsorption sites and reduced adsorption of all PFAS under surface-saturated conditions. At lower initial concentrations (≈1000 ng/L), adsorption in single- and multi-solute systems is similar except at low carbon doses corresponding to the right-hand side of the isotherm. Under these conditions, adsorption in the multi-solute system exceeds monolayer saturation due to multilayer adsorption in constrained mesoporous space (Section 7.2.1). The absence of multilayer adsorption in the corresponding single-solute systems indicates that PFAS aggregation is enhanced by the presence of co-solutes.

Competition between short- and long-chain PFAS arises directly from their molecular similarity and differences in adsorption affinity. As illustrated in Figure 1.1 in the Chapter 1, PFAS share a common molecular backbone and differ primarily in fluorinated chain length and functional head group, typically carboxylate or sulfonate. Because of these similarities, PFAS molecules compete for the same adsorption sites. Under conditions of limited adsorption capacity, long-chain PFAS displace short-chain PFAS due to stronger hydrophobic interactions. In addition to chain length, the functional head group influences adsorption affinity: PFAS with sulfonic head groups consistently exhibit higher adsorption affinity than

carboxylate analogues of the same chain length, a trend observed throughout this Thesis and widely reported in the literature.,[13] and commonly attributed to lower solubility of sulfonic PFAS.[90]

While this Thesis focuses on C4–C8 PFAS, the implications extend to emerging compounds. Ultrashort-chain PFAS, such as trifluoroacetic acid (TFA), are expected to exhibit very low affinity for activated carbon and to be readily displaced by longer-chain PFAS. In contrast, recent work by Sadia et al. (2024) suggests that PFAS precursors may behave differently, with some short-chain precursors exhibiting stronger adsorption than their longer-chain counterparts, potentially due to enhanced electrostatic interactions. Further studies are required to clarify the adsorption mechanisms of PFAS precursors.[143]

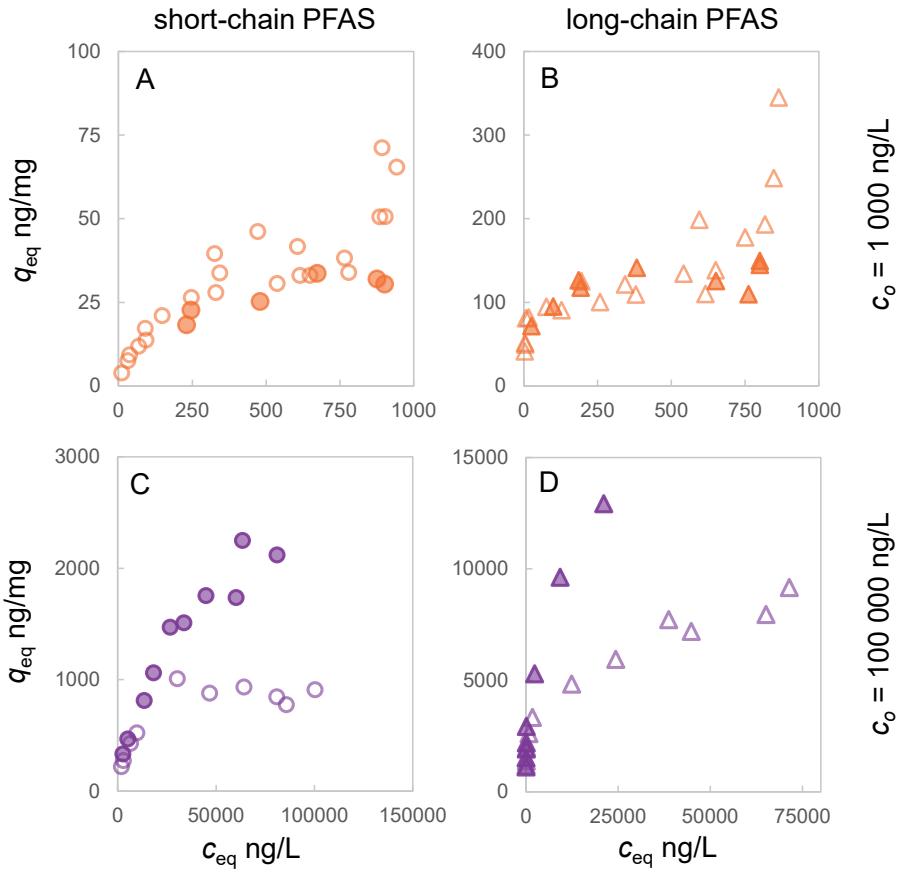


Figure 7.6. Adsorption isotherms for short- (A, C) and long-chain PFAS (B, D) for different initial concentrations on microporous CS carbon. The full data points represent single solute data, and full data points represent multi-solute data obtained as a part of Chapter 3.

7.2.3.1. Strategies to reduce PFAS competition

Competition between PFAS molecules cannot be fully eliminated, as PFAS share similar physicochemical properties and long-chain compounds inherently exhibit higher adsorption affinity. As shown in Chapter 3, the total PFAS isotherm can be divided into three regions, indicating that substantial removal of short-chain PFAS occurs only after long-chain PFAS have been largely removed. One straightforward mitigation strategy is to increase the GAC dose, for example from a typical 5 mg/L to 10 or 20 mg/L, or to increase bed volume by installing multiple GAC filters in series. However, these approaches substantially increase treatment costs.

Introducing additional adsorption sites specifically targeting short-chain PFAS through GAC functionalization represents another potential strategy, but in practice such sites are still likely to be preferentially occupied by long-chain PFAS. At present, the most practical approach for addressing short-chain PFAS is the application of a post-treatment step following GAC, such as ion-exchange resins,[26] particularly because compounds such as TFA are not effectively removed by GAC.[22]

7.2.4. Pore size distribution of activated carbon

AC is widely used in water treatment because of its exceptionally large internal adsorption space, consisting of both pore volume and surface area, which allows contaminants to be concentrated by factors of up to 10,000.[223] For most ACs, the majority of the surface area and pore volume resides within micropores (<2 nm).[30] However, steric hindrance can restrict access of larger molecules to these pores. According to Li et al. (2001), pores must be approximately 1.3–1.8 times larger than the adsorbing molecule to be accessible.[224]

Based on the molecular diameters of the PFAS compounds investigated in this Thesis (0.6–1.26 nm[92]; Table 1.1 in Chapter 1), micropores should theoretically be accessible for PFAS adsorption, particularly for short-chain PFAS. Given that many GACs possess a large fraction of microporous surface area, highly microporous carbons would therefore be expected to perform well for PFAS removal. However, as shown in Chapters 2 and 3, carbons with a higher micropore fraction generally exhibit lower adsorption performance for both short- and long-chain PFAS than more mesoporous carbons. For the highest-performing GACs, mesopores were identified as the capacity-limiting adsorption domain for PFAS.

7.2.4.1. Underlying mechanism

A mechanistic explanation that explains the roles of both micropores and mesopores in PFAS adsorption is that mesopores primarily facilitate mass transfer into the particle interior, while micropores serve as the primary adsorption sites. Under ideal conditions, PFAS molecules rapidly diffuse through mesopores and adsorb in micropores. However, due to inherently slow surface diffusion (Section 7.2.2), these primary sites are not fully utilized, leading PFAS

molecules to accumulate and adsorb in mesopores and, under conditions of limited adsorption space, form multilayers or aggregates (Section 7.2.1).

7.2.4.2. Strategies to overcome pore size limitations

One potential strategy to enhance PFAS adsorption on AC is to modify the pore size distribution in order to improve access to micropores. Although it may seem intuitive that increasing mesoporosity could enhance transport to micropores, our results indicate the opposite: the surface diffusion coefficient (D_s) decreases when the amount of mesopores increases (Section 7.2.2). This demonstrates that increasing mesoporosity does not enhance PFAS transport into micropores and therefore does not lead to more effective utilization of micropore adsorption capacity. Improving micropore accessibility would instead require altering PFAS–carbon interactions during intraparticle transport, shifting the dominant mechanism from surface diffusion toward pore diffusion, as discussed in Section 7.2.1.2.

Rather than attempting to redesign carbons to improve micropore accessibility, a more effective strategy is to optimize mesoporosity, as PFAS adsorption predominantly occurs within mesopores under realistic operating conditions. As discussed in Chapter 3, GACs for drinking water treatment should ideally maintain a minimum micropore volume of approximately 0.3 cm^3/g to avoid micropore limitations, while maximizing mesopore volume to enhance PFAS adsorption capacity. In addition, mesopores should be protected from competition and blockage by NOM through appropriate pretreatment strategies such as ozonation or biodegradation (see Section 7.3.2).

7.2.5. Surface charge of activated carbon

For the two activated carbons investigated in detail in this Thesis (CS and SRD), surface charge properties were intentionally selected to be similar (Chapter 2) in order to isolate the effects of pore size distribution and intraparticle transport. Nevertheless, chemical surface charge is known to strongly influence PFAS adsorption (Chapter 3), and this effect has been widely reported in the literature.[107,225] In general, PFAS adsorption is enhanced on carbons with a low density of charged surface functional groups and on carbons exhibiting a more positive surface charge.

7.2.5.1. Underlying mechanism

Under the pH conditions typical of drinking water and wastewater treatment, legacy PFAS predominantly exist as anions.[7] Electrostatic interactions therefore arise between the negatively charged PFAS headgroups and the surface charge of the adsorbent, leading to either attraction or repulsion (Figure 1.6 in Chapter 1)

On unmodified thermally activated carbon, surface charge primarily originates from oxygen-containing functional groups.[30] These groups can be either acidic (e.g., carboxylic, phenolic) or basic (e.g., carbonyl, lactone), and their relative abundance is commonly determined by

Boehm titration.[226] In addition to basic surface groups, positive charge on carbon can also form through proton adsorption onto π-electron-rich regions of the basal planes.[107] The delocalized electrons within aromatic ring clusters tend to migrate toward the edges once protons adsorb, creating electron-deficient areas of localized positive charge.

For anionic adsorbates such as PFAS, a higher density of positive surface charge, originating from either basic functional groups or proton adsorption onto π-electron-rich regions, combined with a lower concentration of negatively charged acidic sites, enhances adsorption.

7.2.5.2. Strategies to overcome surface charge limitations

Studies on commercially available ACs show that materials with a net positive surface charge delay PFAS breakthrough compared with neutral or negatively charged ACs.[75,76] Such carbons are typically coal-based and thermally activated. However, their inherent positive surface charge is relatively low, suggesting that targeted surface modification may further improve PFAS adsorption performance.

One effective modification strategy is thermal defunctionalisation, which removes oxygen-containing surface groups to improve PFAS adsorption.[74,112] The removal of these groups increases AC surface hydrophobicity. In addition, Saeidi et al. (2020) showed that defunctionalisation increases the density of positive charges associated with π-electron-rich regions, further enhancing PFAS adsorption.[112] Beyond defunctionalisation, increasing positive surface charge through chemical modification has also been explored, most notably by introducing amine functionalities. Aminated surfaces exhibit substantially enhanced PFAS adsorption; however, most existing studies focus on ion-exchange resins, polymers, or inorganic sorbents, and systematic investigation of aminated ACs remains limited.[218]

Kim et al. (2024) compared pristine powdered AC with oxidized (acidic), defunctionalized, and aminated variants. Both defunctionalized and aminated carbons exhibited improved removal of short- and long-chain PFAS, whereas oxidation, which increased surface acidity, reduced adsorption.[225] In Chapter 6 of this Thesis, amination was also shown to enhance desorption of short-chain PFAS during electroregeneration, indicating that PFAS bound via electrostatic interactions to positively charged amine sites can be more readily released under an applied negative potential.

Despite strong evidence from batch studies, surface-modified GACs with enhanced PFAS adsorption, such as defunctionalized or aminated carbons, have not yet been widely implemented or evaluated at pilot or full scale. Moreover, surface charge properties of activated carbons are frequently underreported, which limits comparability across studies and complicates translation of laboratory findings to practical system design

7.2.6. Natural organic matter

Natural organic matter (NOM) is ubiquitous in source waters for drinking water production and represents a key factor limiting PFAS removal (Chapter 5). As shown in Figure 7.7, the presence of 1 mg/L NOM reduces the Langmuir maximum adsorption capacity (q_{max}) for both short- and long-chain PFAS by approximately one order of magnitude compared with NOM-free conditions.

The data in Figure 7.7 correspond to a NOM-to-PFAS ratio of 1 mg/L to 1000 ng/L. In practical treatment scenarios, NOM concentrations can reach up to5 mg/L,[75] while PFAS are typically present at low ng/L levels. Under such conditions, competitive effects are expected to be even more pronounced. Consistent with this expectation, Chapter 5 demonstrates that increasing NOM concentrations lead to substantially earlier PFAS breakthrough, indicating that competition intensifies as the concentration disparity between NOM and PFAS increases. To meet increasingly stringent PFAS regulatory limits,[11,17] effective reduction of NOM prior to GAC filter treatment is therefore essential.

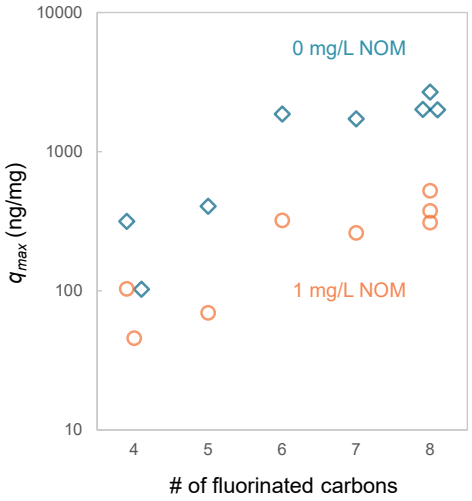


Figure 7.7. Langmuir maximum adsorption capacity (q_{max}) as a function of fluorinated carbons in PFAS molecule. Results are shown for adsorption in the presence of 1 mg/L NOM (orange circles) and under NOM-free conditions (blue diamonds). Data was collected in Chapter 5.

7.2.6.1. Underlying mechanism

Understanding how NOM reduces PFAS adsorption is challenging because NOM is a heterogeneous mixture of compounds whose composition and concentration vary widely between water sources.[161] In Chapter 5, this complexity was addressed by fractionating NOM based on molecular size and chemical characteristics and evaluating PFAS adsorption in both batch and column experiments. These results showed that NOM components with molecular

features similar to PFAS are the strongest competitors for adsorption sites: hydrophilic, low-molecular-weight fractions primarily compete with short-chain PFAS, while hydrophobic, neutral NOM fractions preferentially compete with long-chain PFAS.

In addition to direct competition for adsorption sites, NOM can block pores and reduce PFAS adsorption.[54,75,227] Furthermore NOM adsorbed on AC can reduce PFAS adsorption by introducing additional negative surface charge that electrostatically repels anionic PFAS head groups,[86] but it may also promote PFAS adsorption through hydrophobic interactions between PFAS tails and adsorbed NOM.[13] Finally, NOM has been suggested to promote PFAS aggregation. McCleaf et al. (2017) observed increased long-chain PFAS adsorption in columns and attributed this to NOM-induced aggregation, although it remains unclear whether NOM actively stabilizes aggregates, for example, by serving as nucleation sites for their formation. or whether aggregation arises indirectly from limited adsorption space. Together, these mechanisms illustrate the complex NOM-PFAS-AC interplay summarized in Figure 7.8.

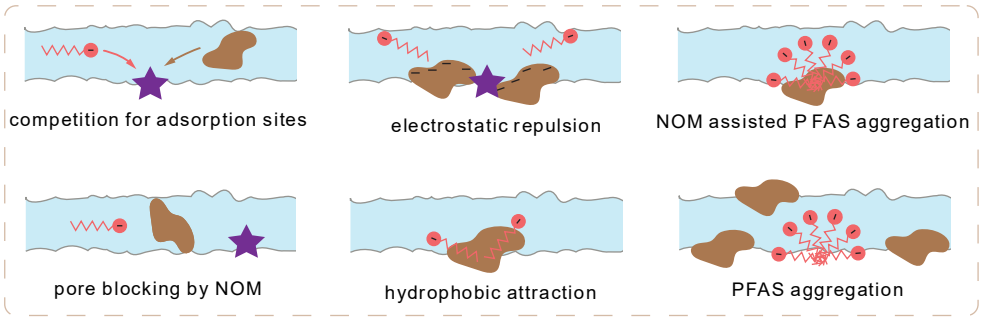


Figure 7.8. PFAS adsorption mechanisms in the presence of NOM. The NOM can reduce PFAS adsorption through direct competition for adsorption sites, pore blockage, and the introduction of additional negative surface charge that electrostatically repels anionic PFAS head groups. Conversely, NOM may enhance PFAS adsorption by providing hydrophobic interaction sites on the carbon surface or by promoting PFAS aggregation, either by acting as nucleation sites for aggregate formation or by reducing limited adsorption space.

7.2.6.2. Strategies to reduce NOM-PFAS competition

Because NOM is the dominant factor limiting PFAS adsorption during water treatment, effective NOM pretreatment upstream of GAC filters is essential to improve PFAS removal. Such pretreatments should specifically target the removal of NOM fractions that compete most strongly with PFAS, particularly low molecular weight, hydrophilic compounds that reduce adsorption of problematic short-chain PFAS. This represents one of the key practical recommendations arising from this Thesis and is discussed in Section 7.3.2. In Chapter 5, PFAS–NOM interactions were investigated using surface water NOM. Future studies can apply the same methodology to clarify interactions between NOM and emerging PFAS for

different water sources. This represents an important direction for future research (see Section 7.4.2.)

7.2.7. Temperature

In Chapter 4, PFAS adsorption was evaluated between 10 and 30 °C at environmentally relevant concentrations. The results show that adsorption of short-chain PFAS decreases with increasing temperature, whereas adsorption of long-chain PFAS remains largely unaffected. To our knowledge, this is the first study to determine temperature-dependent PFAS isotherms under drinking-water–relevant conditions. Consistent with these findings, a long-term monitoring study by Nakazawa et al. (2023) reported desorption of short-chain PFAS from GAC filters during periods of elevated water temperatures (20–29 °C), an effect not observed at lower temperatures (5–19 °C).[35] The authors hypothesised that this behaviour resulted from enhanced replacement of short-chain PFAS by NOM during warmer periods. In contrast, the temperature-dependent isotherm data presented in this Thesis demonstrate that short-chain PFAS adsorption is intrinsically reduced at elevated temperatures, independent of NOM presence.

7.2.7.1. Underlying mechanism

Chapter 4 shows that increasing temperature induces negative lateral interactions in the adsorbed phase, leading to desorption of short-chain PFAS. As temperature increases, molecular mobility on the carbon surface increases, enabling long-chain PFAS, which exhibit higher adsorption affinity, to displace short-chain PFAS. This behaviour is described using the Frumkin isotherm, a mechanistically grounded extension of the Langmuir model that explicitly accounts for lateral interactions and is suitable for predicting breakthrough behaviour, making it directly relevant from an engineering perspective.

In addition, a thermodynamic analysis was performed using isotherm data from Chapter 4 and van 't Hoff equation.[152,228] This analysis showed that adsorption of short-chain PFAS is exothermic, with enthalpy values between −50 and −20 kJ/mol, whereas adsorption of long-chain PFAS is dominated by entropic effects (188–204 J/mol·K) with negligible enthalpy change. Such high entropy values are characteristic of hydrophobic, non-specific adsorption,[133] which is less sensitive to temperature variations than the more site-specific adsorption governing short-chain PFAS.

7.2.7.2. Strategies to address temperature impact on PFAS adsorption

Regardless of the underlying mechanisms, temperature effects must be considered when designing PFAS treatment systems. Higher water temperatures reduce the adsorption of short-chain PFAS on GAC, implying poorer treatment performance during warm seasons and in warm climates compared with colder periods and regions. One practical mitigation strategy is managed aquifer recharge or soil infiltration of surface water.[229] Infiltration through soils can lower and stabilise water temperature prior to abstraction, allowing subsequent GAC treatment to operate under more favourable conditions. In addition to temperature control, infiltration may also reduce NOM concentrations and improve overall treatability.[230]

7.2.8. Overview of factors that limit PFAS adsorption on activated carbon

Table 7.1 provides an overview of the main findings discussed in Section 7.2 and summarizes the factors limiting PFAS adsorption on activated carbon. While Table 7.1 and Section 7.2 identify a range of potential strategies to overcome these limitations and highlight directions for future research, Sections 7.3 and 7.4 focus and discuss in detail the most promising and practically relevant approaches for improving PFAS removal in treatment systems and addressing remaining knowledge gaps.

Table 7.1. Factors limiting PFAS adsorption on activated carbon (AC), importance of these limitations in practice, and approaches to enhance PFAS removal.

Factors limiting PFAS adsorption on AC	Main finding / mechanism	Practical implications	Strategies to enhance PFAS adsorption
Low PFAS concentration (Section 7.2.1)	Isotherm parameters are strongly concentration-dependent. At high initial concentration PFAS form aggregates while at ng/L levels, cooperative adsorption is suppressed.	Most literature isotherms derived at high concentration overestimate PFAS adsorption capacity at drinking-water levels. Column models fail in predicting PFAS breakthrough.	(i) Pre-concentrate PFAS (e.g. nanofiltration) to shift adsorption into a multilayer regime. (ii) Develop adsorbents with high adsorption at ng/L conc. (iii) Apply modelling approaches that extrapolate low-concentration behaviour from high-concentration data.
Slow PFAS kinetics (Section 7.2.2)	PFAS intraparticle transport is dominated by surface diffusion, controlled by PFAS–AC interactions. The surface diffusion coefficient decreases when more adsorption sites are available.	At realistic GAC doses, equilibrium is not reached within practical timescales. In columns, short EBCT limits carbon utilization, causing low loading and early breakthrough.	(i) Increase EBCT or apply multiple GAC filters in series. (ii) Develop adsorbents that enable faster intraparticle PFAS transport.
PFAS competition (Section 7.2.3)	Short-chain PFAS diffuse faster but have lower adsorption affinity while long-chain PFAS bind more strongly and displace short-chain PFAS over time.	Short-chain PFAS often drive early breakthrough. Even when initially removed, short-chain PFAS can reappear due to displacement as the bed loads.	(i) Use multiple GAC filters or higher GAC doses. (ii) Apply post treatment (e.q. ion exchange) targeting short-chain PFAS.
GAC pore size distribution (Section 7.2.4)	PFAS molecules can access micropores, but slow surface diffusion limits their utilization. PFAS therefore accumulate and adsorb mainly in mesopores. Multilayer adsorption occurs in mesopores.	GACs with high microporosity do not necessarily perform better for PFAS removal. Mesopore volume is the capacity-limiting domain under realistic conditions.	(i) Select GAC/adsorbents with high mesopore volume. (ii) Protect mesopores from NOM blockage with adequate pretreatment (e.q. ozonation or biodegradation).
GAC surface charge (Section 7.2.5)	Anionic PFAS are electrostatically repelled by negatively charged (acidic) surface groups. Positive charge, from basic sites or protonated π-electron regions, enhances adsorption.	Adsorption of short- and ultrashort-chain PFAS is highly sensitive to surface charge. Without reporting charge properties, cross-study comparisons and material selection are unreliable.	(i) Use low-acidity or positively charged carbons (often coal-based, thermally activated). (ii) Apply surface modification, e.q. defunctionalisation or amination (needs pilot/full-scale validation).

Table 7.1. Continued

Factors limiting PFAS adsorption on AC	Main finding / mechanism	Practical implications	Strategies to enhance PFAS adsorption
NOM competition (Section 7.2.6)	NOM fractions with molecular features similar to PFAS compete for adsorption sites. Low-molecular-weight hydrophilic NOM limits short-chain PFAS adsorption while hydrophobic neutral NOM limits long-chain PFAS adsorption	PFAS breakthrough occurs earlier as the NOM-to-PFAS concentration ratio increases. NOM is often the dominant factor controlling GAC performance under drinking-water conditions.	(i) Reduce concentrations of competitive NOM fractions prior to GAC adsorption (e.q. biological treatment, ozonation). (ii) Extend studies to emerging PFAS and NOM from different water sources.
Temperature (Section 7.2.7)	Increasing water temperature reduces adsorption of short-chain PFAS.	Higher water temperatures during warm seasons and in warm climates lead to reduced short-chain PFAS removal in surface-water GAC filters.	(i) Consider temperature effects in design and modelling. (ii) Use infiltration-based treatment (e.g. soil passage) to lower and stabilize water temperature.

7.3. Recommendations for application

Based on the mechanistic insights identified in Section 7.2 and summarized in Table 7.1, this Thesis outlines several strategies to improve PFAS removal in water treatment. While Table 7.1 provides a comprehensive overview of potential approaches, this section focuses on the most mature and practically applicable options. These include selecting granular activated carbons (GACs) with appropriate pore structure and surface charge, applying pretreatment to reduce competitive natural organic matter (NOM), and using predictive modelling tools to translate laboratory insights into full-scale system predictions. Together, these approaches offer realistic pathways to improve PFAS removal efficiency and extend filter lifetime.

7.3.1. Ideal activated carbon for PFAS removal

PFAS adsorption on GAC is governed by pore size distribution and surface chemistry. Although PFAS molecules are small enough to access micropores, slow intraparticle diffusion limits their effective use, causing PFAS to accumulate in mesopores, where multilayer adsorption can occur under conditions of limited adsorption space. Consequently, GACs with a high mesopore volume are preferred in water treatment. Surface chemistry further controls adsorption performance: because PFAS are predominantly anionic at typical treatment pH values, GACs with a low density of acidic surface groups are favoured. Thermal defunctionalisation removes acidic groups and increases surface hydrophobicity, while amine functionalisation can further improve adsorption by introducing positively charged sites that promote electrostatic attraction. In summary, GACs for PFAS removal should have:

- high mesopore volume, providing adsorption sites and promoting multilayer adsorption;
- low surface acidity or a positively charged surface, promoting electrostatic and hydrophobic interactions.

The best-performing GACs for PFAS removal identified in this Thesis, such as SRD and F400, are coal-based carbons produced via a reagglomeration process. This production route yields a relatively low surface charge and a high mesopore volume, both of which favour PFAS adsorption. At present, the availability of alternative feedstocks that simultaneously provide high mesoporosity and favourable surface charge properties is limited. In addition, surface modification strategies that enhance PFAS removal, such as thermal defunctionalisation or amination, have not yet been widely implemented in large-scale GAC production.

These same surface and structural properties that are important for GAC are likely beneficial for other adsorbents such as resins and zeolites. However, any new material must be tested under environmentally relevant PFAS concentrations (ng/L range). While experiments at higher concentrations are useful for identifying adsorption mechanisms, performance at trace levels ultimately determines suitability for water treatment. A material can only be considered superior to GAC if it demonstrates improved removal under these realistic conditions.

7.3.2. Removal of competing NOM to increase PFAS adsorption capacity

As discussed in Section 7.3.6 natural organic matter (NOM) is the primary competitor that reduces PFAS adsorption during drinking water treatment. Among the conventional processes used for NOM reduction: coagulation, adsorption, oxidation, biological treatment and membrane filtration, biological treatment appears to be the most suitable for removing low molecular weight NOM compounds,[231] which were identified in the Chapter 5 as competitors with short-chain PFAS for adsorption. A practical option is the use of biological activated carbon, which could be implemented by reducing reactivation frequency to allow biological activity to develop, without major additional investment. However, in many drinking water treatment scenarios, the influent to GAC filters may contain NOM with low biodegradability. In such cases, ozonation can serve as a complementary step to enhance the biodegradability of NOM, thereby improving the overall efficiency of subsequent biological treatment.

7.3.2.1. Ozonation

Ozonation is a well-established water treatment process, primarily used to remove taste, odour, and colour from water. While it does not substantially reduce total NOM concentration, it alters NOM composition by decreasing molecular size and hydrophobicity. When pore blockage is the dominant factor limiting PFAS adsorption, ozonation can be beneficial by reducing the size of NOM molecules and alleviating blockage. Liu et al. (2024) showed that ozonation improved PFAS removal only for GACs with limited microporosity, where reducing NOM-induced micropore blockage increased the accessibility of adsorption sites.[232] This suggests potential benefits for short-chain PFAS, which can adsorb in micropores (Chapter 3).

In contrast, ozonation is unlikely to improve long-chain PFAS removal. It does not effectively remove hydrophobic neutral (HON) fraction, identified in Chapter 5 as the main competitors for long-chain PFAS adsorption. The HON fraction is poorly reactive to ozone due to their saturated carbon content and limited aromaticity.[163] Moreover, ozonation can increase the formation of low-molecular-weight (LWM) acids,[231,233] which structurally resemble PFAS and therefore intensify competition for adsorption sites. Interestingly, Liu et al. (2024) observed little to no benefit of ozonation for F400 carbon, similar to the SRD carbon used in this Thesis, where mesopores rather than micropores limit PFAS adsorption. In such cases, increased LMW NOM may offset any benefits of reduced micropore blockage. Elevated PFAS concentrations after ozonation have also been reported, attributed to the transformation of PFAS precursors.[232]

A more promising approach involves coupling ozonation with biological activated carbon (BAC). Tajdini et al. (2023) compared ozonation, BAC, and combined O_3–BAC pretreatments before PFAS removal using GAC, anion exchange resin, and surface-modified clays.[234] The combined O_3–BAC process achieved the greatest improvement in PFAS removal. This enhancement was attributed to ozonation transforming hydrophobic NOM into hydrophilic,

biodegradable molecules that were subsequently degraded in the BAC. Importantly, the study confirmed that LMW NOM strongly limits PFAS adsorption regardless of adsorbent.

Ozonation can introduce operational and regulatory challenges, particularly in bromide-containing waters, where oxidation of bromide to bromate may occur. Mitigating bromate formation requires careful ozone dose control, pH adjustment, or additional downstream treatment, which increases treatment complexity and cost.[235] Regardless of the need for bromate control, ozonation primarily alters NOM composition rather than removing the low-molecular-weight fractions that most strongly compete with PFAS adsorption. Overall, ozonation alone is therefore unlikely to significantly enhance PFAS removal and may even increase competition. However, when coupled with biological treatment, ozonation can effectively reduce NOM and improve PFAS adsorption on GAC.

7.3.2.2. Adsorption with biodegradation

The BAC filters remove biodegradable NOM through microbial activity on the carbon surface. By degrading adsorbed NOM, microbes can partially regenerate adsorption sites and thereby extend the effective lifetime of the carbon filter. Although BAC is most commonly applied in wastewater treatment, biological activity can also develop in drinking water GAC filters; Zhang et al. (2011) observed stable biofilms after approximately 39,000 bed volumes.[236]

In practice, however, in countries with particularly strict PFAS guidelines, such as The Netherlands, drinking water GAC filters are often thermally reactivated after approximately 10,000–20,000 bed volumes, which potentially prevents meaningful biofilm development. One potential strategy is to operate GAC filters in series, allowing the first filter to evolve into a BAC unit without reactivation, while the second filter is periodically regenerated to maintain PFAS adsorption capacity. Compared with two GAC filters in series, a BAC–GAC configuration may be more cost-effective, as upstream NOM removal reduces competition for adsorption sites and enhances PFAS removal in the downstream GAC. While modelling study by Parniske et al. (2026) suggest that sequential filtration improves micropollutant removal from wastewater effluent,[50] the optimal filter configuration for PFAS removal in drinking water treatment depends strongly on site-specific conditions and cannot be generalized without predictive modelling tools.

7.3.3. Predictive modelling of PFAS breakthrough in the presence of NOM

Predictive modelling of PFAS breakthrough under varying water quality conditions is essential for translating experimental results into the design and operation of GAC treatment systems. Based on the mechanisms identified in this Thesis (Chapters 2, 3, and 5), only modelling approaches that account for direct site competition and surface-diffusion-limited transport are suitable for predicting PFAS fate in practical treatment systems.

7.3.3.1. Modelling equilibrium

There are several mechanistic modelling approaches that can describe direct site competition between PFAS and NOM (Table 7.2). Highly detailed models such as the ideal adsorbed solution theory (IAST) and the fictive component approach (FCA) require extensive adsorption data and are often not suitable for application. IAST requires single-solute isotherms for all competing components, which is impractical for NOM unless it is fractionated and each fraction is quantified, while FCA requires single-solute PFAS isotherms, which is unrealistic given the large and evolving number of relevant PFAS.

The more suitable models are equivalent background compound model (EBCM) and tracer model (TRM). The EBCM also relies on single-solute PFAS isotherms but is less data-intensive than FCA because NOM is represented as a single equivalent competing component rather than a distribution of fictive species. As a result, EBCM can be useful in situations where one or a few PFAS dominate breakthrough and risk, such as local contamination scenarios or waters where a single compound (e.g., TFA at elevated concentrations) largely determines compliance. In contrast, when PFAS occur as complex mixtures without a single dominant compound, the TRM is typically more suitable. TRM relies on mixture isotherms and a total NOM isotherm, rather than single-solute PFAS isotherms, making it better aligned with the type of data routinely available to water utilities.

It should be noted that models in Table 7.2 do not consider pore blockage. While results from Chapter 5 indicate that site competition is the dominant mechanism for reduction of PFAS adsorption in presence of NOM for surface water treatment, pore blockage may become relevant in other water matrices or at higher NOM loads. In systems where pore blockage becomes relevant, extended fixed-bed models that incorporate both site competition and pore blockage are required for accurate prediction. An example is the COMPSORB-GAC model developed by Schideman et al. (2006), which extends the EBCM framework by including into model an additional NOM fraction that causes pore blockage.

Table 7.2. Modelling approaches to describe multi-component PFAS + NOM isotherms

Model	Key concept & characteristics	Model requires isotherm for:		
		Single-solute PFAS	PFAS/NOM mixture	NOM
Ideal adsorbed solution theory (IAST)	Thermodynamic multi-solute equilibrium model based on ideal adsorbed phase; predicts competition using single-solute isotherms of all components. Accurate for defined mixtures but fails for complex NOM.	yes	no	Yes, each fraction
Fictive Component Approach (FCA)	Extends IAST by decomposing NOM into several fictive components with assigned K and n values; captures NOM heterogeneity. Data-intensive but mechanistic.	yes	no	Total NOM isotherm
Tracer Model (TRM)	Empirically corrects micropollutant isotherm parameters using mixture data and DOC isotherm; allows simultaneous description of NOM and micropollutant adsorption.	no	yes	Total NOM isotherm
Equivalent Background Compound Model (EBCM)	Represents NOM as a single "equivalent" background competitor with fitted parameters (K, n, c_0); simple and effective for micropollutant prediction only.	yes	yes	no

7.3.3.2. Modelling kinetics in GAC filters

The choice of kinetic model for PFAS adsorption in GAC filters depends on the dominant mass-transfer mechanism, i.e., whether adsorption is controlled by intraparticle surface diffusion or by external film diffusion. Adsorption kinetics are most commonly described using either the Homogeneous Surface Diffusion Model (HSDM) or the Linear Driving Force (LDF) model. Both account for film diffusion, but they differ in their treatment of intraparticle transport. The LDF model is a simplified approximation of the HSDM and does not explicitly resolve surface diffusion; instead, it assumes a lumped linear driving force. As shown by Sperlich et al. (2008), the LDF model performs adequately when film diffusion dominates mass transfer but fails when intraparticle diffusion is rate-limiting.

Results from this Chapter 2 show that PFAS intraparticle transport is predominantly governed by surface diffusion rather than film diffusion, indicating that the HSDM is the more appropriate modelling framework. This conclusion is consistent with previous studies, including Dixit et al. (2021), who likewise identified surface diffusion as the dominant mechanism for PFAS adsorption in the presence of NOM. These conclusions were obtained from batch experiments conducted at high mixing intensities, designed to minimise external mass-transfer resistance. At lower mixing intensities (30 RPM) film diffusion can become rate-limiting, as demonstrated by Abulikemu et al. (2025). However, even under such conditions, highly hydrophobic PFAS such as PFOS were reported to remain surface-diffusion controlled, with surface diffusion coefficients ($1.6–7.46 \times 10^{-16}$ m²/s) comparable to those obtained in this Thesis.

To date, the relative contributions of surface and film diffusion have been investigated primarily in batch systems. In fixed-bed columns, the balance between these mechanisms may vary with EBCT, flow velocity, and carbon properties, which introduces uncertainty when extrapolating batch-derived parameters to full-scale operation.

7.4. Recommendations for future research

While this Thesis provides new mechanistic insights into PFAS adsorption and removal on AC, several critical knowledge gaps remain. Future research should focus on elucidating the molecular mechanisms governing PFAS multilayer adsorption, expanding the understanding of how NOM from different sources affects the fate of diverse PFAS species, and developing sustainable regeneration technologies such as electroregeneration. Addressing these topics will advance both the scientific understanding and practical implementation of PFAS adsorption.

7.4.1. Understanding PFAS multilayer adsorption

PFAS are amphiphilic surfactants that can self-assemble into aggregates, hemi-micelles, or micelles under right conditions. While such behaviour is documented in aqueous systems, this Thesis provides evidence that similar cooperative adsorption can occur on GAC surfaces. Specifically, S-shaped adsorption isotherms were observed under conditions of limited adsorption space (low carbon doses), indicating multilayer formation within mesopores at environmentally relevant concentrations (Figure 7.1F and 7.6). These findings suggest that PFAS, particularly long-chain, do not adsorb solely as isolated molecules but can form organized structures driven by hydrophobic tail–tail interactions. As discussed in Section 7.2.1, multilayer adsorption for long-chain PFAS occurs once local pore concentrations exceed reported CMC values. Notably, S-shaped isotherms were also observed for short-chain PFAS in multi-solute systems (Figure 7.6), indicating that co-solute effects enhance aggregation either by increasing surface saturation or through direct association between short- and long-chain PFAS molecules. Figure 7.9 shows speculated multilayer formations of PFAS inside GAC pores.

Several complementary approaches can be used in future work to investigate PFAS multilayer adsorption on GACs. First, surfactant-based adsorption models could be systematically applied to S-shaped isotherms to extract mechanistic parameters describing the transition from monolayer to multilayer adsorption.[142] Extensions of the Langmuir isotherm, such Frumkin or two-step adsorption model, are particularly promising, as they can distinguish conditions under which adsorption occurs as isolated molecules from those that promote cooperative aggregation. Applying such models across different PFAS mixtures, concentrations, and pore structures would clarify when and why multilayer adsorption emerges.

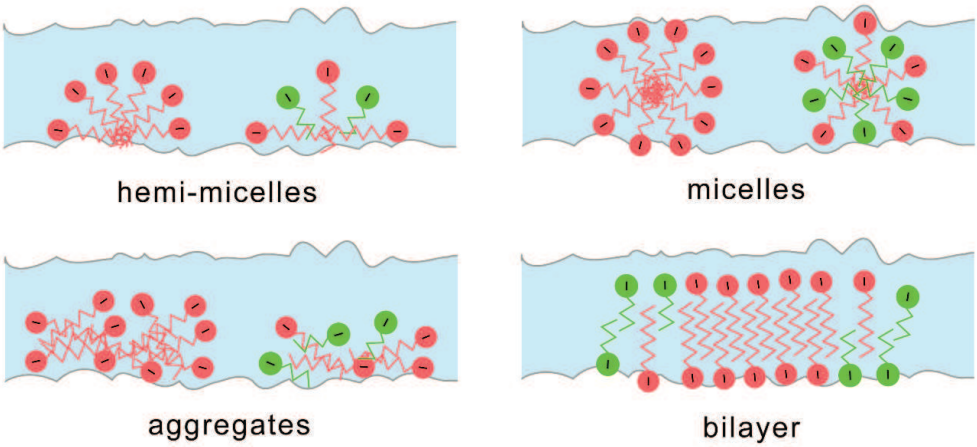


Figure 7.9. Conceptual illustration of multilayer PFAS adsorption within porous adsorbents. Previous studies have proposed that long-chain PFAS (red icons) can adsorb as ordered surface structures, including hemi-micelles, micelles, or bilayers, at sufficiently high local concentrations.[54] Recent work suggests that PFAS may also form less ordered, aggregate-like assemblies within pores.[14,237] In this Thesis (Figure 7.6A), S-shaped isotherms provide indirect evidence that short-chain PFAS (green symbols) can also undergo multilayer adsorption in multi-component systems.

Despite strong indirect evidence from isotherm shape, direct visualization of PFAS aggregates within porous carbon remains experimentally challenging. In this Thesis, attempts were made to image PFAS multilayers using transmission electron microscopy (TEM), inspired by the work of Zaggia et al. (2016), who successfully visualized PFAS aggregates on ion-exchange resins.[85] However, no aggregates could be observed in our case, likely due to sample-preparation artefacts that are unsuitable for GAC. With improved sample preparation, a promising future strategy would be to combine TEM imaging with laser-ablation-based mass spectrometry. In such an approach, TEM could first identify potential aggregate structures within mesopores, after which targeted laser ablation would release material from these regions for chemical analysis.[238] Detection of fluorine would then provide direct confirmation that the observed structures are PFAS. Applying this approach to GAC sampled from full-scale filters of different operational ages would enable direct verification of multilayer PFAS adsorption under realistic treatment conditions and substantially improve predictive adsorption modelling.

Another interesting approach is by Robertson et al. (2025), who used contrast-matching small-angle neutron scattering (CM-SANS) to characterize the structure of adsorbed PFOA molecules on carbons.[237] Their results revealed that PFOA aggregates form within mesopores, not micropores, and that increasing pore size facilitates multilayer adsorption and enhances sorption capacity. Specifically, they found that at 1 mg/L PFOA concentration, aggregates with a cylinder radius of ~0.5 nm and length of ~3 nm formed within mesopores, extending

along the pore wall through hydrophobic tail interactions. At higher concentrations (100 mg/L), aggregates reached a radius of 2.9 nm and length of 46 nm. These findings confirm that PFAS multilayer structures can assemble along mesoporous surfaces; however, the experiments were performed at relatively high PFAS concentrations (1–100 mg/L) and high carbon dose (5 g/L), far above environmentally relevant conditions. Thus, the existence and morphology of PFAS aggregates under typical drinking water treatment conditions remain uncertain.

7.4.2. Determining impact of NOM of varied sources on the fate of legacy PFAS, PFAS precursors and ultrashort-chain PFAS

In Chapter 5, eight legacy PFAS were investigated to elucidate adsorption and competition mechanisms with NOM during GAC treatment. However, thousands of PFAS exist in the environment, including ultrashort-chain PFAS such as TFA, branched isomers, and various precursor compounds that can transform into legacy PFAS through biotic or abiotic pathways.[157,239] These species differ in molecular size, polarity, reactivity, and their interactions with NOM and fate during water treatment remain largely unexplored.

The NOM–PFAS interactions in Chapter 5 were studied using Suwannee River NOM (SRNOM), a standardized surface-water reference material. Accordingly, the findings discussed in Chapter 5, identifying which NOM constituents strongly reduce PFAS adsorption, are directly relevant to water treatment facilities that produce drinking water from surface waters. However, NOM composition and concentration vary substantially across waters.[240,241] Surface water NOM generally occurs at higher concentrations than groundwater, and is dominated by humic and fulvic acids rich in aromatic and hydrophobic moieties.[241] In contrast, groundwater contains more aliphatic, aromatic proteins, and low-molecular-weight compounds,[241] whereas wastewater-derived NOM is enriched in nitrogenous and hydrophilic constituents originating from proteins, amino sugars, and microbial by-products.[242,243] It remains unclear whether the competitive adsorption mechanisms identified in Chapter 5, where hydrophobic neutral NOM interfered with long-chain PFAS and low-molecular-weight hydrophilic NOM affected short-chain PFAS, also apply to groundwater or wastewater NOM.

Therefore, future research should investigate the interactions between a broader range of PFAS and NOM sources. Ultrashort-chain PFAS are of particular concern in drinking water due to their high mobility and poor removability by GAC.[55] Municipal wastewater treatment plants are also major sources of PFAS released into the environment..[244] Several studies have reported higher concentrations of legacy PFAS in wastewater effluents than in influents, attributed to the biodegradation of PFAS precursors during biological treatment. [157,245] The extent and rate of these transformations are likely influenced by both NOM concentration and composition, as shown in studies with biodegradable micropollutants.[246,247] This topic is increasingly relevant as many wastewater treatment plants plan to implement GAC filtration

to meet the 4.4 ng PEQ/L surface water standard. A better understanding of interactions between NOM, PFAS precursors, and transformation processes is therefore essential to predict the fate of both precursors and ultrashort-chain PFAS in treatment systems.

The fractionation-based methodology developed in Chapter 5 provides a framework for disentangling PFAS–NOM interactions. By separating NOM according to molecular size and chemical characteristics and systematically assessing its impact on PFAS adsorption and transformation, future studies can identify which NOM fractions most strongly compete for adsorption sites or influence precursor degradation. This approach can be extended beyond the eight PFAS examined in this Thesis to include ultrashort-chain, branched, and PFAS precursors, establishing relationships between PFAS molecular structure, NOM composition, and adsorption or transformation behaviour. Such insights can also support the evaluation of pretreatments, such as ozonation and biological activated carbon, by clarifying whether they effectively remove the NOM fractions responsible for limiting PFAS adsorption.

7.4.3. Developing electroregeneration of saturated activated carbon filters

Even in well-performing treatment systems, where PFAS adsorption is high or breakthrough is delayed by NOM pretreatment, GAC filters require regeneration. In Dutch drinking water treatment plants, thermal reactivation is typically needed after ~10,000 bed volumes to meet the PFAS guideline of 4.4 ng PEQ/L. This frequent reactivation poses major operational challenges, as filters must be taken offline and GAC transported to external facilities for energy-intensive thermal regeneration, associated with high costs and CO_2 emissions. As an alternative, this Thesis explored electroregeneration as a potential on-site, low-emission regeneration strategy. Chapter 6 demonstrates, as a proof of concept, that electroregeneration can recover nearly all short-chain PFAS responsible for early breakthrough. Further research is required to assess the mechanisms, scalability, and long-term feasibility of this approach.

Future studies should clarify the dominant electroregeneration mechanisms: electrodesorption, pH-driven desorption, and ion-exchange displacement, and how these mechanisms change with GAC saturation level, PFAS properties (chain length, functional group), and GAC properties (surface chemistry, pore size distribution). The influence of NOM on regeneration efficiency has to be explored, as NOM might affect PFAS desorption through competition, pore blockage, or complexation. In addition, applied voltages and electrochemical reactions may alter the surface chemistry or pore structure of GAC, potentially enhancing or reducing subsequent adsorption performance. At the process level, optimization of electrochemical cell design and operating conditions (e.g., electrolyte composition, electrode configuration, applied potential) will be necessary to improve energy efficiency and enable the transition from batch experiments to continuous adsorption–regeneration systems.

7.1.3.1. Management of concentrated PFAS streams

Even if electroregeneration proves to be an effective regeneration method, a critical challenge remains regarding the management of the concentrated PFAS streams produced during this process. The concentrated effluents, enriched with desorbed PFAS, must be treated to prevent secondary contamination. While coupling electroregeneration with advanced oxidation or reduction technologies, such as plasma treatment, photocatalysis, or electrochemical degradation, appears to be a logical next step, these approaches are still at the laboratory or pilot stage and not yet viable for large-scale application.[248] At present, the most mature technology for complete PFAS destruction is high-temperature thermal reactivation of GAC filters (~1000 °C), during which complete PFAS defluorination occurs.[62]

Therefore, an alternative adsorption-based strategy is proposed to reduce the frequency of thermal reactivations while still achieving complete PFAS removal. As demonstrated in Section 7.2.1., PFAS adsorption capacity on GAC is strongly dependent on the initial PFAS concentration. Conventional GAC filters become saturated when treating water with PFAS in the ng/L range; however, these exhausted filters still possess sufficient capacity to adsorb PFAS from mg/L-range concentrated solutions. One promising approach is thus to reuse spent GAC filters, which are no longer effective for dilute drinking water streams, for the treatment of concentrated PFAS effluents generated during electroregeneration. Alternatively, a dedicated adsorption unit, using GAC, PAC, or another suitable adsorbent, could be employed specifically for high-concentration PFAS adsorption. Under these elevated concentrations, multilayer adsorption is expected to occur, enhancing overall removal efficiency. Moreover, the increased ionic strength and humic acid content that might be present in electroregeneration concentrates may further promote micelle formation, facilitating PFAS aggregation. Finally, the addition of co-surfactants during concentrate treatment could be explored as a means to further enhance PFAS capture and maximize overall removal efficiency.

Figure 7.10 illustrates the proposed concept of electroregeneration of PFAS-loaded GAC coupled with subsequent treatment of the resulting concentrated streams. In addition to adsorption, these concentrates could also be treated using foam fractionation, particularly when the effluent contains sufficiently high concentrations of surfactants. In this process, PFAS molecules accumulate at the air–water interface of rising gas bubbles, forming a PFAS-enriched foam. Separation and collapse of the foam yield a highly concentrated foamate and a PFAS-depleted retentate, effectively reducing the treated volume and enabling more targeted downstream treatment.[249] Foam fractionation therefore represents a promising approach for pre-concentrating PFAS prior to destruction. However, unlike the well-established thermal reactivation of GAC, fewer studies have demonstrated complete mineralization or defluorination of PFAS from foam concentrates,[250] indicating that this method is less mature and requires further development before large-scale implementation.

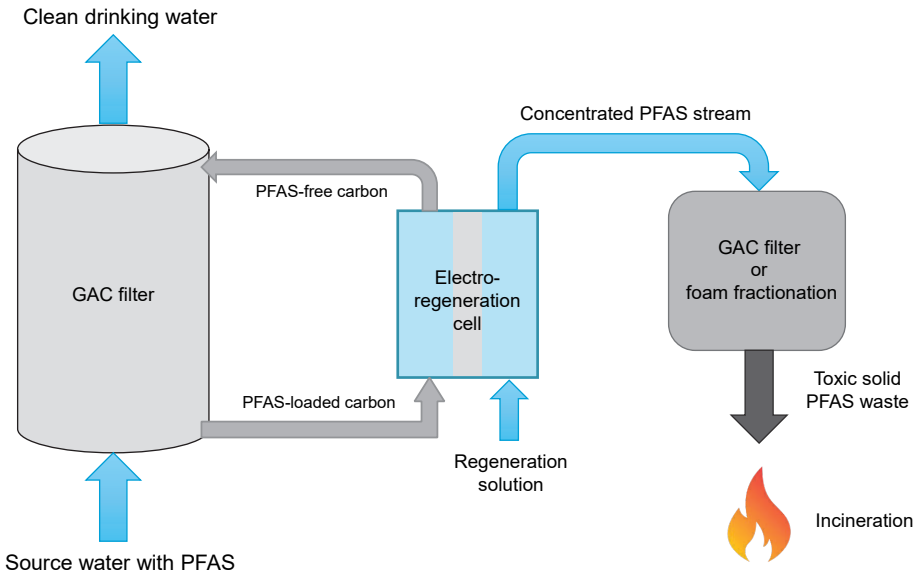


Figure 7.10. Conceptual treatment scheme combining electroregeneration of PFAS-loaded GAC with downstream treatment of the resulting PFAS-concentrated streams.

In conclusion, electroregeneration of adsorbents combined with targeted treatment of concentrated PFAS streams represents a promising step toward a circular and sustainable approach for PFAS removal. Future work should focus on mechanistic understanding, process optimization, and coupling with effective destruction methods to enable full-scale deployment.

7.5. Societal costs and benefits of PFAS removal in drinking water production

The removal of PFAS from drinking water has direct economic and societal implications, as treatment requirements are increasingly driven by stringent regulatory standards intended to protect public health. For European drinking water utilities in 2025, this corresponds to compliance with a total PFAS limit of <100 ng/L.[11] However, several countries have put stricter standards, such as the U.S. EPA limits of 4–10 ng/L (compound-specific)[17] and Dutch PFOA equivalents (PEQ) guideline of <4.4. ng(PEQ)/L[19]. Belkouteb et al. (2020) demonstrated that tightening the effluent target for a GAC filter from 85 ng/L to 10 ng/L increases the treatment cost of GAC filter from 0.02 to 0.10 €/m³ of treated water.[36] The reason for this increase is the need for more frequent regeneration of GAC filter to meet stricter targets. Consequently, any technological or operational improvement that extends GAC bed life and delays PFAS breakthrough can directly reduce treatment costs, provided that the added process itself remains economically justified.

To meaningfully evaluate treatment performance and associated costs, PFAS concentrations should be expressed in a way that is consistent with regulatory limits, i.e., as summed PFAS concentrations. However, the choice of regulatory metric strongly influences which PFAS drive breakthrough and treatment cost. Figure 7.11 compares breakthrough curves obtained in Chapter 5 expressed as (i) the sum of all PFAS, (ii) the sum of short-chain PFAS, and (iii) the sum of long-chain PFAS. When concentrations are expressed according to the current EU regulation (PFAS sum in ng/L), short-chain PFAS dominate early breakthrough and therefore largely determine treatment cost (Figure 7.11A). In contrast, when the same data are converted to PEQ only long-chain PFAS remain critical for compliance (Figure 7.11). It should be noted that these results were obtained under controlled conditions with equal influent concentrations of eight PFAS (1000 ng/L each). In real treatment systems, short-chain PFAS are often present at substantially higher concentrations than long-chain PFAS and can therefore dominate breakthrough behaviour and treatment costs, even under PEQ-based standards.

The following section evaluates strategies to reduce PFAS treatment costs using the current EU regulatory framework, in which compliance is assessed based on total PFAS concentrations (ng/L).

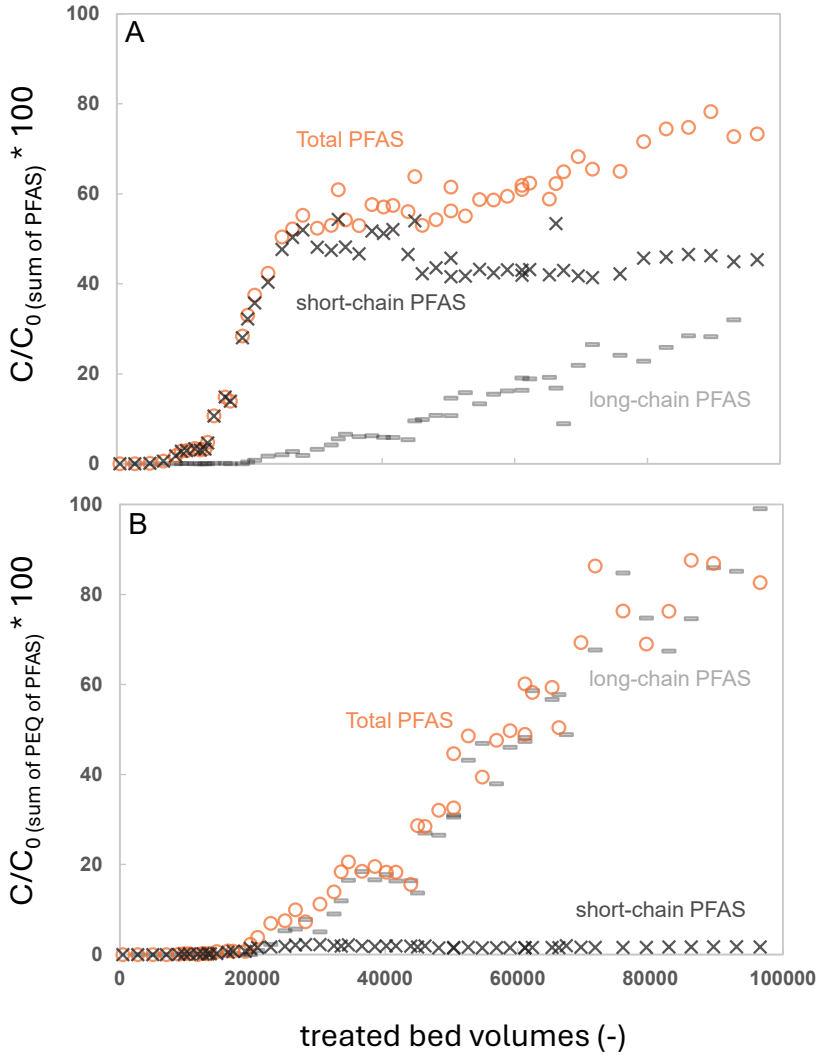


Figure 7.11. Breakthrough curves of PFAS in the presence of 1 mg/L NOM. Data are presented as (A) the sum of all PFAS and (B) the corresponding PFOA-equivalent (PEQ) concentrations. Experimental data points represent the sum of all PFAS (orange circles), short-chain PFAS (black crosses), and long-chain PFAS (black minus symbols). Data was obtained in Chapter 5.

7.5.1. Reducing PFAS treatment cost by removing competing NOM

The most straightforward way to reduce PFAS treatment costs is to lower the concentration of competing NOM. Figure 7.12 shows the summed PFAS breakthrough curves obtained in Chapter 5, conducted under the following conditions: in the presence of 0, 1, and 5 mg/L of NOM, as well as in the presence of 1 mg/L of the >10 kDa NOM fraction (a fraction with a reduced concentration of low-molecular-weight (LMW) compounds). In the presence of 5 mg/L of NOM, breakthrough occurred almost immediately. With 1 mg/L of NOM, breakthrough was observed after approximately 17,000 bed volumes (BV), whereas in the absence of NOM, breakthrough was delayed until around 40,000 BV. When LMW compounds (>10 kDa) were removed, breakthrough occurred at approximately 25,000 BV. The difference in treated bed volumes under these conditions can be used to estimate the potential economic benefit of reducing NOM concentrations prior to PFAS adsorption.

To estimate the cost of PFAS treatment based on the breakthrough curves shown in Figure 7.12, the first step is to determine the regeneration cost of a single GAC filter. Belkouteb et al. (2019) reported a regeneration cost of €892 per m^3 of GAC material (equivalent to approximately €25,000 for a 28 m^3 filter).[36] By dividing the total regeneration cost (€25,000) by the total volume of water treated up to a defined treatment goal, the regeneration cost per cubic meter (€/m^3) of treated water can be calculated. Assuming that the breakthrough behaviour presented in Figure 7.12 is comparable across both high and low ng/L concentration ranges, the resulting cost estimates can be used to evaluate the regeneration costs of GAC filters under conditions relevant to current regulatory limits. The results are presented in Figure 7.13.

The main observation from Figure 7.13 is that the regeneration cost required to achieve a specific treatment goal strongly depends on the NOM concentration in the influent. For example, if the treatment goal is set at sum 20 ng/L of PFAS, the regeneration cost exceeds 0.10 €/m^3 when 5 mg/L of NOM is present, but decreases to approximately 0.05 €/m^3 when the NOM concentration is reduced to 1 mg/L. Clearly, when NOM concentrations in the influent are high, pretreatment is necessary to lower NOM levels and, consequently, reduce GAC regeneration costs. As discussed in Section 7.3.2, ozonation and/or biological activated carbon filtration can be applied as pretreatment steps. The pretreatment should specifically target LMW compounds, as they are the main competitors when short-chain PFAS dominate the total PFAS breakthrough. Figure 7.13 further illustrates that when the concentration of LMW compounds (1 mg/L >10 kDa) is reduced, the regeneration cost to achieve a treatment goal of 20 ng/L decreases to approximately 0.03 €/m^3, compared to 0.05 €/m^3 without pretreatment (1 mg/L NOM)

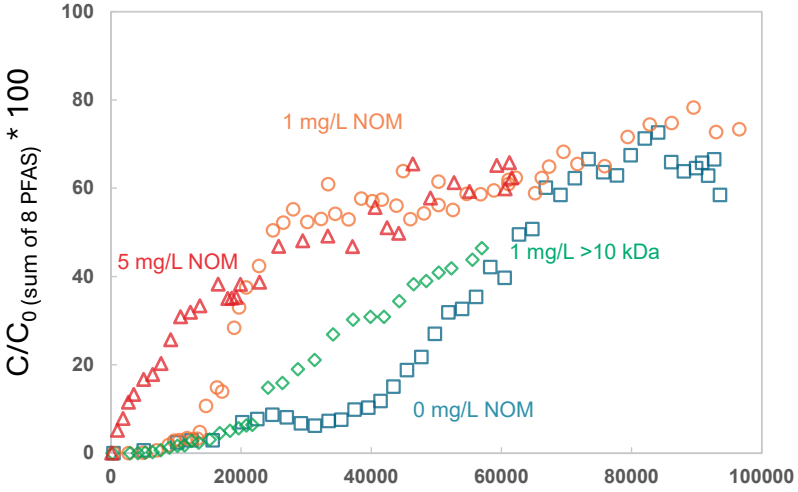


Figure 7.12. Breakthrough curves of the sum of PFAS in the presence of varying concentrations and fractions of Suwannee River NOM (SRNOM): 0 mg/L (blue squares), 1 mg/L (orange circles), 5 mg/L (red triangles), and 1 mg/L of the >10 kDa SRNOM fraction (green diamonds).

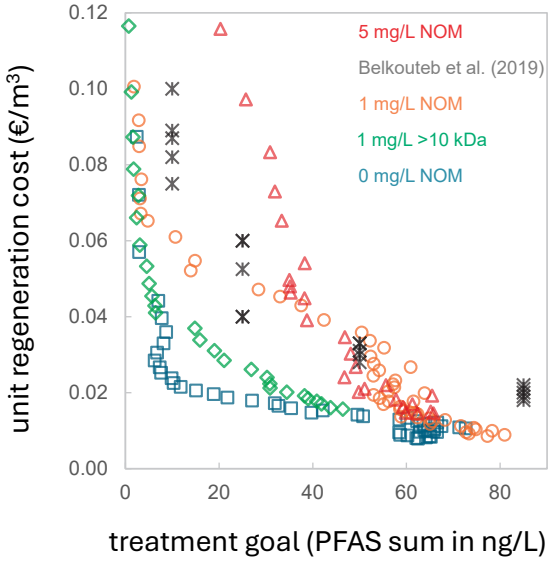


Figure 7.13. Costs of regeneration of a GAC filter as a function of allowed PFAS concentration in the effluent (treatment goal) for breakthrough curves presented on the Figure 7.12. Data from Belkouteb et al. (2019) is also presented for comparison.

The data presented in Figure 7.13 were normalized to the 0–100 ng/L concentration range relevant for regulatory limits by assuming that PFAS breakthrough curves are comparable across both high and low ng/L concentration ranges. This normalization was necessary because the experimental data shown in Figure 7.12 were obtained at an initial PFAS concentration of 1000 ng/L. While this assumption introduces some uncertainty in the exact cost estimates, the calculated regeneration costs align closely with those reported by Belkouteb et al. (2019) for a full-scale treatment plant treating low PFAS concentrations with 1.7 mg/L of NOM.

An important implication of Figure 7.13 is that NOM removal at low concentrations does not necessarily reduce regeneration costs when very stringent PFAS targets are applied. For example, at a treatment goal of 5 ng/L, GAC regeneration costs are nearly identical for influent containing 1 mg/L NOM and for NOM-free water, because the breakthrough curves for these conditions overlap up to ~18,000 bed volumes (Figure 7.12). Within this range, NOM removal does not meaningfully extend filter lifespan. Whether a benefit is realized at early bed volumes therefore depends strongly on the PFAS-to-NOM concentration ratio. At high NOM levels (e.g., 5 mg/L), PFAS breakthrough occurs almost immediately (Figure 7.12), demonstrating severe competitive effects. Even at 1 mg/L NOM, competition is likely to be significant under real treatment conditions, because PFAS concentrations are typically one to two orders of magnitude lower than the 1000 ng/L used in the experiments shown in Figure 7.12. Consequently, recommendation is to do column testing with the site-specific water matrix, alongside a reference experiment in NOM-free water, to assess whether NOM pretreatment provides a tangible benefit for the target effluent concentration. If PFAS concentrations are relatively high and NOM concentrations low, pretreatment may offer limited advantage, and alternative strategies, discussed in the following section, should be considered instead.

7.5.2. Other strategies that can reduce PFAS treatment cost

PFAS removal efficiency generally improves with longer contact times between water and GAC. This can be achieved by reducing the flow rate and increasing the empty bed contact time (EBCT). Belkouteb et al. (2019) reported that doubling the EBCT from 20 to 40 minutes nearly doubled the filter lifetime and reduced GAC regeneration costs by 26%. Higher EBCTs facilitate deeper diffusion of PFAS molecules into the carbon granules, mitigating the kinetic limitations described in Chapter 2 and Section 7.2.2. However, increasing EBCT reduces the total volume of water treated over the same period, which must be carefully considered when evaluating whether GAC filters should be reactivated or operated for longer cycles.

GAC treatment performance, and thus PFAS treatment cost, is strongly influenced by water quality. In particular, the presence of ultrashort-chain PFAS can render GAC ineffective for meeting strict standards. For example, under the Dutch guideline of 4.4 ng PEQ/L, inclusion of trifluoroacetic acid (TFA) poses a major challenge. TFA is frequently detected in surface and groundwater at concentrations around 2000 ng/L or higher. Using a relative potency factor (RPF) of 0.002 for TFA, 2000 ng/L corresponds to approximately 4 ng PEQ/L in the

influent. Since GAC exhibits low adsorption affinity for ultrashort-chain PFAS such as TFA, rapid breakthrough would occur, making traditional GAC treatment insufficient to meet Dutch limit.

The most established technology for removing short- and ultrashort-chain PFAS is ion exchange, that can be employed as a polishing step following GAC filtration. Several studies have shown that ion exchange resins exhibit high adsorption capacities for short-chain PFAS, enabling effective removal.[123,251,252] However, these resins are often expensive and commonly operated as single-use materials that require disposal after exhaustion, or they must be regenerated with concentrated organic solvent and/or inorganic salt solutions that produce secondary waste streams requiring further treatment.[26] Instead of adding a separate treatment step after GAC, an alternative approach to mitigate the rapid breakthrough of short-chain PFAS is to restore GAC adsorption capacity in situ. In this Thesis, we demonstrated that chemical-free recovery of short-chain PFAS adsorption capacity on carbon materials is achievable through electroregeneration, as discussed in Chapter 6.

Although the installation and operating costs of electroregeneration are not yet known, as the technology remains at the proof-of-concept stage, its main current advantage lies in reducing environmental impacts. Electroregeneration avoids the CO_2 and particulate emissions associated with high-temperature regeneration. As PFAS regulations become more stringent and treatment intensity increases, the environmental burden of frequent thermal reactivation is expected to grow. This highlights the need to balance public health benefits from PFAS removal against negative environmental impacts of thermal regeneration. A recent study by Smith et al. (2025) examined this balance and found that, although intensified treatment targeting 4.4 ng PEQ/L provides a net health benefit of 6.9–300 disability-adjusted life years (DALYs) gained per million people annually, the additional thermal regenerations required impose a health burden of 1–35 DALYs lost. The amount of DALYs lost can be substantially mitigated by adopting low-emission regeneration technologies, such as electrochemical reactivation.

Ultimately, the choice of PFAS treatment and regeneration strategy affects not only treatment performance and cost, but also the environmental burden of drinking water production. Assessing PFAS removal in the future will therefore require balancing improved public health protection against the economic and environmental costs of increasingly intensive treatment.

7.6. Conclusions

Advances in understanding PFAS adsorption on Activated Carbon

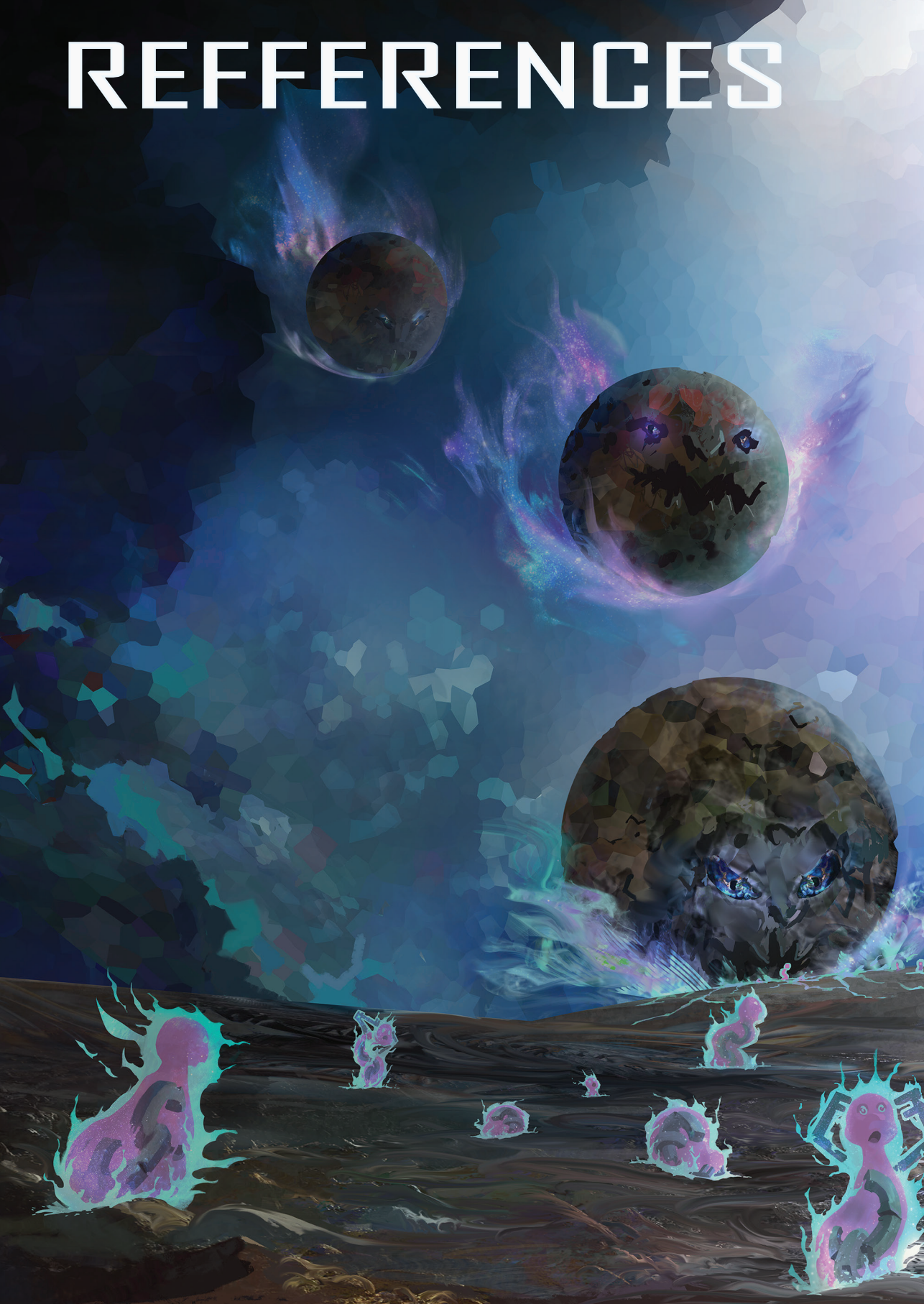
This Thesis shows that the performance of activated carbon (AC) for PFAS removal is primarily limited by (i) trace-level PFAS concentrations, (ii) slow intraparticle PFAS mass transfer, and (iii) competitive interactions between PFAS molecules and between PFAS and natural organic matter (NOM).

(i) Adsorption capacities and isotherm parameters derived at elevated concentrations substantially overestimate adsorption at environmentally relevant ng/L levels. This behaviour arises from the surfactant nature of PFAS and demonstrates that cooperative adsorption and multilayer formation can occur locally within pores, even when bulk concentrations are low.

(ii) Across all systems, PFAS adsorption kinetics were intrinsically slow under realistic GAC-to-water ratios and were best described by surface-diffusion-controlled transport, particularly for hydrophobic long-chain PFAS. As a consequence, PFAS are unable to fully utilize micropore volume and instead accumulate in mesopores, which become the dominant adsorption domain; under right conditions, this accumulation promotes multilayer adsorption.

(iii) In mixtures, short-chain PFAS are displaced over time by longer-chain PFAS with higher affinity for AC, and increasing temperature further reduces short-chain PFAS adsorption by enhancing negative lateral interactions in the adsorbed phase. Adsorption is additionally limited by NOM through site competition, with low-molecular-weight hydrophilic NOM preferentially competing with short-chain PFAS, while hydrophobic neutral NOM fractions primarily interfere with long-chain PFAS adsorption.

REFFERENCES



References

(1) Schrenk, D.; Bignami, M.; Bodin, L.; Chipman, J. K.; del Mazo, J.; Grasl-Kraupp, B.; Hogstrand, C.; Hoogenboom, L.; Leblanc, J. C.; Nebbia, C. S.; Nielsen, E.; Ntzani, E.; Petersen, A.; Sand, S.; Vleminckx, C.; Wallace, H.; Barregård, L.; Ceccatelli, S.; Cravedi, J. P.; Halldorsson, T. I.; Haug, L. S.; Johansson, N.; Knutsen, H. K.; Rose, M.; Roudot, A. C.; Van Loveren, H.; Vollmer, G.; Mackay, K.; Riolo, F.; Schwerdtle, T. Risk to Human Health Related to the Presence of Perfluoroalkyl Substances in Food. *EFSA J.* **2020**, *18* (9). https://doi.org/10.2903/j.efsa.2020.6223.

(2) Plunkett, R. J. *The History of Polytetrafluoroethylene: Discovery and Development*; 1986.

(3) Veritasium. *How One Company Secretly Poisoned The Planet*. https://www.youtube.com/watch?v=SC2eSujzrUY&t=1763s.

(4) Gehrmann, H. J.; Taylor, P.; Aleksandrov, K.; Bergdolt, P.; Bologa, A.; Blye, D.; Dalal, P.; Gunasekar, P.; Herremanns, S.; Kapoor, D.; Michell, M.; Nuredin, V.; Schlipf, M.; Stapf, D. Mineralization of Fluoropolymers from Combustion in a Pilot Plant under Representative European Municipal and Hazardous Waste Combustor Conditions. *Chemosphere* **2024**, *365* (June), 143403. https://doi.org/10.1016/j.chemosphere.2024.143403.

(5) Puts, G. J.; Crouse, P.; Ameduri, B. M. Polytetrafluoroethylene: Synthesis and Characterization of the Original Extreme Polymer. *Chem. Rev.* **2019**, *119* (3), 1763–1805. https://doi.org/10.1021/acs.chemrev.8b00458.

(6) Liljestrand, C. T. PFAS Exposure: A Comprehensive Look at Emerging Facts and Studies, Risk and Liability Assessment, Litigation History, Evolving Regulations and Future Predictions. *Def. Couns. J.* **2022**, *89*, 1.

(7) Buck, R. C.; Franklin, J.; Berger, U.; Conder, J. M.; Cousins, I. T.; Voogt, P. De; Jensen, A. A.; Kannan, K.; Mabury, S. A.; van Leeuwen, S. P. J. Perfluoroalkyl and Polyfluoroalkyl Substances in the Environment: Terminology, Classification, and Origins. *Integr. Environ. Assess. Manag.* **2011**, *7* (4), 513–541. https://doi.org/10.1002/ieam.258.

(8) Organization for Economic Co-operation and Development. Reconciling Terminology of the Universe of Per- and Polyfluoroalkyl Substances: Recommendations and Practical Guidance. *OECD Ser. Risk Manag. - No.61* **2021**, No. 61, 1–45.

(9) Sigmund, G.; Venier, M.; Ågerstrand, M.; Cousins, I. T.; DeWitt, J.; Diamond, M. L.; Field, J.; Ford, A. T.; Joudan, S.; van Leeuwen, S.; Lohmann, R.; Ng, C.; Scheringer, M.; Soehl, A.; Suzuki, N.; Trier, X.; Valsecchi, S.; Vlahos, P.; Young, C. J.; Wang, Z. Scientists' Statement on the Chemical Definition of PFASs. *Environ. Sci. Technol. Lett.* **2025**, *12* (9), 1104–1106. https://doi.org/10.1021/acs.estlett.5c00478.

(10) Wallington, T. J.; Metrangolo, P.; Ameduri, B.; Armelao, L.; Dichiarante, V.; Hori, H.; Kah, M.; Kookana, R.; Krafft, M. P.; Riedel, S.; Walkowiak-Kulikowska, J.; Keinan, E. Comment on "Scientists' Statement on the Chemical Definition of PFASs". *Environ. Sci. Technol. Lett.* **2025**, *12*, 1587–1589. https://doi.org/doi.org/10.1021/acs.estlett.5c00642.

(11) The European Parliament and the Council of the European Union. Directive (EU) 2020/2184. *Off. J. Eur. Union* **2020**, *L 435/1*.

(12) Rayne, S.; Forest, K. Perfluoroalkyl Sulfonic and Carboxylic Acids: A Critical Review of Physicochemical Properties, Levels and Patterns in Waters and Wastewaters, and Treatment Methods. *J. Environ. Sci. Heal. - Part A Toxic/Hazardous Subst. Environ. Eng.* **2009**, *44* (12), 1145–1199. https://doi.org/10.1080/10934520903139811.

(13) Gagliano, E.; Sgroi, M.; Falciglia, P. P.; Vagliasindi, F. G. A.; Roccaro, P. Removal of Poly- and Perfluoroalkyl Substances (PFAS) from Water by Adsorption: Role of PFAS Chain Length, Effect of Organic Matter and Challenges in Adsorbent Regeneration. *Water Res.* **2020**, *171*, 115381. https://doi.org/10.1016/j.watres.2019.115381.

(14) Sobolewski, T. N.; Findlay, J. L.; Hemphill, J. E.; Walker, R. A. Aggregation, Not Micellization: Perfluorooctanoic Acid, Perfluorobutanesulfonic Acid, and Potassium Perfluorooctanesulfonate Behavior in Aqueous Solution. *Langmuir* **2024**, *40* (47), 24820–24831. https://doi.org/10.1021/acs.langmuir.4c02566.

(15) Glüge, J.; Scheringer, M.; Cousins, I. T.; Dewitt, J. C.; Goldenman, G.; Herzke, D.; Lohmann, R.; Ng, C. A.; Trier, X.; Wang, Z. An Overview of the Uses of Per- And Polyfluoroalkyl Substances (PFAS). *Environ. Sci. Process. Impacts* **2020**, *22* (12), 2345–2373. https://doi.org/10.1039/d0em00291g.

(16) Gebbink, W. A.; Van Asseldonk, L.; Van Leeuwen, S. P. J. Presence of Emerging Per- and Polyfluoroalkyl Substances (PFASs) in River and Drinking Water near a Fluorochemical Production Plant in the Netherlands. *Environ. Sci. Technol.* **2017**, *51* (19), 11057–11065. https://doi.org/10.1021/acs.est.7b02488.

(17) US EPA. *National Primary Drinking Water Regulation*; 2024.

(18) Smith, S. J.; Sylvestre, É.; Motelica-Wagenaar, A. M.; Cantoni, B.; Nair, P. S.; Palmeros Parada, M. PFAS Drinking Water Treatment Trade-Offs: Comparing the Health Burden of GAC Treatment to the Health Benefits of Reduced PFAS Exposure. *Environ. Sci. Process. Impacts* **2025**, *27* (7), 1796–1809. https://doi.org/10.1039/d5em00238a.

(19) The European Parliament and the Council of the European Union. Proposal for a Directive 2022/0344 (COD). **2022**.

(20) Zafeiraki, E.; Costopoulou, D.; Vassiliadou, I.; Leondiadis, L.; Dassenakis, E.; Traag, W.; Hoogenboom, R. L. A. P.; van Leeuwen, S. P. J. Determination of Perfluoroalkylated Substances (PFASs) in Drinking Water from the Netherlands and Greece. *Food Addit. Contam. - Part A Chem. Anal. Control. Expo. Risk Assess.* **2015**, *32* (12), 2048–2057. https://doi.org/10.1080/19440049.2015.1086823.

(21) Skutlarek, D.; Exner, M.; Färber, H. Perfluorinated Surfactants in Surface and Drinking Waters. *Environ. Sci. Pollut. Res.* **2006**, *13* (5), 299–307. https://doi.org/10.1065/espr2006.07.326.

(22) Sadia, M.; Nollen, I.; Helmus, R.; Ter Laak, T. L.; Béen, F.; Praetorius, A.; Van Wezel, A. P. Occurrence, Fate, and Related Health Risks of PFAS in Raw and Produced Drinking Water. *Environ. Sci. Technol.* **2023**, *57* (8), 3062–3074. https://doi.org/10.1021/acs.est.2c06015.

(23) Grung, M.; Hjermann, D.; Rundberget, T.; Bæk, K.; Thomsen, C.; Knutsen, H. K.; Haug, L. S. Low Levels of Per- and Polyfluoroalkyl Substances (PFAS) Detected in Drinking Water in Norway, but Elevated Concentrations Found near Known Sources. *Sci. Total Environ.* **2024**, *947* (0579), 174550. https://doi.org/10.1016/j.scitotenv.2024.174550.

(24) Gagliano, E.; Sgroi, M.; Falciglia, P. P.; Vagliasindi, F. G. A.; Roccaro, P. Removal of Poly- and Perfluoroalkyl Substances (PFAS) from Water by Adsorption: Role of PFAS Chain Length, Effect of Organic Matter and Challenges in Adsorbent Regeneration. *Water Res.* **2020**, *171*, 115381. https://doi.org/10.1016/j.watres.2019.115381.

(25) Wanninayake, D. M. Comparison of Currently Available PFAS Remediation Technologies in Water: A Review. *J. Environ. Manage.* **2021**, *283* (October 2020), 111977. https://doi.org/10.1016/j.jenvman.2021.111977.

(26) Dixit, F.; Dutta, R.; Barbeau, B.; Berube, P.; Mohseni, M. PFAS Removal by Ion Exchange Resins: A Review. *Chemosphere* **2021**, *272*, 129777. https://doi.org/10.1016/j.chemosphere.2021.129777.

(27) Li, P.; Zhi, D.; Zhang, X.; Zhu, H.; Li, Z.; Peng, Y.; He, Y.; Luo, L.; Rong, X.; Zhou, Y. Research Progress on the Removal of Hazardous Perfluorochemicals: A Review. *J. Environ. Manage.* **2019**, *250* (February), 109488. https://doi.org/10.1016/j.jenvman.2019.109488.

(28) Horst, J.; McDonough, J.; Ross, I.; Dickson, M.; Miles, J.; Hurst, J.; Storch, P. Water Treatment Technologies for PFAS: The Next Generation. *Groundw. Monit. Remediat.* **2018**, *38* (2), 13–23. https://doi.org/10.1111/gwmr.12281.

(29) Lu, D.; Sha, S.; Luo, J.; Huang, Z.; Zhang Jackie, X. Treatment Train Approaches for the Remediation of Per- and Polyfluoroalkyl Substances (PFAS): A Critical Review. *J. Hazard. Mater.* **2020**, *386* (October 2019), 121963. https://doi.org/10.1016/j.jhazmat.2019.121963.

(30) Worch, E. Adsorption Technology in Water Treatment. *De Gruyter* **2012**, 41–47, 136–162, 297. https://doi.org/10.1515/9783110240238.

(31) Sontheimer, H.; Crittenden, J. C.; Summers, R. S. *Activated Carbon for Water Treatment*; 1988.

(32) Dąbrowski, A. Adsorption - From Theory to Practice. *Adv. Colloid Interface Sci.* **2001**, *93* (1–3), 135–224. https://doi.org/10.1016/S0001-8686(00)00082-8.

(33) Pourret, O.; Bollinger, J. C.; Hursthouse, A.; van Hullebusch, E. D. Sorption vs Adsorption: The Words They Are a-Changin', Not the Phenomena. *Sci. Total Environ.* **2022**, *838* (May), 156545. https://doi.org/10.1016/j.scitotenv.2022.156545.

(34) Schwarzenbach, R. P.; Gschwend, P. M.; Imboden, D. M. Environmental Organic Chemistry (Third Edition). *Wiley* **2017**, 280–282. https://doi.org/10.1002/0471649643.

(35) Nakazawa, Y.; Kosaka, K.; Yoshida, N.; Asami, M.; Matsui, Y. Long-Term Removal of Perfluoroalkyl Substances via Activated Carbon Process for General Advanced Treatment Purposes. *Water Res.* **2023**, *245*, 120559. https://doi.org/10.1016/j.watres.2023.120559.

(36) Belkouteb, N.; Franke, V.; McCleaf, P.; Köhler, S.; Ahrens, L. Removal of Per- and Polyfluoroalkyl Substances (PFASs) in a Full-Scale Drinking Water Treatment Plant: Long-Term Performance of Granular Activated Carbon (GAC) and Influence of Flow-Rate. *Water Res.* **2020**, *182*. https://doi.org/10.1016/j.watres.2020.115913.

(37) Boone, J. S.; Vigo, C.; Boone, T.; Byrne, C.; Ferrario, J.; Benson, R.; Donohue, J.; Simmons, J. E.; Kolpin, D. W.; Furlong, E. T.; Glassmeyer, S. T. Per- and Polyfluoroalkyl Substances in Source and Treated Drinking Waters of the United States. *Sci. Total Environ.* **2019**, *653*, 359–369. https://doi.org/10.1016/j.scitotenv.2018.10.245.

(38) Marsh, H.; Rodríguez-Reinoso, F. *Activated Carbon*; Elsevier Science & Technology Books, 2006. https://doi.org/https://doi.org/10.1016/B978-0-08-044463-5.X5013-4.

(39) Spencer, W.; Senanayake, G.; Altarawneh, M.; Ibana, D.; Nikoloski, A. N. Review of the Effects of Coal Properties and Activation Parameters on Activated Carbon Production and Quality. *Miner. Eng.* **2024**, *212* (April), 108712. https://doi.org/10.1016/j.mineng.2024.108712.

(40) Siipola, V.; Tamminen, T.; Källi, A.; Lahti, R.; Romar, H.; Rasa, K.; Keskinen, R.; Hyväluoma, J.; Hannula, M.; Wikberg, H. Effects of Biomass Type, Carbonization Process, and Activation Method on the Properties of Bio-Based Activated Carbons. *BioResources* **2019**, *13* (3), 5976–6002. https://doi.org/10.15376/biores.13.3.5976-6002.

(41) IUPAC Pore Size Distribution Definition. *IUPAC Compend. Chem. Terminol.* **2008**, *71*, 3853. https://doi.org/10.1351/goldbook.m03853.

(42) McNamara, J. D.; Franco, R.; Mimna, R.; Zappa, L. Comparison of Activated Carbons for Removal of Perfluorinated Compounds from Drinking Water. *J. Am. Water Works Assoc.* **2018**, *110* (1), E2-141. https://doi.org/10.5942/jawwa.2018.110.0003.

(43) Wernert, V.; Nguyen, K. L.; Levitz, P.; Coasne, B.; Denoyel, R. Impact of Surface Diffusion on Transport through Porous Materials. *J. Chromatogr. A* **2022**, *1665*. https://doi.org/10.1016/j.chroma.2022.462823.

(44) Piai, L.; Dykstra, J. E.; Adishakti, M. G.; Blokland, M.; Langenhoff, A. A. M.; van der Wal, A. Diffusion of Hydrophilic Organic Micropollutants in Granular Activated Carbon with Different Pore Sizes. *Water Res.* **2019**, *162*, 518–527. https://doi.org/10.1016/j.watres.2019.06.012.

(45) Cevallos Toledo, R. B.; Aragón-Tobar, C. F.; Gámez, S.; de la Torre, E. Reactivation Process of Activated Carbons: Effect on the Mechanical and Adsorptive Properties. *Molecules* **2020**, *25* (7). https://doi.org/10.3390/molecules25071681.

(46) Vakili, M.; Cagnetta, G.; Deng, S.; Wang, W.; Gholami, Z.; Gholami, F.; Dastyar, W.; Mojiri, A.; Blaney, L. Regeneration of Exhausted Adsorbents after PFAS Adsorption: A Critical Review. *J. Hazard. Mater.* **2024**, *471* (March), 134429. https://doi.org/10.1016/j.jhazmat.2024.134429.

(47) Ateia, M.; Helbling, D. E.; Dichtel, W. R. Best Practices for Evaluating New Materials as Adsorbents for Water Treatment. *ACS Mater. Lett.* **2020**, *2* (11), 1532–1544. https://doi.org/10.1021/acsmaterialslett.0c00414.

(48) Wang, J.; Guo, X. Adsorption Isotherm Models: Classification, Physical Meaning, Application and Solving Method. *Chemosphere* **2020**, *258*, 127279. https://doi.org/10.1016/j.chemosphere.2020.127279.

(49) Wang, J.; Guo, X. Adsorption Kinetic Models: Physical Meanings, Applications, and Solving Methods. *J. Hazard. Mater.* **2020**, *390* (November 2019), 122156. https://doi.org/10.1016/j.jhazmat.2020.122156.

(50) Parniske, J.; Froemelt, A.; Morck, T. Modelling Competitive Adsorption of Organic Micropollutants onto Granular Activated Carbon in Fixed-Bed Adsorbers for Advanced Wastewater Treatment. *Water Res.* **2026**, *288* (PA), 124631. https://doi.org/10.1016/j.watres.2025.124631.

(51) Ochoa-Herrera, V.; Sierra-Alvarez, R. Removal of Perfluorinated Surfactants by Sorption onto Granular Activated Carbon, Zeolite and Sludge. *Chemosphere* **2008**, *72* (10), 1588–1593. https://doi.org/10.1016/j.chemosphere.2008.04.029.

(52) Qiu, Y.; Fujii, S.; Tanaka, S. Removal of Perfluorochemicals from Wastewater by Granular Activated Carbon Adsorption. *Environmeantal Eng. Res.* **2007**, *44* (23), 185–193. https://doi.org/10.11532/proes1992.44.185.

(53) Takagi, S.; Adachi, F.; Miyano, K.; Koizumi, Y.; Tanaka, H.; Mimura, M.; Watanabe, I.; Tanabe, S.; Kannan, K. Perfluorooctanesulfonate and Perfluorooctanoate in Raw and Treated Tap Water from Osaka, Japan. *Chemosphere* **2008**, *72* (10), 1409–1412. https://doi.org/10.1016/j.chemosphere.2008.05.034.

(54) Du, Z.; Deng, S.; Bei, Y.; Huang, Q.; Wang, B.; Huang, J.; Yu, G. Adsorption Behavior and Mechanism of Perfluorinated Compounds on Various Adsorbents-A Review. *J. Hazard. Mater.* **2014**, *274*, 443–454. https://doi.org/10.1016/j.jhazmat.2014.04.038.

(55) Ateia, M.; Maroli, A.; Tharayil, N.; Karanfil, T. The Overlooked Short- and Ultrashort-Chain Poly- and Perfluorinated Substances: A Review. *Chemosphere* **2019**, *220*, 866–882. https://doi.org/10.1016/j.chemosphere.2018.12.186.

(56) Appleman, T. D.; Dickenson, E. R. V.; Bellona, C.; Higgins, C. P. Nanofiltration and Granular Activated Carbon Treatment of Perfluoroalkyl Acids. *J. Hazard. Mater.* **2013**, *260*, 740–746. https://doi.org/10.1016/j.jhazmat.2013.06.033.

(57) McCleaf, P.; Englund, S.; Östlund, A.; Lindegren, K.; Wiberg, K.; Ahrens, L. Removal Efficiency of Multiple Poly- and Perfluoroalkyl Substances (PFASs) in Drinking Water Using Granular Activated Carbon (GAC) and Anion Exchange (AE) Column Tests. *Water Res.* **2017**, *120*, 77–87. https://doi.org/10.1016/j.watres.2017.04.057.

(58) Hansen, M. C.; Børresen, M. H.; Schlabach, M.; Cornelissen, G. Sorption of Perfluorinated Compounds from Contaminated Water to Activated Carbon. *J. Soils Sediments* **2010**, *10* (2), 179–185. https://doi.org/10.1007/s11368-009-0172-z.

(59) Chow, S. J.; Croll, H. C.; Ojeda, N.; Klamerus, J.; Capelle, R.; Oppenheimer, J.; Jacangelo, J. G.; Schwab, K. J.; Prasse, C. Comparative Investigation of PFAS Adsorption onto Activated Carbon and Anion Exchange Resins during Long-Term Operation of a Pilot Treatment Plant. *Water Res.* **2022**, *226* (July), 119198. https://doi.org/10.1016/j.watres.2022.119198.

(60) Liu, C. J.; Werner, D.; Bellona, C. Removal of Per- And Polyfluoroalkyl Substances (PFASs) from Contaminated Groundwater Using Granular Activated Carbon: A Pilot-Scale Study with Breakthrough Modeling. *Environ. Sci. Water Res. Technol.* **2019**, *5* (11), 1844–1853. https://doi.org/10.1039/c9ew00349e.

(61) Xiao, F.; Sasi, P. C.; Yao, B.; Kubátová, A.; Golovko, S. A.; Golovko, M. Y.; Soli, D. Thermal Stability and Decomposition of Perfluoroalkyl Substances on Spent Granular Activated Carbon. *Environ. Sci. Technol. Lett.* **2020**, *7* (5), 343–350. https://doi.org/10.1021/acs.estlett.0c00114.

(62) Sonmez Baghirzade, B.; Zhang, Y.; Reuther, J. F.; Saleh, N. B.; Venkatesan, A. K.; Apul, O. G. Thermal Regeneration of Spent Granular Activated Carbon Presents an Opportunity to Break the Forever PFAS Cycle. *Environ. Sci. Technol.* **2021**, *55* (9), 5608–5619. https://doi.org/10.1021/acs.est.0c08224.

(63) Larasati, A. Chemical Regeneration of Granular Activated Carbon: Development and Evaluation of an Optimal Regenerant Solution. **2020**.

(64) Todeschini, F. C.; Lauer, L. A.; de Almeida, I. R.; Benetti, A. D.; Bernardes, A. M.; da Silva, S. W. Electrochemical Regeneration of Carbendazim-Loaded Granular Activated Carbon. *Sep. Sci. Technol.* **2024**, *59* (5), 878–895. https://doi.org/10.1080/01496395.2024.2340745.

(65) Zhou, J.; Saeidi, N.; Wick, L. Y.; Xie, Y.; Kopinke, F. D.; Georgi, A. Efficient Removal of Trifluoroacetic Acid from Water Using Surface-Modified Activated Carbon and Electro-Assisted Desorption. *J. Hazard. Mater.* **2022**, *436* (February), 129051. https://doi.org/10.1016/j.jhazmat.2022.129051.

(66) Narbaitz, R. M.; Karimi-Jashni, A. Electrochemical Reactivation of Granular Activated Carbon: Impact of Reactor Configuration. *Chem. Eng. J.* **2012**, *197*, 414–423. https://doi.org/10.1016/j.cej.2012.05.049.

(67) Vakili, M.; Bao, Y.; Gholami, F.; Gholami, Z.; Deng, S.; Wang, W.; Kumar Awasthi, A.; Rafatullah, M.; Cagnetta, G.; Yu, G. Removal of HFPO-DA (GenX) from Aqueous Solutions: A Mini-Review. *Chem. Eng. J.* **2021**, *424* (May), 130266. https://doi.org/10.1016/j.cej.2021.130266.

(68) Kancharla, S.; Alexandridis, P.; Tsianou, M. Sequestration of Per- and Polyfluoroalkyl Substances (PFAS) by Adsorption: Surfactant and Surface Aspects. *Curr. Opin. Colloid Interface Sci.* **2022**, *58*, 101571. https://doi.org/10.1016/j.cocis.2022.101571.

(69) Niarchos, G.; Georgii, L.; Ahrens, L.; Kleja, D. B.; Fagerlund, F. A Systematic Study of the Competitive Sorption of Per- and Polyfluoroalkyl Substances (PFAS) on Colloidal Activated Carbon. *Ecotoxicol. Environ. Saf.* **2023**, *264* (August), 115408. https://doi.org/10.1016/j.ecoenv.2023.115408.

(70) Endo, S. Comment on "Experimentally Determined Aqueous Diffusion Coefficients of PFAS Using 19F NMR Diffusion-Ordered Spectroscopy." *ACS ES T Water* **2025**, *5* (1), 488–489. https://doi.org/10.1021/acsestwater.4c01021.

(71) KEMI. Occurrence and Use of Highly Fluorinated Substances and Alternatives. Report from a Government Assignment. **2015**.

(72) Roest, K.; ter Laak, T. L.; Huiting, H.; Siegers, W.; Meekel, N.; Jong, C. de; Jong, M. de; Houten, M. van; Pancras, T.; Plaisier, W.; Dalmijn, J. Performance of Water Treatment Systems for PFAS Removal. Concawe Report. **2021**, *no. 5/21*.

(73) Sörengård, M.; Östblom, E.; Köhler, S.; Ahrens, L. Adsorption Behavior of Per- And Polyfluoralkyl Substances (PFASs) to 44 Inorganic and Organic Sorbents and Use of Dyes as Proxies for PFAS Sorption. *J. Environ. Chem. Eng.* **2020**, *8* (3), 103744. https://doi.org/10.1016/j.jece.2020.103744.

(74) Liu, L.; Liu, Y.; Gao, B.; Ji, R.; Li, C.; Wang, S. Removal of Perfluorooctanoic Acid (PFOA) and Perfluorooctane Sulfonate (PFOS) from Water by Carbonaceous Nanomaterials: A Review. *Crit.*

Rev. Environ. Sci. Technol. **2020**, *50* (22), 2379–2414. https://doi.org/10.1080/10643389.2019.1700751.

(75) Cantoni, B.; Turolla, A.; Wellmitz, J.; Ruhl, A. S.; Antonelli, M. Perfluoroalkyl Substances (PFAS) Adsorption in Drinking Water by Granular Activated Carbon: Influence of Activated Carbon and PFAS Characteristics. *Sci. Total Environ.* **2021**, *795*, 148821. https://doi.org/10.1016/j.scitotenv.2021.148821.

(76) Park, M.; Wu, S.; Lopez, I. J.; Chang, J. Y.; Karanfil, T.; Snyder, S. A. Adsorption of Perfluoroalkyl Substances (PFAS) in Groundwater by Granular Activated Carbons: Roles of Hydrophobicity of PFAS and Carbon Characteristics. *Water Res.* **2020**, *170*. https://doi.org/10.1016/j.watres.2019.115364.

(77) Dixit, F.; Barbeau, B.; Lompe, K. M.; Kheyrandish, A.; Mohseni, M. Performance of the HSDM to Predict Competitive Uptake of PFAS, NOM and Inorganic Anions by Suspended Ion Exchange Processes. *Environ. Sci. Water Res. Technol.* **2021**, *7* (8), 1417–1429. https://doi.org/10.1039/d1ew00145k.

(78) Yu, J.; Lv, L.; Lan, P.; Zhang, S.; Pan, B.; Zhang, W. Effect of Effluent Organic Matter on the Adsorption of Perfluorinated Compounds onto Activated Carbon. *J. Hazard. Mater.* **2012**, *225–226*, 99–106. https://doi.org/10.1016/j.jhazmat.2012.04.073.

(79) Yu, Q.; Zhang, R.; Deng, S.; Huang, J.; Yu, G. Sorption of Perfluorooctane Sulfonate and Perfluorooctanoate on Activated Carbons and Resin: Kinetic and Isotherm Study. *Water Res.* **2009**, *43* (4), 1150–1158. https://doi.org/10.1016/j.watres.2008.12.001.

(80) Geankoplis, C. J.; Leyva-Ramos, R. Model Simulation and Analysis of Surface Diffusion of Liquids in Porous Solids. *Chem. Eng. Sci.* **1985**, *40* (5), 799–807. https://doi.org/10.1016/0009-2509(85)85032-6.

(81) Souza, P. R.; Dotto, G. L.; Salau, N. P. G. Detailed Numerical Solution of Pore Volume and Surface Diffusion Model in Adsorption Systems. *Chem. Eng. Res. Des.* **2017**, *122*, 298–307. https://doi.org/10.1016/j.cherd.2017.04.021.

(82) Burkhardt, J. B.; Burns, N.; Mobley, D.; Pressman, J. G.; Magnuson, M. L.; Speth, T. F. Modeling PFAS Removal Using Granular Activated Carbon for Full-Scale System Design. *J. Environ. Eng.* **2022**, *148* (3), 1–25. https://doi.org/10.1061/(asce)ee.1943-7870.0001964.

(83) Kaur, H.; Bansiwal, A.; Hippargi, G.; Pophali, G. R. Effect of Hydrophobicity of Pharmaceuticals and Personal Care Products for Adsorption on Activated Carbon: Adsorption Isotherms, Kinetics and Mechanism. *Environ. Sci. Pollut. Res.* **2018**, *25* (21), 20473–20485. https://doi.org/10.1007/s11356-017-0054-7.

(84) Gong, Y.; Chen, Z.; Bi, L.; Kang, J.; Zhang, X.; Zhao, S.; Wu, Y.; Tong, Y.; Shen, J. Adsorption Property and Mechanism of Polyacrylate-Divinylbenzene Microspheres for Removal of Trace Organic Micropollutants from Water. *Sci. Total Environ.* **2021**, *781*, 146635. https://doi.org/10.1016/j.scitotenv.2021.146635.

(85) Zaggia, A.; Conte, L.; Falletti, L.; Fant, M.; Chiorboli, A. Use of Strong Anion Exchange Resins for the Removal of Perfluoroalkylated Substances from Contaminated Drinking Water in Batch and Continuous Pilot Plants. *Water Res.* **2016**, *91*, 137–146. https://doi.org/10.1016/j.watres.2015.12.039.

(86) Inyang, M.; Dickenson, E. R. V. The Use of Carbon Adsorbents for the Removal of Perfluoroalkyl Acids from Potable Reuse Systems. *Chemosphere* **2017**, *184*, 168–175. https://doi.org/10.1016/j.chemosphere.2017.05.161.

(87) Du, Z.; Deng, S.; Chen, Y.; Wang, B.; Huang, J.; Wang, Y.; Yu, G. Removal of Perfluorinated Carboxylates from Washing Wastewater of Perfluorooctanesulfonyl Fluoride Using Activated Carbons and Resins. *J. Hazard. Mater.* **2015**, *286*, 136–143. https://doi.org/10.1016/j.jhazmat.2014.12.037.

(88) Franke, V.; McCleaf, P.; Lindegren, K.; Ahrens, L. Efficient Removal of Per- And Polyfluoroalkyl Substances (PFASs) in Drinking Water Treatment: Nanofiltration Combined with Active Carbon or Anion Exchange. *Environ. Sci. Water Res. Technol.* **2019**, *5* (11), 1836–1843. https://doi.org/10.1039/c9ew00286c.

(89) Wu, C.; Klemes, M. J.; Trang, B.; Dichtel, W. R.; Helbling, D. E. Exploring the Factors That Influence the Adsorption of Anionic PFAS on Conventional and Emerging Adsorbents in Aquatic Matrices. *Water Res.* **2020**, *182*, 115950. https://doi.org/10.1016/j.watres.2020.115950.

(90) Higgins, C. P.; Luthy, R. G. Modeling Sorption of Anionic Surfactants onto Sediment Materials: An a Priori Approach for Perfluoroalkyl Surfactants and Linear Alkylbenzene Sulfonates. *Environ. Sci. Technol.* **2007**, *41* (9), 3254–3261. https://doi.org/10.1021/es062449j.

(91) Ahrens, L. Polyfluoroalkyl Compounds in the Aquatic Environment : A Review of Their Occurrence and Fate. *J. Environ. Monit.* **2011**, *13* (20), 20–31. https://doi.org/10.1039/c0em00373e.

(92) Li, M.; Sun, F.; Shang, W.; Zhang, X.; Dong, W.; Dong, Z.; Zhao, S. Removal Mechanisms of Perfluorinated Compounds (PFCs) by Nanofiltration: Roles of Membrane-Contaminant Interactions. *Chem. Eng. J.* **2021**, *406* (July 2020). https://doi.org/10.1016/j.cej.2020.126814.

(93) Yuan, S.; Wang, X.; Jiang, Z.; Zhang, H.; Yuan, S. Contribution of Air-Water Interface in Removing PFAS from Drinking Water: Adsorption, Stability, Interaction and Machine Learning Studies. *Water Res.* **2023**, *236* (December 2022), 119947. https://doi.org/10.1016/j.watres.2023.119947.

(94) Atkinson, A. J.; Apul, O. G.; Schneider, O.; Garcia-Segura, S.; Westerhoff, P. Nanobubble Technologies Offer Opportunities to Improve Water Treatment. *Acc. Chem. Res.* **2019**, No. Table 1. https://doi.org/10.1021/acs.accounts.8b00606.

(95) Do, H. D.; Do, D. D.; Prasetyo, I. On the Surface Diffusion of Hydrocarbons in Microporous Activated Carbon. *Chem. Eng. Sci.* **2001**, *56* (14), 4351–4368. https://doi.org/10.1016/S0009-2509(01)00051-3.

(96) Gilliland, E. R.; Baddour, R. F.; Perkinson, G. P.; Sladek, K. J. Diffusion on Surfaces. I. Effect of Concentration on the Diffusivity of Physically Adsorbed GAsses. *Ind. Eng. Chem. Res.* **1974**, *13* (2), 95–100.

(97) Neretnieks, I. Analysis of Some Adsorption Experiments with Activated Carbon. *Chem. Eng. Sci.* **1976**, *31* (11), 1029–1035. https://doi.org/10.1016/0009-2509(76)87023-6.

(98) Suzuki, M.; Takao, F. Concentration Dependence of Surface Diffusion Coefficient of Propionic Acid in Activated Carbon Particles. *AIChE J.* **1982**, *28* (3), 380–385. https://doi.org/10.1002/aic.690280303.

(99) Leyva-ramos, R. Role of Pore Volume and Surface Diffusion in the Adsorption of Aromatic Compounds on Activated Carbon. **2013**, No. 6, 945–957. https://doi.org/10.1007/s10450-013-9502-y.

(100) Neretnieks, I. Adsorption in Finite Bath and Countercurrent Flow with Systems Having a Nonlinear Isotherm. *Chem. Eng. Sci.* **1976**, *31* (2), 107–114. https://doi.org/10.1016/0009-2509(76)85045-2.

(101) Mohona, T. M.; Ye, Z.; Dai, N.; Nalam, P. C. Adsorption Behavior of Long-Chain Perfluoroalkyl Substances on Hydrophobic Surface : A Combined Molecular Characterization and Simulation Study. *Water Res.* **2023**, *239* (May), 120074. https://doi.org/10.1016/j.watres.2023.120074.

(102) Schönherr, J.; Buchheim, J.; Scholz, P.; Adelhelm, P. Boehm Titration Revisited (Part I): Practical Aspects for Achieving a High Precision in Quantifying Oxygen-Containing Surface Groups on Carbon Materials. *C* **2018**, *4* (2), 21. https://doi.org/10.3390/c4020021.

(103) Ocampo-Perez, R.; Leyva-Ramos, R.; Alonso-Davila, P.; Rivera-Utrilla, J.; Sanchez-Polo, M. Modeling Adsorption Rate of Pyridine onto Granular Activated Carbon. *Chem. Eng. J.* **2010**, *165* (1), 133–141. https://doi.org/10.1016/j.cej.2010.09.002.

(104) Ocampo-Perez, R.; Leyva-Ramos, R.; Mendoza-Barron, J.; Guerrero-Coronado, R. M. Adsorption Rate of Phenol from Aqueous Solution onto Organobentonite: Surface Diffusion and Kinetic Models. *J. Colloid Interface Sci.* **2011**, *364* (1), 195–204. https://doi.org/10.1016/j.jcis.2011.08.032.

(105) Ramakrishna, V. Effect of Biot Number in Batch Studies of Adsorption. *IEJRT* **2013**, *2* (10), 587–595.

(106) Wilke, C. R.; Chang, P. Correlation of Diffusion Coefficients in Dilute Solutions. *AIChE J.* **1955**, 264–270. https://doi.org/10.1002/aic.690010222.

(107) Saeidi, N.; Kopinke, F. D.; Georgi, A. Understanding the Effect of Carbon Surface Chemistry on Adsorption of Perfluorinated Alkyl Substances. *Chem. Eng. J.* **2020**, *381* (August 2019), 122689. https://doi.org/10.1016/j.cej.2019.122689.

(108) Schutta, T. C.; *, Caitlin G. Bresnahana, Timothy C. Ricardb, and M. K. S.; AUS. Impacts of Pore Size in Binding Dynamics of Per-and Polyfluoroalkyl Substances (PFAS) on Modified Graphene Materials. **2025**. https://doi.org/10.1039/D5VA00030K.

(109) Mian, M. M.; Zhu, J.; Jiang, X.; Deng, S. Recent Advances in Activated Carbon Driven PFAS Removal: Structure-Adsorption Relationship and New Adsorption Mechanisms. *Front. Environ. Sci. Eng.* **2025**, *19* (6). https://doi.org/10.1007/s11783-025-1998-3.

(110) Zhang, Y.; Thomas, A.; Apul, O.; Venkatesan, A. K. Coexisting Ions and Long-Chain per- and Polyfluoroalkyl Substances (PFAS) Inhibit the Adsorption of Short-Chain PFAS by Granular Activated Carbon. *J. Hazard. Mater.* **2023**, *460* (July), 132378. https://doi.org/10.1016/j.jhazmat.2023.132378.

(111) Saeidi, N.; Lai, A.; Harnisch, F.; Sigmund, G. A FAIR Comparison of Activated Carbon, Biochar, Cyclodextrins, Polymers, Resins, and Metal Organic Frameworks for the Adsorption of per- and Polyfluorinated Substances. *Chem. Eng. J.* **2024**, *498* (May), 155456. https://doi.org/10.1016/j.cej.2024.155456.

(112) Saeidi, N.; Kopinke, F. D.; Georgi, A. Understanding the Effect of Carbon Surface Chemistry on Adsorption of Perfluorinated Alkyl Substances. *Chem. Eng. J.* **2020**, *381* (September 2019), 122689. https://doi.org/10.1016/j.cej.2019.122689.

(113) Zhi, Y.; Liu, J. Adsorption of Perfluoroalkyl Acids by Carbonaceous Adsorbents: Effect of Carbon Surface Chemistry. *Environ. Pollut.* **2015**, *202*, 168–176. https://doi.org/10.1016/j.envpol.2015.03.019.

(114) Zhou, J.; Saeidi, N.; Wick, L. Y.; Kopinke, F. D.; Georgi, A. Adsorption of Polar and Ionic Organic Compounds on Activated Carbon: Surface Chemistry Matters. *Sci. Total Environ.* **2021**, *794*, 148508. https://doi.org/10.1016/j.scitotenv.2021.148508.

(115) Pranić, M.; Carlucci, L.; van der Wal, A.; Dykstra, J. E. Kinetic and Isotherm Study for the Adsorption of Per- and Polyfluoroalkyl Substances (PFAS) on Activated Carbon in the Low Ng/L Range. *Chemosphere* **2025**, *370*. https://doi.org/10.1016/j.chemosphere.2024.143889.

(116) Nakazawa, Y.; Kosaka, K.; Asami, M.; Matsui, Y. Maximum Desorption of Perfluoroalkyl Substances Adsorbed on Granular Activated Carbon Used in Full-Scale Drinking Water Treatment Plants. *Water Res.* **2024**, *254* (October 2023), 121396. https://doi.org/10.1016/j.watres.2024.121396.

(117) Murray, C. C.; Vatankhah, H.; McDonough, C. A.; Nickerson, A.; Hedtke, T. T.; Cath, T. Y.; Higgins, C. P.; Bellona, C. L. Removal of Per- and Polyfluoroalkyl Substances Using Super-Fine Powder Activated Carbon and Ceramic Membrane Filtration. *J. Hazard. Mater.* **2019**, *366* (November 2018), 160–168. https://doi.org/10.1016/j.jhazmat.2018.11.050.

(118) Xiao, X.; Ulrich, B. A.; Chen, B.; Higgins, C. P. Sorption of Poly- and Perfluoroalkyl Substances (PFASs) Relevant to Aqueous Film-Forming Foam (AFFF)-Impacted Groundwater by Biochars

and Activated Carbon. *Environ. Sci. Technol.* **2017**, *51* (11), 6342–6351. https://doi.org/10.1021/acs.est.7b00970.

(119) Abulikemu, G.; Pressman, J. G.; Sorial, G. A.; Sanan, T. T.; Haupert, L. M.; Burkhardt, J. B.; Smith, S. J.; Kleiner, E. J.; Stebel, E. K.; Gray, B. N.; Gastaldo, C. X.; Hughes, E. W.; Pedigo, S. G.; Wahman, D. G. Perfluoroalkyl Chemical Adsorption by Granular Activated Carbon: Assessment of Particle Size Impact on Equilibrium Parameters and Associated Rapid Small-Scale Column Test Scaling Assumptions. *Water Res.* **2025**, *271* (October 2024), 122977. https://doi.org/10.1016/j.watres.2024.122977.

(120) Summers, R. S.; Roberts, P. V. Activated Carbon Adsorption of Humic Substances. I. Heterodisperse Mixtures and Desorption. *J. Colloid Interface Sci.* **1988**, *122* (2), 367–381. https://doi.org/10.1016/0021-9797(88)90372-4.

(121) Pranić, M.; Zhou, K.; Biesheuvel, P. M.; van der Wal, A.; Dykstra, J. E. Temperature Impacts PFAS Adsorption on Activated Carbon. *ACS ES&T Water* **2025**. https://doi.org/10.1021/acsestwater.5c00343.

(122) Sun, R.; Sasi, P. C.; Alinezhad, A.; Xiao, F. Sorptive Removal of Per- and Polyfluoroalkyl Substances (PFAS) in Organic-Free Water, Surface Water, and Landfill Leachate and Thermal Reactivation of Spent Sorbents. *J. Hazard. Mater. Adv.* **2023**, *10* (March), 100311. https://doi.org/10.1016/j.hazadv.2023.100311.

(123) Riegel, M.; Haist-Gulde, B.; Sacher, F. Sorptive Removal of Short-Chain Perfluoroalkyl Substances (PFAS) during Drinking Water Treatment Using Activated Carbon and Anion Exchanger. *Environ. Sci. Eur.* **2023**, *35* (1). https://doi.org/10.1186/s12302-023-00716-5.

(124) Rahman, M. F. Removal of Perfluorinated Compounds from Ultrapure and Surface Waters by Adsorption and Ion Exchange. *Univ. Waterloo* **2014**, 315.

(125) Senevirathna, S. T. M. L. D.; Tanaka, S. A. of four perfluorinated acids on non ion exchange polymer sorbents; Fujii, S.; Kunacheva, C.; Harada, H.; Shivakoti, B. R.; Dinh, H.; Ariyadasa, T. Adsorption of Four Perfluorinated Acids on Non Ion Exchange Polymer Sorbents. *Water Sci. Technol.* **2011**, *63* (10), 2106–2113. https://doi.org/10.2166/wst.2011.295.

(126) Li, F.; Wei, Z.; He, K.; Blaney, L.; Cheng, X.; Xu, T.; Liu, W.; Zhao, D. A Concentrate-and-Destroy Technique for Degradation of Perfluorooctanoic Acid in Water Using a New Adsorptive Photocatalyst. *Water Res.* **2020**, *185*, 1–14. https://doi.org/10.1016/j.watres.2020.116219.

(127) Dunmyer, M.; Welchert, J.; Bellido-Aguilar, D. A.; Brusseau, M.; Savagatrup, S.; Karanikola, V. Molecular Scale Adsorption Behavior of Per- and Poly-Fluoroalkyl Substances (PFAS) on Model Surfaces. *Chem. Eng. J.* **2024**, *497*, 154286. https://doi.org/10.1016/j.cej.2024.154286.

(128) OECD Guidelines for Adsorption. https://doi.org/10.1097/00001888-199702000-00023.

(129) Carey, G. R.; Hakimabadi, S. G.; Singh, M.; McGregor, R.; Woodfield, C.; Van Geel, P. J.; Pham, A. L. T. Longevity of Colloidal Activated Carbon for in Situ PFAS Remediation at AFFF-Contaminated Airport Sites. *Remediation* **2022**, *33* (1), 3–23. https://doi.org/10.1002/rem.21741.

(130) Schutt, T. C.; Bresnahan, C. G.; Ricard, T. C.; Shukla, M. K. Impacts of Pore Size in Binding Dynamics of Per- and Polyfluoroalkyl Substances (PFAS) on Modified Graphene Materials. *Environ. Sci. Adv.* **2025**, *4* (10), 1587–1593. https://doi.org/10.1039/d5va00030k.

(131) Crone, B. C.; Speth, T. F.; Wahman, D. G.; Smith, S. J.; Abulikemu, G.; Kleiner, E. J.; Pressman, J. G.; Crone, B. C.; Speth, T. F.; Wahman, D. G.; Samantha, J.; Abulikemu, G.; Kleiner, E. J.; Pressman, J. G. Occurrence of Per- and Polyfluoroalkyl Substances (PFAS) in Source Water and Their Treatment in Drinking Water. *Crit. Rev. Environ. Sci. Technol.* **2019**, *49* (24), 2359–2396. https://doi.org/10.1080/10643389.2019.1614848.

(132) Shimizu, S.; Matubayasi, N. Temperature Dependence of Sorption. *Langmuir* **2021**, *37*, 11008–11017. https://doi.org/10.1021/acs.langmuir.1c01576.

(133) Tong, Y.; Mayer, B. K.; McNamara, P. J. Adsorption of Organic Micropollutants to Biosolids-Derived Biochar: Estimation of Thermodynamic Parameters. *Environ. Sci. Water Res. Technol.* **2019**, *5* (6), 1132–1144. https://doi.org/10.1039/c8ew00854j.

(134) Qian, J.; Shen, M.; Wang, P.; Wang, C.; Hu, J.; Hou, J.; Ao, Y.; Zheng, H.; Li, K.; Liu, J. Co-Adsorption of Perfluorooctane Sulfonate and Phosphate on Boehmite: Influence of Temperature, Phosphate Initial Concentration and PH. *Ecotoxicol. Environ. Saf.* **2017**, *137* (November 2016), 71–77. https://doi.org/10.1016/j.ecoenv.2016.11.026.

(135) Omo-Okoro, P. N.; Curtis, C. J.; Karásková, P.; Melymuk, L.; Oyewo, O. A.; Okonkwo, J. O. Kinetics, Isotherm, and Thermodynamic Studies of the Adsorption Mechanism of PFOS and PFOA Using Inactivated and Chemically Activated Maize Tassel. *Water. Air. Soil Pollut.* **2020**, *231* (9). https://doi.org/10.1007/s11270-020-04852-z.

(136) Guo, W.; Huo, S.; Feng, J.; Lu, X. Adsorption of Perfluorooctane Sulfonate (PFOS) on Corn Straw-Derived Biochar Prepared at Different Pyrolytic Temperatures. *J. Taiwan Inst. Chem. Eng.* **2017**, *78*, 265–271. https://doi.org/10.1016/j.jtice.2017.06.013.

(137) Qian, J.; Shen, M.; Wang, P.; Wang, C.; Li, K.; Liu, J.; Lu, B.; Tian, X. Perfluorooctane Sulfonate Adsorption on Powder Activated Carbon: Effect of Phosphate (P) Competition, PH, and Temperature. *Chemosphere* **2017**, *182*, 215–222. https://doi.org/10.1016/j.chemosphere.2017.05.033.

(138) Xu, C.; Chen, H.; Jiang, F. Adsorption of Perflourooctane Sulfonate (PFOS) and Perfluorooctanoate (PFOA) on Polyaniline Nanotubes. *Colloids Surfaces A Physicochem. Eng. Asp.* **2015**, *479*, 60–67. https://doi.org/10.1016/j.colsurfa.2015.03.045.

(139) Kuo, C. Y.; Wu, C. H.; Wu, J. Y. Adsorption of Direct Dyes from Aqueous Solutions by Carbon Nanotubes: Determination of Equilibrium, Kinetics and Thermodynamics Parameters. *J. Colloid Interface Sci.* **2008**, *327* (2), 308–315. https://doi.org/10.1016/j.jcis.2008.08.038.

(140) Tran, H. N.; Lima, E. C.; Juang, R. S.; Bollinger, J. C.; Chao, H. P. Thermodynamic Parameters of Liquid–Phase Adsorption Process Calculated from Different Equilibrium Constants Related to Adsorption Isotherms: A Comparison Study. *J. Environ. Chem. Eng.* **2021**, *9* (6), 106674. https://doi.org/10.1016/j.jece.2021.106674.

(141) Agudelo-Vera, C.; Avvedimento, S.; Boxall, J.; Creaco, E.; de Kater, H.; Nardo, A. Di; Djukic, A.; Douterelo, I.; Fish, K. E.; Rey, P. L. G.; Jacimovic, N.; Jacobs, H. E.; Kapelan, Z.; Solano, J. M.; Pachongo, C. M.; Piller, O.; Quintiliani, C.; Ručka, J.; Tuhovčák, L.; Blokker, M. Drinking Water Temperature around the Globe: Understanding, Policies, Challenges and Opportunities. *Water* **2020**, *12* (4). https://doi.org/10.3390/W12041049.

(142) Ishiguro, M.; Koopal, L. K. Surfactant Adsorption to Soil Components and Soils. *Adv. Colloid Interface Sci.* **2016**, *231*, 59–102. https://doi.org/10.1016/j.cis.2016.01.006.

(143) Sadia, M.; Beut, L. B.; Pranić, M.; Wezel, A. P. va.; Laak, T. L. te. Sorption of Per- and Poly-Fluoroalkyl Substances and Their Precursors on Activated Carbon under Realistic Drinking Water Conditions: Insights into Sorbent Variability and PFAS Structural Effects. *Heliyon* **2024**, *10* (3). https://doi.org/10.1016/j.heliyon.2024.e25130.

(144) Foo, K. Y.; Hameed, B. H. Insights into the Modeling of Adsorption Isotherm Systems. *Chem. Eng. J.* **2010**, *156* (1), 2–10. https://doi.org/10.1016/j.cej.2009.09.013.

(145) Chu, K. H.; Tan, B. C. Is the Frumkin (Fowler–Guggenheim) Adsorption Isotherm a Two- or Three-Parameter Equation? *Colloids Interface Sci. Commun.* **2021**, *45*, 100519. https://doi.org/10.1016/j.colcom.2021.100519.

(146) Miyabe, K.; Guiochon, G. Analysis of Surface Diffusion Phenomena in Reversed-Phase Liquid Chromatography. *Anal. Chem.* **1999**, *71* (4), 889–896. https://doi.org/10.1021/ac9809027.

(147) Ross, I.; McDonough, J.; Miles, J.; Storch, P.; Thelakkat Kochunarayanan, P.; Kalve, E.; Hurst, J.; S. Dasgupta, S.; Burdick, J. A Review of Emerging Technologies for Remediation of PFASs. *Remediation* **2018**, *28* (2), 101–126. https://doi.org/10.1002/rem.21553.

(148) Tang, X.; Ripepi, N. Temperature-Dependent Langmuir's Model in the Coal and Methane Sorption Process: Statistics Relationship. *Trans. Soc. Mining, Metall. Explor.* **2016**, *340*, 61–69. https://doi.org/10.19150/trans.7328.

(149) Saffarionpour, S.; Tam, S. Y. S.; Van der Wielen, L. A. M.; Brouwer, E.; Ottens, M. Influence of Ethanol and Temperature on Adsorption of Flavor-Active Esters on Hydrophobic Resins. *Sep. Purif. Technol.* **2019**, *210*, 219–230. https://doi.org/10.1016/j.seppur.2018.05.026.

(150) Piccin, J. S.; Dotto, G. L.; Pinto, L. A. A. Adsorption Isotherms and Thermochemical Data of FDandC RED N° 40 Binding by Chitosan. *Brazilian J. Chem. Eng.* **2011**, *28* (2), 295–304. https://doi.org/10.1590/S0104-66322011000200014.

(151) Hwang, K. S.; Choi, D. K.; Gong, S. Y.; Cho, S. Y. Adsorption and Thermal Regeneration of Methylene Chloride Vapor on an Activated Carbon Bed. *Chem. Eng. Sci.* **1997**, *52* (7), 1111–1123. https://doi.org/10.1016/S0009-2509(96)00470-8.

(152) Tong, Y.; McNamara, P. J.; Mayer, B. K. Adsorption of Organic Micropollutants onto Biochar: A Review of Relevant Kinetics, Mechanisms and Equilibrium. *Environ. Sci. Water Res. Technol.* **2019**, *5* (5), 821–838. https://doi.org/10.1039/c8ew00938d.

(153) Marcel R. Bóhmer and Luuk K. Koopal. Adsorption of Ionic Surfactants on Variable-Charge Surfaces. 1. Charge Effects and Structure of the Adsorbed Layer. *Langmuir* **1992**, *8* (11), 2585–2848. https://doi.org/doi.org/10.1021/la00047a014.

(154) Brusseau, M. L.; Van Glubt, S. The Influence of Surfactant and Solution Composition on PFAS Adsorption at Fluid-Fluid Interfaces. *Water Res.* **2019**, *161*, 17–26. https://doi.org/10.1016/j.watres.2019.05.095.

(155) García-Mateos, F. J.; Ruiz-Rosas, R.; Marqués, M. D.; Cotoruelo, L. M.; Rodríguez-Mirasol, J.; Cordero, T. Removal of Paracetamol on Biomass-Derived Activated Carbon: Modeling the Fixed Bed Breakthrough Curves Using Batch Adsorption Experiments. *Chem. Eng. J.* **2015**, *279*, 18–30. https://doi.org/10.1016/j.cej.2015.04.144.

(156) Pan, B. C.; Meng, F. W.; Chen, X. Q.; Pan, B. J.; Li, X. T.; Zhang, W. M.; Zhang, X.; Chen, J. L.; Zhang, Q. X.; Sun, Y. Application of an Effective Method in Predicting Breakthrough Curves of Fixed-Bed Adsorption onto Resin Adsorbent. *J. Hazard. Mater.* **2005**, *124* (1–3), 74–80. https://doi.org/10.1016/j.jhazmat.2005.03.052.

(157) Phong Vo, H. N.; Ngo, H. H.; Guo, W.; Hong Nguyen, T. M.; Li, J.; Liang, H.; Deng, L.; Chen, Z.; Hang Nguyen, T. A. Poly-and Perfluoroalkyl Substances in Water and Wastewater: A Comprehensive Review from Sources to Remediation. *J. Water Process Eng.* **2020**, *36* (June), 101393. https://doi.org/10.1016/j.jwpe.2020.101393.

(158) Sun, Y.; Angelotti, B.; Brooks, M.; Dowbiggin, B.; Evans, P. J.; Devins, B.; Wang, Z. W. A Pilot-Scale Investigation of Disinfection by-Product Precursors and Trace Organic Removal Mechanisms in Ozone-Biologically Activated Carbon Treatment for Potable Reuse. *Chemosphere* **2018**, *210*, 539–549. https://doi.org/10.1016/j.chemosphere.2018.06.162.

(159) Sgroi, M.; Anumol, T.; Roccaro, P.; Vagliasindi, F. G. A.; Snyder, S. A. Modeling Emerging Contaminants Breakthrough in Packed Bed Adsorption Columns by UV Absorbance and Fluorescing Components of Dissolved Organic Matter. *Water Res.* **2018**, *145*, 667–677. https://doi.org/10.1016/j.watres.2018.09.018.

(160) Pramanik, B. K.; Pramanik, S. K.; Sarker, D. C. Removal of Emerging Perfluorooctanoic Acid and Perfluorooctane Sulfonate Contaminants from Lake Water. **2017**, *3330*. https://doi.org/10.1080/09593330.2016.1240716.

(161) Levchuk, I.; Rueda Márquez, J. J.; Sillanpää, M. Removal of Natural Organic Matter (NOM) from Water by Ion Exchange – A Review. *Chemosphere* **2018**, *192*, 90–104. https://doi.org/10.1016/j.chemosphere.2017.10.101.

(162) Dejaeger, K.; Criquet, J.; Vanoppen, M.; Vignal, C.; Billon, G.; Cornelissen, E. R. Identification of Disinfection By-Product Precursors by Natural Organic Matter Fractionation: A Review. *Environ. Chem. Lett.* **2022**, *20* (6), 3861–3882. https://doi.org/10.1007/s10311-022-01478-x.

(163) van Gijn, K.; Zhao, Y.; Balasubramaniam, A.; de Wilt, H. A.; Carlucci, L.; Langenhoff, A. A. M.; Rijnaarts, H. H. M. The Effect of Organic Matter Fractions on Micropollutant Ozonation in Wastewater Effluents. *Water Res.* **2022**, *222* (July), 118933. https://doi.org/10.1016/j.watres.2022.118933.

(164) Bai, Y.; Cui, Z.; Ding, D.; Hong, C.; Cui, H.; Hu, Q.; Zhou, M.; Qu, K. The Characteristics of CDOM Structural Composition and the Effect on Indirect Photodegradation of Sulfamerazine. *Sci. Total Environ.* **2023**, *888* (April), 164231. https://doi.org/10.1016/j.scitotenv.2023.164231.

(165) Li, C.; Wang, D.; Xu, X.; Wang, Z. Formation of Known and Unknown Disinfection By-Products from Natural Organic Matter Fractions during Chlorination , Chloramination , and Ozonation. *Sci. Total Environ.* **2017**, *587–588*, 177–184. https://doi.org/10.1016/j.scitotenv.2017.02.108.

(166) Ribeiro Pinela, S.; Larasati, A.; Meulepas, R. J. W.; Gagliano, M. C.; Kleerebezem, R.; Bruning, H.; Rijnaarts, H. H. M. Ultrafiltration (UF) and Biological Oxygen-Dosed Activated Carbon (BODAC) Filtration to Prevent Fouling of Reversed Osmosis (RO) Membranes: A Mass Balance Analysis. *J. Water Process Eng.* **2024**, *57* (November 2023). https://doi.org/10.1016/j.jwpe.2023.104648.

(167) Hua, G.; Reckhow, D. A.; Abusallout, I. Correlation between SUVA and DBP Formation during Chlorination and Chloramination of NOM Fractions from Different Sources. *Chemosphere* **2015**, *130*, 82–89. https://doi.org/10.1016/j.chemosphere.2015.03.039.

(168) Ratpukdi, T.; Intarasuwan, K.; Jutaporn, P.; Khan, E. Interactions between Natural Organic Matter Fractions and Nanoscale Zero-Valent Iron. *Sci. Total Environ.* **2021**, *796*, 148954. https://doi.org/10.1016/j.scitotenv.2021.148954.

(169) Lei, X.; Yao, L.; Lian, Q.; Zhang, X.; Wang, T.; Holmes, W.; Ding, G.; Gang, D. D.; Zappi, M. E. Enhanced Adsorption of Perfluorooctanoate (PFOA) onto Low Oxygen Content Ordered Mesoporous Carbon (OMC): Adsorption Behaviors and Mechanisms. *J. Hazard. Mater.* **2022**, *421* (August 2021), 126810. https://doi.org/10.1016/j.jhazmat.2021.126810.

(170) Hua, G.; Reckhow, D. A. Characterization of Disinfection By-Product Precursors Based on Hydrophobicity and Molecular Size. *AWWA 124th Annu. Conf. Expo. World's Water Event, ACE 2005* **2005**, 3309–3315.

(171) Özdemr, K. Characterization of Natural Organic Matter in Conventional Water Treatment Processes and Evaluation of THM Formation with Chlorine. *Sci. World J.* **2014**, *2014*. https://doi.org/10.1155/2014/703173.

(172) Zhao, Z. Y.; Gu, J. D.; Li, H. B.; Li, X. Y.; Leung, K. M. Y. Disinfection Characteristics of the Dissolved Organic Fractions at Several Stages of a Conventional Drinking Water Treatment Plant in Southern China. *J. Hazard. Mater.* **2009**, *172* (2–3), 1093–1099. https://doi.org/10.1016/j.jhazmat.2009.07.101.

(173) Zhang, X.; Chen, Z.; Shen, J.; Zhao, S.; Kang, J.; Chu, W.; Zhou, Y.; Wang, B. Formation and Interdependence of Disinfection Byproducts during Chlorination of Natural Organic Matter in a Conventional Drinking Water Treatment Plant. *Chemosphere* **2020**, *242*, 125227. https://doi.org/10.1016/j.chemosphere.2019.125227.

(174) Wei, Q. shan; Feng, C. hong; Wang, D. sheng; Shi, B. you; Zhang, L. tian; Wei, Q.; Tang, H. xiao. Seasonal Variations of Chemical and Physical Characteristics of Dissolved Organic Matter

and Trihalomethane Precursors in a Reservoir: A Case Study. *J. Hazard. Mater.* **2008**, *150* (2), 257–264. https://doi.org/10.1016/j.jhazmat.2007.04.096.

(175) Marhaba, T. F.; Van, D.; Lippincott, R. L. Changes in NOM Fractionation through Treatment: A Comparison of Ozonation and Chlorination. *Ozone Sci. Eng.* **2000**, *22* (3), 249–266. https://doi.org/10.1080/01919510008547209.

(176) Ratpukdi, T.; Rice, J. A.; Chilom, G.; Bezbaruah, A.; Khan, E. Rapid Fractionation of Natural Organic Matter in Water Using a Novel Solid-Phase Extraction Technique. *Water Environ. Res.* **2009**, *81* (11), 2299–2308. https://doi.org/10.2175/106143009x407302.

(177) Świetlik, J.; Sikorska, E. Characterization of Natural Organic Matter Fractions by High Pressure Size-Exclusion Chromatography, Specific UV Absorbance and Total Luminescence Spectroscopy. *Polish J. Environ. Stud.* **2006**, *15* (1), 145–153.

(178) Aoki, S.; Fuse, Y.; Yamada, E. Determinations of Humic Substances and Other Dissolved Organic Matter and Their Effects on the Increase of COD in Lake Biwa. *Anal. Sci.* **2004**, *20* (1), 159–164. https://doi.org/10.2116/analsci.20.159.

(179) Korshin, G. V.; Benjamin, M. M.; Sletten, R. S. Adsorption of Natural Organic Matter (NOM) on Iron Oxide: Effects on NOM Composition and Formation of Organo-Halide Compounds during Chlorination. *Water Res.* **1997**, *31* (7), 1643–1650. https://doi.org/10.1016/S0043-1354(97)00007-9.

(180) Tak, S.; Vellanki, B. P. Natural Organic Matter as Precursor to Disinfection Byproducts and Its Removal Using Conventional and Advanced Processes: State of the Art Review. *J. Water Health* **2018**, *16* (5), 681–703. https://doi.org/10.2166/wh.2018.032.

(181) Terry, L. G.; Summers, R. S. Biodegradable Organic Matter and Rapid-Rate Biofilter Performance: A Review. *Water Res.* **2018**, *128*, 234–245. https://doi.org/10.1016/j.watres.2017.09.048.

(182) Toor, R.; Mohseni, M. UV-H2O2 Based AOP and Its Integration with Biological Activated Carbon Treatment for DBP Reduction in Drinking Water. *Chemosphere* **2007**, *66* (11), 2087–2095. https://doi.org/10.1016/j.chemosphere.2006.09.043.

(183) Sarathy, S. R.; Stefan, M. I.; Royce, A.; Mohseni, M. Pilot-Scale UV/H2O2 Advanced Oxidation Process for Surface Water Treatment and Downstream Biological Treatment: Effects on Natural Organic Matter Characteristics and DBP Formation Potential. *Environ. Technol.* **2011**, *32* (15), 1709–1718. https://doi.org/10.1080/09593330.2011.553843.

(184) Imai, A.; Fukushima, T.; Matsushige, K.; Kim, Y. H.; Choi, K. Characterization of Dissolved Organic Matter in Effluents from Wastewater Treatment Plants. *Water Res.* **2002**, *36* (4), 859–870. https://doi.org/10.1016/S0043-1354(01)00283-4.

(185) Shen, M.; Hai, X.; Shang, Y.; Zheng, C.; Li, P.; Li, Y.; Jin, W.; Li, D. Insights into Aggregation and Transport of Graphene Oxide in Aqueous and Saturated Porous Media : Complex Effects of Cations with Different Molecular Weight Fractionated Natural Organic Matter. *Sci. Total Environ.* **2019**, *656*, 843–851. https://doi.org/10.1016/j.scitotenv.2018.11.387.

(186) Munera-Echeverri, J. L.; Martinsen, V.; Strand, L. T.; Zivanovic, V.; Cornelissen, G.; Mulder, J. Cation Exchange Capacity of Biochar: An Urgent Method Modification. *Sci. Total Environ.* **2018**, *642*, 190–197. https://doi.org/10.1016/j.scitotenv.2018.06.017.

(187) Siriwardena, D. P.; James, R.; Dasu, K.; Thorn, J.; Iery, R. D.; Pala, F.; Schumitz, D.; Eastwood, S.; Burkitt, N. Regeneration of Per- and Polyfluoroalkyl Substance-Laden Granular Activated Carbon Using a Solvent Based Technology. *J. Environ. Manage.* **2021**, *289* (February), 112439. https://doi.org/10.1016/j.jenvman.2021.112439.

(188) Larasati, A.; Fowler, G. D.; Graham, N. J. D. Insights into Chemical Regeneration of Activated Carbon for Water Treatment. *J. Environ. Chem. Eng.* **2021**, *9* (4), 105555. https://doi.org/10.1016/j.jece.2021.105555.

(189) Cooney, D. O.; Nagerl, A.; Hines, A. L. Solvent Regeneration of Activated Carbon. *Water Res.* **1983**, *17* (4), 403–410. https://doi.org/10.1016/0043-1354(83)90136-7.

(190) Guo, D.; Shi, Q.; He, B.; Yuan, X. Different Solvents for the Regeneration of the Exhausted Activated Carbon Used in the Treatment of Coking Wastewater. *J. Hazard. Mater.* **2011**, *186* (2–3), 1788–1793. https://doi.org/10.1016/j.jhazmat.2010.12.068.

(191) Dutta, T.; Kim, T.; Vellingiri, K.; Tsang, D. C. W.; Shon, J. R.; Kim, K. H.; Kumar, S. Recycling and Regeneration of Carbonaceous and Porous Materials through Thermal or Solvent Treatment. *Chem. Eng. J.* **2019**, *364* (January), 514–529. https://doi.org/10.1016/j.cej.2019.01.049.

(192) Saeidi, N.; Harnisch, F.; Presser, V.; Kopinke, F. D.; Georgi, A. Electrosorption of Organic Compounds: State of the Art, Challenges, Performance, and Perspectives. *Chem. Eng. J.* **2023**, *471* (March), 144354. https://doi.org/10.1016/j.cej.2023.144354.

(193) Garcia-Rodriguez, O.; Villot, A.; Olvera-Vargas, H.; Gerente, C.; Andres, Y.; Lefebvre, O. Impact of the Saturation Level on the Electrochemical Regeneration of Activated Carbon in a Single Sequential Reactor. *Carbon N. Y.* **2020**, *163*, 265–275. https://doi.org/10.1016/j.carbon.2020.02.041.

(194) Zhou, W.; Meng, X.; Gao, J.; Zhao, H.; Zhao, G.; Ma, J. Electrochemical Regeneration of Carbon-Based Adsorbents: A Review of Regeneration Mechanisms, Reactors, and Future Prospects. *Chem. Eng. J. Adv.* **2021**, *5* (October 2020), 100083. https://doi.org/10.1016/j.ceja.2020.100083.

(195) Ersan, G.; Ersan, M. S.; Perreault, F.; Garcia-Segura, S. Enabling in Situ Electro-Regeneration Systems for PFOA-Laden Spent Activated Carbon Adsorbents Reuse. *J. Environ. Chem. Eng.* **2023**, *11* (6), 111369. https://doi.org/10.1016/j.jece.2023.111369.

(196) Saeidi, N.; Kopinke, F. D.; Georgi, A. Controlling Adsorption of Perfluoroalkyl Acids on Activated Carbon Felt by Means of Electrical Potentials. *Chem. Eng. J.* **2021**, *416* (February), 129070. https://doi.org/10.1016/j.cej.2021.129070.

(197) Román Santiago, A.; Baldaguez Medina, P.; Su, X. Electrochemical Remediation of Perfluoroalkyl Substances from Water. *Electrochim. Acta* **2022**, *403*. https://doi.org/10.1016/j.electacta.2021.139635.

(198) Román Santiago, A.; Yin, S.; Elbert, J.; Lee, J.; Shukla, D.; Su, X. Imparting Selective Fluorophilic Interactions in Redox Copolymers for the Electrochemically Mediated Capture of Short-Chain Perfluoroalkyl Substances. *J. Am. Chem. Soc.* **2023**, *145* (17), 9508–9519. https://doi.org/10.1021/jacs.2c10963.

(199) Verma, S.; Lee, T.; Sahle-Demessie, E.; Ateia, M.; Nadagouda, M. N. Recent Advances on PFAS Degradation via Thermal and Nonthermal Methods. *Chem. Eng. J. Adv.* **2023**, *13* (December 2022), 100421. https://doi.org/10.1016/j.ceja.2022.100421.

(200) Berenguer, R.; Marco-Lozar, J. P.; Quijada, C.; Cazorla-Amorós, D.; Morallón, E. Electrochemical Regeneration and Porosity Recovery of Phenol-Saturated Granular Activated Carbon in an Alkaline Medium. *Carbon N. Y.* **2010**, *48* (10), 2734–2745. https://doi.org/10.1016/j.carbon.2010.03.071.

(201) Arulrajan, A. C.; Ramasamy, D. L.; Sillanpää, M.; van der Wal, A.; Biesheuvel, P. M.; Porada, S.; Dykstra, J. E. Exceptional Water Desalination Performance with Anion-Selective Electrodes. *Adv. Mater.* **2019**, *31* (10), 1–5. https://doi.org/10.1002/adma.201806937.

(202) Kim, C.; Srimuk, P.; Lee, J.; Fleischmann, S.; Aslan, M.; Presser, V. Influence of Pore Structure and Cell Voltage of Activated Carbon Cloth as a Versatile Electrode Material for Capacitive Deionization. *Carbon N. Y.* **2017**, *122*, 329–335. https://doi.org/10.1016/j.carbon.2017.06.077.

(203) Mubita, T. M.; Porada, S.; Biesheuvel, P. M.; van der Wal, A.; Dykstra, J. E. Strategies to Increase Ion Selectivity in Electrodialysis. *Sep. Purif. Technol.* **2022**, *292* (January), 120944. https://doi.org/10.1016/j.seppur.2022.120944.

(204) Zhang, C.; He, D.; Ma, J.; Tang, W.; Waite, T. D. Faradaic Reactions in Capacitive Deionization (CDI) - Problems and Possibilities: A Review. *Water Res.* **2018**, *128*, 314–330. https://doi.org/10.1016/j.watres.2017.10.024.

(205) Zhao, R.; van Soestbergen, M.; Rijnaarts, H. H. M.; van der Wal, A.; Bazant, M. Z.; Biesheuvel, P. M. Time-Dependent Ion Selectivity in Capacitive Charging of Porous Electrodes. *J. Colloid Interface Sci.* **2012**, *384* (1), 38–44. https://doi.org/10.1016/j.jcis.2012.06.022.

(206) Appleman, T. D.; Higgins, C. P.; Quiñones, O.; Vanderford, B. J.; Kolstad, C.; Zeigler-Holady, J. C.; Dickenson, E. R. V. Treatment of Poly- and Perfluoroalkyl Substances in U.S. Full-Scale Water Treatment Systems. *Water Res.* **2014**, *51*, 246–255. https://doi.org/10.1016/j.watres.2013.10.067.

(207) McCleaf, P.; Stefansson, W.; Ahrens, L. Drinking Water Nanofiltration with Concentrate Foam Fractionation—A Novel Approach for Removal of per- and Polyfluoroalkyl Substances (PFAS). *Water Res.* **2023**, *232* (October 2022), 119688. https://doi.org/10.1016/j.watres.2023.119688.

(208) Baldaguez Medina, P.; Ardila Contreras, V.; Hartmann, F.; Schmitt, D.; Klimek, A.; Elbert, J.; Gallei, M.; Su, X. Investigating the Electrochemically Driven Capture and Release of Long-Chain PFAS by Redox Metallopolymer Sorbents. *ACS Appl. Mater. Interfaces* **2023**, *15* (18), 22112–22122. https://doi.org/10.1021/acsami.3c01670.

(209) Ellis, A. C.; Boyer, T. H.; Fang, Y.; Liu, C. J.; Strathmann, T. J. Life Cycle Assessment and Life Cycle Cost Analysis of Anion Exchange and Granular Activated Carbon Systems for Remediation of Groundwater Contaminated by Per- and Polyfluoroalkyl Substances (PFASs). *Water Res.* **2023**, *243* (July), 120324. https://doi.org/10.1016/j.watres.2023.120324.

(210) Smith, S. J.; Lewis, J.; Wiberg, K.; Wall, E.; Ahrens, L. Foam Fractionation for Removal of Per- and Polyfluoroalkyl Substances: Towards Closing the Mass Balance. *Sci. Total Environ.* **2023**, *871* (August 2022), 162050. https://doi.org/10.1016/j.scitotenv.2023.162050.

(211) Buckley, T.; Karanam, K.; Xu, X.; Shukla, P.; Firouzi, M.; Rudolph, V. Effect of Mono- and Di-Valent Cations on PFAS Removal from Water Using Foam Fractionation – A Modelling and Experimental Study. *Sep. Purif. Technol.* **2022**, *286* (January), 120508. https://doi.org/10.1016/j.seppur.2022.120508.

(212) Zhi, Y.; Zhao, X.; Shuai, A.; Jia, Y.; Cheng, X.; Lin, S.; Xiao, F.; Han, L.; Chai, H.; He, Q.; Liu, C. Enhancing Rejection of Short-Chain per- and Polyfluoroalkyl Substances by Tailoring the Surface Charge of Nanofiltration Membranes. *Water Res.* **2025**, *272* (November 2024), 122931. https://doi.org/10.1016/j.watres.2024.122931.

(213) Liu, Y. L.; Sun, M. Ion Exchange Removal and Resin Regeneration to Treat Per- and Polyfluoroalkyl Ether Acids and Other Emerging PFAS in Drinking Water. *Water Res.* **2021**, *207* (August), 117781. https://doi.org/10.1016/j.watres.2021.117781.

(214) Zeidabadi, F. A.; Esfahani, E. B.; McBeath, S. T.; Mohseni, M. Managing PFAS Exhausted Ion-Exchange Resins through Effective Regeneration/Electrochemical Process. *Water Res.* **2024**, *255* (November 2023), 121529. https://doi.org/10.1016/j.watres.2024.121529.

(215) Doornbusch, G. J.; Dykstra, J. E.; Biesheuvel, P. M.; Suss, M. E. Fluidized Bed Electrodes with High Carbon Loading for Water Desalination by Capacitive Deionization. *J. Mater. Chem. A* **2016**, *4* (10), 3642–3647. https://doi.org/10.1039/c5ta10316a.

(216) Borsje, C.; Sleutels, T.; Saakes, M.; Buisman, C. J. N.; ter Heijne, A. The Granular Capacitive Moving Bed Reactor for the Scale up of Bioanodes. *J. Chem. Technol. Biotechnol.* **2019**, *94* (8), 2738–2748. https://doi.org/10.1002/jctb.6091.

(217) Musegades, L. J.; Curtin, O. P.; Cyran, J. D. Determining the Surface PKa of Perfluorooctanoic Acid. *J. Phys. Chem. C* **2024**, *128* (5), 1946–1951. https://doi.org/10.1021/acs.jpcc.3c07235.

(218) Ateia, M.; Alsbaiee, A.; Karanfil, T.; Dichtel, W. Efficient PFAS Removal by Amine-Functionalized Sorbents: Critical Review of the Current Literature. *Environ. Sci. Technol. Lett.* **2019**, *6* (12), 688–695. https://doi.org/10.1021/acs.estlett.9b00659.

(219) Sudo, Y.; Misic, D. M.; Suzuki, M. Concentration Dependence of Effective Surface Diffusion Coefficient in Aqueous Phase Adsorption on Activated Carbon. *Chem. Eng. Sci.* **1978**, *33* (9), 1287–1290. https://doi.org/10.1016/0009-2509(78)85097-0.

(220) Wang, W.; Mi, X.; Zhou, Z.; Zhou, S.; Li, C.; Hu, X.; Qi, D.; Deng, S. Novel Insights into the Competitive Adsorption Behavior and Mechanism of Per- and Polyfluoroalkyl Substances on the Anion-Exchange Resin. *J. Colloid Interface Sci.* **2019**, *557*, 655–663. https://doi.org/10.1016/j.jcis.2019.09.066.

(221) Umeh, A. C.; Hassan, M.; Egbuatu, M.; Zeng, Z.; Al Amin, M.; Samarasinghe, C.; Naidu, R. Multicomponent PFAS Sorption and Desorption in Common Commercial Adsorbents: Kinetics, Isotherm, Adsorbent Dose, PH, and Index Ion and Ionic Strength Effects. *Sci. Total Environ.* **2023**, *904* (June), 166568. https://doi.org/10.1016/j.scitotenv.2023.166568.

(222) Singh, M.; Hakimabadi, S. G.; Van Geel, P. J.; Carey, G. R.; Pham, A. L. T. Modified Competitive Langmuir Model for Prediction of Multispecies PFAS Competitive Adsorption Equilibria on Colloidal Activated Carbon. *Sep. Purif. Technol.* **2024**, *345* (April), 127368. https://doi.org/10.1016/j.seppur.2024.127368.

(223) Aumeier, B. M.; Georgi, A.; Saeidi, N.; Sigmund, G. Is Sorption Technology Fit for the Removal of Persistent and Mobile Organic Contaminants from Water? *Sci. Total Environ.* **2023**, *880* (April), 163343. https://doi.org/10.1016/j.scitotenv.2023.163343.

(224) Li, L.; Quinlivan, P. A.; Knappe, D. R. U. Effects of Activated Carbon Surface Chemistry and Pore Structure on the Adsorption of MTBE from Natural Water. *ACS Div. Environ. Chem. Prepr.* **2001**, *41* (2), 448–453.

(225) Kim, G.; Mengesha, D. N.; Choi, Y. Adsorption Dynamics of Per- and Polyfluoroalkyl Substances (PFAS) on Activated Carbon: Interplay of Surface Chemistry and PFAS Structural Properties. *Sep. Purif. Technol.* **2024**, *349* (May), 127851. https://doi.org/10.1016/j.seppur.2024.127851.

(226) Schönherr, J.; Buchheim, J.; Scholz, P.; Adelhelm, P. Boehm Titration Revisited (Part I): Practical Aspects for Achieving a High Precision in Quantifying Oxygen-Containing Surface Groups on Carbon Materials. *C* **2018**, *4* (2), 21. https://doi.org/10.3390/c4020021.

(227) Dixit, F.; Barbeau, B.; Mostafavi, S. G.; Mohseni, M. PFOA and PFOS Removal by Ion Exchange for Water Reuse and Drinking Applications: Role of Organic Matter Characteristics. *Environ. Sci. Water Res. Technol.* **2019**, *5* (10), 1782–1795. https://doi.org/10.1039/c9ew00409b.

(228) Inglezakis, V. J.; Zorpas, A. A. Heat of Adsorption, Adsorption Energy and Activation Energy in Adsorption and Ion Exchange Systems. *Desalin. Water Treat.* **2012**, *39* (1–3), 149–157. https://doi.org/10.1080/19443994.2012.669169.

(229) Ore, A.; Sigmund, G.; Specker, J.; Helmus, R.; Aguilar-Alarcón, P.; Schriks, M.; van Wezel, A. P.; Sutton, N. B. Removal, Transport, and Transformation of Organic Micropollutants in Managed Aquifer Recharge: Insights from Target and Non-Target Analyses. *Water Res.* **2025**, *287* (August). https://doi.org/10.1016/j.watres.2025.124409.

(230) Abdelrady, A.; Sharma, S.; Sefelnasr, A.; Kennedy, M. The Fate of Dissolved Organic Matter (DOM) during Bank Filtration under Different Environmental Conditions: Batch and Column Studies. *Water (Switzerland)* **2018**, *10* (12). https://doi.org/10.3390/w10121730.

(231) Zhang, Y.; Zhao, X.; Zhang, X.; Peng, S. A Review of Different Drinking Water Treatments for Natural Organic Matter Removal. *Water Sci. Technol. Water Supply* **2015**, *15* (3), 442–455. https://doi.org/10.2166/ws.2015.011.

(232) Liu, Z.; Peldszus, S.; Sauvé, S.; Barbeau, B. Enhanced Removal of Trace-Level per- and Polyfluoroalkyl Substances (PFAS) from Drinking Water Using Granular Activated Carbon (GAC): The Role of Ozonation. *Chemosphere* **2024**, *368* (August). https://doi.org/10.1016/j.chemosphere.2024.143758.

(233) Yavich, A. A.; Lee, K. H.; Chen, K. C.; Pape, L.; Masten, S. J. Evaluation of Biodegradability of NOM after Ozonation. *Water Res.* **2004**, *38* (12), 2839–2846. https://doi.org/10.1016/j.watres.2004.03.040.

(234) Tajdini, B.; Vatankhah, H.; Murray, C. C.; Liethen, A.; Bellona, C. Impact of Effluent Organic Matter on Perfluoroalkyl Acid Removal from Wastewater Effluent by Granular Activated Carbon and Alternative Adsorbents. *Water Res.* **2023**, *241* (May), 120105. https://doi.org/10.1016/j.watres.2023.120105.

(235) Von Gunten, U. Ozonation of Drinking Water: Part II. Disinfection and by-Product Formation in Presence of Bromide, Iodide or Chlorine. *Water Res.* **2003**, *37* (7), 1469–1487. https://doi.org/10.1016/S0043-1354(02)00458-X.

(236) Zhang, D. Y.; Li, W. G.; Zhang, S. M.; Liu, M.; Zhao, X. Y.; Zhang, X. C. Bacterial Community and Function of Biological Activated Carbon Filter in Drinking Water Treatment. *Biomed. Environ. Sci.* **2011**, *24* (2), 122–131. https://doi.org/10.3967/0895-3988.2011.02.006.

(237) Robertson, M.; Lamb, B.; Griffin, A.; He, L.; Ma, B.; Qiang, Z. Critical Role of Pore Size on Perfluorooctanoic Acid Adsorption Behaviors in Carbonaceous Sorbents. *Mater. Horizons* **2025**, *12* (9), 2935–2944. https://doi.org/10.1039/d4mh01771d.

(238) Sylvester, P. J.; Jackson, S. E. A Brief History of Laser Ablation Inductively Coupled Plasma Mass Spectrometry (LA-ICP-MS). *Elements* **2016**, *12* (5), 307–310. https://doi.org/10.2113/gselements.12.5.307.

(239) O'Connor, J.; Bolan, N. S.; Kumar, M.; Nitai, A. S.; Ahmed, M. B.; Bolan, S. S.; Vithanage, M.; Rinklebe, J.; Mukhopadhyay, R.; Srivastava, P.; Sarkar, B.; Bhatnagar, A.; Wang, H.; Siddique, K. H. M.; Kirkham, M. B. Distribution, Transformation and Remediation of Poly- and per-Fluoroalkyl Substances (PFAS) in Wastewater Sources. *Process Saf. Environ. Prot.* **2022**, *164* (June), 91–108. https://doi.org/10.1016/j.psep.2022.06.002.

(240) Baghoth, S. A.; Maeng, S. K.; Salinas Rodríguez, S. G.; Ronteltap, M.; Sharma, S.; Kennedy, M.; Amy, G. L. An Urban Water Cycle Perspective of Natural Organic Matter (NOM): NOM in Drinking Water, Wastewater Effluent, Storm Water, and Seawater. *Water Sci. Technol. Water Supply* **2008**, *8* (6), 701–707. https://doi.org/10.2166/ws.2008.146.

(241) Xue, C.; Yu, Y.; Huang, X. Comparison of Organic Matter Properties and Disinfection By-Product Formation between the Typical Groundwater and Surface Water. *Water (Switzerland)* **2022**, *14* (9). https://doi.org/10.3390/w14091418.

(242) Huang, M. H.; Li, Y. M.; Gu, G. W. Chemical Composition of Organic Matters in Domestic Wastewater. *Desalination* **2010**, *262* (1–3), 36–42. https://doi.org/10.1016/j.desal.2010.05.037.

(243) Hu, H.; Ma, H.; Ding, L.; Geng, J.; Xu, K.; Huang, H.; Zhang, Y.; Ren, H. Concentration, Composition, Bioavailability, and N-Nitrosodimethylamine Formation Potential of Particulate and Dissolved Organic Nitrogen in Wastewater Effluents: A Comparative Study. *Sci. Total Environ.* **2016**, *569–570*, 1359–1368. https://doi.org/10.1016/j.scitotenv.2016.06.218.

(244) Ziayad, A.; Alazaiza, M. Y. D.; Mohammed, B. J. K. An Overview of Per- and Polyfluoroalkyl Substances (PFAS) in the Environment: Source, Fate, Risk and Regulations. *Water* **2020**, 1–28. https://doi.org/10.3390/w12123590.

(245) Coggan, T. L.; Moodie, D.; Kolobaric, A.; Szabo, D.; Shimeta, J.; Crosbie, N. D.; Lee, E.; Fernandes, M.; Clarke, B. O. An Investigation into Per- and Polyfluoroalkyl Substances (PFAS) in Nineteen Australian Wastewater Treatment Plants (WWTPs). *Heliyon* **2019**, *5* (8), e02316. https://doi.org/10.1016/j.heliyon.2019.e02316.

(246) H.R. Branco, R.; Meulepas, R. J. W.; van Veelen, H. P. J.; Rijnaarts, H. H. M.; Sutton, N. B. Influence of Redox Condition and Inoculum on Micropollutant Biodegradation by Soil and Activated Sludge Communities. *Sci. Total Environ.* **2023**, *897* (April), 165233. https://doi.org/10.1016/j.scitotenv.2023.165233.

(247) Luo, Y.; Atashgahi, S.; Rijnaarts, H. H. M.; Comans, R. N. J.; Sutton, N. B. Influence of Different Redox Conditions and Dissolved Organic Matter on Pesticide Biodegradation in Simulated Groundwater Systems. *Sci. Total Environ.* **2019**, *677*, 692–699. https://doi.org/10.1016/j.scitotenv.2019.04.128.

(248) Radjenovic, J.; Duinslaeger, N.; Avval, S. S.; Chaplin, B. P. Facing the Challenge of Poly- And Perfluoroalkyl Substances in Water: Is Electrochemical Oxidation the Answer? *Environ. Sci. Technol.* **2020**, *54* (23), 14815–14829. https://doi.org/10.1021/acs.est.0c06212.

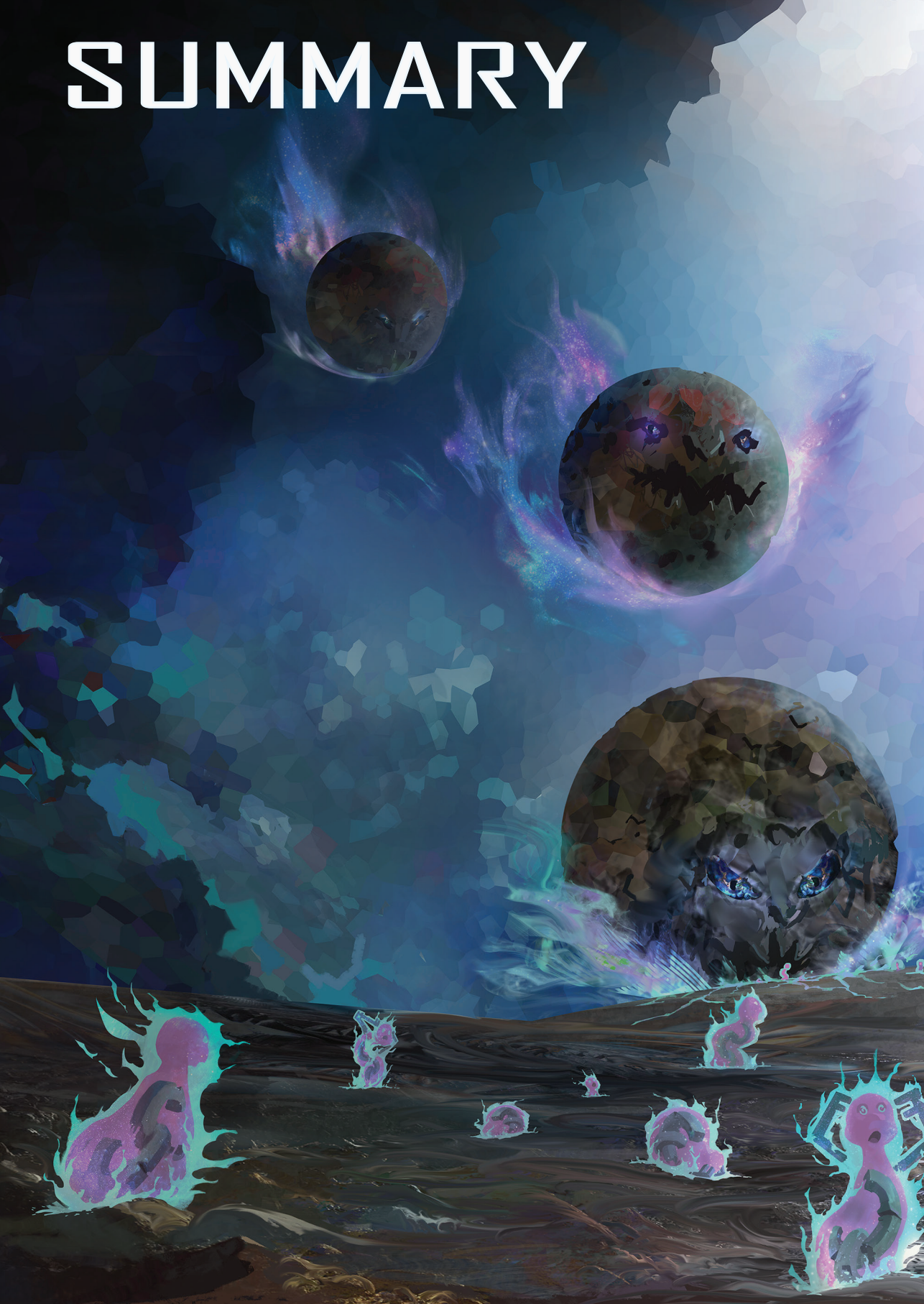
(249) Smith, S. J.; Wiberg, K.; McCleaf, P.; Ahrens, L. Pilot-Scale Continuous Foam Fractionation for the Removal of Per- and Polyfluoroalkyl Substances (PFAS) from Landfill Leachate. *ACS ES T Water* **2022**, *2* (5), 841–851. https://doi.org/10.1021/ACSESTWATER.2C00032.

(250) Shields, E. P.; Krug, J. D.; Roberson, W. R.; Jackson, S. R.; Smeltz, M. G.; Allen, M. R.; Burnette, R. P.; Nash, J. T.; Virtaranta, L.; Preston, W.; Liberatore, H. K.; Wallace, M. A. G.; Ryan, J. V.; Kariher, P. H.; Lemieux, P. M.; Linak, W. P. Pilot-Scale Thermal Destruction of Per- and Polyfluoroalkyl Substances in a Legacy Aqueous Film Forming Foam. *ACS ES T Eng.* **2023**, *3* (9), 1308–1317. https://doi.org/10.1021/acsestengg.3c00098.

(251) Liu, C.; Chu, J.; Cápiro, N. L.; Fortner, J. D.; Pennell, K. D. In-Situ Sequestration of Perfluoroalkyl Substances Using Polymer-Stabilized Ion Exchange Resin. *J. Hazard. Mater.* **2022**, *422* (May 2021). https://doi.org/10.1016/j.jhazmat.2021.126960.

(252) Li, D.; Lee, C. S.; Zhang, Y.; Das, R.; Akter, F.; Venkatesan, A. K.; Hsiao, B. S. Efficient Removal of Short-Chain and Long-Chain PFAS by Cationic Nanocellulose. *J. Mater. Chem. A* **2023**, *11* (18), 9868–9883. https://doi.org/10.1039/d3ta01851b.

SUMMARY



Summary

The removal of per- and polyfluoroalkyl substances (PFAS) by activated carbon (AC) and the regeneration of AC under conditions relevant for drinking water treatment were investigated in this PhD Thesis. The work was motivated by increasingly stringent regulatory limits for PFAS in drinking water, the growing relevance of short-chain PFAS, and the low removal of PFAS by granular activated carbon (GAC) filters operated at trace concentrations. By combining systematic batch experiments, mechanistic modelling, and regeneration studies, this Thesis provides a coherent framework to understand why PFAS adsorption is fundamentally limited at ng/L levels and how these limitations can be mitigated in practice.

A central finding of this Thesis is that PFAS adsorption on AC behaves fundamentally differently at environmentally relevant concentrations than at the elevated concentrations that dominate the scientific literature. Adsorption isotherm parameters were shown to depend strongly on the initial PFAS concentration used to reach equilibrium. Isotherms derived at µg/L–mg/L levels substantially overestimate adsorption capacity at ng/L concentrations, primarily because high concentrations promote cooperative adsorption phenomena such as aggregation and multilayer formation that are suppressed at trace levels. As a result, adsorption data obtained at high concentrations cannot be directly extrapolated to predict GAC performance in drinking water treatment.

PFAS adsorption kinetics were inherently slow under conditions relevant to drinking-water treatment. Intraparticle transport was shown to be governed predominantly by surface diffusion rather than pore diffusion, with surface diffusion coefficients decreasing when more adsorption sites are available, at lower PFAS concentrations, and in carbons with higher mesopore volume. As a consequence of surface diffusion controlling PFAS intraparticle transport, long equilibration times are required in batch systems and long empty bed contact times are required in column systems to achieve high PFAS removal.

Competitive adsorption between different PFAS was identified as a key mechanism controlling PFAS removal in GAC systems. Long-chain PFAS consistently outcompete short-chain PFAS due to stronger hydrophobic interactions, and in some cases, desorption of short-chain PFAS. This competition occurs both dynamically, due to differences in adsorption kinetics, and at equilibrium under conditions of limited adsorption space.

The role of AC properties was clarified by decoupling pore size distribution, surface chemistry, and transport effects. A higher micropore surface area did not result in increased PFAS adsorption. Instead, mesopores dominate PFAS adsorption because slow intraparticle transport prevents effective utilization of micropores. Carbons with high mesopore volume were identified as most effective for PFAS removal. Surface charge further influences adsorption:

carbons with a low concentration of acidic surface groups or a net positive surface charge exhibit enhanced PFAS adsorption, particularly for short-chain compounds.

Natural organic matter (NOM) was identified as the dominant external factor limiting PFAS adsorption in water matrices often found in drinking water treatment. NOM reduced PFAS adsorption capacity by at least an order of magnitude, with low-molecular-weight NOM fractions identified as the most competitive species. These findings explain the rapid PFAS breakthrough observed in GAC filters and demonstrate that effective PFAS removal cannot be achieved by GAC alone without addressing NOM competition.

Temperature effects further limited PFAS removal. Increasing temperature reduced adsorption of short-chain PFAS, reflecting a lower affinity of these compounds for activated carbon at higher temperatures, whereas adsorption of long-chain PFAS was largely temperature-independent. As a result, short-chain PFAS removal performance may vary seasonally, which should be considered in treatment system design.

To translate these mechanistic insights into practice, this Thesis evaluated strategies to improve PFAS removal and reduce operational costs of drinking water treatment. The results indicate that selecting GACs with high mesopore volume and favourable surface charge, removing competing NOM through biological treatment or combined O_3–BAC processes, and applying predictive modelling frameworks that explicitly account for adsorption site competition and surface-diffusion-limited transport are the most promising near-term approaches.

Finally, this Thesis explored electroregeneration as a potential alternative to frequent thermal reactivation of GAC filters. Electroregeneration was shown to preferentially desorb short-chain PFAS and concentrate them into a smaller volume, demonstrating its potential to extend filter lifetime and reduce the environmental footprint of PFAS removal. While further development is required before full-scale implementation, these results provide a proof of concept for a more sustainable regeneration strategy.

In conclusion, this Thesis demonstrates that PFAS removal by activated carbon at drinking-water concentrations operates at the limits of adsorption. Low influent concentrations, slow intraparticle transport, strong competition from NOM and co-occurring PFAS, and temperature effects collectively limit adsorption performance. By identifying these limitations and linking these to measurable material properties and operating conditions, this work provides a mechanistic basis for improving PFAS treatment design, modelling, and regeneration of activated carbon filters, while clearly defining the conditions under which activated carbon can, and cannot, adsorb PFAS effectively.

ACKNOWLEDGMENTS



to all my friends,

about the cover,

and about me

Acknowledgments

While this section is called *Acknowledgments*, as I sit down to write them, I find myself doing something slightly different. Rather than simply listing the things people should be thanked for, I allowed my mind to wander and put my thoughts on paper. Sometimes those thoughts are achievements or acts of kindness that deserve recognition, but often they are memories, impressions, and reflections on the people who have shaped my PhD journey, and how I see them.

I will write about people more or less in the chronological order in which I met them.

Dear **Father and Mother**. Everything that I am today is because of how you raised me. While I hate many things about myself, I can also say that I am proud of who I have become. For that, I am deeply grateful to you.

Dear **Maarten,** I believe you are the most intelligent person mentioned here, and I think you would agree. It is safe to say that you are the person most responsible for me coming to Wetsus and, later, starting a PhD at Wageningen. I remember writing quite an elaborate email as a Master's student, asking for an internship at Wetsus and sending it to you, thinking there was perhaps a 1% chance that you would respond. To my surprise, only a few minutes later you replied, said that I could come, and put me in contact with Slawek. After my internship finished, you sent several emails, contacted people, and in the end found a PhD position for me. It has always been a pleasure to work with you. You taught me a great deal: how to treat data properly, how to present it clearly, and that, no matter what, simplicity is something worth pursuing in science.

Dear **Slawek,** I feel like we are very similar. Perhaps it is our Slavic ancestry, or perhaps it is because we both enjoy spending time in the lab. During my year at Wetsus, you trusted me with experiments. You allowed me to make mistakes, learn from them, and gave me enough freedom to try new things. At the same time, you knew how much was needed to get the work done and when it was time to stop. As someone who rarely stops and often thinks results are not good enough, that balance made me very productive. You were never a boss to me. Coming from a country where the opposite is often the norm, you were a breath of fresh air. While I always knew that I wanted to do science, that feeling came largely from how I was raised, and I saw it as something I was supposed to do. Your attitude, supervision, and personality ultimately made me realize that I genuinely love science, and that I do not have to pursue it simply because it is something I am good at.

Dear **Max,** You are my oldest friend. You are incredibly kind. As I write these words and think about you, I cannot help but get teary-eyed. There were several times during the last six years of my stay in The Netherlands when I felt alone, when I felt like I just wanted to

run away somewhere. But you were always there to talk to, to calm me down, and to make sure that everything was alright. I remember one year being stuck alone in my room during New Year's Eve, thinking that life should not be like this. You called me, we talked for quite some time, and ever since then, every year, you have made sure that I am doing well at that time and not alone. You were the one who introduced me to the wonderful world of Dungeons & Dragons, and we spent several years playing together, with many more wonderful years still to come.

Dear **Wybren**, or, as I like to describe you to other people, my hot Dutch friend, you have been part of my life for a very long time. We started our internship together, and even after it ended, you kept in touch. You have no idea how much that means to me. You always make an effort to organize things for us to do, and our monthly video game sessions never fail to leave me in laughter. Your enthusiasm, humour, and perspective on life always put me in a positive state of mind. Somehow, you also always seem to end up in some kind of funny trouble. Because of that, I have to say that, out of everyone mentioned here, you are by far the most exciting person to be around. For better or worse :D.

Dear **Wanda**, you have no idea how fascinating it was to be around you. I always felt like your mind was a painting by Van Gogh mixed with stories written by Lovecraft. Because of you, I realized how much I enjoy being around expressive people, people who are not afraid to show what is on their minds and share the world as they see it. Thank you for all the years we spent together at FKIT. From the bottom of my heart, I wish you happiness, purpose, and fulfilment in whatever path you choose.

Dear **Antony**, it is impossible to forget all the time we spent in the lab, with our setups next to each other, discussing how to run experiments and often complaining about why our setups were not working the way they should. You really made those days memorable, and somewhere along the way we became close friends. Thank you for introducing me to Indian culture, and I must admit that the best chicken biryani I have ever had was the one you made, and that is coming from someone who actually went to India!

Dear **Sam,** you have really grown on me over the years, and I am starting to appreciate and enjoy your attitude more and more. You were the first truly Dutch person I interacted with, and I will let you decide what exactly that means. You get things done. My favorite memory with you was during our trip to India for Anthony's wedding. While I was half sick, wandering through the rainy, monsoon-soaked streets of Chennai, lost, frustrated, and unable to find our hotel, you somehow managed to find me and save me from the random sinkholes scattered throughout the streets.

Dear **Kestral**, I have always thought of you as a happy and lovely person. Somehow, you always manage to laugh regardless of the situation. Thank you for making my time in the

lab during my internship so enjoyable, and later for bringing Kikko to visit me from time to time. Our adventures in India, surviving the traffic, elephants, pineapples, and everything else that came our way, are something I will never forget.

Dear **Kikko**, thank you for taking such good care of Sam and Kestral. Please continue being a good boy.

Dear **Sebastian,** it is never boring to be around you. You are very confident, and you are not afraid to show it. Thank you for sharing the India trip with me and for helping me survive Indian pineapples. Out of all the people I know, you would easily win the prize for falling asleep the fastest in the most random places.

My dear **Jouke,** my dear supervisor, when I think about who you are and the impact you have had on me, the first thing that comes to mind is that you genuinely cared. You cared about me as a person. You cared that I felt well, that I grew into a good scientist, and you helped shape me into one. We had many deep discussions, not only about research, but also about life, the future, and the things that mattered to me. You really cared, and I always felt that. Thank you for trusting me with so many things in the lab, for guiding me, and for helping me with models, writing, and countless other challenges along the way. You were always there to help me get back on my feet when things were not going well and to remind me that I should be proud of my achievements. Your door was always open to me and whatever problems I happened to bring with me. Thank you for being tough when I desperately needed it and kind when I needed that as well. Thank you for giving me this PhD even after I initially declined it, and for helping me decide what to do after. You have been exactly the kind of supervisor I needed, and for that I am deeply grateful.

Dear **Bert**, I very much appreciate all the feedback you have given me throughout my PhD. You have an exceptional ability to quickly recognize what needs to be done and communicate it clearly and directly. Your comments were always sharp, precise, and to the point. Thank you for being my Promotor and all the support you provided along the way. I hope we can stay in touch and continue working together in the future.

Dear **Laura**, you were the first person from ETE that I met. In many ways, the path you took before me helped shape the path my own PhD would follow. You taught me how to perform adsorption experiments, and you introduced me to the Micropollutant group, which became a major part of both my social life at ETE. During my first year, you were always there whenever I had a question related to adsorption, and even after you left, you remained approachable and willing to discuss research problems and new ideas. Thank you for your kindness and for helping me navigate the many questions and challenges I encountered along the way.

Dear **Liesbeth**, I always found you very approachable. I come from a culture where secretaries are often the people who have to deal with everyone else's stress and problems, and as a result are usually quite stressed themselves. It was therefore a breath of fresh air to have someone like you to turn to whenever I had an administrative problem. Thank you for dealing with mine, and the problems of many other PhD students, in such a friendly and welcoming manner.

Dear **Selin**, you really were the first friend I made at ETE. You are incredibly fun to be around, and I feel like we have so many things in common, from having the same supervisor and favourite song to having to deal with Jorn. It is difficult to choose a favourite memory, as there are so many, but the one that stands out the most is our trip to Utrecht, which started with the pursuit of a suit and somehow ended in a Belgian church. Thank you for all the memories, and I hope many more are still to come.

Dear **Livio**, without you, I probably would not have been able to spend so much time doing my favourite thing: spending my supervisor's money! Thank you for developing the PFAS method with me, and for all the times you helped solve problems with measurements, instruments, and everything in between. The thing I admire most about you is how deeply you care about the things you love and how unafraid you are to show it. I t makes you genuine, and I honestly think the world would be a better place if more people were like that.

Dear **Jill,** it was a pleasure to have you as an office mate for a while and to organize the PhD trip together. Thank you for giving me the banana plant. Unfortunately, it died. If you ever find another one to give away, I promise that this one will grow to at least two meters tall.

Dear **Pradip**, thank you for entrusting your plant to me after you left our office. I am happy to say that it is still doing well, and I will carry it with me wherever I go.

Dear **Alessia**, my dear Paranimph. I really admire your problem-solving approach to life. You are one of those rare people who can look at a situation, clearly understand what is happening, and immediately see a way forward. More than once, when a problem appeared and I was already panicking and preparing for some radical solution, you were the person who calmed me down and helped me figure out what actually needed to be done. Without you, I would never have found the courage to tell Ele that I liked her, and without you all those lunches would have felt much emptier. My favourite memory is from the PhD trip to Sweden and Denmark, when I was busy texting my future girlfriend and paying absolutely no attention to the world around me as we walked through the streets of Stockholm. Meanwhile, you were guiding me under the hand, making sure I did not walk into a streetlight or end up under a car. Thank you for all your guidance, and thank you for always being so easy-going and comfortable to talk to. With you, I could share problems, hopes, dreams, and plans for the future without hesitation. You were, by far, the calmest part of my PhD journey.

Dear **Zhaolu**, you are the most adorable person at ETE. You are kind, warm, and bring a positive energy that somehow manages to lift the mood of an entire room. That is probably why I so often find myself ending up in your office, just to chat for a few minutes (and steal Anran's food). I have greatly enjoyed all of our conversations, whether they were shared over bubble tea or regular tea. We started our PhDs together, and because of that, the memories we created hold a special place in my mind. The conferences and trips we shared, the problems we faced in the lab and outside of it, all of those moments are memories that I treasure. By far, you are my favourite person to have lunch or dinner with, mostly because you often cannot finish your meal, which means there is more food for me. Thank you for being such an amazing friend.

Dear **Alladin**, you are a very kind and intelligent person. Like, seriously. You are also a great artist. You make beautiful figures, and you even drew a beautiful tree for me. I like trees. Thank you for all the times we played tennis together. I enjoyed it very much, and I hope we can play many more matches in the future. You were one of the first friends I made at ETE. I am sorry that I could not be your paranymph during your defence, but the fact that you asked me means a great deal to me. Thank you

Dear **John**, I deeply regret that I was not able to finish my PhD in time for you to be there. You were the first person I asked to be my paranymph, and that was because you were the first colleague I truly and completely trusted. I shared my secrets, hopes, and wishes with you. I always felt that we were very similar in what we wanted to get out of life, and in the way we find fulfilment by taking care of the people who matter to us. There are so many good memories that we shared, but my favourite one is still the evening I came to your room for dinner. You were terribly hungover, and I asked you to have a drink with me because I had something important to tell you. Of course, you wanted absolutely nothing to do with alcohol at that moment, but as soon as I told you that I liked a certain someone, you simply said, "Okei Marko, we drink." That is a memory I will always treasure.

Dear **Yue**, while it has been a while since I last saw or spoke to you, I remember you as someone calm, kind, and always wanting to make the people around you happy. The football game I played with you was my first in ten years, and, strangely enough, I have not played another one since. Because of that, I do not think I will ever forget that moment. For a brief time, it felt like being a kid again. Thank you for helping me choose my Chinese name.

Dear **Chang**, you were always working hard and staying late in the office. You had many students, and all of them seemed to enjoy working with you. You were cheerful, but also never afraid to complain about the latest problems in the lab. I always enjoyed stopping by your office and simply listening to you talk. It was somehow both entertaining and reassuring. I do miss that.

Dear **Hooman**, when I think of you, the first word that comes to mind is an calm man. I enjoyed all the volleyball games and beers we shared together. In fact, I am pretty sure I still owe you a beer or two.

Dear **Rikke**, you remind me of an overpowered character from a fantasy novel, the kind of character who somehow succeeds at everything they attempt. In your case, I imagine that character would be a bard who dabbles in magic, or rather science, and ends up becoming far more powerful than anyone expected. Thank you for using your bardic skills to create several of the graphics that can be found in this thesis. I always enjoy playing DnD with you. Your characters have a unique charm and personality that make them memorable long after the session is over. I hope we end up sharing many more sessions together in the future.

Dear **Joao**, you were only in my office only for few months, but in those few months I felt like I had gained a lifelong friend. I enjoyed talking with you about the past and the future, and I greatly enjoyed the drinks we shared together at The Desire. Even though you are now an entire continent away, I still look forward to our monthly chats. Thank you for visiting me in Utrecht, and I promise that one day I will come and visit you in Brazil.

Dear **Micropollutant** people, Alessia, Anne, Chenxiao, Claudia, Gabriel, Han, Jill, Marija, Merel, Nena, Nikoline, Nora, Reiner, Selina, Shuhao, Silvana, Stefan, Thomas, and Zhaolu, and all the other people who were part of this group during my PhD, thank you for making every second Monday more enjoyable with your problems. Seriously, I always found our meetings surprisingly enjoyable. There was something very satisfying about listening to each other's struggles and trying to find solutions together. Because of all of you, I learned a great deal, both scientifically and personally, and you made me feel much more like I belonged at ETE. We attended four conferences together, three Micropols and one SETAC. Traveling with you, exploring new places, and sharing those experiences was a lot of fun. Thank you for all the discussions, ideas, and memories.

Dear **Nora**, thank you for creating the OMP group. It was the place at ETE where I felt the closest connection to my research.

Dear **Jinsong**, you are a very cheerful and warm person, and that is why I enjoy your company a lot. I also feel that we share many of the same struggles, both in science and in figuring out what the future holds for us. Thank you for helping me during the start of my PhD with adsorption. I will always appreciate your kindness.

Dear **Koen**, our adventures in Portugal holds a special place in my heart. I will never forget watching the sunset over the port of Porto, our port wine experience, the oversized Portuguese sandwiches, and, of course, the seagull sandwich. Those memories still make me

smile. I am also looking forward to sharing many more ice creams at Ciccuto together in the future.

Dear **Thomas**, your sense of humour is definitely unfiltered. That said, it never fails to make me smile. Thank you for helping me with writing my Rubicon proposal. One memory that I will never forget is our fishing trip. Even though we did not catch anything, it was the first time I had gone fishing since I was a kid, and that alone made it special.

Dear **Dainis**, I have always found you to be a very kind person, someone who genuinely cares about their PhD students and makes sure they feel supported. Thank you for bringing that spirit to ETE. I hope we get to share many more beers together in the future.

Dear **Betty**, thank you for tolerating my chaos in the lab and for all your help with the LC-MS. Thank you for always offering me food when I was starving, and for bringing those amazing crickets. They taste great.

Dear **Doortje**, thank you for often snuggling with me in bed. Even though I am fully aware that you only care about me because I feed you, I forgive you for that because you are simply too adorable.

Dear **Ine**, thank you for trusting me with your room and your cat. The last five years in Wageningen have been pleasant and quiet, and over that time I have grown very fond of your place.

Dear **Sha**, your sense of humor is truly out of this world, and words alone are not enough to describe it. Thank you for helping me choose my Chinese name, and thank you for welcoming me into the Chinese community. The dinners at your place were always amazing. Just thinking about them makes me hungry. I still hope to have that hot pot again someday!

Dear **Weishan**, there are many memories that I will treasure, but the one that stands above all the others is our Chinese New Year dinner. It was followed by me discovering that you can play the guitar remarkably well, and you discovering that I should probably be forbidden from singing. I am always looking forward to our Friday table tennis games, and I hope we will play many more matches together in the future.

Dear **Xiao Fang**, it is incredibly easy to talk to you. It does not matter whether it is about problems, work, something funny, or something completely random. Conversations with you always seem to flow naturally. You really have my kind of humor: authentic, direct, and never afraid to call people out or make fun of them in a wholesome way. I enjoyed sharing paranymph duties with you during Minh's defense, and I always enjoyed our conversations

about life and the future over bubble tea. If one day I can have even 10% of the confidence that you possess, I think I would be unstoppable. You are truly amazing.

Dear **Minh,** with you, I truly gained a lifelong friend. I could probably spend two pages writing about all the good memories we shared, but you already did that in your thesis, so instead I will focus on what happened after you returned to Vietnam. I struggled when you left. A good friend had moved to the other side of the world. Yet, despite the distance, you were always there whenever I needed someone to talk to. It was therefore very special to visit you in Vietnam. Experiencing Vietnam with you was unforgettable. All the food, the pho, bánh mì, amazing desserts, and spring rolls. By far, Vietnamese cuisine is my favourite. The crazy Vietnamese streets, the questionable karaoke bars, the beautiful nature, mountains, and fields, and the sweaty 40°C weather. The beautiful streets of Hanoi, named after the things that were once sold there. Watching the Mekong Delta from a skyscraper while rain poured down from the sky. All of those memories, experienced together with you, have a special place in my heart. I will visit again. Many more times.

Dear **Marko**, around this time, I also got to know you. The first thing I really liked about you was how much you try to take care of the people around you, even though you sometimes forget to take care of yourself. So please do not forget to do that, because you cannot take care of others if you do not take care of yourself first. I know how afraid you are of standing in front of others and being the centre of attention, but trust me, you are doing great. I can see the sense of achievement you feel when your words reach other people. Remember to relax in those moments. Nothing bad is going to happen. Finally, I really hope your biggest dream in life comes true: to plant a tree and then spend the next fifty years watching it grow. And if it does not, that is fine too. We are all built upon the foundations of dreams that never came true. They shaped who we are, just as much as the dreams we achieved. Be proud of yourself.

Dear **Elizabeth**, as you know, you are my favorite player to DM. I feel like you have a wonderfully vivid imagination, and in that way I feel very close to you. The more I think about it, the more I realize how many similarities we share, both in the challenges we face in life and in the people we aspire to become. I am incredibly happy that you ended up in my office. You brought the best smells (after Yulian, of course) with your teas and delicious noodles. Thank you for always taking care of and watering my plants whenever I was away. Thank you for all the walks we shared, talking about the future, our hopes, and our wishes. Thank you for the delicious dinners, the conversations, and the laughter. I know that in you I have found a friend for life, and I hope we will share many more adventures, both at the table and beyond.

Dear **Milan**, thank you for being hot.

To the random reader who found this, while there are millions of words of wisdom I could write here and pretend to be clever by sharing them with you, I will simply tell you something that has helped me throughout life. It may help you, or it may not.

Be authentic in every aspect of your life.

You do not need to put on a mask when giving a presentation, attending an interview, talking to a random girl or guy you like, writing a scientific paper, or facing someone you dislike. No matter how much people push you to do certain things in a certain way, life becomes much easier when you live it according to who you are.

That is all.

Dear **Ke**, I really enjoyed all of the dinners we shared together. You always prepared so many dishes, and every single one of them was delicious. Thank you for trusting me with your samples. You are a kind and caring person, and a wonderful father.

Dear **Lanqing**, thank you for giving me the most unique gift I have ever received. I am still working my way through it, tearing out one page at a time.

Dear **Amit,** the dates you brought were among the best things I have ever tasted. While we did not spend a great deal of time together, a couple of beers were enough for me to feel like I had made a friend. I hope to visit you soon and enjoy more of those amazing dates.

Dear **Jorn**, my dear paranymph, sometimes I feel like we are two sides of the same coin, much to the misfortune of those around us, and especially our girlfriends. It is always fun to sweat together, whether it is during tennis, ping-pong, or trying to get a good pull. I love your impressions of other people, and I really miss having you at our DnD table. I really miss that long, cheesy beard of yours. The bromance we shared is something I keep looking for in other people, but it is never quite the same. There is something about you that shows you have never forgotten what it means to be a child and simply enjoy life, and that makes you incredibly fun to be around. You are a charismatic person and a fantastic presenter. You walk into a room, take control of it, and people genuinely enjoy having you around. I cherish our dinners together, and the secrets, dreams, and desires we shared during them. I trust you deeply, my dear friend. Both you and Selin have had such a profound impact on my PhD journey, and I hope that wherever the future takes me, I will not end up too far away from two of you.

Dear **Kaiyue**, I really admire your confidence and courage. There is no messing with you. You know what you want, and you are not afraid to go after it. Without a doubt, I believe you will do exceptionally well in life.

Dear **Mark**, it was great having you in the office. I enjoyed organizing borrels together, playing chess and Catan, and sharing beers. I still hope that one day I will finally manage to beat you at chess.

Dear **Yme**, you are incredibly chill, easy to be around, and you have excellent taste in music. I feel like I could walk into your office at any moment, ask what you are listening to, and discover some obscure song I have never heard before that would immediately earn a permanent place on my playlist. You do the best impressions of people (sorry Jorn), and somehow always seem to end up in the coolest places, whether it is a music festival, a cinema, or an art exhibition. Spending time with you always leaves me with a new recommendation, a good story, or both.

Dear **Silvana**, you organize the best dinners. They are always elegant and thoughtfully prepared, with special ingredients that somehow always turn out to be delicious. I still think fondly of your potatoes, the special South American teas, and the Spanish ham. I am sorry that I missed your PhD defence. Thank you for all the walks we shared together, listening to me, and for sharing your hopes, dreams, and desires for the future with me.

Dear **PhD trip** committee, Alessia, Carlos, Chang, Jill, Yue, and Yujun, it was fun, stressful, and chaotic to organize this trip. But we did it. Honestly, I do not remember much of the trip anymore. I think the adrenaline and stress I felt every day somehow erased most of my memories of it. Therefore, I am extremely grateful to the next PhD Trip Committee: Corne, Ding, Han, Ralf, Reiner, Shuhao, Weishen, Yifan, and Yulian, for allowing me to join the trip to Germany. For those few days, I finally got to experience what it feels like to be on a PhD trip without having to organize it. Thank you all for making these trips happen.

Dear **Halimat**, you are a strong woman, and there is no messing around with you. I have heard that you make amazing African food, and I sincerely hope that one day I will get the chance to taste it

Dear **Claudia**, there was a period during my PhD when I was feeling horrible, and I was fortunate to have you to talk to. Somehow, you always managed to give me compliments in front of other people, and you have no idea how much that meant for my confidence. Spending time with you was always a lot of fun, and your energy had a way of spreading to everyone around you, including me. Thank you for that.

Dear **Huub**, thank you for building the kind of environment at ETE that made me feel at home and gave me a sense of belonging. I have always found you to be a very kind person, someone who genuinely cares about his PhD students and goes the extra mile to make sure they are doing well and successfully completing their PhDs. Thank you for creating a place where people can grow, both as scientists and as individuals.

Dear **Annemiek**, thank you for that one walk we shared. One of the most important realizations of my PhD came out of it: that I truly enjoy this beautiful, foresty village of Wageningen, and that I should not be ashamed of wanting to stay here and build a life in a place that makes me happy. From the bottom of my heart, thank you for helping me realize that.

Dear **Elena**, my dear Love, thank you for enabling me to be the person I want to be. Thank you for being Italian, and for introducing me to so many wonderful foods and traditions. Thank you for showing me what it means to be part of a loving family, and thank you for being a nerd who is always willing to play games with me. Together, we have shared so many adventures, from Northern Italy to Japan, London, and Canada. Every one of those memories is precious to me. I know that I am a danger to your wallet, but I promise to make up for it by loving every atom of your being, every single day.

Dear **Tea**, you are incredibly organized. I remember looking through some of your work almost two years after you had left and thinking, "okei, I know exactly what happened here". Finding out that we came from the same small town in Croatia and somehow both ended up in a same small town in the Netherlands made me smile. We had the same teachers, shared some of the same memories, and talking about it all felt wonderfully nostalgic. It was a sad day for me, and for many others, when you left the Netherlands. We still miss you very much.

Dear **Kaiyuan**, honestly, the amount of work you did during your Master's thesis for me was probably enough to complete a PhD of your own. Thank you for all the sampling and for analysing the never-ending amount of my samples. I always enjoy our tennis and squash games, our discussions about life and the future, and our dinners at Campus Plaza. Thank you for all your help, and for being such great company throughout the years.

Dear **Gabriel**, my fellow sorption and DnD geek. I think the thing I admire most about you is how genuine you are. It does not take long for someone to figure out who you are and what you stand for. I honestly think more people should strive to be as open and authentic as you are. The world would be a nicer place because of it. I often found help in you, whether because things were not adsorbing as they should, or when I was feeling down and doubting what I was doing, or when I needed advice on how to make rocks fall onto our fellow players. One of the most memorable things you ever told me was that it does not matter how many papers you publish; what matters is how many people want to work with you and how many people value your help. Thank you for that. While I may have been unlucky with papers at times, I have been incredibly lucky to meet you and many other people who are excited to work with me in the future. You genuinely care about others and often go far beyond what anyone expects to help them. You bring a unique kind of positive energy to ETE. Thank you for starting the DnD group at ETE. I did not even realize how much I needed that. And, finally, thank you for making that delicious aubergine and tomato pasta dish.

Dear **Ding**, you are an incredibly hard worker, always in the lab taking care of your reactors. You genuinely care about your work, and you should be applauded for it. Both you and Sunny are such wonderful people, always bringing me beautiful gifts and little pieces of Chinese culture. My favourite was the red Chinese Horse New Year blessing that you gave me. Honestly, I forgot what is written on it, but the horse looks super cute. Thank you for all the thoughtful presents that you made for me over the years.

Dear **Manuela**, thank you for welcoming me as a guest PhD student into your group in Milan. I greatly enjoyed the environment you created, which made my time there both enjoyable and productive. I learned a lot, both scientifically and personally, and I am grateful for the opportunity you gave me.

Dear **Beatrice**, you always struck me as a very cheerful and positive person, and a pleasure to be around. Thank you for teaching me so many new things about adsorption, especially when it comes to column experiments. I learned a great deal from you. I hope we will have the opportunity to work on many more projects together in the future.

Dear **Alessandro**, thank you for all the trips we shared, both in real life to Japan, Sardinia, and Canada, and in fantasy to worlds filled with elementals, dwarves, elves, and goliaths. I have always found you to be a very calm and collected person who works hard and genuinely tries to do the right thing. You are also super calm in bed, which is great as I cannot sleep if somebody makes noises.

Dear **Anne**, thank you for telling me that you would miss me at ETE if I left. Sometimes we say things to people without realizing how much those words can mean to them, and your words meant a great deal to me. I always enjoyed discussing our research together, and I still remember your stories about China.

Dear **Merel**, as I am writing this, I am not yet sure whether I will have a party after my PhD defense. If I decide not to, one of the things I would miss most is your amazingly edited video of everything I did during my PhD. You are funny, kind, and not quite as Dutch as the others. I hope we get to play many more board games and solve many more jigsaw puzzles together in the future.

Dear **Bochi**, you are such a unique person that it is difficult to describe you in words. The fact that, in only six months at Wageningen, you somehow became involved with so many different people and friend groups, many of whom did not even know each other, says a lot about the kind of person you are. Thank you for working with me on our paper, and thank you for the amazing gifts from China. Your tea set is used very frequently at ETE and receives a great deal of praise. I hope to visit you in China soon.

Dear **Nick**, you have no idea how much I needed, and how much I enjoyed, playing table tennis with you during our breaks. Even though it pains me a little to admit it, you are better at it than I am. Having someone to chase and eventually beat gives me plenty of motivation. By the way, you are the best back cracker at ETE, and you can always realign my back. I hope we will play many more DnD games together in the future. You always seem to find the most unorthodox solutions to the problems we face. You are a great player, and it is truly a pleasure to DM for you.

Dear **Sijie**, thank you for the amazing snacks that always seemed to appear in your office, and for the friendly conversations with special Chinese tea. I am very happy that you came to ETE and that I had the chance to get to know you. One day, when you return to China, I promise I wil come and visit you there.

Dear **Jip**, I very much enjoyed supervising you. You have a talent for asking the right questions, and you were often demanding of yourself in the best possible way, always thinking carefully about how to present and communicate your work. You truly were a pleasure to supervise. I will remember you as a very charismatic person and an excellent presenter. I sincerely hope that our paths cross again in the future.

Dear **Nina**, forgive me for not being able to find enough work for you during your internship. Even so, thank you for doing such a great job with the small tasks that I managed to find here and there. You were the Croatian that I needed at a time when I was starting to forget my own language. The ping pong games we shared were a lot of fun, and I often needed them to forget about the struggles of my PhD for a while. Our trips together were wonderful, and the one to the beach is a memory that I will treasure forever.

Dear **Connie**, you are incredibly chill, fun, and easy to be around. It took me all of five minutes to realize how much we have in common and to become friends. Thank you for introducing me to card games that I knew very little about, and thank you for all the cards you have given me over the years. I always enjoyed spending time with you, and I hope we will share many more games in the future.

Dear **Advait,** thank you for making a model for me, and forgive me for never using it. You are very calm, but also sharp, with a unique sense of humour. You have a way of saying something unexpectedly funny. That made spending time with you enjoyable.

Dear **Chenxiao**, you have a pretty cool experimental setup that you built. I really envy it, as the only thing I did during my PhD was work with plastic bottles. Well done for building such a setup, and you should be proud of yourself. I always enjoyed our conversations and exchanging ideas about adsorption and biodegradation. And as for how to properly distinguish between the two... I am fairly convinced that nobody will ever completely figure that out.

Dear **new PhDs of ETE** who started around the time I finished and who will start in future, I did not get to know you well enough to thank you for anything in particular. But I can tell you that ETE is a great place to work. Be free, ask people for help, and do not let anything limit you except your own brain.

Dear **Selina**, there are two things that lift me up when I come into the office in the morning. One is your smile, and the second is an invitation to go for a coffee.

Dear **Julian**, I do not know how you do it, but you always smell good. I am sure those French perfumes help, but you are the one choosing them, so the credit still goes to you. You are also the calmest person I know. If I had to pick one person out of a group of a thousand who trains Kung Fu, I would choose you without hesitation. You just have that Aura. Ping-pong is always fun with you, and I am looking forward to more games once they put our table back.

Dear **Ralf**, you are my favourite person to run into at the market on Saturday mornings. I very much enjoyed the PhD trip that you organized, and thank you for making it possible for me to join it. I will never forget the eels, and at some point I am definitely going to steal them. I also have very fond memories of the events at your place, the New Year's celebrations, and the 5th of May gatherings. Thank you for all the good times and for bringing people together

Dear **Amin**, I feel like we share the struggle of method development in the lab and the frustration of things not working the way they should. Still, I do believe that in the end it will all work out somehow. It was fun playing table tennis with you while we still had the table. I hope they put it back soon.

Dear **Rik,** the Munich karaoke with you was a lot of fun. The dancing, the singing, and everything in between. Who would have guessed that going to a random Indian bar would lead to one of my favorite moments of the past year? Thank you for sharing those moments with me.

Dear **Adriaan**, you are unexpectedly cool for a chairholder. Jumping out of the box like a toy, wanting to go play table tennis with us (which we still have to do), and being willing to take stroopwafels to my friend in Vietnam. Thank you for bringing such a casual vibe to ETE. It really helps make people feel comfortable and at ease.

The people of **office Z1013**: Alessio, Ding, Elizabeth, Jill, Joao, Kaiyue, Lanqing, Mark, Minh, Qamar, Selina, and Yulian,. I hate you all for making my office such a wonderful place that I cannot imagine working anywhere else. From the bottom of my heart, thank you.

Dear **Lab Team**: Betty, Katja, Livio, Lucian, Nick, Pieter, and Thomas, thank you for dealing with me and all of my laboratory adventures. Finding shaker space, dealing with me occasionally destroying shakers, finding freezer space, ordering endless bottles, and helping solve

all the practical problems that somehow kept appearing. I am sure it was not always easy. But I want you to know that you made everything feel easy. No matter what problem I came to you with, you always dealt with it efficiently and successfully. A lot of what I achieved during my PhD would simply not have been possible without your help. Thank you.

Dear **Secretaries**: Adriana, Liesbeth, Marjolein, Petra, and Wies, you are all incredibly approachable, relaxed, and a pleasure to interact with. Before starting my PhD, everything I knew about secretaries was that they were stressed people whom nobody liked talking to. Thank you for completely changing that perception for me. Throughout my PhD, you helped solve many administrative problems and made dealing with them feel easy. I am very grateful for all the help and kindness you showed to me and my PhD friends over the years.

Dear **Modutech team**, Vinnie and Michiel thank you for quickly repairing the shakers I broke. Without your help, I would not have been able to break them again. Ilse, thank you for measuring the PSD for me at the start of my PhD. Without that, I would not have been able to begin my PhD so efficiently. And to all of you, as well as Julian, thank you for helping all of my PhD friends with their struggles in the lab.

Dear **Simon**, you did not stay at ETE for very long, but I feel like we managed to connect quickly. It seemed as if almost every hobby, wish for the future, and aspect of our personalities was somehow similar. The more I got to know you, the more I realized how much we had in common. I hope that I can visit you in Norway, or that you will visit the Netherlands again soon, so that I can get to know you even better.

Dear **Xingang**, I can see that you genuinely care about your students. I enjoyed listening to your life experiences and hearing how you experienced Europe and other cultures, over a few beers. I hope I can visit you in China soon.

Dear **Phoenix**, thank you for showing me that being a great DM is often just about trusting yourself and improvising when needed. I love your cheerful personality, geeky attitude, and fucking awesome clothes. (Yes, if I am to keep this book PG-13, I am allowed one f-word, and I am using it here.)

Dear **Delft people**, Kim and Akhilesh, I am only just getting to know you, but you are my adsorption people. It is a pleasure to work with you, and I am very much looking forward to our future collaborations. In just a few weeks in Delft, I felt like I could completely geek out about adsorption, and I think our expertise complements each other extremely well. I have a feeling that we will do some very interesting work together in the years to come.

At the end, there are two groups of people that I have to acknowledge, because without them I do not think I would have been able to finish my PhD at all.

The first group are all the creative, imaginative, and when needed chaotic people with whom I played **DnD**, both in person: Gabriel, Elizabeth, Nick, Eline, Phoenix, Jorn, Rikke, Alessandro; and online: Max, Lost, Bel, and Zeph. All the universes, stories, adventures, and characters that we created and lived through have become such a profound part of who I am that they continue to shape my thoughts, my values, and the way I approach life.

And the second group are **my students**: Casper, Dan, Haikal, Hanna, Ilse, Ivan, Jip, Kaiyuan, Mike, Nina, Tea, and Zhilin. This PhD would not have been possible without you. Through all the interactions we shared, you made me realize how much I love supervising, teaching, and helping others grow. Interacting with you gave me energy and motivation during the difficult moments of my PhD, and reminded me why I am doing it in the first place. To help others. Thank you for trusting me and allowing me to be a small part of your journeys.

About the Cover

Anyone who knows me knows how much I love stories and imaginary worlds. Growing up with all the things that shaped a millennial boy: The Lord of the Rings, Star Wars, anime and video games, left a deep mark on how I see the world and who I am. Because of that, I decided that the cover of this thesis should tell a story. The artwork was created by the amazing Belgian artist Kim van Deun. Please check out her work.

In this story, set in a faraway universe, the world is about to end. Giant carbonized meteors are falling onto a planet split by two oceans. The inhabitants of this world live partially submerged between them. And as the meteors approach, their destruction seems inevitable.

The only hope of stopping the coming apocalypse is a lone hero standing against the falling doom. Like many heroes, he is different from those around him. He is smaller, unable to live like the others, and has spent his entire life as an outsider. Yet, because he is different, he is the Chosen One, and he is the one who must stand and fight while the world collapses around him.

…

So how does any of this relate to the content of a PhD thesis about PFAS adsorption?

Well, the hero is actually a short-chain PFAS, one that resists removal by activated carbon. The frightened inhabitants are long-chain PFAS, waiting to be removed by the approaching meteors. And the meteor itself is, of course, activated carbon.

There was a deliberate decision to depict PFAS as the hero and carbon as the villain on this cover. This may seem peculiar, because throughout my PhD it was exactly the opposite: activated carbon was my hero and PFAS was my enemy. My goal was to remove PFAS, not to save it. Yet I wanted this cover to tell the story from the opposite point of view. I wanted to step into the perspective of the thing I spent years trying to eliminate.

I think we humans have a tendency to divide the world into heroes and villains, right and wrong, us and them. I have never liked that way of thinking. I try to be the kind of person who can understand both sides of a story, even when I prefer one of them.

In the end, who was right and who was wrong will matter very little on the fields of destruction. And those fields of destruction will continue to exist as long as each side refuses to understand the other, and refuses to be kind and compassionate toward those who are on the opposing end.

At least, that is what I believe.

List of publications

Related to this Thesis:

Pranić, M.; Carlucci, L.; van der Wal, A.; Dykstra, J. E. Kinetic and Isotherm Study for the Adsorption of Per- and Polyfluoroalkyl Substances (PFAS) on Activated Carbon in the Low Ng/L Range. Chemosphere 2025, 370. doi.org/10.1016/j.chemosphere.2024.143889

Pranić, M.; Zhou, K.; Biesheuvel, P. M.; van der Wal, A.; Dykstra, J. E. Temperature Impacts PFAS Adsorption on Activated Carbon. ACS ES&T Water 2025. doi.org/10.1021/acsestwater.5c00343

Zhou, K., **Pranic, M**., Rutten, S.M., Porada, S., Post, J.W., van der Wal, A., Dykstra, J. E (2025) Electroregeneration of activated carbon filters: concentrating short-chain PFAS, ACS ES&T Water , doi.org/10.1021/acsestwater.5c00819

Pranic, M., Cantoni, B., de Ridder, D.J., Antonelli, M., Dykstra, J. E, van der Wal, A., (2026) Which natural organic matter components limit PFAS removal by activated carbon? Chem. Eng. J. doi.org/10.1016/j.cej.2026.178076

Pranić, M.; Sigmund, G.; Martin, P.; Hofmann, T.; van der Wal, A.; Dykstra, J. E. Total PFAS isotherms as a framework to select adsorbents for PFAS removal (in preparation)

Other:

Pranić, M.; Kimani, E. M.; Biesheuvel, P. M.; Porada, S. Desalination of Complex Multi-Ionic Solutions by Reverse Osmosis at Different pH Values, Temperatures, and Compositions. ACS Omega 2021, 6 (30), 19946–19955. doi.org/10.1021/acsomega.1c02931

Kimani, E. M.; **Pranić, M.;** Porada, S.; Kemperman, A. J. B.; Ryzhkov, I. I.; van der Meer, W. G. J.; Biesheuvel, P. M. The Influence of Feedwater pH on Membrane Charge Ionization and Ion Rejection by Reverse Osmosis: An Experimental and Theoretical Study. J. Membr. Sci. 2022, 660. doi.org/10.1016/j.memsci.2022.120800

Saida, M.; Beut, L. B.; **Pranić, M.;** van Wezel, A. P.; ter Laak, T. L. Sorption of Per- and Polyfluoroalkyl Substances and Their Precursors on Activated Carbon under Realistic Drinking Water Conditions: Insights into Sorbent Variability and PFAS Structural Effects. Heliyon 2024, 10 (3). doi.org/10.1016/j.heliyon.2024.e25130

Yu, B.; **Pranić, M.;** Rizzo, S.; Sikma, M. A.; Gosselt, A. N. C.; van der Vis, S.; Sutton, N. B.; Sigmund, G. Urine from Intensive Care Patients as a Hotspot for Pharmaceutical Emissions and Sorbent-Based Treatment. Environ. Sci. Technol. Lett. 2025, 12 (7), 862–868. doi.org/10.1021/acs.estlett.5c00375

Netherlands Research School for the
Socio-Economic and Natural Sciences of the Environment

D I P L O M A

for specialised PhD training

The Netherlands research school for the
Socio-Economic and Natural Sciences of the Environment
(SENSE) declares that

Marko Pranić

born on 15/03/1994 in Bjelovar, Croatia

has successfully fulfilled all requirements of the
educational PhD programme of SENSE.

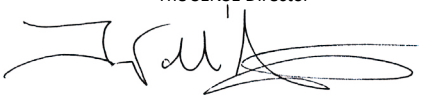
Wageningen, 01 July 2026

SENSE coordinator PhD education



Dr Ir Peter Vermeulen

The SENSE Director



Dr Jampel Dell'Angelo

The SENSE Research School declares that **Marko Pranić** has successfully fulfilled all requirements of the educational PhD programme of SENSE with a workload of 41.8 EC, including the following activities:

SENSE PhD Courses

- A1: Environmental Research in Context (2021)
- A2 Research in context activity: 'Co-organizer of Physics of Membrane Processes 2022' (2022)

Other PhD and Advanced MSc Courses

- The Art of Modelling, (2021)
- Communication styles,WUR (2021)
- Adobe Indesign: Scientific publications & layout, WUR Library (2021)
- Strathclyde Adsorption Summer School, University of Strathclyde (2022)
- Adobe Illustrator: Scientific Artwork & Infographics, WUR Library (2022)
- PhD trip to Denmark and Sweden (2023)

Management and Didactic Skills Training

- Chair of the organization committee for the PhD trip (2022-2023)
- Supervision of two MSc student with thesis (2024-2025)

External training at a foreign research institute

- Guest PhD in the group of Manuella Antonelli, Department of Civil and Environmental Engineering (DICA), Politecnico di Milano, Italy, (29/021/2024 – 05/2024)

Oral Presentations

- *Why is adsorption of PFAS on activated carbon limited? - Insights from isotherm and kinetic experiments in the low ng/L concentration range.* Wetsus Workshop, 20/04/ 2023, Leeuwarden, The Netherlands
- *What limits the adsorption of PFAS on activated carbon*. 13th Micropol and Ecohazard Conference, 16-20/06/ 2024, Taipei, Taiwan
- *What limits the adsorption of PFAS on activated carbon*. SETAC Europe 2025, 11-15/05/ 2025, Wien, Austria

The research described in this Thesis was financially supported by Evides Water Company N.V. (Rotterdam, The Netherlands)

Financial support from Wageningen University for printing this thesis is gratefully acknowledged

Cover design by Kim Van Deun - https://eyesintheforest.com/
Layout and printed by ProefschriftMaken | proefschriftmaken.nl

